



UNIVERSITÄT
BAYREUTH

Describing Charge Transfer in Extended Donor-Acceptor Systems with Density Functional Theory

Andreas Karolewski

Genehmigte Abhandlung zur Erlangung des akademischen Grades eines Doktors der Naturwissenschaften (Dr. rer. nat.) im Promotionsprogramm Fotophysik synthetischer und biologischer multichromophorer Systeme (Graduiertenkolleg 1640 der Deutschen Forschungsgemeinschaft) der Bayreuther Graduiertenschule für Mathematik und Naturwissenschaften

von

Andreas Karolewski
geboren in Erfurt

Tag der Einreichung: 17. Oktober 2013
Tag des Kolloquiums: 05. Dezember 2013

Prüfungsausschuss:

Prof. Dr. Stephan Kümmel (1. Gutachter)
Prof. Dr. G. Matthias Ullmann (2. Gutachter)
Prof. Dr. Mukundan Thelakkat (Vorsitzender)
Prof. Dr. Matthias Schmidt

Abstract

It is a long-standing problem of (time-dependent) density functional theory ((TD)DFT) that traditional functionals severely underestimate charge transfer (CT) excitations. In particular, the theoretical description of donor-acceptor (DA) systems is plagued by this shortcoming. DA systems are frequently used as light absorbing components in organic photovoltaic devices. The lowest electronic excitation in these molecules is usually influenced by CT.

In order to support the systematic development of new DA systems that are needed to improve the efficiency of organic solar cells it is a prerequisite for theory to reliably predict the electronic properties of this system class.

We demonstrate that the tuned range-separated hybrid (RSH) approach predicts these excitations in accordance with experiment. The approach can be regarded as an implicitly defined density functional within the generalized Kohn-Sham (GKS) scheme of DFT. Its main ingredient is the range-separation parameter that determines the splitting between long- and short-range exchange. It is obtained from first principles by enforcing the ionization potential theorem of GKS theory.

We consider DA systems of various sizes that are composed of thiophene as donor and benzothiadiazole or naphthalene diimide as acceptor. We show how the optical and electronic properties can be tailored by changing the conjugation length and the arrangement of the donor and acceptor components. We also address the downsides that accompany the use of tuned RSH functionals. Due to the way the approach is implicitly defined anew for each system it is not size consistent. By calculating ground state properties of atoms and diatomic molecules we report size consistency errors and demonstrate consequences of the size consistency violation, *e.g.*, the incorrect prediction of binding energies.

In order to reliably predict CT excitations within the Kohn Sham scheme of DFT the exchange correlation potential approximation has to incorporate particle number discontinuities. A candidate potential with the necessary features is the Becke-Johnson potential that is based on semi-local ingredients and is therefore computationally attractive for the treatment of very large systems. We show, however, that the potential cannot be applied in TDDFT because it is not a functional derivative and violates the zero-force theorem. We discuss a procedure on the basis of density path integrals that transforms the BJ potential into a functional derivative of a corresponding energy expression.

Zusammenfassung

Seit langem besteht bei der Anwendung zeitabhängiger Dichtefunktionaltheorie (DFT) basierend auf traditionellen Funktionalen das Problem, dass Ladungstransferanregungsenergien falsch berechnet werden. Dies trifft insbesondere auf die theoretische Beschreibung von Donor-Akzeptor(DA)-Systemen zu, welche verhäuft als lichtabsorbierende Komponenten in organischen Solarzellen verwendet werden. Die niedrigste Anregung wird in diesen Systemen im allgemeinen durch Ladungstransfer beeinflusst. Um die systematische Entwicklung neuer DA-Systeme zur Effizienzsteigerung organischer Solarzellen zu unterstützen, muss die Theorie in der Lage sein die elektronischen Eigenschaften dieser Systeme möglichst zuverlässig vorherzusagen.

Wir zeigen, dass ein Ansatz, der auf der Justierung reichweitenseparierter Hybridfunktionale (RSH) beruht, diese Anregungsenergien im Einklang mit experimentellen Ergebnissen prognostiziert. Dieser Ansatz kann als implizit definiertes Dichtefunktional betrachtet werden, welches in das Gerüst des generalisierten Kohn-Sham(GKS)-Ansatzes der DFT eingegliedert ist. Der Hauptbestandteil des Funktional ist der Reichweitenseparationsparameter, der die Reichweite von lang- und kurzreichweitigem Austauschanteil bestimmt. Er wird durch die Einhaltung des Ionisationspotential-Satzes der GKS Theorie nichtempirisch festgelegt.

Die Berechnungen in dieser Arbeit werden für DA-Systeme verschiedener Größe durchgeführt, bei denen Thiophen als Donor und 2,1,3-Benzothiadiazol bzw. Naphthalindiimid als Akzeptor eingesetzt wird. Wir zeigen, wie sich die optischen und elektronischen Eigenschaften durch die Änderung der Konjugationslänge und die Anordnung von Donor- und Akzeptor-Komponenten maßschneidern lassen. Weiterhin untersuchen wir die Nachteile, die durch die Verwendung von justierten RSH-Funktionalen auftreten. Durch die implizite Definition des Funktional wird der Reichweitenseparationsparameter für jedes System neu festgelegt. Infolgedessen wird die Größenkonsistenz verletzt. Wir führen Grundzustandsrechnungen an Atomen und zweiatomigen Molekülen durch um den dabei auftretenden Größenkonsistenzfehler zu bestimmen. Dieser hat weitreichende Folgen für die korrekte Vorhersagbarkeit von Grundzustandseigenschaften wie z.B. Bindungsenergien.

Um Ladungstransferanregungen innerhalb der Kohn-Sham-Theorie der DFT qualitativ richtig beschreiben zu können, muss das genäherte Austauschkorrelationspotential ein unstetiges Verhalten beim Übergang zwischen ganzzahligen Teilchenzahlen enthalten. Ein Kandidat mit dieser Eigenschaften ist das Becke-Johnson(BJ)-Potential. Es hängt nur von semilokalen Größen ab und ist damit auch für die Behandlung sehr großer Systeme geeignet. Unsere Untersuchungen dieses Potentials zeigen jedoch, dass es sich nicht in der zeitabhängigen DFT verwenden läßt, da es keine Funktionalableitung ist und damit das Zero-Force-Theorem verletzt. Schließlich analysieren wir ein auf Dichtepfadintegralen basierendes Verfahren, mit dem das BJ-Potential in eine Funktionalableitung eines zugehörigen Energieausdrucks umgewandelt werden kann.

Preface

List of Included Publications and Manuscripts

1. *Communication: Tailoring the optical gap in light-harvesting molecules*,
A. Karolewski, T. Stein, R. Baer, and S. Kümmel,
J. Chem. Phys. **134**, 151101 (2011).
2. *Using optimally tuned range separated hybrid functionals in ground-state calculations: Consequences and caveats*,
A. Karolewski, L. Kronik, and S. Kümmel,
J. Chem. Phys. **138**, 204115 (2013).
3. *Optical absorption in donor-acceptor polymers – alternating vs. random*,
A. Karolewski, A. Neubig, M. Thelakkat, and S. Kümmel,
Phys. Chem. Chem. Phys. **15**, 20016 (2013).
4. *Electronic excitations and the Becke-Johnson potential: The need for and the problem of transforming model potentials to functional derivatives*
A. Karolewski, R. Armiento, and S. Kümmel,
Phys. Rev. A **88**, 052519 (2013).
5. *The influence of donor and acceptor ordering on the fundamental and the optical gap*,
A. Karolewski and S. Kümmel,
Manuscript.

List of Other Publications

1. *Polarizabilities of Polyacetylene from a Field-Counteracting Semilocal Functional*,
A. Karolewski, R. Armiento, and S. Kümmel,
J. Chem. Theory Comput. **5**, 712 (2009)

Contents

Abstract	iii
Zusammenfassung	iv
Preface	v
List of Included Publications and Manuscripts	v
List of Other Publications	v
Contents	vi
1 Introduction	1
Part I Fundamentals and Concepts	7
2 Density Functional Theory	8
2.1 Schrödinger Equation and Hohenberg-Kohn Theorems	8
2.2 The Kohn-Sham Scheme	10
2.3 Splitting into Exchange and Correlation	12
2.4 Exact Properties of the Exchange Correlation Functional	13
2.5 Exchange Correlation Functional Approximations	15
3 Time-Dependent Density Functional Theory	20
3.1 Time-Dependent Kohn-Sham Equations	20
3.2 Time Propagation	22
3.3 Linear Response	23
3.4 Adiabatic Approximation	26
3.5 Zero-Force Theorem	26
4 Generalized Kohn-Sham Scheme	28
4.1 The Generalized Kohn-Sham Scheme in Static DFT	28
4.2 Approximations	30
4.3 The Generalized Kohn-Sham Scheme in TDDFT	35
4.4 Eigenvalue Gaps in Kohn-Sham and Generalized Kohn-Sham Theory	36

5	Charge Transfer Excitations in Donor-Acceptor Systems	39
5.1	Long-Range Charge Transfer Excitations in TDDFT	39
5.2	Tuned Range-Separated Hybrid Functionals	42
5.3	Partial Charge Transfer Excitations in Donor-Acceptor Systems	45
5.4	Influence of Donor-Acceptor Arrangements on Excitation Energies	46
5.5	Downsides of the Tuning Approach	51
6	Direct Potential Approximation	54
6.1	Becke-Johnson Potential	54
6.2	Transforming Potential Expressions into Functional Derivatives	56
	Acknowledgments	59
	List of Abbreviations	61
	Bibliography	63
Part II	Publications	73
	Publication 1	75
	Publication 2	81
	Publication 3	95
	Publication 4	107
	Publication 5	119
	Erklärung	132

Introduction

It is a well known problem that the future energy needs of the global population will not be covered by conventional energy sources like oil, gas and nuclear fission. Ultimately, the energy demand will have to be harvested from the sun's radiation on the earth's surface. This goal could be achieved indirectly, *e.g.*, via biomass, wind or hydro power or directly via solar thermal or photovoltaic technologies. Photovoltaic cells based on conventional inorganic materials are a well established and frequently applied technology. In Germany alone it accounted for 4.7% of the annual electricity production in 2012.¹ In recent years much research effort has been directed into the development of their organic counterpart – organic photovoltaic (OPV) cells.^{2–8} OPV cells have some notable advantages over inorganic solar cells. They are processable in solution via inkjet printing, one has the possibility to use flexible substrate materials, they are light weight and allow a cost effective fabrication with a low energy demand.^{9–11} The semiconducting organic materials between the electrodes can be polymers, oligomers or low molecular weight molecules.

A very simple model for an organic solar cell is the combination of a hole conducting material (electron donor, \bar{D}) and an electron conducting material (electron acceptor, \bar{A}) between two electrodes. In this model, the conversion of light into electricity can be divided into several steps:^{12,13}

1. The formation of an excited state \bar{D}^* (also called exciton) in \bar{D} by the absorption of light ($\hbar\omega$). For simplicity, we only assume light absorption in \bar{D} although it can generally also occur in \bar{A} .
2. The migration or diffusion of the exciton to the \bar{D}/\bar{A} interface before it decays back to the ground state.
3. The charge transfer of an electron across the \bar{D}/\bar{A} interface forming a bound pair of positively charged donor (\bar{D}^+) and negatively charged acceptor (\bar{A}^-).

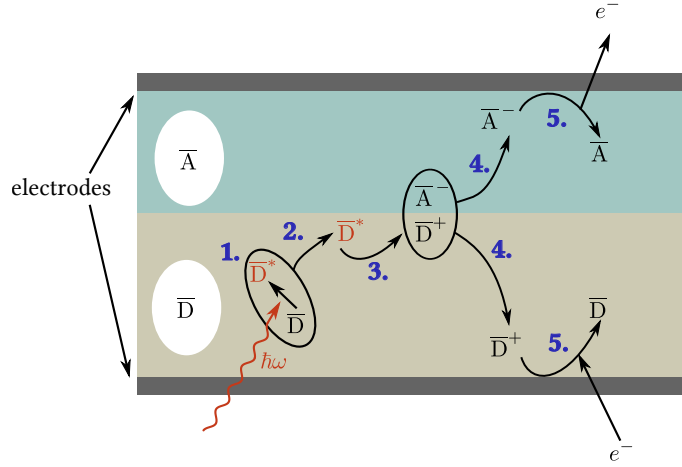


Figure 1.1. Schematic illustration of the processes that occur in a simplified ideal OPV cell that only consists of a layer of \bar{D} , a layer of \bar{A} and the electrodes (for an explanation see text). Note that the active layer of modern cells is usually a blend of \bar{D} and \bar{A} which forms a heterojunction.

4. The dissociation of the Coulomb bound pair \bar{D}^+/\bar{A}^- towards the electrodes.
5. The collection of the separated charges (also called holes in \bar{D} and electrons in \bar{A}) at the respective electrodes.

A schematic illustration of these processes is depicted in Fig. 1.1. The maximum energy that can be harvested from one absorbed photon is defined by the difference of the ionization potential (IP) of \bar{D} and the electron affinity (EA) of \bar{A} , $IP^{\bar{D}} - EA^{\bar{A}}$.⁵ The IP and EA are the energies that are required for the removal and addition of an electron, respectively. An energy level diagram of all energies relevant for OPV cells is shown in Fig. 1.2. This graph is of importance since we will discuss these energy levels several times in the following chapters. One of these energies, that remained unmentioned so far, is the fundamental gap ΔE_f , the difference between IP and EA (*cf.* Fig. 1.2 (b))

In order to improve the solar cell efficiency systematically and provide guidance for the design of new materials it is necessary to understand all of the above mentioned processes (1.) to (5.). Along with experimental studies, theoretical simulations can help to achieve this goal. For this purpose it is necessary to successfully model the underlying dynamical processes and reliably predict the materials properties, *e.g.*, optical and electronic properties or charge carrier mobilities.

In this thesis we focus on the theoretical prediction of the first excitation energy, the IP and the EA of conjugated donor-acceptor (DA) systems. These

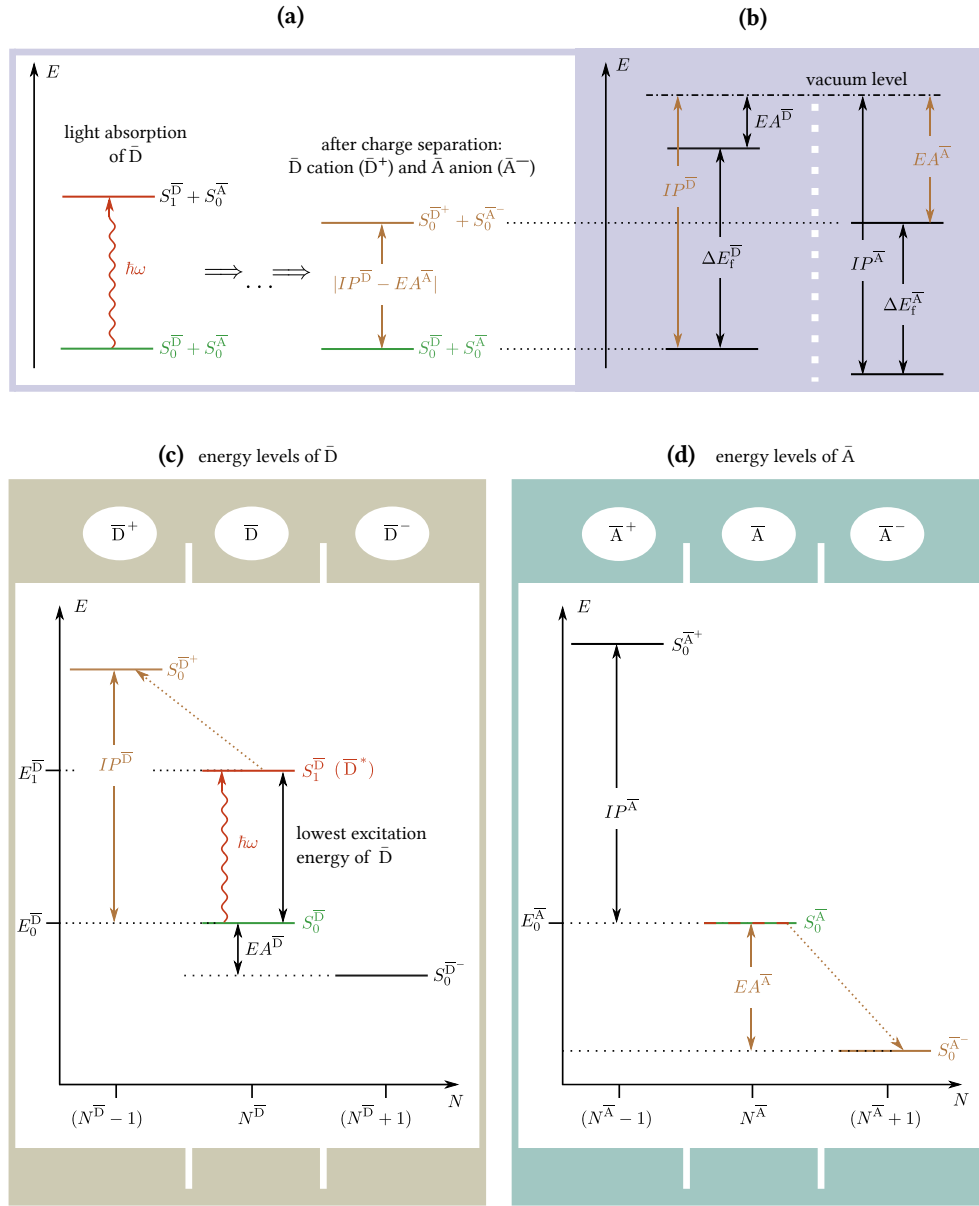


Figure 1.2. (a): Illustration of the energy that is absorbed in process (1.) of Fig. 1.1 due to light absorption ($\hbar\omega$) of \bar{D} . Furthermore, we illustrate the upper energy limit that can be harvested at the electrodes ($IP^{\bar{D}} - EA^{\bar{A}}$). S_0 denotes the electronic ground state and S_1 the first excited state corresponding to the ground state energy E_0 and the energy of the first excited state E_1 . (b): Energy levels IP and EA of \bar{D} and \bar{A} with respect to the vacuum level. Note that the levels are aligned with respect to the gap defined in (b). The difference of IP and EA defines the fundamental gap (c): Energy levels of \bar{D} including an illustration of the light absorption process (1.) and the formation of a positively charged ion after the charge separation at the interface. (d): Energy levels of \bar{A} including an illustration of the formation of a negatively charged ion after the charge separation at the interface. Note, that the colors in (a) to (d) and in Fig. 1.1 are used consistently.

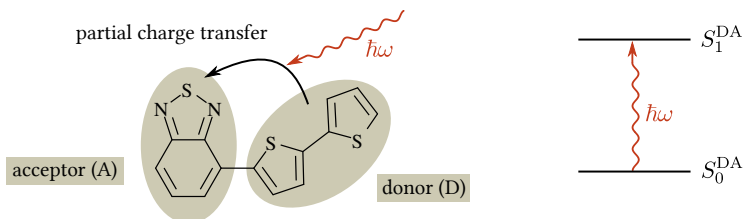


Figure 1.3. DA system with thiophene as the D and 2,1,3-benzothiadiazole as the A component. We discuss this system among others in Chap. 5.

systems consist of an arrangement of electron-rich donor (D) and electron-deficient acceptor (A) units along the conjugated molecular backbone. In Fig. 1.3 we show an exemplary DA system that is part of our examinations in Chap. 5. The optical properties of this class of materials are ideal for light absorption in organic solar cells.^{14–17} The lowest absorption peak is very broad, low in energy and high in oscillator strength which is necessary to build thin film cells that harvest the major part of the solar spectrum. In the simple schemes of Figs. 1.1 and 1.2, DA systems are usually employed as the light absorbing hole-conducting component \bar{D} (although the electron-conducting part \bar{A} could in principle also act as an light absorbing component).

The method of choice to describe DA systems from first principles is density functional theory (DFT). Due to its excellent compromise between computational efficiency and accuracy it enables the description of organic systems that contain several hundred atoms. Such system sizes are relevant for this work and already far outside the reach of high-quality ab-initio wave-function based methods.

An important characteristic of the lowest excitation in DA systems is the partial occurrence of photo-induced charge transfer (CT). Upon the absorption of light, electronic density is transferred from the electron rich to the electron poor component (*cf.* Fig. 1.3). Thus, these excitations exhibit a non-local character that standard DFT methods fail to describe correctly. The main part of this thesis will address this issue, starting with an analysis of the shortcomings of standard DFT causing the poor description of CT to the application and development of methods to overcome these shortcomings. Attached to this thesis are five publications. Four of them are published and one is attached as a manuscript. We refer to these works as **Pub. 1** to **Pub. 5**.

Following this introductory chapter, we discuss the fundamental concepts of DFT and time-dependent DFT (TDDFT) in Chaps. 2 and 3 of this thesis. TDDFT is an extension of DFT that is required for the calculation of excitation energies. Chaps. 2 and 3 are based on the so-called Kohn-Sham (KS) scheme, the first realization of DFT of practical relevance for which many theorems and exact conditions exist. In Chap. 4 we introduce the generalized Kohn-

Sham (GKS) scheme as a second realization of DFT. This scheme allows more flexibility in constructing new approximations. One of these new approximations is the so-called range-separated hybrid (RSH) approach that contains one free parameter that cannot be determined analytically. In Chap. 5 we use the tuned RSH approach to set this parameter according to an exact condition and apply the approach to several DA systems (Pub. 1, Pub. 3 and Pub. 5). By critically comparing the theoretical predictions with experimental absorption spectra we demonstrate that this method is, within the GKS scheme, able to reliably predict CT excitations of DA systems. At the end of Chap. 5 we analyze the downsides of the tuned RSH approach which is topic of Pub. 2. In Chap. 6 we introduce Pub. 4 and provide an overview of its results. We discuss the development of a new approach that tackles the CT issue within the KS scheme.

Preliminary Notes

First, we use Hartree atomic units throughout the entire thesis. Second, in the field of DA systems we only consider singlet excitation energies. Furthermore, note that all our calculations of organic molecules are based on the single molecule approach, *i.e.*, we only consider one molecule in vacuum at zero temperature. Nevertheless, we compare the theoretical predictions of the absorption energies with experimental measurements of the same molecule in solution at room temperature. Compared to the single molecule approach the results are influenced by vibrations of the nuclei, distortions from the ground state geometry and intermolecular interactions (solvent–molecule and molecule–molecule). We discuss these influences in Pub. 1 and Pub. 3.

Part I

Fundamentals and Concepts

Density Functional Theory

In the first section of this chapter we set the basic framework of **DFT** starting from the stationary many body Schrödinger equation. In the following sections we introduce the Kohn-Sham scheme, an important practical realization of **DFT**, and discuss its most relevant properties and approximations. For a detailed introduction to **DFT** we refer the reader to Refs. 18–22 upon which the following sections are based.

2.1 Schrödinger Equation and Hohenberg-Kohn Theorems

In the following we only consider time-independent systems. **DFT** for time-dependent systems is introduced in the subsequent chapter. The formal starting point of this thesis is a quantum mechanical many-particle system consisting of nuclei and electrons. We restrict our studies to non-relativistic systems and separate the dynamics of electrons and nuclei by using the Born-Oppenheimer approximation,²³ *i.e.*, we only consider systems where the response of the electrons to the dynamics of the nuclei is immediate. Following our assumptions the electrons can be described by the non-relativistic time-independent Schrödinger equation

$$\hat{H}\Psi = E\Psi \quad (2.1)$$

with the many-electron Hamiltonian

$$\hat{H} = \underbrace{-\sum_{i=1}^N \frac{\nabla_i^2}{2}}_{\hat{T}} + \underbrace{\sum_{i=1}^N v(\mathbf{r}_i)}_{\hat{V}} + \underbrace{\sum_{i<j}^N \frac{1}{|\mathbf{r}_i - \mathbf{r}_j|}}_{\hat{U}}. \quad (2.2)$$

The three contributions to the Hamiltonian are the kinetic energy of the electrons \hat{T} , the external potential \hat{V} given by the nuclei, and the electron-electron repulsion energy \hat{U} . The many-electron wave-function Ψ of a system

of N electrons is a function of N spin ($\sigma_i = \uparrow, \downarrow$) and $3N$ spatial coordinates (\mathbf{r}_i)

$$\Psi = \Psi(\sigma_1, \mathbf{r}_1, \dots, \sigma_N, \mathbf{r}_N) . \quad (2.3)$$

In principle, the ground state Ψ_0 and the ground state energy E_0 can be determined by the Rayleigh-Ritz variational principle²⁴ as the state of minimum energy

$$\hat{H}\Psi_0 = E_0\Psi_0 \quad E_0 = \min_{\Psi} \langle \Psi | \hat{H} | \Psi \rangle . \quad (2.4)$$

However, even for simple atoms a direct minimization involves the search for the minimizing wave-function in a $3N$ dimensional space of functions. To circumvent this complex minimization problem one can reformulate Eq. (2.4) into a minimization problem of only three dimensional functions. This leads us to density functional theory (DFT), an approach that uses the electron density $n(\mathbf{r})$ as the basic variable instead of the many-electron wave-function. The density is given by the expectation value of the density operator $\hat{n}(\mathbf{r}) = \sum_{i=1}^N \delta(\mathbf{r} - \mathbf{r}_i)$

$$n(\mathbf{r}) = \langle \Psi | \hat{n}(\mathbf{r}) | \Psi \rangle \quad (2.5)$$

$$= N \sum_{\{\sigma_i\}} \int d^3r_2 \dots \int d^3r_N |\Psi(\sigma_1, \mathbf{r}, \sigma_2, \mathbf{r}_2, \dots, \sigma_N, \mathbf{r}_N)|^2 . \quad (2.6)$$

The theoretical framework of DFT was established by two simple theorems proven by Hohenberg and Kohn in 1964.²⁵ The *first Hohenberg-Kohn theorem* states that the ground state electron density $n(\mathbf{r})$ of an interacting electron system uniquely determines the external potential $v(\mathbf{r})$, except for a constant. Thus, \hat{H} and all quantities that can be derived from \hat{H} are also uniquely determined by the density whose integral gives

$$\int d^3r n(\mathbf{r}) = N . \quad (2.7)$$

The theorem in its original form assumes a non-degenerate ground state. However, it can be generalized for degenerate ground states. Furthermore, only densities that correspond to an existing potential v were considered. Densities that have no corresponding potential are called non- v -representable. Such densities exist, however, they do not restrict the use of DFT in practical applications.

The *second Hohenberg-Kohn theorem* states that the total energy $E[n]$ can be defined as a functional of the density with the ground state energy E_0 being the global minimum of this functional. It enables the reformulation of the Rayleigh-Ritz variational principle for the three-dimensional density space

$$E_0 = \min_n E[n] . \quad (2.8)$$

One can construct the energy functional via

$$E[n] = F[n] + V[v, n] . \quad (2.9)$$

The external potential functional $V[v, n]$ can be obtained straightforwardly

$$V[v, n] = \int d^3r n(\mathbf{r}) v(\mathbf{r}) . \quad (2.10)$$

The remainder is defined by a universal functional

$$F[n] = \min_{\Psi \rightarrow n} \langle \Psi | \hat{T} + \hat{U} | \Psi \rangle . \quad (2.11)$$

Here the minimization is constrained to those Ψ that yield the density n . The definition of $F[n]$ is of conceptual importance for the density variational principle. The remaining problem is to find an explicit density functional expression of $F[n]$. Finding this functional is as difficult as solving the Schrödinger equation for all possible systems with interaction \hat{U} because $F[n]$ is the same for all these systems. Without a good approximation of $F[n]$ an explicit density minimization is not feasible in practice.

To ensure the correct total number of electrons (*cf.* Eq. (2.7)) we introduce a Lagrange multiplier μ and rewrite Eq. (2.8) as an Euler equation

$$\delta \left[F[n] + V[v, n] - \mu \int d^3r n(\mathbf{r}) \right] = 0 \quad \Longrightarrow \quad \frac{\delta F}{\delta n(\mathbf{r})} + v(\mathbf{r}) = \mu . \quad (2.12)$$

2.2 The Kohn-Sham Scheme

Below we introduce a scheme that enables us to approximate $F[n]$. It was introduced by Kohn and Sham in 1965²⁶ and replaces the direct variation with respect to the density with an auxiliary non-interacting orbital system that is solved self-consistently. The Kohn-Sham (KS) scheme is the most often used practical implementation of DFT. Although it is used to construct approximations for $F[n]$ the scheme is in principle exact.

Kohn and Sham have proven that it is sufficient to carry out the energy minimization of Eq. (2.8) for a system of non-interacting auxiliary particles. In contrast to the real electrons, these particles are subject to an effective external potential, the so called KS potential v_{KS} . The ground state wave-function of a non-interacting system is a Slater determinant. Hence, we can write the ground state density as (*cf.* Eq. (2.5))

$$n(\mathbf{r}) = n_{\uparrow}(\mathbf{r}) + n_{\downarrow}(\mathbf{r}) = \sum_{\sigma=\uparrow,\downarrow} \sum_{j=1}^{N_{\sigma}} |\phi_{j\sigma}(\mathbf{r})|^2 \quad (2.13)$$

with

$$N = N_{\uparrow} + N_{\downarrow} . \quad (2.14)$$

The orbitals $\phi_{j\sigma}$ are called KS orbitals and can be obtained as solutions of a simple one-electron Schrödinger equation, the so-called KS orbital equation.

The spin resolved form²⁷ of this equation is given by

$$\left(-\frac{\nabla^2}{2} + v_\sigma^{\text{KS}}(\mathbf{r})\right)\phi_{j\sigma}(\mathbf{r}) = \epsilon_{j\sigma}\phi_{j\sigma}(\mathbf{r}) \quad (2.15)$$

where the **KS** potential is defined as

$$v_\sigma^{\text{KS}}(\mathbf{r}) = v(\mathbf{r}) + \int d^3r' \frac{n(\mathbf{r}')}{|\mathbf{r} - \mathbf{r}'|} + v_{\text{xc},\sigma}[\{n_\sigma\}](\mathbf{r}). \quad (2.16)$$

It consists of three potential terms. The first is the external potential of Eq. (2.10). The second is the Hartree potential v_{H} . It is the functional derivative of the classical electrostatic interaction energy, the Hartree energy

$$U_{\text{H}}[n] = \frac{1}{2} \int d^3r \int d^3r' \frac{n(\mathbf{r})n(\mathbf{r}')}{|\mathbf{r} - \mathbf{r}'|}. \quad (2.17)$$

The unknown potential $v_{\text{xc},\sigma}$ in Eq. (2.16) is the so-called exchange-correlation (**xc**) potential which is defined as the functional derivative of the **xc** energy E_{xc}

$$v_{\text{xc},\sigma}[\{n_\sigma\}](\mathbf{r}) = \frac{\delta E_{\text{xc}}[\{n_\sigma\}]}{\delta n_\sigma(\mathbf{r})}. \quad (2.18)$$

E_{xc} in turn is defined as the difference of the non-interacting kinetic energy ($T_{\text{ni}}[n]$) and the Hartree energy ($U_{\text{H}}[n]$) from $F[n]$ of the real interacting system

$$E_{\text{xc}}[\{n_\sigma\}] = F[\{n_\sigma\}] - T_{\text{ni}}[n] - U_{\text{H}}[n]. \quad (2.19)$$

Thus, the **xc** energy includes the non-classical part of the electron-electron interaction and a part of the kinetic energy that cannot be described by a Slater determinant. With this definition we are able to calculate the main contributions to $F[n]$. The only part of $F[n]$ that remains unknown is E_{xc} that needs to be approximated. We can rewrite the Euler equation (Eq. (2.12)) to

$$\frac{\delta E[n]}{\delta n_\sigma} = \frac{\delta T_{\text{ni}}[n]}{\delta n_\sigma} + \frac{\delta U_{\text{H}}[n]}{\delta n_\sigma} + \frac{\delta E_{\text{xc}}[\{n_\sigma\}]}{\delta n_\sigma} + \frac{\delta V[v, n]}{\delta n_\sigma} = \mu. \quad (2.20)$$

For the non-interacting **KS** system with the effective potential v_σ^{KS} we obtain

$$\frac{\delta E_{\text{KS}}[n]}{\delta n_\sigma} = \frac{\delta T_{\text{ni}}[n]}{\delta n_\sigma} + \frac{\delta V[v^{\text{KS}}, n]}{\delta n_\sigma} = \mu \quad (2.21)$$

as $F[n] = T_{\text{ni}}[n]$ in the non-interacting case. By comparing the last two equations we can make the following important conclusion: If we define the **KS** potential v^{KS} as in Eq. (2.16) both Eqs. (2.20) and (2.21) are identical and lead to the same density n . Thus, we only need to solve the **KS** orbital equation of the non-interacting **KS** system to obtain the density for the real system of interacting electrons. However, since v^{KS} depends on the unknown

density it is not possible to solve the equation directly. It can only be solved iteratively until self-consistency is achieved.

After the minimization the ground state energy $E_{\text{KS},0}$ of the non-interacting KS system is given by the sum of the occupied orbital energies

$$E_{\text{KS},0} = T_{\text{ni}}[n] + V[v^{\text{KS}}, n] = \sum_{\sigma=\uparrow,\downarrow} \sum_{j=1}^{N_\sigma} \epsilon_{j\sigma}. \quad (2.22)$$

Using this equation we can calculate the ground state energy of the real system with the converged KS orbitals via

$$E_0 = \sum_{\sigma=\uparrow,\downarrow} \sum_{j=1}^{N_\sigma} \epsilon_{j\sigma} - U_{\text{H}}[n] + E_{\text{xc}}[\{n_\sigma\}] - V[v^{\text{xc}}, n]. \quad (2.23)$$

2.3 Splitting into Exchange and Correlation

It is common to split the xc energy into two parts, the exchange energy E_{x} and the correlation energy E_{c} . The exchange energy is defined as the exchange Fock integral evaluated with the Slater determinant of the KS orbitals Φ_{KS}

$$E_{\text{x}} = \langle \Phi_{\text{KS}} | \hat{U} | \Phi_{\text{KS}} \rangle - U_{\text{H}} \quad (2.24)$$

$$= -\frac{1}{2} \sum_{\sigma=\uparrow,\downarrow} \sum_{i,j=1}^{N_\sigma} \int d^3r \int d^3r' \frac{\phi_{i\sigma,\text{KS}}^*(\mathbf{r}) \phi_{j\sigma,\text{KS}}^*(\mathbf{r}') \phi_{j\sigma,\text{KS}}(\mathbf{r}) \phi_{i\sigma,\text{KS}}(\mathbf{r}')}{|\mathbf{r} - \mathbf{r}'|} \quad (2.25)$$

Hence, the correlation energy is defined as

$$E_{\text{c}} = F[n] - T_{\text{ni}}[n] - U_{\text{H}}[n] - E_{\text{x}}[\{\phi_i[\{n_\sigma\}]\}] \quad (2.26)$$

$$= \left(\langle \Psi | \hat{T} | \Psi \rangle - \langle \Phi_{\text{KS}} | \hat{T} | \Phi_{\text{KS}} \rangle \right) + \left(\langle \Psi | \hat{U} | \Psi \rangle - \langle \Phi_{\text{KS}} | \hat{U} | \Phi_{\text{KS}} \rangle \right). \quad (2.27)$$

It contains part of the electron-electron interaction energy that is not described by E_{x} and U_{H} and a part of the kinetic energy that is not described by the KS kinetic energy T_{ni} . One may view this separation as a further step to split the energy into parts that are known and a small rest to be approximated. However, in practice, usually both parts, E_{x} and E_{c} , are approximated. Thus, splitting in exchange and correlation is more a matter of convention than necessity.

Correspondingly, the xc potential can be split into its exchange and correlation counterparts

$$v_{\text{xc},\sigma}(\mathbf{r}) = v_{\text{x},\sigma}(\mathbf{r}) + v_{\text{c},\sigma}(\mathbf{r}) = \frac{\delta E_{\text{x}}[\{n_\sigma\}]}{\delta n_\sigma(\mathbf{r})} + \frac{\delta E_{\text{c}}[\{n_\sigma\}]}{\delta n_\sigma(\mathbf{r})}. \quad (2.28)$$

2.4 Exact Properties of the Exchange Correlation Functional

In the previous section we introduced the **KS** equations, a scheme to determine the ground state energy and density. The scheme is in principle exact if the **KS** functional $E_{\text{xc}}[n]$ were known exactly. However, in practice, this functional has to be approximated. Although it is only a small fraction of the total energy the approximation should still be as accurate as possible since it contains all non-classical many-body effects. For example, the main contribution to chemical bonding effects arises from this energy.²⁰

Helpful for the construction of approximations are the known exact properties of $E_{\text{xc}}[n]$. A useful strategy is to fulfill as many of these properties as possible in order to improve the predictive power of **DFT**. In the following we will summarize some of the properties that are especially important for the description of **CT** phenomena and this work in general.

Size Consistency

Size consistency means that the energies of two well separated, independent subsystems A and B should be equal to the energy of a large combined system that contains both subsystems

$$E(\text{A}) + E(\text{B}) \stackrel{!}{=} E(\text{A} + \text{B}) . \quad (2.29)$$

This is a very fundamental principle that applies to **DFT** as well as any other electronic structure theory. A violation of size consistency can cause various failures, *e.g.*, incorrect binding energies, dissociation properties and potential energy surfaces.

Asymptotic Behavior

An electron in a finite neutral system that moves far away from the other electrons and the nuclei should see the Coulomb potential of a single positive effective charge. The potentials v_{H} and v fall off with $\frac{N}{r}$ and $-\frac{N}{r}$, respectively, and therefore cancel each other. Thus, the **xc** potential fulfills

$$v_{\text{xc}}(\mathbf{r}) \xrightarrow{r \rightarrow \infty} -\frac{1}{r} . \quad (2.30)$$

KS energy eigenvalues ϵ_j

The energy level of the highest occupied **KS** orbital of a finite system of N electrons equals minus the exact vertical ionization energy IP ²⁸

$$\epsilon_N(N) = -IP(N) = E_0(N) - E_0(N - 1) \quad (2.31)$$

2. DENSITY FUNCTIONAL THEORY

where $E_0(Z)$ is the ground state energy of a Z -electron system. Similarly, one can write for the electron affinity EA

$$\epsilon_{N+1}(N+1) = -IP(N+1) = E_0(N+1) - E_0(N) = -EA(N). \quad (2.32)$$

Except for the highest occupied **KS** eigenvalue the $\{\epsilon_j\}$'s have no rigorous physical meaning. In particular, differences between occupied and unoccupied energy levels are not the excitation energies of the real interacting system although they represent a zero-order approximation.²⁹

Derivative Discontinuity

By extending **DFT** to systems with non-integer particle numbers N' Perdew showed that the total energy $E(N')$ of a finite system changes linearly with N' between adjacent integers and has a derivative discontinuity at each integer, *i.e.*, the chemical potential $\mu = \frac{\partial E}{\partial N'}$ jumps discontinuously at $N' = N \in \mathbb{N}$.³⁰ Thus, IP and EA of Eqs. (2.31) and (2.32) can be related to $\frac{\partial E}{\partial N'}$

$$\mu = \begin{cases} -IP(N) = E(N) - E(N-1) = \lim_{\delta \rightarrow 0} \frac{\partial E}{\partial N'} \Big|_{N-\delta} \\ -EA(N) = E(N+1) - E(N) = \lim_{\delta \rightarrow 0} \frac{\partial E}{\partial N'} \Big|_{N+\delta} \end{cases} \quad (2.33)$$

The jump of the chemical potential at integer particle numbers defines the fundamental gap ΔE_f

$$\Delta E_f = IP(N) - EA(N). \quad (2.34)$$

Because the functional derivatives of the Hartree energy $U_H[n]$ and external energy $V[v, n]$ are continuous we conclude from the Euler equation of **DFT** (Eq. (2.20)) and Eq. (2.33)

$$\Delta E_f = \lim_{\delta \rightarrow 0} \left\{ \left(\frac{\delta T_{\text{ni}}[n]}{\delta n(\mathbf{r})} \Big|_{N+\delta} - \frac{\delta T_{\text{ni}}[n]}{\delta n(\mathbf{r})} \Big|_{N-\delta} \right) + \underbrace{\left(\frac{\delta E_{\text{xc}}[n]}{\delta n(\mathbf{r})} \Big|_{N+\delta} - \frac{\delta E_{\text{xc}}[n]}{\delta n(\mathbf{r})} \Big|_{N-\delta} \right)}_{\Delta_{\text{xc}}} \right\} \quad (2.35)$$

The derivative discontinuity of the **xc** energy is Δ_{xc} . Thus, $v_{\text{xc}}(\mathbf{r})$ jumps by Δ_{xc} (independent of \mathbf{r}) at integer particle numbers.³¹ From the Euler equation of the non-interacting system (Eq. (2.21)) we deduce

$$\lim_{\delta \rightarrow 0} \left(\frac{\delta T_{\text{ni}}[n]}{\delta n(\mathbf{r})} \Big|_{N+\delta} - \frac{\delta T_{\text{ni}}[n]}{\delta n(\mathbf{r})} \Big|_{N-\delta} \right) = \Delta_{\text{KS}} = \epsilon_{N+1}(N) - \epsilon_N(N). \quad (2.36)$$

Overall, we can write the fundamental gap as the sum of the **KS** orbital gap and the derivative discontinuity of the **xc** energy functional

$$\Delta E_f = [\epsilon_{N+1}(N) - \epsilon_N(N)] + \Delta_{\text{xc}}. \quad (2.37)$$

2.5. Exchange Correlation Functional Approximations

In common notation the highest occupied orbital is called “**HOMO**” and the lowest unoccupied orbital “**LUMO**”. Thus,

$$\Delta E_f = \epsilon_{\text{HOMO}}^{(N+1)} - \epsilon_{\text{HOMO}}^{(N)} = \left(\epsilon_{\text{LUMO}}^{(N)} - \epsilon_{\text{HOMO}}^{(N)} \right) + \Delta_{\text{xc}} \quad (2.38)$$

and

$$\epsilon_{\text{HOMO}}^{(N+1)} = -EA(N) = \epsilon_{\text{LUMO}}^{(N)} + \Delta_{\text{xc}}. \quad (2.39)$$

Self-Interaction

In a system with only one electron no electron-electron interaction is present. Thus, the **KS** potential must be $v_{\text{KS}} = -\frac{\nabla^2}{2} - \frac{1}{r}$. This implies that the **xc** potential has to cancel the electron self-interaction contribution of the Hartree potential that is even present in the one-electron case

$$v_{\text{xc}}(\mathbf{r}) = -v_{\text{H}}(\mathbf{r}) = -\int d^3r' \frac{n(\mathbf{r}')}{|\mathbf{r} - \mathbf{r}'|}. \quad (2.40)$$

For a system with many electrons it is harder to find a condition that an approximate **xc** potential must fulfill in order to cancel the (many-electron) self-interaction error of the Hartree potential.^{32–34} A condition that accounts for part of the self-interaction is³⁵

$$E_{\text{xc}} \left[|\phi_{j\sigma}|^2, 0 \right] = -U_{\text{H}} \left[|\phi_{j\sigma}|^2 \right] \quad (2.41)$$

for any occupied **KS** orbital with corresponding single orbital density $|\phi_{j\sigma}|^2$. Functionals that fulfill this condition are called one-electron self-interaction free functionals. Eq. (2.41) can be reformulated to

$$E_{\text{x}} \left[|\phi_{j\sigma}|^2, 0 \right] = -U_{\text{H}} \left[|\phi_{j\sigma}|^2 \right] \quad \text{and} \quad E_{\text{c}} \left[|\phi_{j\sigma}|^2 \right] = 0, \quad (2.42)$$

i.e., the exchange energy compensates the self-interaction error (cf. Eq. (2.25)).

2.5 Exchange Correlation Functional Approximations

In the following we provide an overview of commonly used **xc** functional approximations.

Local and Semi-Local Functionals

The local density approximation (**LDA**) is the oldest and crudest **xc** functional approximation and it was already introduced in early **DFT** works.^{25,26} It is based on the homogeneous electron gas (or liquid) which has a homogeneous density \bar{n} and homogeneous energy density $e_{\text{xc}}^{\text{hom}}(\bar{n})$. The exchange part of this energy density is known exactly in its analytic form. For the correlation part

2. DENSITY FUNCTIONAL THEORY

analytical parametrizations^{36,37} based on accurate numerical quantum Monte Carlo calculations³⁸ exist.

The idea behind the **LDA** is to assign the energy density of the homogeneous electron gas to every point \mathbf{r} in space, but, to evaluate it with the density $n(\mathbf{r})$ of the system at this point. Thus, we obtain the **LDA** energy

$$E_{\text{xc}}^{\text{LDA}}[n] = \int d^3r e_{\text{xc}}^{\text{hom}}(\bar{n}) \Big|_{\bar{n} \rightarrow n(\mathbf{r})} = \int d^3r e_{\text{xc}}^{\text{LDA}}[n](\mathbf{r}) \quad (2.43)$$

and the **LDA** potential

$$v_{\text{xc}}^{\text{LDA}}(\mathbf{r}) = \frac{\delta E_{\text{xc}}^{\text{LDA}}}{\delta n(\mathbf{r})} = \frac{de_{\text{xc}}^{\text{LDA}}[n]}{dn}(\mathbf{r}). \quad (2.44)$$

The crucial point of this approximation is the assumption that the **xc** energy per particle and the **xc** potential only depend locally on the density whereas the exact $e_{\text{xc}}[n](\mathbf{r})$ and $v_{\text{xc}}[n](\mathbf{r})$ depend on the density $n(\mathbf{r}')$ at all points in space \mathbf{r}' . One would naively expect that the **LDA** is an acceptable approximation only in the limit of slowly varying densities (small $\frac{|\nabla n(\mathbf{r})|}{n(\mathbf{r})}$). However, in practice this requirement does not have to be fulfilled in order to obtain reasonable results for many systems.

One step beyond the strictly local **LDA** are functionals that are called generalized gradient approximations (**GGAs**). The idea is to construct *semi-local* functionals that also depend on the gradient of the density and thus, introduce some non-locality. **GGAs** have the following general structure

$$E_{\text{xc}}^{\text{GGA}}[n_{\uparrow}, n_{\downarrow}] = \int d^3r e_{\text{xc}}^{\text{GGA}}[n_{\uparrow}, n_{\downarrow}, \nabla n_{\uparrow}, \nabla n_{\downarrow}](\mathbf{r}). \quad (2.45)$$

Over the years many different **GGA** expressions have been developed. The aim of construction is to fulfill as many known constraints for E_{xc} as possible. An overview of important constraints can be found in Ref. 20. Additionally, in some expressions empirical parameters were introduced that can be fitted to experimental data or to a more accurate quantum mechanical calculation. Below we provide a list of a few **GGA** examples that are used in this work.

- The Becke exchange functional from 1988 (**B88**) contains one empirical parameter fitted to Hartree-Fock (**HF**) energy calculations.³⁹
- The Lee, Yang, and Parr correlation functional (**LYP**) contains four fitting parameters.⁴⁰ It is based on a correlation energy formula⁴¹ developed to improve **HF** and fitted to data for the He atom.
- The Perdew, Burke, and Ernzerhof exchange correlation functional (**PBE**) is a widely used **GGA** functional. It is completely non-empirical and only built on the basis of fulfilling known constraints.⁴²

LDA and GGA calculations work surprisingly well for many properties such as total energies and bond lengths of different material classes. The main reason is error cancellation: Neither the exchange nor the correlation potential expressions are good approximations to the exact exchange and correlation potentials. However, integrated properties like the energy are predicted with acceptable accuracy. The reason is that the xc energy approximations fulfill many constraints of the exact xc energy, *e.g.*, sum rules.²⁰ Deficiencies in the exchange and correlation functional cancel out.

To have an even more flexible framework to fulfill additional constraints the so-called meta-GGAs were developed.^{43,44} They include the Laplacian of the density or the kinetic energy density $\tau_\sigma = \frac{1}{2} \sum |\phi_{j\sigma}|^2$ as additional elements. However, for those meta-GGAs that depend on $\tau_\sigma[\{\phi_{i\sigma}\}]$ it is not straightforward to evaluate the functional derivative $\frac{\delta E}{\delta n}$ due to the orbital dependence of the xc energy functional. Strictly speaking such functionals are orbital functionals and are commonly treated in the GKS framework (*cf.* Sec. 4.1). Although meta-GGAs provide some improvements over ordinary GGAs they generally also do not correct the famous shortcomings of (semi-) local DFT that are:

- Lack of a discontinuity in the xc potential at integer particle numbers which can lead to fractionally charged dissociation fragments.³²
- Freedom from self-interaction error. However, some meta-GGAs partially cancel the self-interaction error.
- Wrong asymptotic behavior. Except for the B88 potential that falls off with $-\frac{\alpha}{r^2}$ the other xc potential approximations of this class decay exponentially for $r \rightarrow \infty$.

The consequences of these shortcomings are wrong dissociation properties (like fractionally charged fragments), wrong ionization properties (since $\epsilon_{\text{HOMO}} = -IP$ cannot be fulfilled) and the incorrect prediction of non-local properties such as CT. For the purpose of this work semi-local functionals are not suitable.

Orbital Functionals

Functionals of this group depend explicitly on the orbitals and only implicitly on the density (at least partly). In the KS scheme the xc potential (even of an orbital dependent functional) is defined as the multiplicative potential that is obtained via a functional derivative with respect to the density

$$v_{\text{xc},\sigma}[n_\uparrow, n_\downarrow](\mathbf{r}) = \frac{\delta E_{\text{xc}}[\{\phi_{j\sigma}[n_\sigma]\}]}{\delta n_\sigma(\mathbf{r})}. \quad (2.46)$$

Because the orbitals itself are functionals of the density $\phi_{j\sigma}[n_\sigma]$ the derivative is formally well defined. However, the density functional of the orbitals is

not known explicitly which makes an analytical evaluation of the derivative impossible. To circumvent this problem one can use a formalism that was originally introduced to construct a local potential for HF theory.^{45,46} Eq. (2.46) can be rewritten as an integral equation for $v_{xc,\sigma}$, the so-called optimized effective potential (OEP) equation.⁴⁷ The solution of this equation, the OEP, can only be obtained numerically by a computationally demanding procedure. However, various schemes exist that solve the OEP equation approximately, *e.g.*, the Krieger, Li, and Iafrate approximation.^{48,49}

One of the most important orbital functionals evaluated in KS theory with the OEP method (or one of its approximations) is the exact exchange (EXX) functional

$$E^{\text{EXX}}[\{\phi_{j\sigma,\text{KS}}[n_\sigma]\}] = -\frac{1}{2} \sum_{\sigma=\uparrow,\downarrow} \sum_{i,j=1}^{N_\sigma} \int d^3r \int d^3r' \frac{\phi_{i\sigma,\text{KS}}^*(\mathbf{r}) \phi_{j\sigma,\text{KS}}^*(\mathbf{r}') \phi_{j\sigma,\text{KS}}(\mathbf{r}) \phi_{i\sigma,\text{KS}}(\mathbf{r}')}{|\mathbf{r} - \mathbf{r}'|}. \quad (2.47)$$

This energy defines the exact exchange potential of KS theory

$$v^{\text{EXX(KS)}}[n_\uparrow, n_\downarrow](\mathbf{r}) = \frac{\delta E^{\text{EXX}}[\{\phi_{j\sigma}[n_\sigma]\}]}{\delta n_\sigma(\mathbf{r})}. \quad (2.48)$$

It cures many shortcomings of (semi-)local functionals since it has the correct asymptotic behavior, is self-interaction free according to Eq. (2.41), and contains a discontinuity at integer particle numbers. However, a serious drawback of using the EXX expression is the difficulty of finding a compatible correlation expression. Semi-local correlation functionals benefit from error cancellation with the corresponding semi-local exchange functional. For this reason, they are not adequate for a combination with the EXX functional.⁵⁰

In order to circumvent the problem of the incompatibility of EXX with semi-local correlation (to some extent), two functional classes have been developed that are in widespread use. The first class are called hybrid functionals which mix only a fraction of EXX with semi-local exchange and correlation. The second class only treats the long-range part of the electron-electron exchange exactly and uses semi-local functionals for the short-range part. Both approaches are usually not treated within the OEP approach (although it is possible) but as orbital specific potentials in the GKS framework. We will discuss these approaches in Sec. 4.2.

Another orbital functional concept, the so-called self-interaction correction (SIC), is based on the idea to correct the self-interaction error of standard functionals. A possible way of doing this, is subtracting the one-electron self-interaction error of each occupied orbital³⁵ from the approximate xc functional

$$E_{xc}^{\text{SIC}} = E_{xc}^{\text{approx}}[n_\uparrow, n_\downarrow] - \sum_{\sigma=\uparrow,\downarrow} \sum_j^{N_\sigma} \left(E_{\text{H}}[|\phi_{j\sigma}|^2] + E_{xc}^{\text{approx}}[|\phi_{j\sigma}|^2, 0] \right). \quad (2.49)$$

2.5. Exchange Correlation Functional Approximations

The orbital dependence of E_{xc}^{SIC} in fact causes a non-local density dependence. Furthermore, the potential that is obtained from an **OEP** procedure exhibits a discontinuity at integer particle numbers. However, Eq. (2.49) is not invariant under unitary orbital transformation of the occupied orbitals. Details on handling this issue and the performance for describing non-local properties with this functional concept can be found in Refs. 50–57.

Time-Dependent Density Functional Theory

In this chapter we set the **DFT** framework for calculating the excitation energies Ω_k of a finite electron system. We define the excited states as the solutions of the stationary many-body Schrödinger equation

$$\hat{H}\Psi_k = E_k\Psi_k \quad \text{and} \quad \Omega_k = E_k - E_0. \quad (3.1)$$

However, from the non-interacting **KS** equation we can only obtain the electronic ground state energy E_0 . The unoccupied orbital levels correspond to excitations of non-interacting **KS** particles that do not reflect the real excited states. In practice, we have to go beyond static **KS** theory in order to access the excitation energies of the real system although they are in principle accessible.²⁹ This extension of static **DFT** is called **TDDFT**. An overview of this field is given in Refs. [22,58–62](#).

3.1 Time-Dependent Kohn-Sham Equations

In this section we extend the framework of **DFT** to the time domain. The starting point is the time-dependent Schrödinger equation

$$i\frac{\partial}{\partial t}\Psi(t) = \hat{H}(t)\Psi(t) \quad (3.2)$$

that determines the time evolution of an interacting electron system which is in an initial state Ψ_0 at time t_0 . The time-dependent Hamiltonian $\hat{H}(t)$ is defined analogous to Eq. (2.2) with the only difference that the operator of the external potential is generally time-dependent

$$\hat{V} = \sum_{i=1}^N v(\mathbf{r}_i, t). \quad (3.3)$$

3.1. Time-Dependent Kohn-Sham Equations

Now and for the rest of this work we only consider situations where the system is in its ground state until t_0 . This is mostly the case in practical applications. The time-dependent external potential can then be written in the form

$$v(\mathbf{r}, t) = v_0(\mathbf{r}) + v_1(\mathbf{r}, t)\theta(t - t_0). \quad (3.4)$$

The foundation of **TDDFT** was laid by Runge and Gross⁶³ who proofed that a one-to-one correspondence between the time-dependent density $n(\mathbf{r}, t)$ and a Taylor-expandable $v(\mathbf{r}, t)$ (up to a purely time-dependent function) exists. Thus, due to the Runge-Gross theorem $\hat{H}(t)$ and $\Psi(t)$ as well as any physical observable $\hat{O}(t)$ can be expressed as a functional of the density. For practical applications of **TDDFT** we want to calculate the density $n(\mathbf{r}, t)$ of the real system – similar to the static theory – by solving a single particle time-dependent Schrödinger equation. Therefore, we need to map the interacting system to a non-interacting model system that can be described by a single Slater determinant $\Phi(t)$ and yields the same density. Due to the one-to-one correspondence in the Runge-Gross theorem the external potential of this model system is uniquely determined by this density. The existence of the potential (up to a purely time-dependent function) was proven by van Leeuwen.⁶⁴

Hence, we can introduce the time-dependent Kohn-Sham (**TD-KS**) equation that describes the non-interacting model system,

$$\left[-\frac{\nabla^2}{2} + v_{\text{KS},\sigma}(\mathbf{r}, t) \right] \phi_{j\sigma}(\mathbf{r}, t) = i \frac{\partial}{\partial t} \phi_{j\sigma}(\mathbf{r}, t), \quad (3.5)$$

where the **TD-KS** potential is defined as

$$v_{\text{KS},\sigma}(\mathbf{r}, t) = v(\mathbf{r}, t) + \int d^3r' \frac{n(\mathbf{r}', t)}{|\mathbf{r} - \mathbf{r}'|} + v_{\text{xc},\sigma}[\{n_\sigma\}](\mathbf{r}, t) \quad (3.6)$$

and the time-dependent density is

$$n(\mathbf{r}, t) = \sum_{\sigma=\uparrow,\downarrow} \sum_{j=1}^{N_\sigma} |\phi_{j\sigma}(\mathbf{r}, t)|^2. \quad (3.7)$$

Since the system is in its ground state at t_0 the initial condition is

$$\phi_{j\sigma}(\mathbf{r}, t_0) = \phi_{j\sigma}^0(\mathbf{r}), \quad (3.8)$$

where the $\{\phi_j^0\}$ are the orbitals obtained from static **KS** theory.

The time-dependent **xc** potential contains all exchange and correlation effects and is the only part of $v_{\text{KS}}(t)$ that has to be approximated in practice. Here, we introduced it as part of the **TD-KS** potential. In contrast to the static **KS** scheme $v_{\text{xc}}(t)$ cannot be defined as the functional derivative of an **xc** energy functional as for time-dependent systems no energy minimization principle exists. However, in order to systematically derive approximations

3. TIME-DEPENDENT DENSITY FUNCTIONAL THEORY

for $v_{\text{xc}}(t)$ it would be beneficial to have a functional that has $v_{\text{xc}}(t)$ as its functional derivative. Van Leeuwen⁶⁵ defined such a functional, the **xc** action functional \mathcal{A}_{xc} where

$$v_{\text{xc},\sigma}(\mathbf{r}, t) = \left. \frac{\delta \mathcal{A}_{\text{xc}}}{\delta n(\mathbf{r}, \tau)} \right|_{n=n_\sigma(\mathbf{r}, t)}. \quad (3.9)$$

This requires a generalization of the density space via the use of the Keldysh formalism and the introduction of the pseudo-time τ .^{60,65}

Note that the **TD-KS** equation remains valid if the system is not in its ground state at t_0 as assumed above (Eq. (3.4)). However, in this case $v_{\text{KS}}(t)$ and $v_{\text{xc}}(t)$ also become functionals of the initial many-body state Ψ_0 and the initial non-interacting state Φ_0 (apart from the dependence on the density).

3.2 Time Propagation

A practical scheme to solve the **TD-KS** equation involves several approximations. In order to obtain the initial orbitals ϕ_j^0 the static **KS** equations have to be solved numerically with a suitable approximation for v_{xc}^0 . Furthermore, we need an approximation for the time-dependent **xc** potential which we will refer to in Sec. 3.4. Apart from that we need a self-consistent scheme that solves the **TD-KS** equation and accounts for the time-dependence of the density. This will be discussed in the following.

In contrast to the static **KS** equation we have an additional self-consistency problem due to the time-dependence. The potential $v_{\text{KS},\sigma}[n](\mathbf{r}, t)$ depends on the density over the whole space and for all times $t' < t$. The problem can be addressed globally or via a step-by-step propagation in time. A global scheme is very involved because it requires the storage of the density for all times $t' < t$. The other less memory demanding scheme is far more common and will be addressed in the following.

The solution of Eq. (3.5) is given by applying the time evolution operator to the initial orbitals

$$\phi_{j\sigma}(t) = \hat{U}_\sigma(t, t_0) \phi_{j\sigma}(t_0), \quad (3.10)$$

where

$$\hat{U}_\sigma(t, t_0) = \hat{\mathcal{T}} \exp \left[-i \int_{t_0}^t dt' \hat{h}_{\text{KS},\sigma}(t') \right]. \quad (3.11)$$

$\hat{\mathcal{T}}$ is the time ordering operator and $\hat{h}_{\text{KS},\sigma}(t') = -\frac{\nabla^2}{2} + v_{\text{KS},\sigma}(\mathbf{r}, t')$. In order to do a step-by-step propagation we discretize the time in N_t steps $t_{i+1} = t_i + \Delta t$ with a step size of Δt and use

$$\hat{U}_\sigma(t, t_0) = \prod_{i=0}^{N_t-1} \hat{U}_\sigma(t_i + \Delta t, t_i), \quad (3.12)$$

where $t_{N_t} = t$. Now, the orbitals of each time step can be calculated from the previous time step by

$$\phi_{j,\sigma}(t_{i+1}) = \hat{U}_\sigma(t_i + \Delta t, t_i) \phi_{j,\sigma}(t_i). \quad (3.13)$$

If Δt is sufficiently small we can approximate $\hat{U}_\sigma(t_i + \Delta t, t_i)$. However, a straightforward approximation would require the knowledge of the Hamiltonian $\hat{h}_{\text{KS},\sigma}(t')$ (and related to that of the density at times t') up to time $t_i + \Delta t$. Unfortunately, at time t_i we only know the **KS** orbitals and the density for times $t' \leq t_i$. A summary of approximations that account for this difficulty can be found in Refs. 66,67.

The procedure above allows us to calculate the time-dependent density via Eq. (3.7). Thus, we have in principle access to any physical observable (based on the Runge-Gross theorem). As in static **DFT**, this is generally not a straightforward task in practice. Here we only want to discuss the moments of the density since they are explicitly known in terms of the density and can be used to calculate the excitation energies. For this purpose one has to prepare a time-dependent density that contains the required information. This is achieved by applying a boost excitation $v(\mathbf{r}, t) = v_0(\mathbf{r}) - \mathbf{r} \cdot \mathbf{k}_{\text{boost}} \delta(t - t_0)$ to the system that equally excites all frequencies. Thus, the initial orbitals of the system become⁵⁸

$$\phi_{j,\sigma}(\mathbf{r}, t_0^+) = \exp(i\mathbf{r} \cdot \mathbf{k}_{\text{boost}}) \phi_{j,\sigma}^0(\mathbf{r}). \quad (3.14)$$

After the boost the orbitals are propagated in time under the influence of the fixed ions (v_0). The frequently used time-dependent dipole moment

$$\mathbf{d}(t) = - \int d^3r \mathbf{r} n(\mathbf{r}, t) \quad (3.15)$$

filters the dipole-active excitations from the spectrum. From its Fourier transform $\tilde{\mathbf{d}}(\omega)$ we then calculate the positive definite dipole power spectrum

$$D(\omega) = \sum_{i=1}^3 |\tilde{d}_i(\omega)|^2 \quad (3.16)$$

whose peak positions indicate the excitation energies of the dipole-active states.⁶⁸⁻⁷¹ Dipole-forbidden excitation energies can be accessed by calculating higher moments of the density.^{70,71}

3.3 Linear Response

If we only want to determine the response of a system in its ground state to a small perturbation it is not necessary to solve the full **TD-KS** equation. In this section we describe the linear response formalism of **TDDFT** and demonstrate

3. TIME-DEPENDENT DENSITY FUNCTIONAL THEORY

that the linear response is sufficient to calculate the excitation spectrum which is one of the central tasks of this approach.

In the following we assume a weak time-dependent perturbation v_1 (*cf.* Eq. (3.4)) and Taylor-expand the density response in powers of v_1

$$n(\mathbf{r}, t) - n_0(\mathbf{r}) = n_1(\mathbf{r}, t) + n_2(\mathbf{r}, t) + n_3(\mathbf{r}, t) + \dots \quad (3.17)$$

The linear density response is given by

$$n_1(\mathbf{r}, t) = \int dt' \int d^3r' \chi(\mathbf{r}, t, \mathbf{r}', t') v_1(\mathbf{r}', t') \quad (3.18)$$

where χ is the time-dependent density response function. Its Fourier transform is given by²²

$$\chi(\mathbf{r}, \mathbf{r}', \omega) = \lim_{\eta \rightarrow 0^+} \sum_{k=1}^{\infty} \left[\frac{\langle \Psi_0 | \hat{n}(\mathbf{r}) | \Psi_k \rangle \langle \Psi_k | \hat{n}(\mathbf{r}') | \Psi_0 \rangle}{\omega - \Omega_k + i\eta} - \frac{\langle \Psi_k | \hat{n}(\mathbf{r}) | \Psi_0 \rangle \langle \Psi_0 | \hat{n}(\mathbf{r}') | \Psi_k \rangle}{\omega + \Omega_k + i\eta} \right] \quad (3.19)$$

with the eigenstates $\{\Psi_k\}$ and excitation energies $\Omega_k = (E_k - E_0)$ of the interacting system. Hence, the poles of χ are the excitation energies that we want to calculate with **TDDFT**. By means of the **TD-KS** equation (Eq. (3.5)) we can relate χ to the response function of the non-interacting **KS** system

$$\chi_{\text{KS}}(\mathbf{r}, \mathbf{r}', \omega) = 2 \lim_{\eta \rightarrow 0^+} \sum_{i,a} \left[\frac{\xi_{ia}(\mathbf{r}) \xi_{ia}^*(\mathbf{r}')}{\omega - (\epsilon_a - \epsilon_i) + i\eta} - \frac{\xi_{ia}^*(\mathbf{r}) \xi_{ia}(\mathbf{r}')}{\omega + (\epsilon_a - \epsilon_i) + i\eta} \right] \quad (3.20)$$

where $\xi_{ia}(\mathbf{r}) = \phi_i^*(\mathbf{r})\phi_a(\mathbf{r})$, ϕ_i are occupied and ϕ_a are unoccupied ground state **KS** orbitals (here and in the following indices i, i' label occupied and a, a' unoccupied orbitals). All ingredients of χ_{KS} are known from a ground state **KS** calculation. The relation to χ of the interacting system is

$$\chi(\mathbf{r}, \mathbf{r}', \omega) = \chi_{\text{KS}}(\mathbf{r}, \mathbf{r}', \omega) + \int d^3r_1 \int d^3r_2 \chi_{\text{KS}}(\mathbf{r}, \mathbf{r}', \omega) \left[\frac{1}{|\mathbf{r}_1 - \mathbf{r}_2|} + f_{\text{xc}}(\mathbf{r}_1, \mathbf{r}_2, \omega) \right] \chi(\mathbf{r}, \mathbf{r}', \omega). \quad (3.21)$$

In this equation f_{xc} is the Fourier transform of the **xc** kernel which is the functional derivative of v_{xc} with respect to the density

$$f_{\text{xc}}(\mathbf{r}, \mathbf{r}', t - t') = \left. \frac{\delta v_{\text{xc}}[n](\mathbf{r}, t)}{\delta n(\mathbf{r}', t')} \right|_{n_0(\mathbf{r})}. \quad (3.22)$$

Thus, $f_{\text{xc}} + \frac{1}{|\mathbf{r}_1 - \mathbf{r}_2|}$ shifts the poles of χ_{KS} (the **KS** transition energies $\epsilon_a - \epsilon_i$) towards the poles of χ (the real excitation energies Ω_k). Calculating the $\{\Omega_k\}$'s in practice is achieved by solving the eigenvalue problem^{72,73}

$$\begin{pmatrix} \mathbb{A} & \mathbb{B} \\ \mathbb{B}^* & \mathbb{A}^* \end{pmatrix} \begin{pmatrix} \mathbf{X} \\ \mathbf{Y} \end{pmatrix} = \Omega \begin{pmatrix} \mathbb{I} & 0 \\ 0 & -\mathbb{I} \end{pmatrix} \begin{pmatrix} \mathbf{X} \\ \mathbf{Y} \end{pmatrix} \quad (3.23)$$

with the matrix elements

$$(\mathbb{A})_{ia,i'a'} = \delta_{ii'}\delta_{aa'}(\epsilon_a - \epsilon_i) + (ia|i'a') + (ia|f_{xc}|i'a') \quad (3.24)$$

$$(\mathbb{B})_{ia,i'a'} = (ia|a'i') + (ia|f_{xc}|a'i') \quad (3.25)$$

and the two-electron integrals

$$(ia|i'a') = \int d^3r \int d^3r' \frac{\xi_{ia}(\mathbf{r})\xi_{i'a'}^*(\mathbf{r}')}{|\mathbf{r} - \mathbf{r}'|} \quad (3.26)$$

$$(ia|f_{xc}|i'a') = \int d^3r \int d^3r' \xi_{ia}(\mathbf{r})f_{xc}(\mathbf{r}, \mathbf{r}', \omega)\xi_{i'a'}^*(\mathbf{r}'). \quad (3.27)$$

Eq. (3.23) is known as the Casida equation. A more compact form of this equation can be found if one assumes that the KS orbitals are real and f_{xc} is frequency independent (then, \mathbb{A} and \mathbb{B} are real)

$$\mathbb{C}\mathbf{Z} = \Omega^2\mathbf{Z} \quad (3.28)$$

with

$$\begin{aligned} \mathbb{C} &= (\mathbb{A} - \mathbb{B})^{(1/2)} (\mathbb{A} + \mathbb{B}) (\mathbb{A} - \mathbb{B})^{(1/2)} \\ (\mathbb{C})_{ia,i'a'} &= \delta_{ii'}\delta_{aa'}(\epsilon_a - \epsilon_i)^2 + 4\sqrt{(\epsilon_a - \epsilon_i)(\epsilon_{a'} - \epsilon_{i'})} [(ia|i'a') + (ia|f_{xc}|i'a')] \end{aligned} \quad (3.29)$$

and

$$\mathbf{Z} = (\mathbb{A} - \mathbb{B})^{(1/2)} (\mathbf{X} - \mathbf{Y}). \quad (3.30)$$

The transition density (or eigenmode) for each excitation energy (eigenvalue) Ω_k is given by

$$n_{1(k)}(\mathbf{r}) = \sum_{ia} \left[\xi_{ia}^*(\mathbf{r}) X_{ia(k)} + \xi_{ia}(\mathbf{r}) Y_{ia(k)} \right]. \quad (3.31)$$

It can be used to visualize the density changes for the excited state k . The oscillator strengths are given by

$$f_{(k)} = \frac{2}{3} \sum_{m=1}^3 \left| \mathbf{R}_m^T (\mathbb{A} - \mathbb{B})^{1/2} \mathbf{Z}_{(k)} \right|^2 \quad (3.32)$$

where

$$(\mathbf{R}_m)_{ia} = \int d^3r r_m \xi_{ia}(\mathbf{r}). \quad (3.33)$$

In practice efficient schemes exist that only determine a few of the lowest excitation energies since only those are usually of interest. In contrast to the dipole power spectrum of Sec. 3.2, linear response TDDFT also includes dipole-forbidden excitations. However, the disadvantageous aspects of the approach are the effort to analytically derive the xc kernel instead of only the xc potential and the restriction to the linear response regime only. Consequently, non-linear effects as caused, *e.g.*, by the application of strong external fields, cannot be extracted from the Casida equation.

3.4 Adiabatic Approximation

So far we have not discussed what the density dependence of $v_{\text{xc}}[n](\mathbf{r}, t)$ implies. In contrast to the static **KS** formalism v_{xc} (and thus v_{KS}) does not only depend on the density $n(\mathbf{r}', t')$ at all points in space \mathbf{r}' but also on all points in time $t_0 < t' < t$. Hence, besides the non-locality in space the **xc** potential has a non-local dependence on the density in time. All effects that are related to this history dependence are called memory effects.

In practice it is very difficult to find approximations for v_{xc} that take the history dependence into account. The most common approximations only depend on the instantaneous density, *i.e.*, they ignore the history dependence completely. In this so-called adiabatic approximation the **xc** potential is the instantaneous ground state potential evaluated with the time-dependent density

$$v_{\text{xc}}^{\text{A}}[n](\mathbf{r}, t) = v_{\text{xc}}^0[n_0] \Big|_{n_0 \rightarrow n(\mathbf{r}, t)} . \quad (3.34)$$

This drastic approximation is similar to the **LDA** approximation of ground state **KS** theory which ignores the spatial non-locality completely. In the limit of a slowly varying density the adiabatic approximation is exact. Surprisingly, in practice it works well for many situations and can even be reliable when the density changes rapidly in time.⁷⁴ Besides the low computational cost another advantage is that via Eq. (3.34) any ground state functional has its adiabatic counterpart. Thus, it provides a large range of already available approximations for **TDDFT**.

A consequence of the approximation for linear response calculations is that the **xc** kernel is local in time

$$f_{\text{xc}}^{\text{A}}(\mathbf{r}, \mathbf{r}', t - t') = \frac{\delta v_{\text{xc}}^0[n_0](\mathbf{r})}{\delta n_0(\mathbf{r}')} \delta(t - t') = \frac{\delta E_{\text{xc}}^0[n_0]}{\delta n_0(\mathbf{r}') \delta n_0(\mathbf{r})} \delta(t - t') \quad (3.35)$$

and therefore, that its Fourier transform is frequency independent.

Note that all thoughts above assumed explicit density functionals. If we use orbital dependent functionals in the adiabatic approximation we effectively gain a history dependent functional since the time-dependent orbitals $\phi_i(t)$ depend on the density $n(t')$ at all prior times t' . Thus, by using orbital dependent functionals one can at least partly include memory effects.⁵⁰

3.5 Zero-Force Theorem

In this section we introduce the zero-force theorem, one of the most important known conditions for the time-dependent **xc** potential in **TDDFT**. As demonstrated in **Pub. 4** and Sec. 6.2 this theorem has important consequences for **xc** potential approximations that are constructed directly without a corresponding action functional (or energy functional in the case of the adiabatic approximation).

The center of mass coordinate $\mathbf{R}(t)$ of a many-electron system satisfies Newton's third law

$$\ddot{\mathbf{R}}(t) = \frac{d^2}{dt^2} \int d^3r \mathbf{r} n(\mathbf{r}, t) = - \int d^3r n(\mathbf{r}, t) \nabla v(\mathbf{r}, t). \quad (3.36)$$

Eq. (3.36) can be derived using the quantum mechanical equation of motion.⁷⁵ Analogously, one can derive an equation for the non-interacting **KS** system with the center of mass coordinate $\mathbf{R}_{\text{KS}}(t)$ subjected to v_{KS} . Since the **KS** system reproduces the same density it follows that $\mathbf{R}(t) = \mathbf{R}_{\text{KS}}(t)$ and we obtain

$$0 = \ddot{\mathbf{R}}(t) - \ddot{\mathbf{R}}_{\text{KS}}(t) = - \int d^3r n(\mathbf{r}, t) [\nabla v(\mathbf{r}, t) - \nabla v_{\text{KS}}(\mathbf{r}, t)]. \quad (3.37)$$

Inserting the **KS** potential from Eq. (3.6) we arrive at the so-called *zero-force theorem*

$$0 = \int d^3r n(\mathbf{r}, t) \nabla v_{\text{xc}}(\mathbf{r}, t). \quad (3.38)$$

because the Hartree potential explicitly satisfies the above equation.²²

The theorem can also be deduced from the “generalized translational invariance” of the **xc** action functional:⁷⁶ A transformation $\mathbf{r} = \mathbf{r}' + \mathbf{x}(t)$ with an arbitrary time-dependent function \mathbf{x} results in the transformed density $n'(\mathbf{r}', t) = n(\mathbf{r} + \mathbf{x}(t), t)$. The **xc** action functional is invariant under this transformation ($A_{\text{xc}}[n'] = A_{\text{xc}}[n]$) and the **xc** potential has to fulfill

$$v_{\text{xc}}[n'](\mathbf{r}', t) = v_{\text{xc}}[n](\mathbf{r} + \mathbf{x}(t), t). \quad (3.39)$$

If an approximation for the action functional is generalized translationally invariant, then its corresponding potential obeys the zero-force theorem.⁷⁶ In other words, an **xc** potential that is a functional derivative and fulfills Eq. (3.39) also fulfills the zero force theorem.⁷⁷

The theorem also translates to linear response theory as a condition for the **xc** kernel^{75,78}

$$\int d^3r' f_{\text{xc}}(\mathbf{r}, \mathbf{r}', \omega) \nabla' n_0(\mathbf{r}') = \nabla v_{\text{xc}}^0(\mathbf{r}) \quad (3.40)$$

or equally

$$\int d^3r \int d^3r' n_0(\mathbf{r}) n_0(\mathbf{r}') \nabla' f_{\text{xc}}(\mathbf{r}, \mathbf{r}', \omega) = 0 \quad (3.41)$$

where the subscript “0” indicates ground state quantities. Note that the frequency dependence of the kernel has to be such that it averages out in the integration of the left hand side of Eq. (3.40).²²

Generalized Kohn-Sham Scheme

In Sec. 2.2 we introduced one possible realization of DFT which is in principle exact – the KS scheme. In the following we go beyond KS DFT and present the generalized Kohn-Sham (GKS) scheme, a framework for many other in principle exact realizations of DFT. The scheme provides more flexibility for finding new approximate approaches that are of great importance for present-day application of DFT and also for this work. However, this flexibility comes at the cost of losing some of the formal properties of KS DFT.

4.1 The Generalized Kohn-Sham Scheme in Static DFT

The basis of the KS scheme is the mapping of the real interacting electron system into a system of non-interacting auxiliary KS particles. On the basis of Ref. 79 we now present a generalization of this scheme, the so-called GKS scheme. In the GKS scheme one is mapping the interacting system into a model system that is partially interacting but can still be described by a single Slater determinant. This means that part of the electron-electron interaction is taken into account and at the same time a computationally favorable description with a single-particle Schrödinger equation is possible. The scheme includes the standard KS scheme as a special case.

In KS theory the universal functional $F[n]$ is divided into three parts

$$F[n] = T_{\text{ni}}[n] + U_{\text{H}}[n] + E_{\text{xc}}[n], \quad (4.1)$$

where the last term on the right side is the unknown functional $E_{\text{xc}}[n]$ to be approximated. In GKS theory $F[n]$ is divided into

$$F[n] = F_{\text{S}}[n] + R_{\text{S}}[n] \quad (4.2)$$

where F_{S} is a known functional and R_{S} is the unknown remainder density functional. The density functional F_{S} is obtained by the definition of a Slater

determinant dependent functional S

$$F_S = \min_{\Phi \rightarrow n} S[\Phi] = \min_{\{\phi_i\} \rightarrow n} S[\{\phi_i\}] \quad (4.3)$$

where $\{\phi_i\}$ are the orbitals that form the Slater determinant Φ . The crux of this setup is that different choices for S are possible. Each choice defines a new realization of the **GKS** scheme with a different remainder functional $R_S[n]$. The ground state density is obtained by the minimization of the total energy

$$E_0 = \min_n E[n] = \min_n \left(F_S[n] + R_S[n] + \int d^3r n(\mathbf{r}) v(\mathbf{r}) \right) \quad (4.4)$$

$$= \min_{\{\phi_i\} \rightarrow n} \left(S[\{\phi_i\}] + R_S[n[\{\phi_i\}]] + \int d^3r n([\{\phi_i\}], \mathbf{r}) v(\mathbf{r}) \right). \quad (4.5)$$

A Lagrange procedure leads to single orbital equations of the form

$$\left(\hat{O}_{S,j}[\{\phi_i\}] + v_{R_S} + v \right) \phi_j = \epsilon_j \phi_j \quad \text{with } j = 1, \dots, N, \quad (4.6)$$

the so-called **GKS** equations, where $\hat{O}_{S,j}[\{\phi_i\}]$ is an orbital dependent non-local operator defined by

$$\frac{\delta S[\{\phi_i\}]}{\delta \phi_j^*} = \hat{O}_{S,j}[\{\phi_i\}] \phi_j \quad (4.7)$$

and

$$v_{R_S}(\mathbf{r}) = \frac{\delta R_S[n]}{\delta n(\mathbf{r})} \quad (4.8)$$

is the remainder potential. F_S and R_S as well as $\hat{O}_{S,j}[\{\phi_i\}]$ and v_{R_S} are universal. They only depend on the choice of S but not on the external potential v . Solving Eq. (4.6) self-consistently will yield a set of orbitals, the **GKS** orbitals, that form the exact ground state density of the interacting electron system.

Below we want to further elucidate the **GKS** scheme by looking at two example realizations (a) and (b) defined by two different choices for $S[\Phi]$.

(a) In the first case S is chosen to be the kinetic energy of a Slater determinant.

$$S[\Phi] = \langle \Phi | \hat{T} | \Phi \rangle \quad (4.9)$$

The resulting energy functional F_S is equal to the non-interacting kinetic energy functional T_{ni} and we obtain the standard **KS** scheme with

$$R_S[n] = U_{\text{H}}[n] + E_{\text{x}}[n] + E_{\text{c}}[n]. \quad (4.10)$$

Eq. (4.6) reduces to the standard **KS** equation with

$$\hat{O}_S[\{\phi_i\}] = -\frac{\nabla^2}{2}. \quad (4.11)$$

- (b) In the second case we choose S as the sum of kinetic energy and electron-electron interaction energy evaluated with a Slater determinant

$$S[\Phi] = \langle \Phi | \hat{T} + \hat{U} | \Phi \rangle . \quad (4.12)$$

The resulting \hat{O}_S is the sum of single particle kinetic energy and the HF operator. Thus, due to the unknown remainder potential the GKS equations for this case are a formally exact alteration of the HF equations

$$\begin{aligned} & \left[-\frac{1}{2}\nabla^2 + v(\mathbf{r}) + \int d^3r' \frac{n(\mathbf{r}')}{|\mathbf{r} - \mathbf{r}'|} + v_{R_S}(\mathbf{r}) \right] \phi_j(\mathbf{r}) \\ & - \int d^3r' \sum_{i=1}^N \frac{\phi_i^*(\mathbf{r}')\phi_i(\mathbf{r})}{|\mathbf{r} - \mathbf{r}'|} \phi_j(\mathbf{r}') = \epsilon_j \phi_j(\mathbf{r}) \quad \text{with } j = 1, \dots, N \end{aligned} \quad (4.13)$$

with

$$\begin{aligned} \hat{O}_{S,j}[\{\phi_i\}] &= -\frac{1}{2}\nabla^2 + \int d^3r' \frac{n(\mathbf{r}')}{|\mathbf{r} - \mathbf{r}'|} + \hat{v}_j^{\text{Fock}}[\{\phi_i\}] \\ \hat{v}_j^{\text{Fock}}[\{\phi_i\}] &= -\frac{1}{\phi_j(\mathbf{r})} \int d^3r' \sum_{i=1}^N \frac{\phi_i^*(\mathbf{r}')\phi_i(\mathbf{r})}{|\mathbf{r} - \mathbf{r}'|} \phi_j(\mathbf{r}') . \end{aligned} \quad (4.14)$$

The scheme is known as the so-called Hartree-Fock Kohn-Sham (HF-KS) scheme.^{18,79}

Comparing the standard KS equation (Eq. (2.15)) with the GKS equation (Eq. (4.6)) reveals a prominent difference between both DFT approaches. Whereas the former scheme leads to single particle equations with a local multiplicative potential, the latter generally leads to equations that contain non-local potentials (orbital specific integral operators) and thus, reflect the interaction that is present in the GKS model system. One example is the operator of Eq. (4.14).

4.2 Approximations

From the previous section we already know that the standard KS scheme is a special case of the GKS scheme. Thus, all the approximations of Sec. 2.5 can be seen as approximations for $R_S[n]$ for the choice $S[\Phi] = \langle \Phi | \hat{T} | \Phi \rangle$. However, in this section we want to discuss choices for $S[\Phi]$ and compatible approximations for $R_S[n]$ that go beyond the framework of KS theory. The GKS scheme provides an alternative to the OEP approach to treat orbital functionals in DFT. The advantage is that the required orbital specific potential can always be derived in analytic form in contrast to the xc potential of OEP. However, some concepts of KS theory are no longer valid such as the strict definition of the derivative discontinuity.

All the following approximations have one common ingredient. They include in some way part or all of the EXX energy expression of Eq. (2.25).

Exact Exchange – Hartree Fock

As discussed in the previous section, for the choice $S[\Phi] = \langle \Phi | \hat{T} + \hat{U} | \Phi \rangle$ and $R_S[n] = 0$ we obtain the HF equations. HF is the analog to an exact exchange calculation in KS theory (EXX-OEP). The energy expressions of both HF and EXX-OEP are identical. Nevertheless, they can lead to different energy values (although usually very similar). The reason is that the former is evaluated with HF orbitals that arise from a non-local orbital specific potential, whereas the latter is evaluated with KS orbitals that arise from the multiplicative and local OEP. Hence, the exact (unknown) remainder functional $R_S[n]$ that contains all the correlation effects must be different from E_c in KS theory although the energy expressions are formally the same

$$R_S[n] = \langle \Psi | \hat{F} | \Psi \rangle - \langle \Phi_{\text{GKS}}^{\text{HF}} | \hat{T} | \Phi_{\text{GKS}}^{\text{HF}} \rangle - \langle \Phi_{\text{GKS}}^{\text{HF}} | \hat{U} | \Phi_{\text{GKS}}^{\text{HF}} \rangle \quad (4.15)$$

$$E_c[n] = \langle \Psi | \hat{F} | \Psi \rangle - \langle \Phi_{\text{KS}}^{\text{OEP}} | \hat{T} | \Phi_{\text{KS}}^{\text{OEP}} \rangle - \langle \Phi_{\text{KS}}^{\text{OEP}} | \hat{U} | \Phi_{\text{KS}}^{\text{OEP}} \rangle . \quad (4.16)$$

However, finding a suitable correlation remainder functional for HF is as difficult as for EXX in KS theory. Note that due to the small difference between the EXX-OEP and the EXX-HF energy the definition of exchange in DFT and HF-based quantum chemistry methods is slightly different. Since we obtain the HF energy from an unconstrained minimization with respect to the orbitals and the OEP energy with the constraint of generating a local potential we can state $E^{\text{HF}} \leq E^{\text{EXX-OEP}}$. We further elaborate on differences between EXX-OEP and EXX-HF in Sec. 4.4.

Hybrid Functionals

In a hybrid functional one part of the exchange interaction is treated exactly and the rest with a semi-local expression.⁸⁰ The functional is complemented with a suitable semi-local correlation functional and has the general form

$$\begin{aligned} S[\Phi] &= \langle \Phi | \hat{T} + a\hat{U} | \Phi \rangle \\ R_S[n] &= (1 - a) \left(U_{\text{H}}[n] + E_{\text{x}}^{\text{sl}}[n] \right) + E_{\text{c}}^{\text{sl}}[n] \end{aligned} \quad (4.17)$$

Note that the (rarely used) analogous xc functional of KS theory

$$E_{\text{xc}}^{\text{hybrid}}[n] = aE^{\text{EXX}}[n] + (1 - a)E_{\text{x}}^{\text{sl}}[n] + E_{\text{c}}^{\text{sl}}[n] \quad (4.18)$$

would lead to different results⁸¹ for the same reasons as explained above. The semi-local approximations $E_{\text{x}}^{\text{sl}}[n]$ and $E_{\text{c}}^{\text{sl}}[n]$ of Eq. (4.17) are usually taken from KS theory, although the exact exchange and correlation contributions to the exact hybrid remainder potential would be different from KS theory. Also note that the Hartree energy is partially included in S and partially included in R_S . However, nothing would change if we would include it only in S or only in R_S since the corresponding potential v_{H} is multiplicative in both cases.

The parameter a is typically in the range of 0.2–0.25 and was first deduced from empirical fitting and later $a = 0.25$ was confirmed from theoretical argumentation.⁸² The most often used hybrid approach is the **B3LYP** functional,⁸³ which is also the most frequently used approximation of **DFT** in general. It accounts for 80% of all **DFT** calculations according to an analysis of functional names in titles and abstracts of the ISI Web of Science.⁸⁴ **B3LYP** is defined as

$$\begin{aligned}
 S[\Phi] &= \langle \Phi | \hat{T} + a\hat{U} | \Phi \rangle \\
 R_S[n] &= (1 - a) \left(U_H[n] + E_x^{\text{LDA}}[n] \right) + a_x \left(E_x^{\text{B88}}[n] - E_x^{\text{LDA}}[n] \right) \\
 &\quad + a_c E_c^{\text{LYP}}[n] + (1 - a_c) E_c^{\text{LDA}}[n].
 \end{aligned} \tag{4.19}$$

It contains three parameters ($a = 0.2$, $a_x = 0.72$, $a_c = 0.81$) that are fitted to experimental atomization energies, ionization potentials, proton affinities, and total atomic energies.⁸⁵ It is a pragmatically constructed functional that has a good average performance for many thermochemical properties of many different systems.⁸⁴

Another commonly used hybrid approach is the **PBE0** functional. It combines 25% **EXX** with an correspondingly adjusted **PBE** functional and is free of empirical parameters.^{82,86}

Due to the mixing with **EXX**, hybrid functionals reduce the self-interaction error and improve the asymptotic behavior to $\xrightarrow[r \rightarrow \infty]{} -\frac{a}{r}$. However, these corrections are not sufficient for a reliable description of non-local properties such as **CT** excitations. Nevertheless, they are generally an improvement over standard semi-local **KS** approximations.

Range-Separated Hybrid Functionals

Finding a functional expression that is able to overcome the incompatibility between semi-local correlation functionals and **EXX** is the main motivation for the **RSH** functional approach. The basic idea is to split the electron-electron interaction into a short-range and a long-range part^{87,88}

$$\frac{1}{|\mathbf{r} - \mathbf{r}'|} = \underbrace{\frac{1 - u(\gamma|\mathbf{r} - \mathbf{r}'|)}{|\mathbf{r} - \mathbf{r}'|}}_{\text{short-range}} + \underbrace{\frac{u(\gamma|\mathbf{r} - \mathbf{r}'|)}{|\mathbf{r} - \mathbf{r}'|}}_{\text{long-range}}, \tag{4.20}$$

where

$$u(\gamma r) \xrightarrow[\gamma r \rightarrow 0]{} 0 \quad \text{and} \quad u(\gamma r) \xrightarrow[\gamma r \rightarrow \infty]{} 1, \tag{4.21}$$

and treat both ranges with different functional approximations. Here, we only consider one specific splitting scheme: The short-range (short electron-electron distances) is evaluated with a semi-local exchange functional and the long-range (large electron-electron distances) is treated exactly. Electron correlation is described by a semi-local functional without applying a splitting scheme. The

approach uses standard semi-local **DFT** for small electron-electron distances and therefore incorporates the important error cancellation between exchange and correlation of semi-local **DFT**. At the same time it contains important properties of exact exchange like the correct $-\frac{1}{r}$ asymptotic behavior for large electron-electron distances where they are particularly important. Therefore, it is an ideal candidate for a functional that can be used for the calculation of thermochemical properties as well as non-local properties such as **CT**. However, some of the properties of **EXX** are no longer captured to the full extent like the one-electron self-interaction correction which is only included in the long-range part.

The general form of an **RSH** functional in the **GKS** scheme is given by

$$\begin{aligned} S[\Phi] &= \langle \Phi | \hat{T} | \Phi \rangle + U_{\text{H}}[\{\phi_{j,\sigma}\}] + E_{\text{x,LR}}^{\text{EXX}}[\{\phi_{j,\sigma}\}] \\ R_{\text{S}}[n] &= E_{\text{x,SR}}^{\text{sl}}[n] + E_{\text{c}}^{\text{sl}}[n] \end{aligned} \quad (4.22)$$

with

$$\begin{aligned} E_{\text{x,LR}}^{\text{EXX}}[\{\phi_{j,\sigma}\}] &= -\frac{1}{2} \sum_{\sigma=\uparrow,\downarrow} \sum_{i,j=1}^{N_{\sigma}} \int d^3r \int d^3r' \\ &\times \frac{u(\gamma|\mathbf{r}-\mathbf{r}'|)}{|\mathbf{r}-\mathbf{r}'|} \phi_{i\sigma}^*(\mathbf{r}) \phi_{j\sigma}^*(\mathbf{r}') \phi_{j\sigma}(\mathbf{r}) \phi_{i\sigma}(\mathbf{r}'). \end{aligned} \quad (4.23)$$

The screening function u could be any function fulfilling Eq. (4.21), *e.g.*,

$$u(\gamma r) = \begin{cases} \text{erf}(\gamma r) \\ 1 - \exp(-\gamma r) \end{cases}. \quad (4.24)$$

A common choice for u is the error-function as it facilitates the evaluation of the two-electron integrals in Gaussian-type basis set codes. The splitting for this case is illustrated in Fig. 4.1.

For the correlation part in Eq. (4.22) a standard functional approximation can be used, whereas the semi-local short-range functional $E_{\text{x,SR}}^{\text{sl}}[n]$ has to be redesigned in order to reflect the screened interaction (first term on the right hand side of Eq. (4.20)).^{87,89–91} The crucial ingredient of the functional is the so-called range-separation parameter γ . Its inverse determines the separation length between short- and long-range. For $|\mathbf{r}-\mathbf{r}'| < 0.5\gamma^{-1}$ the first term and for $|\mathbf{r}-\mathbf{r}'| > 0.5\gamma^{-1}$ the second term on the right hand side of Eq. (4.20) dominates (if the error function is used for u). The parameter can be either determined empirically^{92–96} or by a non-empirical fitting procedure^{97,98} (*cf.* Sec. 5.2 and **Pub. 2**). Over the years a couple of different **RSH** functionals have been developed.^{90,91,95,99} They mostly differ in the functional that is used for the correlation and the short-range exchange. Some functionals use a hybrid functional for the short-range exchange instead of an ordinary semi-local functional.^{92,96} In Fig. 4.2 we illustrate the difference between standard **RSH** and standard hybrid functionals.

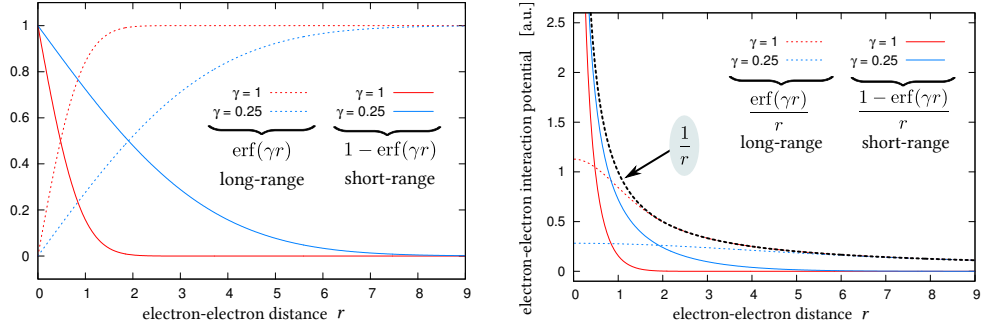


Figure 4.1. *Left:* Splitting function $u(\gamma r) = \text{erf}(\gamma r)$ as a function of electron-electron distance $r = |\mathbf{r} - \mathbf{r}'|$ for two different γ values. In comparison we show $1 - u(\gamma r)$. *Right:* Long- and short-range electron-electron interaction potential for $u(\gamma r) = \text{erf}(\gamma r)$ and two different γ values.

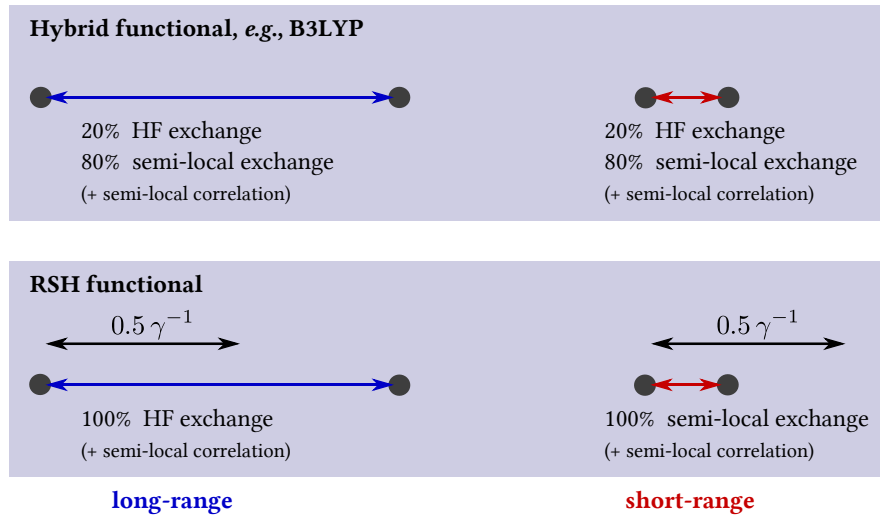


Figure 4.2. Schematic illustration of the exchange contributions for standard RSH and standard hybrid functionals. The left side illustrates large ($|\mathbf{r} - \mathbf{r}'| \gg 0.5\gamma^{-1}$) and the right side very small ($|\mathbf{r} - \mathbf{r}'| \ll 0.5\gamma^{-1}$) electron-electron distances.

The two **RSH** functionals that we apply in this work are the Baer, Neuhauser, Livshits (**BNL**)^{94,99} functional and the **RSH** functional of Scuseria and co-workers (ω **PBE**)⁹¹. The former combines short-range **LDA**⁸⁹ with **LYP** correlation and the latter combines short-range **PBE**⁹¹ with **PBE** correlation.

As already mentioned, **RSH** functionals are not completely one-electron self-interaction-free. However, they are approximately many-electron self-interaction-free since the total energy as a function of fractional particle number is nearly a straight line and shows the correct derivative discontinuity in the total energy.^{98,100–104} Note that **RSH** functionals can in principle be also implemented in the **KS-OEP** framework. The performance of such an approach has to be investigated in future work.

4.3 The Generalized Kohn-Sham Scheme in TDDFT

Similarly to ground state **DFT** one can also introduce a time-dependent variant of the **GKS** scheme (Sec. 4.1) in **TDDFT**. If we use the adiabatic approximation we obtain time-dependent versions of the non-local potential operator \hat{O} and the multiplicative remainder potential v_{R_S} via

$$\begin{aligned}\hat{O}_{S,j}[\{\phi_i\}](\mathbf{r}, t) &= \hat{O}_S^0[\{\phi_i^0\}] \Big|_{\{\phi_i^0\} \rightarrow \{\phi_i(\mathbf{r}, t)\}} \\ v_{R_S}[n](\mathbf{r}, t) &= v_{R_S}^0[n_0] \Big|_{n_0 \rightarrow n(\mathbf{r}, t)} .\end{aligned}\tag{4.25}$$

Using these potentials in combination with the external potential as the effective potential for the **GKS** particles we arrive at the time-dependent generalized Kohn-Sham (**TD-GKS**) equations

$$\begin{aligned}\left(\hat{O}_{S,j}[\{\phi_i\}](\mathbf{r}, t) + v_{R_S,\sigma}(\mathbf{r}, t) + v(\mathbf{r}, t)\right) \phi_{j\sigma}(\mathbf{r}, t) &= i \frac{\partial}{\partial t} \phi_{j\sigma}(\mathbf{r}, t) \\ &\text{with } j = 1, \dots, N .\end{aligned}\tag{4.26}$$

Whereas the **TD-KS** equation is justified by the theorems of Runge and Gross⁶³ and van Leeuwen⁶⁴, the **TD-GKS** equation is not covered by these theorems. Although the mapping to a different interacting system is included, the theorems are based on the one-to-one correspondence between the density and *one* unique potential. This is in conflict with the orbital specific potential operator of Eq. (4.26) that is different for each orbital. An extension of the foundations of **TDDFT** to include the **TD-GKS** scheme is still matter of research. However, if the only non-local ingredient of \hat{S} is the Fock operator, the Runge-Gross theorem is still sound and legitimates the use of the time-dependent **GKS** equations.^{97,98} The **GKS** scheme is extensively used in **TDDFT** calculations, especially the adiabatic version of hybrid functionals such as **B3LYP**.

To obtain a linear response formalism for the frequently used hybrid and **RSH** functionals one can use **HF** theory. The time-dependent **HF** equations

are derived from the time-dependent Schrödinger equation using the **HF** assumption that the time-dependent wave function can be written as a Slater determinant of time-dependent orbitals. The excitation energies in **HF** approximation can be obtained via a linear response formalism similar to the one of **TDDFT**.⁵⁹ The combination of both schemes yields the **GKS** linear response equations for hybrid and **RSH** functionals (*cf.* Eq. (3.23))

$$\begin{pmatrix} \mathbb{A} & \mathbb{B} \\ \mathbb{B}^* & \mathbb{A}^* \end{pmatrix} \begin{pmatrix} \mathbf{X} \\ \mathbf{Y} \end{pmatrix} = \Omega \begin{pmatrix} \mathbb{I} & 0 \\ 0 & -\mathbb{I} \end{pmatrix} \begin{pmatrix} \mathbf{X} \\ \mathbf{Y} \end{pmatrix} \quad (4.27)$$

where

$$(\mathbb{A})_{ia,i'a'} = \delta_{ii'}\delta_{aa'}(\epsilon_a - \epsilon_i) + (ia|i'a') - (ii'|\eta|aa') + (ia|\tilde{f}_{xc}|i'a') \quad (4.28)$$

$$(\mathbb{B})_{ia,i'a'} = (ia|a'i') - (ia'|\eta|ai') + (ia|\tilde{f}_{xc}|a'i') \quad (4.29)$$

are the matrix elements with the interaction

$$\eta(\mathbf{r} - \mathbf{r}') = \begin{cases} a \frac{1}{|\mathbf{r} - \mathbf{r}'|} & \text{hybrid functional} \\ \frac{\omega(\gamma|\mathbf{r} - \mathbf{r}'|)}{|\mathbf{r} - \mathbf{r}'|} & \text{RSH functional} \end{cases} \quad (4.30)$$

and the respective kernels

$$\tilde{f}_{xc}(\mathbf{r}, \mathbf{r}') = \begin{cases} (1 - a_{\text{HF}})f_x(\mathbf{r}, \mathbf{r}') + f_c(\mathbf{r}, \mathbf{r}') & \text{hybrid functional} \\ f_x^{\text{SR}}(\mathbf{r}, \mathbf{r}') + f_c(\mathbf{r}, \mathbf{r}') & \text{RSH functional} \end{cases} \quad (4.31)$$

where the adiabatically approximated kernels

$$f_{x/c}(\mathbf{r}, \mathbf{r}') = \frac{\delta v_{x/c}^0[n_0](\mathbf{r})}{\delta n_0(\mathbf{r}')} \quad (4.32)$$

are derived from the semi-local potentials $v_{x/c}^0[n_0](\mathbf{r})$.

4.4 Eigenvalue Gaps in Kohn-Sham and Generalized Kohn-Sham Theory

Due to the many possible realizations of the **GKS** scheme it is difficult to analyze its properties in general. Therefore, we only consider schemes that are relevant for this work, namely the hybrid and **RSH GKS** schemes. Both functional concepts incorporate in some way the exchange Fock operator as the non-local operator. To understand the consequences thereof we analyze the limit of exact exchange for both **KS-OEP** and **GKS-HF** under the neglect of correlation.

As already mentioned in Sec. 4.2, due to unequal orbitals the energies of **KS-OEP** and **GKS-HF** are generally different, although usually only slightly. The

4.4. Eigenvalue Gaps in Kohn-Sham and Generalized Kohn-Sham Theory

difference between both schemes becomes more important on the orbital level. In **KS** theory all orbitals are obtained from the same effective potential. In the case of exact exchange this potential has the correct $-\frac{1}{r}$ asymptotic behavior. In **HF** theory the orbitals are subject to different potentials. Whereas the potential for the occupied orbitals ($j \leq N$) has the correct $-\frac{1}{r}$ asymptotic behavior, the unoccupied orbitals ($j > N$) see a potential that falls off exponentially (*cf.* Eq. (4.14) for $j > N$ and $r \rightarrow \infty$). Thus, an unoccupied **HF** level “feels” the potential of N electrons and an unoccupied **KS** level the potential of $N - 1$ electrons far away from the system. The consequence are qualitatively different levels. The former approximately reflects an additional electron and therefore an electron affinity, the latter can be regarded as a first approximation of an excitation energy.^{29,105}

If both schemes are completed with their corresponding exact correlation functional, one can show that the **GKS(HF)** eigenvalues are shifted with respect to the exact **KS** eigenvalues by approximately⁷⁹

$$\epsilon_j^{\text{GKS(HF)}} \approx \epsilon_j^{\text{KS}} + \langle \phi_j | \hat{v}_j^{\text{Fock}} - v^{\text{EXX(KS)}} | \phi_j \rangle, \quad (4.33)$$

where \hat{v}_j^{Fock} is the Fock exchange potential (Eq. (4.14)) and $v^{\text{EXX(KS)}}$ the **EXX-OEP** potential (Eq. (2.48)). To arrive at this relation, differences in the correlation functional and differences due to the evaluation of Eq. (4.33) with **KS** and **GKS** orbitals are neglected.

This shift has a direct effect on the eigenvalue gap of the highest occupied and lowest unoccupied orbitals in both schemes

$$\begin{aligned} \Delta_{\text{GKS(HF)}} &= \epsilon_{\text{LUMO}}^{\text{GKS(HF)}}(N) - \epsilon_{\text{HOMO}}^{\text{GKS(HF)}}(N) \\ &\approx \epsilon_{\text{LUMO}}^{\text{KS}}(N) - \epsilon_{\text{HOMO}}^{\text{KS}}(N) + \Delta_x \\ &= \Delta_{\text{KS}} + \Delta_x \end{aligned} \quad (4.34)$$

where Δ_x is the exchange part of the derivative discontinuity (Sec. 2.4) that follows from^{48,79,106}

$$\Delta_x = \langle \phi_{N+1} | \hat{v}_j^{\text{Fock}} - v^{\text{EXX(KS)}} | \phi_{N+1} \rangle - \langle \phi_N | \hat{v}_j^{\text{Fock}} - v^{\text{EXX(KS)}} | \phi_N \rangle. \quad (4.35)$$

Hence, the exchange derivative discontinuity is approximately incorporated in the eigenvalue gap of **GKS** theory based on the non-local **HF** operator. For the fundamental gap we can write (*cf.* Eq. (2.38))

$$\begin{aligned} \Delta E_f &= \left(\epsilon_{\text{LUMO}}^{\text{KS}}(N) - \epsilon_{\text{HOMO}}^{\text{KS}}(N) \right) + \Delta_{\text{xc}} \\ &\approx \left(\epsilon_{\text{LUMO}}^{\text{GKS(HF)}}(N) - \epsilon_{\text{HOMO}}^{\text{GKS(HF)}}(N) \right) + \Delta_c. \end{aligned} \quad (4.36)$$

Since indications exist that the correlation contribution to the derivative discontinuity, Δ_c , is negative and cancels a fraction of Δ_x ,^{81,107,108} the **HF** eigenvalue difference is generally considered to be larger than the fundamental

gap. Furthermore, in both schemes the highest occupied orbital energy is exactly the negative of the (vertical relaxed) ionization potential¹⁰⁹

$$\epsilon_{\text{HOMO}}^{\text{GKS(HF)}}(N) = \epsilon_{\text{HOMO}}^{\text{KS}}(N) = -IP. \quad (4.37)$$

Standard **DFT** approximations do not necessarily fulfill the above equation, *e.g.*, semi-local **KS** functional approximations usually average over the derivative discontinuity and one obtains^{61,110}

$$\epsilon_{\text{HOMO}}^{\text{sl}}(N) \approx -\frac{1}{2}(IP + EA). \quad (4.38)$$

Hybrid functionals contain a fraction a of **HF** exchange and the remainder functional is treated approximately with semi-local functionals. Therefore, the eigenvalue gap lies between the small **KS** gap and the larger **HF** gap and the **HOMO** orbital energy is between the limits of Eq. (4.37) and Eq. (4.38), depending on the choice of a . For the commonly used values of the parameter a between 0.2 and 0.25 the gap of a hybrid functional is still closer to the **KS** gap than to the **HF** gap. Hence, the hybrid gap (**B3LYP**, **PBE0**) is usually rather close to the optical gap than to the fundamental gap (especially for organic molecules).

Similar arguments hold for **RSH** functionals. The eigenvalue gaps are also in between semi-local **KS** eigenvalue gaps and the **HF** eigenvalue gap depending on the choice of the range-separation parameter γ . In the limit of $\gamma \rightarrow 0$ the **RSH** approach becomes a standard semi-local functional approach and the gap is correspondingly small. In the other limit ($\gamma \rightarrow \infty$) one obtains **HF** combined with semi-local correlation and therefore, the gap is approximately the **HF** gap as semi-local correlation functionals do not exhibit a derivative discontinuity. Standard choices for γ are between $0.3 a_0^{-1}$ and $0.5 a_0^{-1}$. This corresponds to a separation distance of $1.7 - 1.0 a_0$, at which the Coulomb interaction is equally split into short-range and long-range (for the error function as separation function). Typically, the eigenvalue gap is already close to the **HF** or fundamental gap if γ is chosen within this range.

At the end we remark, that the strict definition of the **xc** derivative discontinuity defined for the **KS** scheme (see Sec. 2.4) is not valid in the **GKS** scheme. For each choice of the non-local operator \hat{S} the discontinuity of the remainder potential is different. Note that one already changes to a different realization of the **GKS** scheme if only the hybrid mixing parameter a or the range-separation parameter γ are varied.

Charge Transfer Excitations in Donor-Acceptor Systems

Charge transfer (CT) excitations are photoinduced electronic excitations in which electron density (charge) moves from one region, the donor (D) region, to another spatially separated region, the acceptor (A) region. These two regions can be situated on different molecules or on different moieties of the same molecule. CT excitations are not correctly described by standard DFT using semi-local or hybrid functionals. Although these methods accurately predict valence excitations of many different systems, they severely underestimate CT excitation energies up to several eV.^{111–115} In this thesis we mainly focus on the description of CT in alternating donor-acceptor (DA) conjugated molecular chains. In this case the spatial separation between D and A is small since they are covalently bound. However, to demonstrate the failure of semi-local and standard hybrid DFT in predicting CT we discuss the limit of large separation between D and A in the following section. We also discuss the potential of RSH functionals that we apply successfully to DA systems in the subsequent Secs. 5.2 to 5.5. For an accurate description, we define the range-separation parameter by a non-empirical implicit functional definition.

5.1 Long-Range Charge Transfer Excitations in TDDFT

In the limit of large separation between D and A, *i.e.*, if the overlap between orbitals of D and A can be neglected due to their exponential decay, the minimum energy that is required to move one electron from D to A is exactly given by¹¹⁶

$$\Omega_{\text{CT}} = IP_{\text{D}} - EA_{\text{A}} - \frac{1}{R}, \quad (5.1)$$

where R is the distance between **D** and **A**. The energy equivalent to the ionization potential of **D** (IP_D) minus the electron affinity of **A** (EA_A) has to be applied to remove an electron from **D** and move it to **A**. At a finite distance R one additionally gains the electrostatic interaction energy between D^+ and A^- . In optical absorption spectroscopy such excitations cannot be observed. They are dark excitations due to the vanishing orbital overlap between **D** and **A** and thus the vanishing transition dipole moments. However, we can still calculate Ω_{CT} on the basis of linear response theory. In the following, we demonstrate why standard **TDDFT** functionals fail to correctly predict long-range **CT** excitations and show that **RSH** functionals have the potential to cure this deficiency.

Charge Transfer in KS Theory

If we assume for simplicity that the pole Ω_{CT} does not overlap with other poles in the response function of Eq. (3.19) and is the lowest excitation energy of the system we can use the single pole approximation^{117–119} for the highest occupied and the lowest unoccupied orbital energies. For **TD-KS** theory Eq. (3.23) reduces to

$$\begin{aligned} \Omega_{CT}^{KS} \approx & \epsilon_{LUMO}^{KS} - \epsilon_{HOMO}^{KS} + 2 \int d^3r \int d^3r' \\ & \times \phi_L^{(A)}(\mathbf{r}) \phi_H^{(D)}(\mathbf{r}) \left[\frac{1}{|\mathbf{r} - \mathbf{r}'|} + f_{xc}(\mathbf{r}, \mathbf{r}', \omega_{KS}) \right] \phi_L^{(A)}(\mathbf{r}') \phi_H^{(D)}(\mathbf{r}'). \end{aligned} \quad (5.2)$$

If we use a standard semi-local functional within the adiabatic approximation the kernel f_{xc} is not frequency dependent and spatially local. Therefore, the two-electron integral becomes zero due to the exponentially decaying overlap between the **HOMO** orbital $\phi_H^{(D)}$ on **D** and the **LUMO** orbital $\phi_L^{(A)}$ on **A**. According to Eqs. (2.31), (2.39) and (4.38) we obtain

$$\Omega_{CT}^{sl} \approx \epsilon_{LUMO}^{sl} - \epsilon_{HOMO}^{sl} \quad (5.3)$$

$$\leq IP_D - EA_A - \Delta_{xc}. \quad (5.4)$$

Thus, besides the missing R dependence semi-local functionals underestimate **CT** excitation energies at least by the derivative discontinuity.¹¹⁴ Note that in principle **KS-TDDFT** is exact. The exact frequency dependent kernel f_{xc} has a singularity at $w_{KS} = \epsilon_{LUMO}^{KS} - \epsilon_{HOMO}^{KS}$ and is spatially non-local. The consequence is a finite integral in Eq. (5.2) that accounts for the derivative discontinuity and exhibits the correct $\frac{1}{R}$ dependence.^{120–122} Generally, one has to go beyond the adiabatic approximation to obtain such a frequency dependent kernel. Even the exact **xc** potential can lead to wrong results if used in combination with the adiabatic linear response formalism.^{121,123,124} Approximate functionals need to incorporate a correct description of the **xc** derivative discontinuity and have to be self-interaction free. Promising

functionals with these features are orbital dependent functionals such as [EXX](#) and self-interaction corrected functionals (*cf.* [Sec. 2.5](#)).

Charge Transfer in GKS Theory

Now we analyze how hybrid and [RSH](#) functional approximations treated within the [GKS](#) scheme perform for the limit of a large separation between [D](#) and [A](#). All two-electron integrals of the matrices [A](#) and [B](#) of [Eq. \(4.28\)](#) except for $(ii'|η|aa')$ vanish in this limit if we apply the same argument as before in [KS](#) theory. With the same assumption made in [Eq. \(5.2\)](#) we approximately obtain

$$\begin{aligned} \Omega_{\text{CT}}^{\text{GKS}} &\approx \epsilon_{\text{LUMO}}^{\text{GKS}} - \epsilon_{\text{HOMO}}^{\text{GKS}} - \int d^3r \int d^3r' \\ &\quad \times \phi_{\text{L}}^{(\text{A})}(\mathbf{r}) \phi_{\text{L}}^{(\text{A})}(\mathbf{r}) \eta(\mathbf{r} - \mathbf{r}') \phi_{\text{H}}^{(\text{D})}(\mathbf{r}') \phi_{\text{H}}^{(\text{D})}(\mathbf{r}') \end{aligned} \quad (5.5)$$

with $\eta(\mathbf{r} - \mathbf{r}') = \begin{cases} a \frac{1}{|\mathbf{r} - \mathbf{r}'|} & \text{hybrid functional} \\ \frac{\omega(\gamma|\mathbf{r} - \mathbf{r}'|)}{|\mathbf{r} - \mathbf{r}'|} & \text{RSH functional} \end{cases}$

Thus, we arrive at

$$\Omega_{\text{CT}} \approx \begin{cases} \epsilon_{\text{LUMO}}^{\text{hyb}} - \epsilon_{\text{HOMO}}^{\text{hyb}} - \frac{a}{R} & \text{hybrid} \\ \epsilon_{\text{LUMO}}^{\text{HF}} - \epsilon_{\text{HOMO}}^{\text{HF}} - \frac{1}{R} & \text{HF, hybrid with } a \rightarrow 1 \\ \epsilon_{\text{LUMO}}^{\text{RSH}} - \epsilon_{\text{HOMO}}^{\text{RSH}} - \frac{1}{R} & \text{RSH.} \end{cases} \quad (5.6)$$

At first we notice that [HF](#) and [RSH](#) functionals exhibit the correct R dependence that is only partly fulfilled by hybrid functionals. However, the size of the eigenvalue gap is decisive for correctly predicting the [CT](#) excitation energy. From [Sec. 4.4](#) we know that [HF](#) eigenvalue gaps usually overestimate the fundamental gap by the correlation contribution to the derivative discontinuity whereas hybrid and [RSH](#) functional eigenvalue gaps resemble the fundamental gap if a and γ , respectively, are chosen correctly. Hence, although [HF](#) describes long-range [CT](#) qualitatively correct, quantitative agreement with experiment in practically relevant situations is usually not achieved due to the lack of a suitable correlation functional. Standard hybrid functionals with a mixing parameter of $a = 0.2 - 0.25$ usually improve the description of [CT](#) energies compared to semi-local [DFT](#). Yet, they still seriously underestimate them. ^{113,115,125} The Becke half-and-half functional⁸⁰ ($a = 0.5$) yields further improvement, but the amount of [HF](#) exchange is usually still not sufficient.⁵⁹ Furthermore, for $a > 0.25$ hybrid functionals lose their main capability – the accurate prediction of thermochemical properties and also the correct description of valence excitations. Whether [RSH](#) functionals reliably predict long-range [CT](#) excitation energies is a question of a suitably chosen range-separation parameter γ .

5.2 Tuned Range-Separated Hybrid Functionals

How does one choose an appropriate value for γ ? One could adapt a similar approach as in hybrid functionals and treat γ as a universal empirical parameter which can be fitted to an appropriately chosen reference data set. However, calculations indicate and one can analytically motivate that γ is in fact a functional of the density (which is so far unknown)^{98,99,126–128} and as such is system dependent. Whether it is possible to find such a functional is still matter of research. Another approach, that avoids this problem is to define γ as an implicit functional. This can be achieved by still treating γ as a constant, but as one that is determined implicitly for each system by fulfilling physical conditions. For the correct prediction of long-range CT excitations it is necessary to demand two conditions to be fulfilled.

1. The HOMO orbital energy must equal the negative ionization potential, *i.e.*,

$$\epsilon_{\text{HOMO}}(N) = -IP(N). \quad (5.7)$$

2. The derivative discontinuity must vanish, *i.e.*,

$$\epsilon_{\text{LUMO}}(N) = \epsilon_{\text{HOMO}}(N + 1). \quad (5.8)$$

For the former one can easily define a corresponding non-empirical tuning condition to determine γ by calculating the IP approximately from total energy differences (*cf.* Eq. (2.31)). This condition reads

$$T_N(\gamma) = \epsilon_{\text{HOMO}}^\gamma(N) + E^\gamma(N - 1) - E^\gamma(N) = \min. \quad (5.9)$$

The optimal γ that minimizes T_N has to be determined in an iterative procedure of successive ground state calculations as demonstrated in Fig. 5.1 for the system NDI-1 of **Pub. 1**. An RSH calculation that employs the optimal γ leads to a HOMO energy that is close to the measured ionization potential.⁹⁴

Equally important for the prediction of CT excitations is the second condition. However, a physical condition that connects the electron affinity EA with the LUMO energy level does not exist. To circumvent this issue we can enforce Eq. (5.9) for the $N + 1$ system using

$$T_{N+1}(\gamma) = \epsilon_{\text{HOMO}}^\gamma(N + 1) + E^\gamma(N) - E^\gamma(N + 1) = \min. \quad (5.10)$$

which leads to a second tuning condition for the electron affinity. In order to fulfill both tuning conditions T_N and T_{N+1} simultaneously with only one parameter γ we have to introduce a third combined tuning condition

$$T_{LS}(\gamma) = \sqrt{T_N^2(\gamma) + T_{N+1}^2(\gamma)} = \min. \quad (5.11)$$

These conditions are examined in detail in **Pub. 2**. In organic chemistry the three range-separation parameters that minimize T_{LS} , T_N and T_{N+1} are usually

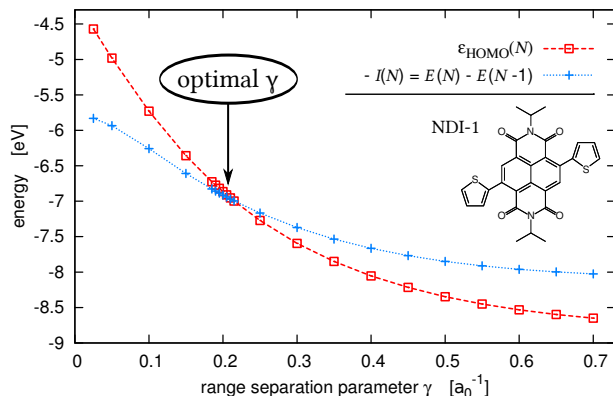


Figure 5.1. Visualization of the procedure for determining the optimal γ for NDI-1. Successive ground state calculation with different γ values lead to the optimal γ that minimizes the tuning condition T_N (Eq. (5.9)). The BNL RSH approach was employed. Numerical details can be found in **Pub. 1**.

very similar. Furthermore, it was found that the derivative discontinuity from tuned RSH calculations of this class of materials is approximately zero^{98,128} as we demanded at the beginning and thus,

$$\epsilon_{\text{LUMO}}(N) \approx -EA(N) \quad (5.12)$$

and

$$\Delta E_f \approx \epsilon_{\text{LUMO}} - \epsilon_{\text{HOMO}} \quad (5.13)$$

We visualized these frontier orbital eigenvalues in Fig. 5.2 and compare them to the respective levels in KS theory.

Tuned RSH calculations also indicate the system dependence of γ since they yield different γ for different systems.^{128–131} Furthermore, it can be observed that γ^{-1} grows with the size of a system.^{129,130} In Fig. 5.3 we show this size dependence for the oligomers of thiophene and benzothiadiazole from **Pub. 3**. At a certain system size γ^{-1} saturates (also *cf.* **Pub. 1**). This effect could be related to the saturation of the conjugation length.¹³⁰

From the last equations we can infer that long-range CT excitations are correctly described (*i.e.*, according to Eq. (5.1)) by tuned RSH functionals. This finding has been confirmed by calculations.^{94,132} It is accomplished by the transformation into a special GKS scheme that has a vanishing derivative discontinuity. The predictive power of the approach depends on the minimum value of T_{LS} that can be achieved by γ optimization. Finally, if a fraction of exact exchange is included in the short-range functional the tuning also improves the straight-line behavior of the energy as a function of the particle number^{98,102,103,133} and thus reduces the many-electron self-interaction error.

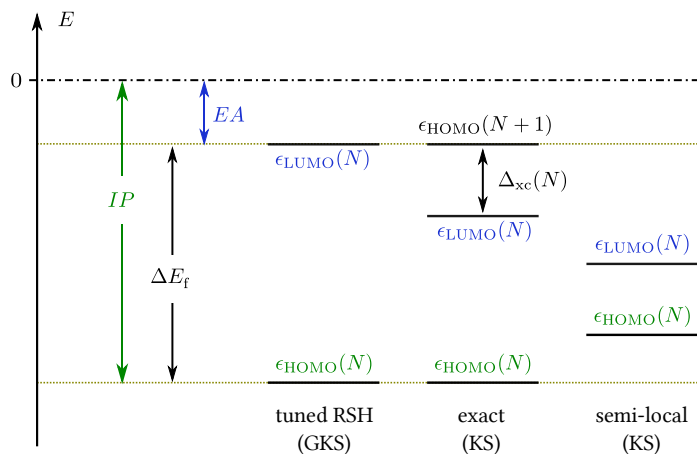


Figure 5.2. Schematic illustration of the HOMO and LUMO orbital eigenvalues for tuned RSH, exact KS and semi-local KS compared to the ionization potential, the electron affinity and the fundamental gap. For the illustration we assume that the tuning conditions are exactly fulfilled. Although for real systems the picture can change, the eigenvalues of organic molecules are usually close to this scheme.

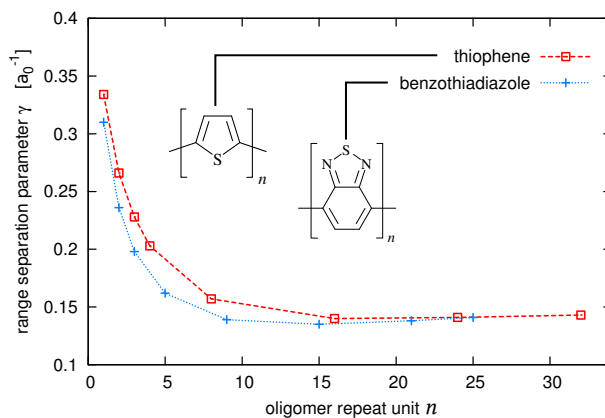


Figure 5.3. Size dependence of the range-separation parameter γ for thiophene and benzothiadiazole oligomers. Numerical details can be found in **Pub. 3**.

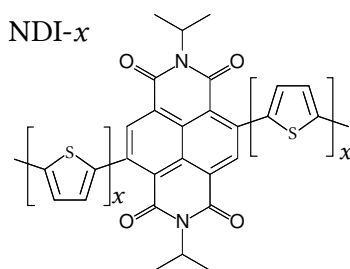


Figure 5.4. Schematic for structure of NDI- x .

5.3 Partial Charge Transfer Excitations in Donor-Acceptor Systems

So far we only discussed CT excitations with a complete transfer of an electron from **D** to **A**. These excitations occur in systems that have a vanishing overlap of **D** and **A** orbitals and therefore, cannot be observed via ultraviolet–visible (UV/vis) absorption spectroscopy. Of more relevance in practice are systems with covalently bound **D** and **A** moieties. Excitations in these systems that combine the **D** and **A** part are referred to as being of mixed CT and valence character instead of CT character only. They can be observed with UV/vis spectroscopy due to a sufficient orbital overlap. The lowest excitation energy (or optical gap) is usually an excitation with only partial CT character. As explained in the introduction such **DA** systems are used in organic photovoltaic devices as low gap light absorbing materials.

Semi-local functionals also underestimate excitation energies of partial CT character for covalently bound **DA** systems. For standard hybrid functionals we cannot draw a simple picture as for long-range CT. The performance depends on the specific system. In the field of organic chemistry standard hybrid approaches such as **B3LYP** and **PBE0** reliably predict vertical excitation energies^{134–139} as the small amount of **HF** exchange leads to a sufficient opening of the optical gap. Excitations in smaller systems with little CT flavor might still be correctly described¹⁴⁰ whereas a description of larger systems or systems with more CT character fails (*cf.* **Pub. 1**).

In **Pub. 1** we examine the performance of the tuned **RSH** approach for a **DA** system based on naphthalene diimide as **A** with x symmetrically attached thiophene rings as **D** (**NDI- x** , see Fig. 5.4). The lowest excitation energy carries appreciable oscillator strength and lies in the visible range. Thus, it is a system with partial CT character that is of practical relevance. We show that the tuning approach reliably predicts the lowest excitation energy in accordance with experimental results. Conversely, a standard hybrid functional (**B3LYP**) underestimates the first excitation energy, while an **RSH** functional

without tuning (ω B97(x)⁹⁵) overestimates it. Furthermore, the results in **Pub. 1** demonstrate that the tuning approach is also applicable to systems with a D-A-D arrangement instead of a D-A arrangement only. With the tuning approach we are able to predict the dependence of the lowest excitation energy on the donor strength by increasing the number of thiophene rings attached to the system. We determine the system size where the saturation of the excitation energy sets in. Thus, we have shown that we are able to predict optical properties of low molecular weight systems relevant for OPV application by employing the tuned RSH approach. Such calculations could help to design efficient OPV materials by tailoring their optical properties. Note that in **Pub. 1** we employed a tuning condition that is slightly different from Eq. (5.11) as it combines the absolute values of T_N and T_{N1} . However, for organic systems the difference is generally small as the optimal range-separation parameters obtained from both conditions are usually nearly identical.

Materials based on naphthalene and thiophene are interesting for OPV application also from a yet different perspective. Polymers of this DA combination show very high mobilities in organic field effect transistor (OFET) measurements.¹⁴¹ In order to determine the mobilities of the low molecular weight systems of **Pub. 1**, I examined NDI-1 films as a side project of this thesis. Instead of thiophene we used 3-hexylthiophene as donor to improve the solubility. In Fig. 5.5 (a) we demonstrate that these additional (well separated) hexyl chains have a negligible influence on the lowest absorption energy (confirmed by calculations on a different system in **Pub. 3**). To fabricate films we spin-coated NDI-1 in chloroform solution on a quartz substrate. This causes a redshift of the first excitation energy by approximately 0.3 eV (*cf.* Fig. 5.5 (b)). An additional annealing step does not improve the optical properties of the film. In Fig. 5.6 we show photographs of the polycrystalline film and the film after annealing (obtained by polarized light microscopy). The photograph of the annealed film illustrates that the film exhibits poor wetting properties. As a consequence, we were not able to measure the mobilities of NDI-1 based OFET's (see also Ref. 142).

5.4 Influence of Donor-Acceptor Arrangements on Excitation Energies

The lowest excitation energy is defined as the difference of the ground and the first excited state energy. Two other energies that are important for OPV devices are the ionization potential IP and the electron affinity EA whose difference defines the fundamental gap ΔE_f . In contrast to the first excitation energy these energies are based on processes that change the total charge of the system by the removal or addition of an electron, respectively. The difference between the ionization potential of the hole conducting material (\bar{D}) and the

5.4. Influence of Donor-Acceptor Arrangements on Excitation Energies

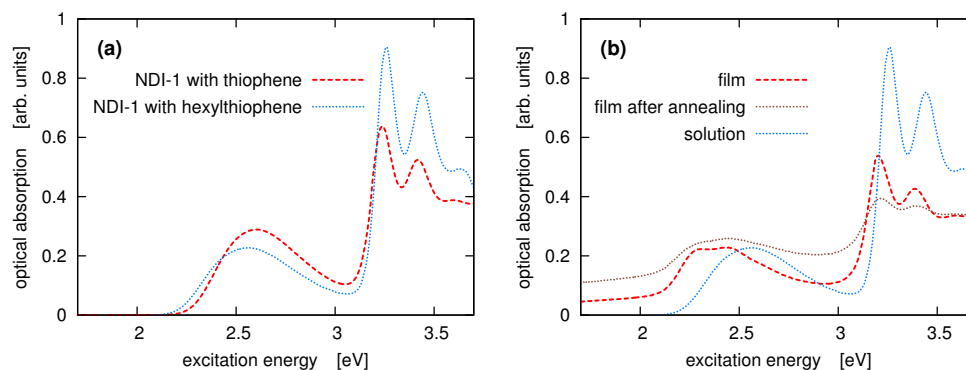


Figure 5.5. (a): Comparison of UV/vis absorption spectra of **NDI-1** with thiophene and 3-hexylthiophene as donor component in solution (solvent: chloroform). (b): UV/vis absorption spectra of **NDI-1** with 3-hexylthiophene as donor in solution, as film and as film after annealing at room temperature (annealing details *cf.* Fig. 5.6).

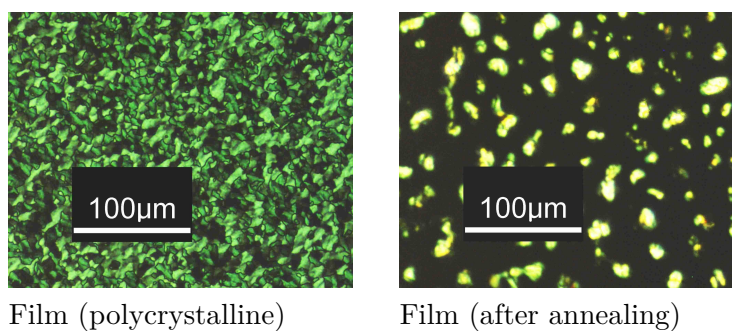


Figure 5.6. **NDI-1** films on quartz substrate. *Left:* Polycrystalline film directly after spin coating at room temperature (parameters: $\approx 100 \mu\text{l}$ solution with a concentration of 0.57 wt%. The speed of rotation was 2000 r min^{-1}). *Right:* Film after annealing demonstrating the poor wetting properties of the film (parameters: 5 min at 150°C).

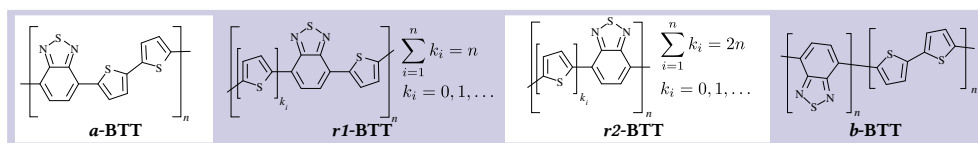


Figure 5.7. Schematic of the $\langle q \rangle$ -BTT oligomer structures. $\langle q \rangle = a$ (alternating), $r1$, $r2$ (random), b (diblock). All four systems are composed of $2n$ thiophene and n benzothiadiazole units and were examined for $n = 1, \dots, 12$. Numerical details can be found in **Pub. 3** and **Pub. 5**.

electron affinity of the electron conducting material (\bar{A}), $IP^{\bar{D}} - EA^{\bar{A}}$, defines the upper energy limit that can be harvested from an OPV cell.¹² Thus, next to the first excitation energy, that is crucial for the absorption, these energies are important for the solar cell efficiency. All mentioned energies are illustrated schematically in Fig. 1.2 of the introductory chapter.

In **Pub. 3** and **Pub. 5** we examine the influence that the specific arrangement of **D** and **A** moieties has on the excitation energies of **DA** systems. The insights that we gain from this analysis are important for the understanding of **DA** systems and provide guidance for the design of future OPV materials. We investigate four different oligomer arrangements of thiophene as donor and benzothiadiazole as acceptor material, an alternating (a -BTT), two different random ($r1$ -BTT and $r2$ -BTT) and a diblock arrangement (b -BTT). The structures of these systems are shown in Fig. 5.7. A central aspect of **Pub. 3** is the comparison with experimental absorption spectra. Both, calculations and experiments, predict that the lowest excitation energy only slightly changes if we rearrange the **D** and **A** units from a -BTT to $r1$ -BTT. However, the striking difference between theory and experiment is the saturation length and related to that the maximum achievable effective conjugation lengths. This leads to a large discrepancy between the lowest excitation energies in theory and experiment for larger oligomers (up to 0.7 eV). We discuss different factors that could cause the disagreement and ultimately lead to the breakdown of the single molecule approach to simulate experimental absorption spectra.

Furthermore, **Pub. 3** and **Pub. 5** demonstrate that **CT** only plays a minor role in the extended **DA** systems of this work, surprisingly, even in the diblock arrangement b -BTT. Note that we cannot use the simple picture that we have drawn for long-range **CT** in Sec. 5.1 since many close lying occupied and unoccupied orbitals contribute to the lowest excitation. However, the results demonstrate that the use of a functional that goes beyond standard semi-local or hybrid functionals is important. In Fig. 5.8 we show that B3LYP ($a = 0.2$) underestimates and the Becke half-and-half functional⁸⁰ ($a = 0.5$) overestimates the absorption energies for large chain lengths. Note, that the graph also shows (for one chain length) that the absorption energy does not depend on the choice of the **RSH** functional.

5.4. Influence of Donor-Acceptor Arrangements on Excitation Energies

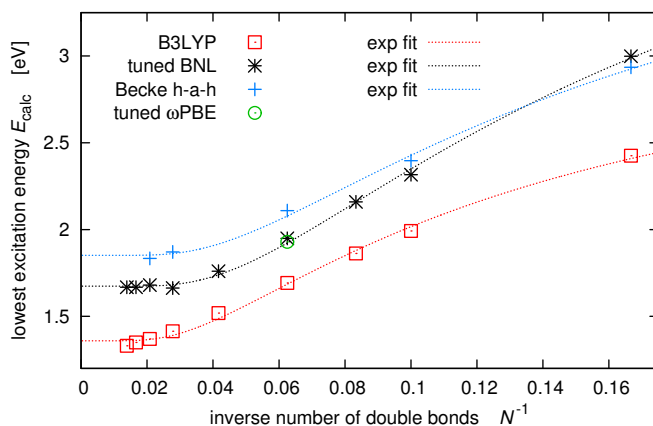


Figure 5.8. Lowest excitation energy as a function of the inverse number of double bonds. The graph compares tuned BNL calculations with the standard hybrid B3LYP and the Becke half-and-half functional. Furthermore, one data point is obtained from a tuning calculation with the ω PBE RSH approach.

Besides these quantitative deviations between the hybrid and the RSH approach we can also find qualitative differences. To investigate the nature of an excitation we analyze its natural transition orbitals.¹⁴³ For the lowest excitation of *b*-BTT we show the most dominant orbital pair in Fig. 5.9 for the BNL and the B3LYP functional. Whereas BNL predicts an excitation with only little CT character, the B3LYP orbital pair indicates an excitation dominated by CT. The failure of B3LYP results from the insufficient amount of incorporated exact exchange. An amount of 50 % exact exchange ($a = 0.5$) reproduces the RSH natural transition orbital plots.

The success of the tuning approach even for these covalently bound DA systems is related to the fact that the derivative discontinuity vanishes if the optimal γ determined from Eq. (5.9) or Eq. (5.11) is used in the calculation. This is demonstrated in Fig. 5.10 for the system *a*-BTT with $n = 2$. Thus, the HOMO and LUMO energy levels correctly predict the *IP* and *EA*, respectively.^{98,128,129}

In **Pub. 5** we further demonstrate that the *IP* and *EA* only change slightly upon changing the DA arrangement (for the systems in Fig. 5.7). All *IP*'s are close to the respective value of poly-thiophene and all *EA*'s are close to the respective value of poly-benzothiadiazole. This can be explained by analyzing orbital plots of the HOMO and the LUMO. They are mainly located on only D and A moieties, respectively. Thus, contrary to the excitation process with no considerable CT the electron ionization and electron absorption takes place on different parts of the molecule for *r1*-BTT, *r2*-BTT and *b*-BTT. Utilizing this effect in organic solar cells could improve the charge transfer and separation

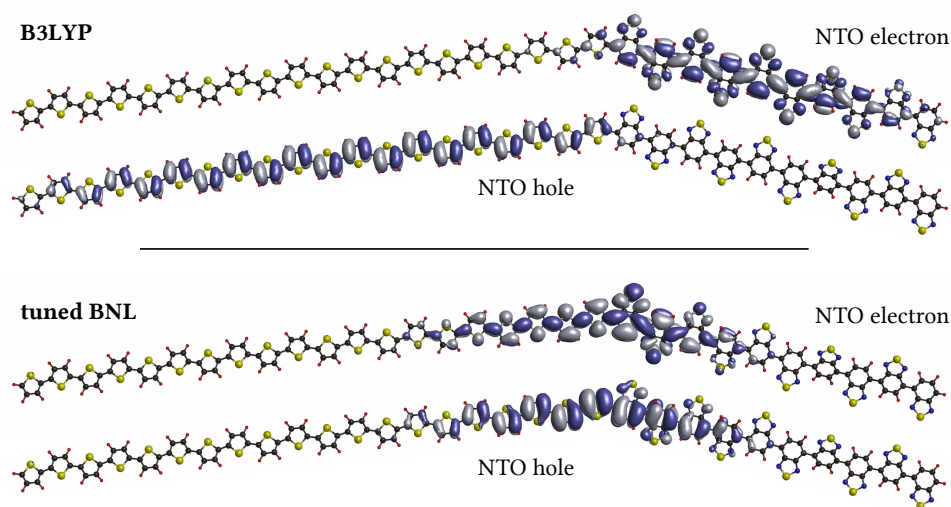


Figure 5.9. Comparison of the most dominant natural transition orbitals of the lowest excitation of *b*-BTT for B3LYP and tuned BNL. Numerical details can be found in **Pub. 3**.

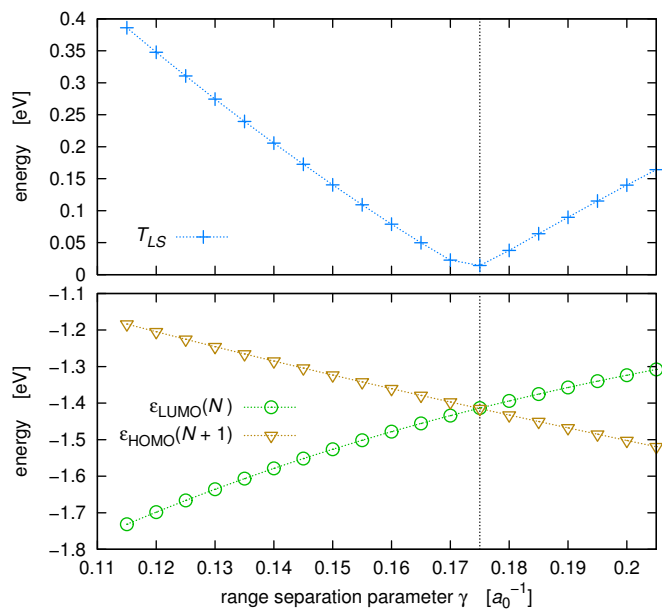


Figure 5.10. The range-separation parameter that minimizes T_{LS} also minimizes the derivative discontinuity. This connection is also valid for a covalently bound DA system with only partial CT. In this case *a*-BTT with $n = 2$.

across the interface of the hole and electron conducting material if the **DA** systems are specifically arranged.

In contrast to the *IP*'s and *EA*'s (and the fundamental gap) the first excitation energy changes considerably by rearranging *a*-BTT to *r2*-BTT and *b*-BTT (by ≈ 0.4 eV). We explain this effect by analyzing structural properties such as the bond length alternation and the planarity which influence the lowest excitation more severely than the *IP* and *EA*. By comparing the excitation energies to the ones of the separated **D** and **A** system (poly-thiophene and poly-benzothiadiazole) we conclude that the optical gap is only reduced by approximately 0.5 eV if **D** and **A** subunits are combined. Thus, the low optical gap of **DA** polymers is mainly achieved by an increase of the effective conjugation length which reduces the gap by approximately 1.5 eV for the examined system.

5.5 Downsides of the Tuning Approach

This work and various other studies demonstrate that the tuning of **RSH** functionals is essential for the correct prediction of full or partial **CT** excitations.^{98,132,144,145} Tuning overcomes the shortcomings of **RSH** functionals with an empirically fitted range-separation parameter which fail to predict these complicated excitations due to the missing system dependence of γ .^{132,144,145} It enables us to define γ implicitly as a functional of the density and still employ a non-empirical approach. However, this approach also leads to serious drawbacks which we analyze in **Pub. 2**.

The main conceptual deficiency is the violation of size consistency (*cf.* Sec. 2.4). This can be understood from two different points of view: One possibility is to view γ as a parameter that is redetermined non-empirically for each system. Thus, a different γ means that we use a different functional (and even a different **GKS** scheme) for each system. Consequently, the total energies of different systems cannot be compared, which manifests itself in the violation of size consistency.

The second perspective treats tuned **RSH** functionals as implicitly defined functionals where $\gamma[n]$ is determined by a tuning procedure. As a consequence, the functional has a highly non-local dependence on the density which causes the size consistency violation. Furthermore, a functional $\gamma[n]$ would imply an additional term in the **GKS** potential of the form

$$\frac{\partial E_{\text{x,LR}}^{\text{EXX}}[\{\phi_{j,\sigma}\}]}{\partial \gamma} \frac{\delta \gamma[n]}{\delta \phi_i}. \quad (5.14)$$

As $\gamma[n]$ is unknown such a term cannot be derived and we have to treat γ as a constant when taking the functional derivative. As a result, we obtain an inconsistent potential-energy pair by determining γ via a tuning step. A

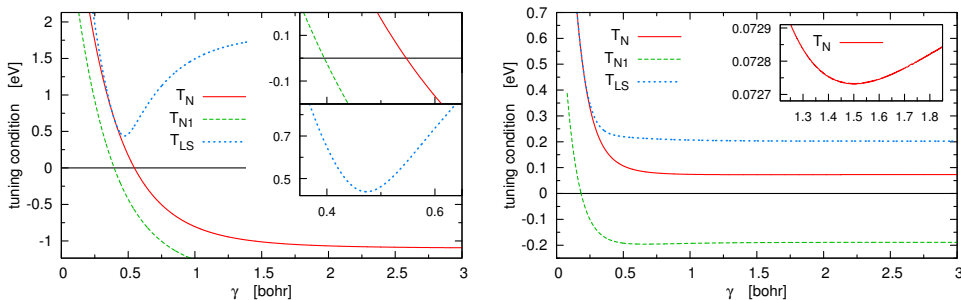


Figure 5.11. Tuning conditions defined in Eqs. (5.9) to (5.11) as a function of γ . *Left:* Cl atom. The optimal γ 's for all three tuning conditions differ substantially. *Right:* Na atom. For the T_N and the T_{LS} tuning the optimal γ is not well defined. T_{LS} only has a shallow minimum and the optimal γ of T_N would be very large ($\gamma \rightarrow \infty$).

different kind of inconsistency between potential and energy will be discussed in Chap. 6 within the KS scheme.

In **Pub. 2** we analyze the consequences of the size consistency violation for ground state DFT. As test systems we chose atoms and diatomic molecules. They exhibit very different optimal γ 's and, because of that, one is able to produce large size consistency errors by comparing the energies of these systems. We report errors of several electron volts and demonstrate that the approach is not suitable for predicting binding energies. Furthermore, we show that the tuning approach could lead to an incorrect prediction of the spin configuration and qualitatively wrong potential energy surfaces. For the latter we show spurious dependencies on the spin states of the cation and anion. For our tests we used the BNL and ω PBE functional. It is noteworthy that for ω PBE the errors are considerably smaller although the system dependence of the optimal γ is similar for both systems. The reason might be the improved compatibility between semi-local exchange and correlation in the case of ω PBE. For excitation gaps deviations between different RSH approaches are usually small (*cf.* **Pub. 3** and Ref. 145).

Pub. 2 also reveals that the tuning does not always work as reliably as in the case of organic molecules. For atoms and diatomic molecules the optimal γ values obtained from T_N , T_{N1} and T_{LS} differ notably, can hardly be determined or are not well defined at all as is the case for alkali and earth alkali atoms. This is demonstrated in Fig. 5.11. These results are related to the strong size dependence of γ .^{129,130} (*cf.* **Pub. 1**) Since there is a considerable size difference between the charged ions and the neutral system the optimal γ 's are different for T_N and T_{N1} . Another consequence of the deviations between the optimal γ 's of T_N and T_{N1} is the finding that the HOMO-LUMO eigenvalue difference does not reflect the fundamental gap as good as in the case of organic

molecules.

The analysis of **Pub. 2** demonstrates that the tuned **RSH** approach has to be modified in order to be a generally usable functional approach that is size consistent. A modification of the approach would also be beneficial from another point of view. So far, the tuning condition only takes frontier orbitals into account and works favorably for all properties that only depend on those orbital levels such as the lowest excitation energies. However, other properties like higher lying excitations, bond lengths and total energies depend on all orbitals and therefore usually require different γ values in the current **RSH** functional setup. Fitting γ to binding energies and other thermochemical properties usually results in $\gamma = 0.3 - 0.7$ ^{91,93,95,146-148} whereas fitting to optical gaps and ionization energies results in lower values.^{94,126,127} Furthermore, heterogeneous systems, in which the **HOMO** is dominantly located on only one part of the system, might not be described correctly. In this case, a range-separation parameter that is only determined from the energy level of this orbital would not reflect the whole system.

To overcome these deficiencies one could employ a different separation function to split long- and short-range exchange (which would correspond to a distance dependent $\gamma(|\mathbf{r} - \mathbf{r}'|)$) or construct an explicit functional $\gamma[n]$. To circumvent the latter rather difficult task we suggest a yet different approach at the end of **Pub. 2**.

Direct Potential Approximation

In this chapter we address a group of functionals that does not fit into the categories of **KS xc** functionals introduced in Sec. 2.5. Contrary to the general approach of constructing an expression for the **xc** energy and obtaining the **xc** potential via the functional derivative of this energy, one can also construct an **xc** potential expression directly without the corresponding energy expression. Examples for such functionals are the exchange potential of van Leeuwen and Baerends¹⁴⁹ and the exchange potential of Becke and Johnson¹⁵⁰ (**BJ**). Approximate solutions of the **OEP** scheme also fall into this category (*cf.* Sec. 2.5) since the resulting potentials do not fulfill the **OEP** equation and, therefore, are potentials without a corresponding energy.

In the following section we discuss the **BJ** potential as one directly constructed potential and examine its prospects as an alternative access to the calculation of complicated **CT** excitations of large systems. We will see that for this task it is essential for a potential to be a functional derivative. Possible ways to transform a directly constructed potential expression into a functional derivative with a corresponding energy expression will be discussed in Sec. 6.2.

6.1 Becke-Johnson Potential

In 2006 Becke and Johnson proposed a simple potential expression that resembles the exact exchange **OEP** potential for closed shell atoms.¹⁵⁰ The **BJ** potential consists of two parts

$$v_{\sigma}^{\text{BJ}}(\mathbf{r}) = v_{x\sigma}^{\text{h}}(\mathbf{r}) + v_{\sigma}^{\text{c}}(\mathbf{r}). \quad (6.1)$$

The first part is the Coulomb potential of the exchange hole $\hat{\rho}_{x\sigma}$ (also called Slater potential)

$$v_{x\sigma}^{\text{h}}(\mathbf{r}) = - \int d^3r' \frac{\hat{\rho}_{x\sigma}(\mathbf{r}, \mathbf{r}')}{|\mathbf{r} - \mathbf{r}'|} \quad (6.2)$$

where

$$\hat{\rho}_{x\sigma}(\mathbf{r}, \mathbf{r}') = \frac{|\sum_{i=1}^N \varphi_{i\sigma}^*(\mathbf{r}) \varphi_{i\sigma}(\mathbf{r}')|^2}{n_{\sigma}(\mathbf{r})}. \quad (6.3)$$

The second part is a simple semi-local correction term

$$v_{\sigma}^c(\mathbf{r}) = C \sqrt{\frac{2\tau_{\sigma}(\mathbf{r})}{n_{\sigma}(\mathbf{r})}}, \quad (6.4)$$

where $C = \frac{1}{\pi} \sqrt{\frac{5}{12}}$ and $\tau_{\sigma} = \frac{1}{2} \sum |\phi_{j\sigma}|^2$. The **BJ** potential contains many important features of the exact exchange potential that makes it an ideal candidate for the calculation of long-range **CT** excitations of large systems. Most importantly, plots of the **BJ** potential for closed shell atoms show step structures that are related to the exchange derivative discontinuity as in the exact **KS** exchange potential.^{48,150–152} The origin of this feature, that is generally attributed to non-local potential ingredients, is solely the semi-local correction term of the **BJ** potential. Furthermore, the Coulomb potential of the exchange hole provides the correct $-\frac{1}{r}$ asymptotic behavior.

However, the complete potential does not exhibit the desired asymptotic behavior. Due to the term v_{σ}^c , the **BJ** potential does not decay to zero but to a constant determined by the eigenvalue of the highest occupied orbital. If a homogeneous electric field F is applied in the z direction, it asymptotically approaches a term linear in z . One can easily correct this wrong behavior by extending the **BJ** potential by yet another term and obtains¹⁵²

$$v_{\sigma}^{\text{extBJ}}(\mathbf{r}) = v_{\sigma}^{\text{BJ}}(\mathbf{r}) - \sqrt{-2\epsilon_{H\sigma}} - \frac{Fz}{\sqrt{-2\epsilon_{H\sigma}}}, \quad (6.5)$$

where $\epsilon_{H\sigma}$ is the eigenvalue of the highest occupied orbital with spin σ . This extended **BJ** potential reliably predicts the longitudinal linear static polarizabilities of hydrogen chains and acetylene oligomers.^{144,152} Standard (semi-)local and hybrid functionals severely overestimate polarizabilities of extended conjugated molecules^{153–155} as they lack the response term of the exact exchange potential that counteracts the applied electric field.^{154,156–158} The **BJ** potential has such a term, which can be seen as a further prerequisite for the reliable prediction of long-range **CT**.

Since a semi-local replacement of the hole potential $v_{x\sigma}^h$ is feasible^{150,159} the **BJ** potential can be transformed into a completely semi-local approach. Hence, it serves as an ideal candidate for the calculation of larger systems, where the application of the tuned **RSH** approach of Sec. 5.2 and exact exchange or self-interaction corrected **OEP** approaches would be computationally demanding. In **Pub. 4** we examine different semi-local hole potentials and check if they serve as appropriate replacements of the potential in Eq. (6.2) and, at the same time, are suitable for the transformation procedure of the next section.

To improve the functional concept it is necessary to find a corresponding correlation functional. This would open the door to a simultaneous calculation of electronic response and thermochemical properties. The hope is that it could be easier to combine one of the well-known semi-local correlation functionals with this approach than with approaches that are based on exact exchange. A further development step would be the replacement of $\epsilon_{H\sigma}$ and Fz in Eq. (6.5) by semi-local quantities.

6.2 Transforming Potential Expressions into Functional Derivatives

Constructing a direct approximation for the **xc** potential instead of the energy provides a convenient access to features that are important for describing non-local electronic response like **CT**. It might be easier to include properties like the **xc** derivative discontinuity or the correct asymptotic behavior into a potential since they can be directly identified therein. However, this approach also has a major disadvantage, namely the missing energy functional. Although it is not required for the self-consistent solution of the **KS** equations or to access many properties like the dipole moment (and successively, the polarizabilities¹⁶⁰), one cannot calculate the total energy and properties that depend on it.

In the case of the **BJ** potential, which is itself an approximation to the exact exchange **OEP** potential, one could circumvent this issue and use the exact exchange energy as a corresponding energy expression. Such an approach leads to reasonable energy values.¹⁶¹ However, searching for a corresponding energy functional would not solve the main issue that comes with this approach. We discuss this issue in the following. Directly constructing an approximation for the **xc** potential will generally lead to an expression that is not a functional derivative, no matter how close the potential is to the exact **xc** potential. Therefore, a corresponding energy whose functional derivative would lead to this directly constructed potential does not exist. This is also the case for the **BJ** potential.^{144,162} The non-trivial requirement that an **xc** potential in the **KS** framework has to fulfill in order to be a functional derivative is given by¹⁶³

$$\frac{\delta v_{xc}(\mathbf{r})}{\delta n(\mathbf{r}')} = \frac{\delta v_{xc}(\mathbf{r}')}{\delta n(\mathbf{r})} \quad (6.6)$$

which is equivalent to

$$\frac{\delta^2 E_{xc}}{\delta n(\mathbf{r})\delta n(\mathbf{r}')} = \frac{\delta^2 E_{xc}}{\delta n(\mathbf{r}')\delta n(\mathbf{r})}. \quad (6.7)$$

The use of a potential that is not a functional derivative is not justified by **KS** theory (*cf.* Sec. 2.2 and Eq. (2.18) therein). However, this does not mean that such a potential is not useful in practice, *e.g.*, the Krieger, Li,

and Iafate (KLI) approximation⁴⁸ to the OEP equation is not obtained as a functional derivative and still useful in practice. Yet, such a potential lacks properties of a proper xc potential, *e.g.*, satisfying the zero-force theorem (Eq. (3.38)), which could cause consequences in practice. In **Pub. 4** we examine the BJ potential regarding the consequences that arise due to the violation of the zero-force theorem. The theorem is strongly violated for the Na₅ cluster and leads to an unstable time propagation (*cf.* Sec. 3.2). It is another evidence that the BJ potential is not a functional derivative and that the potential in this form cannot be used for calculating CT excitations reliably.

The question is if we can save the idea of having a semi-local potential expression to calculate CT excitations in a computationally inexpensive way. In **Pub. 4** we examine a procedure that maps a given potential that is not a functional derivative into a potential that is functional derivative. We define an energy functional that is based on the given potential by performing a density line integral with a parameter λ from $\rho_{\lambda=0}(\mathbf{r}) = 0$ to $\rho_{\lambda=1}(\mathbf{r}) = n(\mathbf{r})$ ¹⁶³

$$\tilde{E}[n] = \int_0^1 d\lambda \int d^3r v_{xc}([\rho_\lambda], \mathbf{r}) \frac{d\rho_\lambda(\mathbf{r})}{d\lambda}. \quad (6.8)$$

If the inserted potential v_{xc} already is a functional derivative of an energy $E_{xc}[n]$, then Eq. (6.8) restores the same energy functional $\tilde{E}_{xc}[n] = E_{xc}[n]$. Otherwise Eq. (6.8) defines a new xc density functional with the corresponding potential

$$\tilde{v}_{xc}[n](\mathbf{r}) = \frac{\delta}{\delta n(\mathbf{r})} \tilde{E}_{xc}[n] \quad (6.9)$$

that is different from the original expression and is a functional derivative per definition. The hope is that all crucial features of the original potential are preserved by the mapping. We illustrate the transformation procedure in Fig. 6.1. Note that the mapping from $v_{xc}[n]$ to $\tilde{v}_{xc}[n]$ is not unique. In fact, there exists an infinite number of density paths ρ_λ and therefore an infinite number of mappings. In **Pub. 4** we applied the mapping to the BJ correction term v_σ^c and the B88 exchange hole potential for two different density paths ρ_λ (which allow an analytical evaluation of Eq. (6.8)). In both cases the newly defined potentials differ substantially from the original expression for one-orbital densities. Thus, the transformation does not preserve the attractive features of the BJ potential although it is very close to the exact KS exchange potential (which is a functional derivative).

One might argue that a more satisfying mapping is possible if we could find a better density path for Eq. (6.8), that minimizes the discrepancies between $v_{xc}[n]$ and $\tilde{v}_{xc}[n]$. However, so far we do not know any indication how to find such a path and whether the integral of Eq. (6.8) can be performed analytically. The path dependence of the procedure is analogous to the path dependence of the mechanical work for a non-conservative force in classical mechanics. Note that the whole chapter is based on the KS framework, *i.e.*, we assume

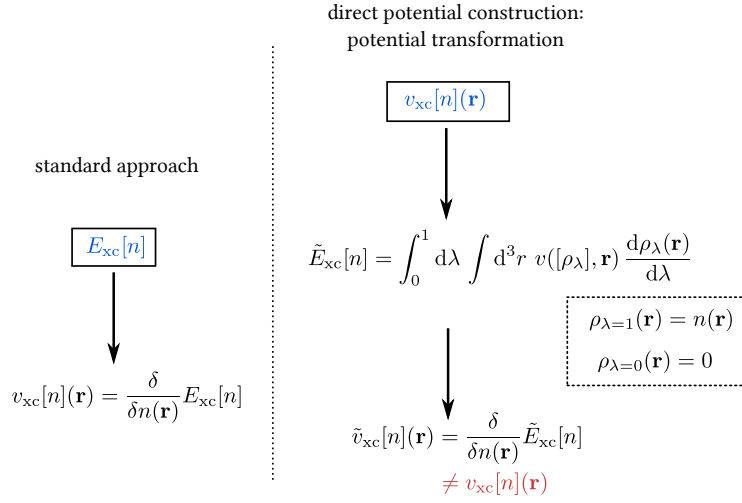


Figure 6.1. *Left:* Standard functional development approach starting with the construction of an energy functional. *Right:* Mapping of a directly constructed potential approximation into a potential that is functional derivative.

multiplicative potentials in contrast to the generally orbital specific potential of GKS theory.

We conclude that the direct potential approximation approach and, in particular, the BJ potential, is an attractive idea to handle non-local electronic response in DFT. The BJ potential is an ideal candidate due to its dependence on only semi-local ingredients. However, the line integral procedure is not suitable to transform directly constructed potentials into functional derivatives. Thus, so far it is not possible to transform the BJ potential into a proper functional that would obey the zero-force theorem. Further development of direct potential expressions might focus on approaches that directly fulfill Eq. (6.6). It is also possible to analyze how the BJ potential incorporates the derivative discontinuity and try to built this feature into a semi-local energy density.¹⁶⁴

Acknowledgments

I am grateful to everyone who supported me directly or indirectly during my work on this thesis. Thanks to all research fellows I was working with, to all members and alumni of the group of Stephan Kümmel and many others from the department of physics at the University of Bayreuth, and to the group of Leor Kronik at the Weizmann Institute of Science. Especially, I want to thank ...

Stephan Kümmel, the supervisor of my thesis and my boss. I am thankful that he treated me like a friend and that he is not the kind of person who just squeezes PhD students for more papers. I greatly acknowledge all the opportunities for working abroad and visiting conferences. I will never forget the positive aura of expertise, patience, enthusiasm, calm and trust that I experienced so many times when entering his office.

Leor Kronik, the second mentor of my thesis. Most of the above words about Stephan also apply to Leor. I thank him for inviting me to the Weizmann Institute of Science, organizing a warm winter in Israel for me and the many inspiring discussions about my thesis. I also greatly acknowledge endless discussions with *Eli Kraisler* and *Sivan Refaely-Abramson* and that they made my time in Israel unforgettable. I also thank *Ofer Sinai*, *Anna Hirsch* and *Ariel Biller* for their warm support.

Mukundan Thelakkat, the third mentor of my thesis, and *Anne Neubig* from Makromolekulare Chemie I for the great experimental collaboration. I gained many insights into the work of experimental chemists and was also allowed in the lab to produce organic films and field effect transistors of the same systems that I calculated. We immensely reduced many gaps like optical gaps, HOMO–LUMO gaps and language gaps between theoretical physicists and experimental chemists. I also thank *Ruth Lohwasser* for her support.

John P. Perdew for discussions and sharing his perspective of density functional theory with me during my visit to Tulane University. I also thank *Jianwei Sun* for discussions and his support during my time in New Orleans.

Roi Baer and *Tamar Stein* from the Hebrew University of Jerusalem for their support in setting up QChem and discussions about range-separated hybrids.

Monika Birkelbach, *Claudia Masuch*, *Markus Hilt*, and *Bernhard Winkler* from the University of Bayreuth and *Ana Naamat* from the Weizmann Institute

of Science for administrative and technical support.

I especially want to thank the people I meet (nearly) every day. They are the reason why I was always happy when going to work in the morning.

Linn Leppert, my office mate for four years and a very close friend for a couple of years more. I cannot think of any topic that did not went through a deep discussion in our office. I deeply admire Linn's general education and her talents. She inspired me in so many ways through her endless source of well-thought opinions on many important questions in life.

Tobias Schmidt, my functional derivative peer, very close friend for so many years and nearly-brother. Thanks to him for always knowing when I needed support and some cheering up.

Matthias Dauth, *Thiago Branquinho de Queiroz* and *Dirk Hofmann* for many discussions about DFT. Thanks to all members of the Kümmel group for the excellent atmosphere. When I left the other offices I was usually smiling or exhausted from all the laughing, especially after a visit with Matze and Tobi.

Fritz, my life coach and close friend.

My parents *Rita* and *Klaus* and my brother *Dominik* for “never” questioning what I was actually doing all the time at university.

After this long list of positive experiences during my PhD time it is hard to imagine why I will finally submit my thesis and end my nice time in Bayreuth. I have my reasons. *Resa*. You were always my light. Now, the light (and we) do not have to travel 230 km anymore.

I thank Linn, Tobi, Matze, Thiago and Resa for proof-reading my thesis.

For financial support I am grateful to German Academic Exchange Service (DAAD), Research Training Group 1640 “Photophysics of Synthetic and Biological Multichromophoric Systems” (*Jürgen Köhler*, *Mukundan Thelakkat*, *Stephan Kümmel*) of Deutsche Forschungsgemeinschaft, Elite Study Program Macromolecular Science (*Hans-Werner Schmidt*) of the Elite Network of Bavaria, the German-Israeli Foundation, the Wilhelm und Else Heraeus-Stiftung and the University of Bayreuth.

List of Abbreviations

A	acceptor: electron-deficient unit in DA systems	
\bar{A}	electron conducting material (acceptor) of an OPV device	
B3LYP	Becke 3-parameter hybrid functional with Lee-Yang-Parr correlation ⁸³	
B88	Becke exchange functional from 1988	16
BJ	Becke-Johnson potential approximation	
BNL	Baer, Neuhauser, Livshits functional ^{94,99}	35
<q>-BTT	DA arrangements of $2n$ thiophene (T) as donor and n 2,1,3-benzothiadiazole (B) as acceptor, $\langle q \rangle = a$ (alternating), $r1$ and $r2$ (random), b (diblock)	
CT	charge transfer	4
DFT	density functional theory	4
D	donor: electron-rich unit in DA systems	
\bar{D}	hole conducting material (donor) of an OPV device	
DA	donor-acceptor	2
EXX	exact exchange	18
GGA	generalized gradient approximation	16
GKS	generalized Kohn-Sham	4
HF	Hartree-Fock	16
HF-KS	Hartree-Fock Kohn-Sham scheme	30
HOMO	highest occupied (molecular) orbital	
KLI	Krieger, Li, and Iafrate approximation	56
KS	Kohn-Sham	4
LDA	local density approximation	15
LUMO	lowest unoccupied (molecular) orbital	
LYP	Lee, Yang, and Parr correlation functional	16
NDI-1	see NDI-x with $x = 1$	

NDI-<i>x</i>	<i>N, N</i> -diisopropyl-2,6-di(<i>x</i>) naphthalene-1,4,5,8-tetracarboxylic acid diimide (<i>x</i> stands for 1: thiophen-2-yl, 2: α -bithiophen-5-yl, etc. up to α -septithiophene (details in Pub. 1)	
OEP	optimized effective potential.....	18
OFET	organic field effect transistor.....	46
OPV	organic photovoltaic device.....	1
PBE	Perdew, Burke, and Ernzerhof exchange correlation functional	16
PBE0	Hybrid functional based on the PBE generalized gradient functional without empirical parameters.	
RSH	range-separated hybrid functional.....	5
sl	semi-local density dependence (used in the context of xc functional approximations)	
TDDFT	time-dependent DFT	4
TD-GKS	time-dependent generalized Kohn-Sham.....	35
TD-KS	time-dependent Kohn-Sham.....	21
UV/vis	ultraviolet–visible spectroscopy.....	45
xc	exchange-correlation.....	11
ω PBE	RSH functional of Scuseria and co-workers.....	35
ω B97(x)	range-separated hybrid functional of Chai and Head-Gordon ⁹⁵	

Bibliography

- [1] Bundesministerium für Umwelt, Naturschutz und Reaktorsicherheit (BMU), *Zeitreihen zur Entwicklung der erneuerbaren Energien in Deutschland*, accessed Oct. 12, 2013, <http://www.erneuerbare-energien.de/die-themen/datenservice/zeitreihen-entwicklung-ab-1990/>.
- [2] C. W. Tang, *Appl. Phys. Lett.*, 1986, **48**, 183.
- [3] B. O'Regan and M. Grätzel, *Nature*, 1991, **353**, 737–740.
- [4] N. S. Sariciftci, D. Braun, C. Zhang, V. I. Srdanov, A. J. Heeger, G. Stucky and F. Wudl, *Appl. Phys. Lett.*, 1993, **62**, 585.
- [5] M. C. Scharber, D. Mühlbacher, M. Koppe, P. Denk, C. Waldauf, A. J. Heeger and C. J. Brabec, *Adv. Mater.*, 2006, **18**, 789–794.
- [6] S. Günes, H. Neugebauer and N. S. Sariciftci, *Chem. Rev.*, 2007, **107**, 1324–1338.
- [7] R. Kroon, M. Lenes, J. C. Hummelen, P. W. M. Blom and B. de Boer, *Polym. Rev.*, 2008, **48**, 531–582.
- [8] B. Kippelen and J.-L. Brédas, *Energy Environ. Sci.*, 2009, **2**, 251–261.
- [9] F. C. Krebs, *Sol. Energ. Mat. Sol. Cells*, 2009, **93**, 394–412.
- [10] M. Hösel, R. R. Søndergaard, M. Jørgensen and F. C. Krebs, *Energy Technol.*, 2013, **1**, 102–107.
- [11] C. Koidis, S. Logothetidis, S. Kassavetis, C. Kapnopoulos, P. Karagiannidis, D. Georgiou and A. Laskarakis, *Sol. Energ. Mat. Sol. Cells*, 2013, **112**, 36–46.
- [12] J.-L. Brédas, J. E. Norton, J. Cornil and V. Coropceanu, *Acc. Chem. Res.*, 2009, **42**, 1691–1699.
- [13] T. M. Clarke and J. R. Durrant, *Chem. Rev.*, 2010, **110**, 6736–6767.

- [14] S. Cho, J. H. Seo, S. H. Park, S. Beaupré, M. Leclerc and A. J. Heeger, *Adv. Mater.*, 2010, **22**, 1253–1257.
- [15] Y. Liang, Z. Xu, J. Xia, S.-T. Tsai, Y. Wu, G. Li, C. Ray and L. Yu, *Adv. Mater.*, 2010, **22**, E135–E138.
- [16] G.-Y. Chen, Y.-H. Cheng, Y.-J. Chou, M.-S. Su, C.-M. Chen and K.-H. Wei, *Chem. Commun.*, 2011, **47**, 5064–5066.
- [17] K.-H. Ong, S.-L. Lim, H.-S. Tan, H.-K. Wong, J. Li, Z. Ma, L. C. H. Moh, S.-H. Lim, J. C. de Mello and Z.-K. Chen, *Adv. Mater.*, 2011, **23**, 1409–1413.
- [18] R. G. Parr and W. Yang, *Density-Functional Theory of Atoms and Molecules*, Oxford University Press, 1989.
- [19] R. M. Dreizler and E. K. E. K. U. Gross, *Density Functional Theory: An Approach to the Quantum Many- Body Problem*, Springer-Verlag, 1990.
- [20] J. P. Perdew and S. Kurth, in *A Primer in Density Functional Theory*, ed. C. Fiolhais, F. Nogueira and M. A. L. Marques, Springer Berlin Heidelberg, 2003, pp. 1–55.
- [21] E. Engel and R. M. Dreizler, *Density Functional Theory: An Advanced Course*, Springer, 2011.
- [22] C. A. Ullrich, *Time-Dependent Density-Functional Theory: Concepts and Applications*, Oxford University Press, 2012.
- [23] M. Born and R. Oppenheimer, *Ann. Phys.*, 1927, **389**, 457–484.
- [24] W. Ritz, *J. Reine Angew. Math.*, 1909, **135**, 1–61.
- [25] P. Hohenberg and W. Kohn, *Phys. Rev.*, 1964, **136**, B864–B871.
- [26] W. Kohn and L. J. Sham, *Phys. Rev.*, 1965, **140**, A1133–A1138.
- [27] U. v. Barth and L. Hedin, *J. Phys. C: Solid State Phys.*, 1972, **5**, 1629.
- [28] C.-O. Almbladh and U. von Barth, *Phys. Rev. B*, 1985, **31**, 3231–3244.
- [29] A. Görling, *Phys. Rev. A*, 1996, **54**, 3912–3915.
- [30] J. P. Perdew, R. G. Parr, M. Levy and J. L. Balduz, *Phys. Rev. Lett.*, 1982, **49**, 1691–1694.
- [31] J. P. Perdew and M. Levy, *Phys. Rev. Lett.*, 1983, **51**, 1884–1887.
- [32] A. Ruzsinszky, J. P. Perdew, G. I. Csonka, O. A. Vydrov and G. E. Scuseria, *J. Chem. Phys.*, 2006, **125**, 194112–194112–8.

- [33] P. Mori-Sánchez, A. J. Cohen and W. Yang, *J. Chem. Phys.*, 2006, **125**, 201102–201102–4.
- [34] A. Ruzsinszky, J. P. Perdew, G. I. Csonka, O. A. Vydrov and G. E. Scuseria, *J. Chem. Phys.*, 2007, **126**, 104102–104102–8.
- [35] J. P. Perdew and A. Zunger, *Phys. Rev. B*, 1981, **23**, 5048–5079.
- [36] S. H. Vosko, L. Wilk and M. Nusair, *Can. J. Phys.*, 1980, **58**, 1200–1211.
- [37] J. P. Perdew and Y. Wang, *Phys. Rev. B*, 1992, **45**, 13244–13249.
- [38] D. M. Ceperley and B. J. Alder, *Phys. Rev. Lett.*, 1980, **45**, 566–569.
- [39] A. D. Becke, *Phys. Rev. A*, 1988, **38**, 3098–3100.
- [40] C. Lee, W. Yang and R. G. Parr, *Phys. Rev. B*, 1988, **37**, 785–789.
- [41] R. Colle and O. Salvetti, *Theoret. Chim. Acta*, 1975, **37**, 329–334.
- [42] J. P. Perdew, K. Burke and M. Ernzerhof, *Phys. Rev. Lett.*, 1996, **77**, 3865–3868.
- [43] J. P. Perdew, S. Kurth, A. Zupan and P. Blaha, *Phys. Rev. Lett.*, 1999, **82**, 2544–2547.
- [44] J. Tao, J. P. Perdew, V. N. Staroverov and G. E. Scuseria, *Phys. Rev. Lett.*, 2003, **91**, 146401.
- [45] R. T. Sharp and G. K. Horton, *Phys. Rev.*, 1953, **90**, 317–317.
- [46] J. D. Talman and W. F. Shadwick, *Phys. Rev. A*, 1976, **14**, 36–40.
- [47] T. Grabo, T. Kreibich and E. K. U. Gross, *Mol. Eng.*, 1997, **7**, 27–50.
- [48] J. B. Krieger, Y. Li and G. J. Iafrate, *Phys. Rev. A*, 1992, **45**, 101–126.
- [49] J. B. Krieger, Y. Li and G. J. Iafrate, *Phys. Rev. A*, 1992, **46**, 5453–5458.
- [50] S. Kümmel and L. Kronik, *Rev. Mod. Phys.*, 2008, **80**, 3–60.
- [51] A. Ruzsinszky, J. P. Perdew, G. I. Csonka, G. E. Scuseria and O. A. Vydrov, *Phys. Rev. A*, 2008, **77**, 060502.
- [52] C. D. Pemmaraju, S. Sanvito and K. Burke, *Phys. Rev. B*, 2008, **77**, 121204.
- [53] T. Körzdörfer, S. Kümmel and M. Mundt, *J. Chem. Phys.*, 2008, **129**, 014110–014110–12.

- [54] T. Körzdörfer, M. Mundt and S. Kümmel, *Phys. Rev. Lett.*, 2008, **100**, 133004.
- [55] D. Hofmann, T. Körzdörfer and S. Kümmel, *Phys. Rev. Lett.*, 2012, **108**, 146401.
- [56] D. Hofmann and S. Kümmel, *J. Chem. Phys.*, 2012, **137**, 064117–064117–17.
- [57] D. Hofmann and S. Kümmel, *Phys. Rev. B*, 2012, **86**, 201109.
- [58] M. A. L. Marques and E. K. U. Gross, in *A Primer in Density Functional Theory*, ed. C. Fiolhais, F. Nogueira and M. A. L. Marques, Springer Berlin Heidelberg, 2003, pp. 144–184.
- [59] A. Dreuw and M. Head-Gordon, *Chem. Rev.*, 2005, **105**, 4009–4037.
- [60] M. Marques, *Time-Dependent Density Functional Theory*, Springer, 2006.
- [61] M. E. Casida, *J. Mol. Struct.: THEOCHEM*, 2009, **914**, 3–18.
- [62] M. A. L. Marques, N. T. Maitra and F. M. S. Nogueira, *Fundamentals of Time-Dependent Density Functional Theory*, Springer, 2012.
- [63] E. Runge and E. K. U. Gross, *Phys. Rev. Lett.*, 1984, **52**, 997–1000.
- [64] R. van Leeuwen, *Phys. Rev. Lett.*, 1999, **82**, 3863–3866.
- [65] R. van Leeuwen, *Phys. Rev. Lett.*, 1998, **80**, 1280–1283.
- [66] A. Castro, M. A. L. Marques and A. Rubio, *J. Chem. Phys.*, 2004, **121**, 3425–3433.
- [67] A. Castro and M. a. L. Marques, in *Time-Dependent Density Functional Theory*, ed. M. A. L. Marques, C. A. Ullrich, F. Nogueira, A. Rubio, K. Burke and E. K. U. Gross, Springer Berlin Heidelberg, 2006, pp. 197–210.
- [68] K. Yabana and G. F. Bertsch, *Phys. Rev. B*, 1996, **54**, 4484–4487.
- [69] F. Calvayrac, P. Reinhard and E. Suraud, *Ann. Phys.*, 1997, **255**, 125–162.
- [70] M. Mundt and S. Kümmel, *Phys. Rev. B*, 2007, **76**, 035413.
- [71] M. Mundt, *Ph.D. thesis*, Universität Bayreuth, 2007.
- [72] M. E. Casida, in *Recent Advances in Density Functional Methods*, ed. D. P. Chong, WORLD SCIENTIFIC, 1995, vol. 1, pp. 155–192.

- [73] M. E. Casida, in *Theoretical and Computational Chemistry*, ed. J.M. Seminario, Elsevier, 1996, vol. Volume 4, pp. 391–439.
- [74] M. Thiele, E. K. U. Gross and S. Kümmel, *Phys. Rev. Lett.*, 2008, **100**, 153004.
- [75] E. K. U. Gross, J. F. Dobson and M. Petersilka, in *Density Functional Theory II*, ed. P. R. F. Nalewajski, Springer Berlin Heidelberg, 1996, pp. 81–172.
- [76] G. Vignale, *Phys. Rev. Lett.*, 1995, **74**, 3233–3236.
- [77] M. Mundt, S. Kümmel, R. van Leeuwen and P.-G. Reinhard, *Phys. Rev. A*, 2007, **75**, 050501.
- [78] G. Vignale, *Phys. Lett. A*, 1995, **209**, 206–210.
- [79] A. Seidl, A. Görling, P. Vogl, J. A. Majewski and M. Levy, *Phys. Rev. B*, 1996, **53**, 3764–3774.
- [80] A. D. Becke, *J. Chem. Phys.*, 1993, **98**, 1372–1377.
- [81] T. Körzdörfer and S. Kümmel, *Phys. Rev. B*, 2010, **82**, 155206.
- [82] J. P. Perdew, M. Ernzerhof and K. Burke, *J. Chem. Phys.*, 1996, **105**, 9982–9985.
- [83] P. J. Stephens, F. J. Devlin, C. F. Chabalowski and M. J. Frisch, *J. Phys. Chem.*, 1994, **98**, 11623–11627.
- [84] S. F. Sousa, P. A. Fernandes and M. J. Ramos, *J. Phys. Chem. A*, 2007, **111**, 10439–10452.
- [85] A. D. Becke, *J. Chem. Phys.*, 1993, **98**, 5648–5652.
- [86] C. Adamo and V. Barone, *J. Chem. Phys.*, 1999, **110**, 6158–6170.
- [87] A. Savin and H.-J. Flad, *Int. J. Quant. Chem.*, 1995, **56**, 327–332.
- [88] T. Leininger, H. Stoll, H.-J. Werner and A. Savin, *Chem. Phys. Lett.*, 1997, **275**, 151–160.
- [89] A. Savin, in *Recent Developments and Applications of Modern Density Functional Theory*, ed. J. M. Seminario, Elsevier, 1996, pp. 327–357.
- [90] H. Iikura, T. Tsuneda, T. Yanai and K. Hirao, *J. Chem. Phys.*, 2001, **115**, 3540–3544.
- [91] T. M. Henderson, B. G. Janesko and G. E. Scuseria, *J. Chem. Phys.*, 2008, **128**, 194105–194105–9.

- [92] T. Yanai, D. P. Tew and N. C. Handy, *Chem. Phys. Lett.*, 2004, **393**, 51–57.
- [93] J.-W. Song, T. Hirose, T. Tsuneda and K. Hirao, *J. Chem. Phys.*, 2007, **126**, 154105–154105–7.
- [94] E. Livshits and R. Baer, *Phys. Chem. Chem. Phys.*, 2007, **9**, 2932–2941.
- [95] J.-D. Chai and M. Head-Gordon, *J. Chem. Phys.*, 2008, **128**, 084106–084106–15.
- [96] M. A. Rohrdanz, K. M. Martins and J. M. Herbert, *J. Chem. Phys.*, 2009, **130**, 054112–054112–8.
- [97] R. Baer, E. Livshits and U. Salzner, *Annu. Rev. Phys. Chem.*, 2010, **61**, 85–109.
- [98] L. Kronik, T. Stein, S. Refaely-Abramson and R. Baer, *J. Chem. Theory Comput.*, 2012, **8**, 1515–1531.
- [99] R. Baer and D. Neuhauser, *Phys. Rev. Lett.*, 2005, **94**, 043002.
- [100] O. A. Vydrov, G. E. Scuseria and J. P. Perdew, *J. Chem. Phys.*, 2007, **126**, 154109–154109–9.
- [101] T. Tsuneda, J.-W. Song, S. Suzuki and K. Hirao, *J. Chem. Phys.*, 2010, **133**, 174101–174101–9.
- [102] S. Refaely-Abramson, S. Sharifzadeh, N. Govind, J. Autschbach, J. B. Neaton, R. Baer and L. Kronik, *Phys. Rev. Lett.*, 2012, **109**, 226405.
- [103] M. Srebro and J. Autschbach, *J. Phys. Chem. Lett.*, 2012, **3**, 576–581.
- [104] T. Stein, J. Autschbach, N. Govind, L. Kronik and R. Baer, *J. Phys. Chem. Lett.*, 2012, **3**, 3740–3744.
- [105] A. Savin, C. Umrigar and X. Gonze, *Chem. Phys. Lett.*, 1998, **288**, 391–395.
- [106] A. Görling and M. Levy, *Phys. Rev. A*, 1995, **52**, 4493–4499.
- [107] M. Städele, J. A. Majewski, P. Vogl and A. Görling, *Phys. Rev. Lett.*, 1997, **79**, 2089–2092.
- [108] M. Städele, M. Moukara, J. A. Majewski, P. Vogl and A. Görling, *Phys. Rev. B*, 1999, **59**, 10031–10043.
- [109] A. Görling and M. Levy, *J. Chem. Phys.*, 1997, **106**, 2675–2680.
- [110] J. P. Perdew and M. Levy, *Phys. Rev. B*, 1997, **56**, 16021–16028.

- [111] D. J. Tozer, R. D. Amos, N. C. Handy, B. O. Roos and L. Serrano-ANDRES, *Mol. Phys.*, 1999, **97**, 859–868.
- [112] Z.-L. Cai, K. Sendt and J. R. Reimers, *J. Chem. Phys.*, 2002, **117**, 5543–5549.
- [113] A. Dreuw, J. L. Weisman and M. Head-Gordon, *J. Chem. Phys.*, 2003, **119**, 2943–2946.
- [114] D. J. Tozer, *J. Chem. Phys.*, 2003, **119**, 12697–12699.
- [115] A. Dreuw and M. Head-Gordon, *J. Am. Chem. Soc.*, 2004, **126**, 4007–4016.
- [116] R. S. Mulliken, *J. Am. Chem. Soc.*, 1952, **74**, 811–824.
- [117] M. Petersilka, U. J. Gossmann and E. K. U. Gross, *Phys. Rev. Lett.*, 1996, **76**, 1212–1215.
- [118] X. Gonze and M. Scheffler, *Phys. Rev. Lett.*, 1999, **82**, 4416–4419.
- [119] H. Appel, E. K. U. Gross and K. Burke, *Phys. Rev. Lett.*, 2003, **90**, 043005.
- [120] O. Gritsenko and E. J. Baerends, *J. Chem. Phys.*, 2004, **121**, 655–660.
- [121] N. T. Maitra, *J. Chem. Phys.*, 2005, **122**, 234104–6.
- [122] M. Hellgren and E. K. U. Gross, *Phys. Rev. A*, 2012, **85**, 022514.
- [123] T. Ziegler, M. Seth, M. Krykunov, J. Autschbach and F. Wang, *J. Mol. Struct.: THEOCHEM*, 2009, **914**, 106–109.
- [124] J. Autschbach, *ChemPhysChem*, 2009, **10**, 1757–1760.
- [125] Y. Tawada, T. Tsuneda, S. Yanagisawa, T. Yanai and K. Hirao, *J. Chem. Phys.*, 2004, **120**, 8425–8433.
- [126] M. A. Rohrdanz and J. M. Herbert, *J. Chem. Phys.*, 2008, **129**, 034107–034107–9.
- [127] B. M. Wong and J. G. Cordaro, *J. Chem. Phys.*, 2008, **129**, 214703–214703–8.
- [128] S. Refaely-Abramson, R. Baer and L. Kronik, *Phys. Rev. B*, 2011, **84**, 075144.
- [129] T. Stein, H. Eisenberg, L. Kronik and R. Baer, *Phys. Rev. Lett.*, 2010, **105**, 266802.

- [130] T. Körzdörfer, J. S. Sears, C. Sutton and J.-L. Brédas, *J. Chem. Phys.*, 2011, **135**, 204107–204107–6.
- [131] N. Kuritz, T. Stein, R. Baer and L. Kronik, *J. Chem. Theory Comput.*, 2011, **7**, 2408–2415.
- [132] T. Stein, L. Kronik and R. Baer, *J. Am. Chem. Soc.*, 2009, **131**, 2818–2820.
- [133] M. Srebro and J. Autschbach, *J. Chem. Theory Comput.*, 2012, **8**, 245–256.
- [134] M. Parac and S. Grimme, *Chem. Phys.*, 2003, **292**, 11–21.
- [135] J. Tao, S. Tretiak and J.-X. Zhu, *J. Phys. Chem. B*, 2008, **112**, 13701–13710.
- [136] J. Tao, S. Tretiak and J.-X. Zhu, *J. Chem. Phys.*, 2008, **128**, 084110.
- [137] P. Elliott, F. Furche and K. Burke, in *Reviews in Computational Chemistry*, ed. K. B. Lipkowitz and T. R. Cundari, John Wiley & Sons, Inc., 2009, p. 91–165.
- [138] D. Jacquemin, V. Wathelet, E. A. Perpète and C. Adamo, *J. Chem. Theory Comput.*, 2009, **5**, 2420–2435.
- [139] E. A. Perpète and D. Jacquemin, *J. Mol. Struct.: THEOCHEM*, 2009, **914**, 100–105.
- [140] D. Rappoport and F. Furche, *J. Am. Chem. Soc.*, 2004, **126**, 1277–1284.
- [141] H. Yan, Z. Chen, Y. Zheng, C. Newman, J. R. Quinn, F. Dötz, M. Kastler and A. Facchetti, *Nature*, 2009, **457**, 679–686.
- [142] E. Ahmed, G. Ren, F. S. Kim, E. C. Hollenbeck and S. A. Jenekhe, *Chem. Mater.*, 2011, **23**, 4563–4577.
- [143] R. L. Martin, *J. Chem. Phys.*, 2003, **118**, 4775–4777.
- [144] A. Karolewski, R. Armiento and S. Kümmel, *J. Chem. Theory Comput.*, 2009, **5**, 712–718.
- [145] L. Pandey, C. Doiron, J. S. Sears and J.-L. Brédas, *Phys. Chem. Chem. Phys.*, 2012, **14**, 14243–14248.
- [146] I. C. Gerber and J. G. Ángyán, *Chem. Phys. Lett.*, 2005, **415**, 100–105.
- [147] M. J. G. Peach, T. Helgaker, P. Sałek, T. W. Keal, O. B. Lutnæs, D. J. Tozer and N. C. Handy, *Phys. Chem. Chem. Phys.*, 2006, **8**, 558–562.

- [148] O. A. Vydrov and G. E. Scuseria, *J. Chem. Phys.*, 2006, **125**, 234109.
- [149] R. van Leeuwen and E. J. Baerends, *Phys. Rev. A*, 1994, **49**, 2421–2431.
- [150] A. D. Becke and E. R. Johnson, *J. Chem. Phys.*, 2006, **124**, 221101–221101–4.
- [151] R. v. Leeuwen, O. Gritsenko and E. J. Baerends, *Z. Phys. D: At., Mol. Clusters*, 1995, **33**, 229–238.
- [152] R. Armiento, S. Kümmel and T. Körzdörfer, *Phys. Rev. B*, 2008, **77**, 165106.
- [153] B. Champagne, E. A. Perpète, S. J. A. van Gisbergen, E.-J. Baerends, J. G. Snijders, C. Soubra-Ghaoui, K. A. Robins and B. Kirtman, *J. Chem. Phys.*, 1998, **109**, 10489.
- [154] S. J. A. van Gisbergen, P. R. T. Schipper, O. V. Gritsenko, E. J. Baerends, J. G. Snijders, B. Champagne and B. Kirtman, *Phys. Rev. Lett.*, 1999, **83**, 694–697.
- [155] M. van Faassen, P. L. de Boeij, R. van Leeuwen, J. A. Berger and J. G. Snijders, *Phys. Rev. Lett.*, 2002, **88**, 186401.
- [156] P. Mori-Sánchez, Q. Wu and W. Yang, *J. Chem. Phys.*, 2003, **119**, 11001.
- [157] S. Kümmel, L. Kronik and J. P. Perdew, *Phys. Rev. Lett.*, 2004, **93**, 213002.
- [158] N. T. Maitra and M. van Faassen, *J. Chem. Phys.*, 2007, **126**, 191106.
- [159] F. Tran, P. Blaha and K. Schwarz, *J. Phys.: Condens. Matter*, 2007, **19**, 196208.
- [160] S. Kümmel and L. Kronik, *Comput. Mater. Sci.*, 2006, **35**, 321–326.
- [161] A. P. Gaiduk and V. N. Staroverov, *J. Chem. Phys.*, 2008, **128**, 204101–204101–6.
- [162] A. P. Gaiduk and V. N. Staroverov, *J. Chem. Phys.*, 2009, **131**, 044107–044107–7.
- [163] R. van Leeuwen and E. J. Baerends, *Phys. Rev. A*, 1995, **51**, 170–178.
- [164] R. Armiento and S. Kümmel, *Phys. Rev. Lett.*, 2013, **111**, 036402.

Part II

Publications

Publication 1

Communication: Tailoring the optical gap in light-harvesting molecules

A. Karolewski, T. Stein, R. Baer, and S. Kümmel,
J. Chem. Phys. **134**, 151101 (2011).

© 2011 American Institute of Physics
DOI: 10.1063/1.3581788

1

Own Contribution

I did all calculations and wrote the first version of the manuscript. T. Stein gave me a first introduction into the use of QChem.

Communication: Tailoring the optical gap in light-harvesting molecules

A. Karolewski,¹ T. Stein,² R. Baer,² and S. Kümmel^{1,a)}¹Theoretical Physics IV, University of Bayreuth, D-95440 Bayreuth, Germany²Fritz Haber Center for Molecular Dynamics, Hebrew University, Jerusalem 91904, Israel

(Received 31 January 2011; accepted 1 April 2011; published online 21 April 2011)

Systematically varying the optical gap that is associated with charge-transfer excitations is an important step in the design of light-harvesting molecules. So far the guidance that time-dependent density functional theory could give in this process was limited by the traditional functionals' inability to describe charge-transfer excitations. We show that a nonempirical range-separated hybrid approach allows to reliably predict charge-transfer excitations for molecules of practically relevant complexity. Calculated absorption energies agree with measured ones. We predict from theory that by varying the number of thiophenes in donor-acceptor-donor molecules, the energy of the lowest optical absorption can be tuned to the lower end of the visible spectrum. Saturation sets in at about five thiophene rings.
© 2011 American Institute of Physics. [doi:10.1063/1.3581788]

Harvesting solar energy in organic electronic devices is an attractive option for satisfying future energy needs. An important aspect of such devices is to capture as large a part of the solar spectrum as possible and use the corresponding energy for charge separation. Therefore, systems in which the energy of optically active excitations with considerable charge-transfer (CT) character can be tuned in a well controlled way are of great interest. Synthesizing such systems can be a challenge, therefore *a priori* guidance from theory is highly desirable. Density functional theory (DFT) and time-dependent density functional theory (TDDFT) are generally very popular for computational studies of electronic systems due to their favorable ratio of accuracy to computational load.¹ However, in the past TDDFT has become (in)famous for its inability to accurately predict CT excitations.^{2,3} Theoretically, the reason for this deficiency is well understood.^{4,5} Commonly used functionals lack the steplike structures in the exchange-correlation (xc) potential that reflect particle-number discontinuities. The latter are a property of the exact time-dependent xc potential,⁶ but are not reproduced by standard functionals.

Orbital functionals incorporate particle number discontinuities by construction⁷ and, therefore, offer the potential to describe CT excitations with TDDFT. However, achieving the subtle balancing of self-interaction errors that is necessary for a quantitatively correct description of the above-mentioned steplike structures is a difficult task.⁸ Based on the range-separated hybrid functional idea that has proved a quite successful development in general,⁹⁻¹⁴ a functional has recently been devised¹⁵ based on two fundamental ideas. First, the range separation parameter must be system dependent and second, this system dependence can be determined in a nonempirical way by ensuring that the functional consistently agrees as close as possible with Mulliken's rule.^{16,17}

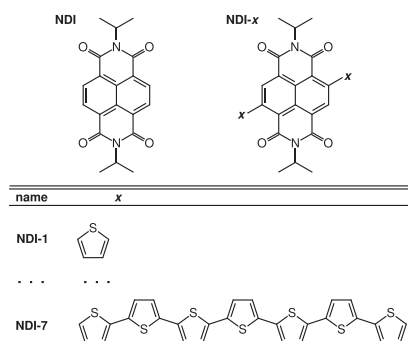
In previous studies, the new approach (there and in the following termed γ BNL functional) was applied to model systems with an emphasis on excitations of long-range CT character. However, from a light-harvesting perspective one is interested in excitations that can be excited optically. In this paper we show that the γ BNL functional works reliably in the practically most important case of excitations between closely connected molecular subunits and excitations of mixed valence and CT character that carry appreciable oscillator strength.

We calculated the photoresponse of a series of donor-acceptor systems carrying thiophenes as donor and naphthalene diimide (NDI) as acceptor. For some of the molecules we could compare the theoretical results to recently measured experimental data.¹⁸ Close agreement between theory and experiment is obtained. We demonstrate that the absorption energy can indeed be changed in an appreciable energy range by extending the donor parts of the molecules, and we theoretically predict the limit of how much the absorption energy can be modified in this way. With five thiophenes the lower end of the visible range is reached.

We study the molecules *N,N*-diisopropyl-2,6-di(*x*) naphthalene-1,4,5,8-tetracarboxylic acid diimide (*x* stands for 1: thiophen-2-yl, 2: α -bithiophen-5-yl, etc. up to α -septithiophene) which we abbreviate as NDI-*x* in the following. Their structure is schematically depicted in Fig. 1. We calculated the molecular geometry by minimizing the ground-state energy using the B3LYP functional¹⁹ and the def2-SV(P) basis set. B3LYP is known to yield reliable geometries for organic systems. However, we also checked the influence that using a different functional and basis set for the geometry optimization has on the excitation energies that are reported below. If the geometry is optimized using the PBE-GGA (Ref. 20) the B3LYP excitation energies change by 0.1 eV and if we use the def2-TZVP basis set, they change by 0.03 eV. Thus, the results are rather robust.

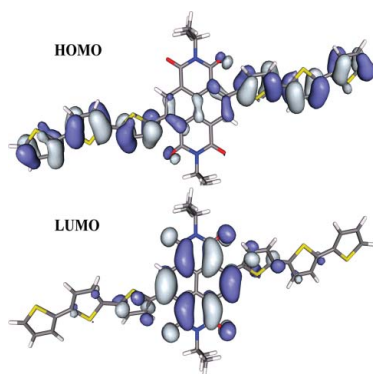
The NDI-*x* system is of practical interest because the lowest excitation energy of NDI-*x* is in the visible range and

^{a)}Author to whom correspondence should be addressed. Electronic mail: stephan.kuettel@uni-bayreuth.de.

FIG. 1. Structural formula of NDI and NDI- x .

has CT character. The CT character is visible in standard linear response TDDFT by looking at the particle-hole amplitudes of the excitation of interest. For example, for NDI-3 with B3LYP the excitation is dominantly (with an amplitude of 0.997) a transition from the HOMO to the LUMO. Inspecting these orbitals, shown in Fig. 2, clearly reveals the CT character of the corresponding excitation. However, it also shows that there is an appreciable overlap between the orbitals, making this a more complicated situation than the very long-range CT excitations which are frequently discussed in TDDFT literature^{7,21} and for which bare exact exchange can be sufficient. As shown in detail below, the NDI- x excitation carries appreciable oscillator strength.

Another aspect which makes the situation that we study here more complicated, but also more interesting, is the fact that NDI- x is not just a donor-acceptor system, but a donor-acceptor-donor arrangement. Combining alternating donor and acceptor units is one of the strategies for designing low band gap materials. This strategy has been successfully utilized to harvest the solar spectrum efficiently.²²⁻²⁴ Polymers based on NDI and thiophene units are known compounds for the use as electron acceptor (n type) materials. Such polymers have shown high electron mobilities up to

FIG. 2. Plot of HOMO and LUMO for NDI-3. The plots were obtained from DFT calculations with the γ BNL functional, see text. Orbitals from the B3LYP functional look almost identical.

0.8 cm²/Vs in organic field effect transistors.²⁵ A decisive question is the strength of the donor unit (i.e., the number of thiophene units) which is ideal for obtaining the maximum red-shift of the absorption band in the resulting donor-acceptor polymer.

In our study the conjugated electronic system of the donor subunits is varied by varying the number of thiophenes. As this changes the energy of the lowest optical absorption, NDI- x molecules with varying x absorb light at different wavelengths. Combining them in a device may thus allow to absorb a broader part of the electromagnetic spectrum while still using molecules that are chemically very similar, the latter being a major advantage for processing and device building.

It is not *a priori* clear, though, how much the absorption energy can be lowered by increasing the number of thiophene rings. Intuitively one expects that there must be a saturation effect, but at which extension, i.e., number of thiophene rings, the saturation sets in is hard to predict on general grounds. However, as we demonstrate in the following, the range-separated hybrid functional that we use here allows to predict it.

For NDI without thiophene donors the spectrum shows onset of absorption with a clear peak at about 3.25 eV and vibrational structure at higher energies.¹⁸ On going over to NDI-1 by adding thiophenes the peak structure at 3.25 eV and higher energies remains, but a new broad peak appears which is centered around 2.6 eV. Thus, the onset of optical absorption is shifted to lower energies. In NDI-2 this peak shifts further to 2.2 eV, i.e., to yet lower energies. This shows that the absorption can be tuned by increasing the donor system size. It is these low lying absorption peaks in NDI- x that are of practical interest and which will be the focus of our theoretical study.

Our calculations were carried out on NDI- x with short N -alkyl (isopropyl) substituents. We verified that the length of the N -alkyl substituents does not influence the electronic excitations. For calculating the absorption spectra of the NDI- x systems we adopt a range-separated hybrid functional.¹⁶ The physical idea behind this approach is to split the exchange term in a long-range and a short-range part via $r^{-1} = r^{-1} \text{erf}(\gamma r) + r^{-1} \text{erfc}(\gamma r)$. The short-range term is treated by means of a semilocal expression and the long-range term is treated exactly. Thus, the γ BNL functional does incorporate exact exchange which will contribute to cancel the spurious electronic self-interaction that is at the heart of the CT problems encountered with semilocal functionals. The range separation parameter γ defines the distance at which exact exchange becomes dominant, and the choice of γ is crucial for the quality of the theoretical results. In previous studies of the γ BNL approach, the most successful strategy was to adjust γ such that the ionization energy of the neutral donor and the acceptor anion correspond as close as possible to the HOMO eigenvalue of the neutral donor and the acceptor anion, respectively. This appears as a natural condition when a clear distinction between the donor and acceptor molecules is possible.

In our present study this is not the case. In NDI- x , one cannot distinguish unambiguously between donor and accep-

tor as the constituents are covalently bound and as we are looking at a donor-acceptor-donor instead of just a donor-acceptor system. Therefore, we employ a different strategy¹⁷ for adjusting γ which works with the molecule as a whole without the need to specify donor and acceptor. Yet, the fundamental physical principle according to which we adjust γ remains the same: The highest occupied eigenvalue of DFT should agree with the first ionization potential as calculated from total energy differences. For a given value of γ one can determine how well this condition is satisfied by evaluating the criterion

$$J2(\gamma) = |\epsilon_{\text{HOMO}}^{\gamma}(N) + \text{IP}^{\gamma}(N)| + |\epsilon_{\text{HOMO}}^{\gamma}(N+1) + \text{IP}^{\gamma}(N+1)|, \quad (1)$$

where $\epsilon_{\text{HOMO}}^{\gamma}$ is the HOMO energy and IP^{γ} is the ionization potential of the N and $N+1$ electron system, respectively. The range separation parameter γ is then adjusted in an iterative procedure such that $J2$ is minimized for each system. We stress that this adjustment is a nonempirical step as no experimental or other empirical information enters and as enforcing Eq. (1) simply amounts to enforce as good as possible an exact constraint which the ultimate functional would automatically fulfill.

Following this procedure we have calculated for NDI-1 to NDI-7 the values of γ which minimize $J2$ (see Table I). These were then used in TDDFT calculations of the excitation energies and oscillator strengths. Figure 3(a) shows the first excitation energies that were obtained in this way with the $J2$ -optimized γ BNL functional.^{26,34} For the reasons of clarity only the lowest excitation energy, which is the practically relevant one, is shown for each molecule. The experimentally measured excitation energies for NDI-1 and NDI-2 are marked as vertical lines in the plot.¹⁸ The γ BNL results for NDI-1 and NDI-2 are in good agreement with the corresponding experimental values, underestimating the experiment by about or less than 0.1 eV. A certain underestimation is plausible²⁷ as the experiments were conducted at room temperature and the calculations assumed 0 K. Thus, these results show that TDDFT can predict excitations of mixed CT and valence character with very reasonable accuracy.

The comparison with the lower panel of Fig. 3(b) shows that this is not a trivial result. Here, the excitations that are obtained from the popular B3LYP functional are shown. Clearly and as expected,²¹ B3LYP does not describe the CT excitations properly and the deviation between B3LYP on the one hand and the γ BNL results and experiment on the other is growing with increasing system size, i.e., with growing num-

TABLE I. First row: Range separation parameter γ for NDI- x obtained from minimizing the $J2$ criterion. γ was varied in steps of 0.005 (for NDI-6 and NDI-7 in steps of 0.001). Second row: The minimum value of $J2$ which was obtained at the end of the γ optimization. Hartree atomic units are used.

System	NDI-1	NDI-2	NDI-3	NDI-4	NDI-5	NDI-6	NDI-7
γ	0.180	0.160	0.145	0.140	0.135	0.132	0.131
$J2$	0.0040	0.0043	0.0042	0.0040	0.0034	0.0031	0.0028

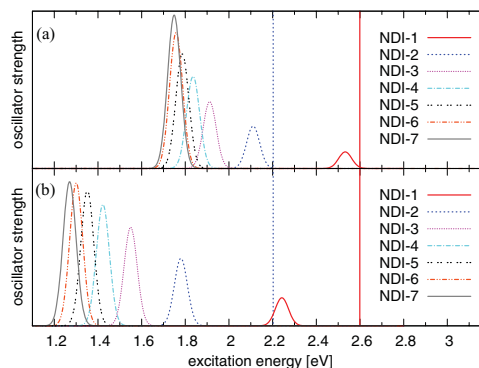


FIG. 3. First absorption peaks of the NDI- x systems calculated with linear response TDDFT. The peaks are broadened by Gaussian functions with a variance of 0.03 eV. The vertical lines indicate the maxima of the lowest experimentally observed absorption peaks (Ref. 18). a: γ BNL. b: B3LYP.

ber of thiophene rings. As a further test we have also used the ω B97 and the ω B97x xc-functionals. For NDI-3, the lowest excitation is at 2.81 and 2.69 eV, respectively, i.e., at unrealistic energies.

For understanding why the γ BNL approach is able to predict complicated excitations of mixed valence and CT character reliably one has to realize the decisive role which is played by the step in which γ is adjusted to fulfill Eq. (1). In this step the functional adapts to the system size and the character of the excitation. One may argue that the adjustment procedure makes γ a density functional—though a very implicit and also unfortunately very nonlocal one. This is confirmed by the optimal γ -values for the NDI- x systems that we report in Table I.

From NDI-1 to NDI-7 the system size increases and γ decreases. This is understandable as γ indicates the length at which exact exchange dominates the electron-electron interaction. To conserve the same characteristic balance between semilocal exchange and exact exchange γ has to increase from NDI-7 to NDI-1 as the average distance between donor and acceptor decreases.

The second row of Table I shows the minimum value of $J2$ that was obtained for each system. All values are close to zero, which indicates that optimizing γ with respect to the ionization potential theorem is a possible and reasonable strategy. Furthermore, we note that the minimum values that we obtain are nearly identical for NDI-1 to NDI-7. Thus, one can argue that the predictive power of γ BNL does not change with system size and that the calculated excitation energies of NDI-3 to NDI-7 can be expected to be of the same quality as the ones of NDI-1 and -2, which were verified by comparison with the experiments. Thus, we can use the TDDFT results to predict how much the lowest optical absorption can be shifted by adding thiophene rings to NDI.

However, before we do so we have to clarify two additional issues that are relevant for relating the TDDFT results to the experiments. First, we note that the theoretical numbers reported above were obtained for molecules in vacuum whereas the experimental excitations were

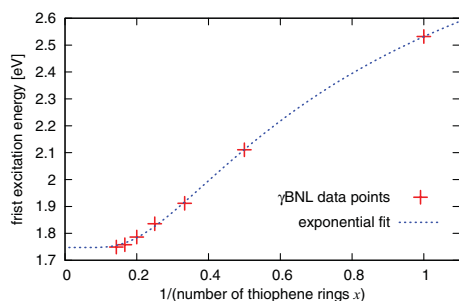


FIG. 4. Exponential fit of the calculated excitation energies to obtain the “infinite chain limit” value.

measured on molecules in a chloroform solution.¹⁸ We checked the influence of the chloroform solvent on our calculations with TURBOMOLE (COSMO) (Ref. 28) and QCHEM (CHEMSOL).²⁹ This changed the excitation energies by about 0.01 eV, showing that the solvent influence on the electronic transitions can here be neglected. Second, we carefully checked the influence of the basis set. Using a smaller basis set, e.g., 6-31G(d,p) instead of 6-311G(d,p), shifts the excitation energies closer to the experimental values by up to 0.07 eV. However, it is the 6-311G(d,p) basis set which we consider as numerically sufficient and whose numbers we, therefore, report here.

Having thus clarified the reliability of our numbers we finally proceed to investigate how far the lowest absorption of NDI- x molecules can be shifted to exploit the visible spectrum. Figure 4 shows the lowest absorption energies of the NDI- x molecules as a function of the inverse number of thiophene rings x . The amount by which the absorption energy drops on adding another thiophene ring falls off dramatically from NDI-1 to NDI-7. We extrapolate to the “infinite chain limit” by fitting an exponential function to the calculated excitation energies,^{30–33} and obtained a value of 1.75 eV, at the edge of the visible spectrum. Using a Kuhn or a combined Kuhn-exponential fit²⁷ results in a similar fit. In view of the accuracy limits of our theoretical prediction, NDI-5 with its absorption at 1.79 eV can be considered as being close to this limit.

In summary, we have investigated donor-acceptor-donor systems with NDI acting as the acceptor and thiophene rings acting as donors. Excitation energies were calculated using

TDDFT with a range-separated hybrid approach that fulfills the ionization potential theorem as close as possible via nonempirical adjustment of the range separation parameter. We showed that the practically relevant excitation in the NDI- x systems is predominantly of CT character. Our results are in agreement with the experimental numbers for NDI-1 and NDI-2. We predict that the NDI- x systems with up to $x=5$ rings already allows to cover the absorption up to the lower end of the visible range. TDDFT emerges as a powerful tool for helping in the design of light-harvesting molecules.

We acknowledge discussions with A. Neubig, M. Thelakkat, and T. Körzdörfer, and financial support by Deutsche Forschungsgemeinschaft (DFG) GRK1640 and the GIF.

- ¹D. Rappoport and F. Furche, *J. Am. Chem. Soc.* **126**, 1277 (2004).
- ²A. Dreuw and M. Head-Gordon, *J. Am. Chem. Soc.* **126**, 4007 (2004).
- ³K. Burke, J. Werschnik, and E. K.U. Gross, *J. Chem. Phys.* **123**, 062206 (2005).
- ⁴D. Tozer, *J. Chem. Phys.* **119**, 12697 (2003).
- ⁵N. Maitra, *J. Chem. Phys.* **122**, 234104 (2005).
- ⁶M. Mundt and S. Kümmel, *Phys. Rev. Lett.* **95**, 203004 (2005).
- ⁷S. Kümmel and L. Kronik, *Rev. Mod. Phys.* **80**, 3 (2008).
- ⁸R. J. Magyar and S. Tretiak, *J. Chem. Theory Comput.* **3**, 976 (2007).
- ⁹H. Iikura *et al.*, *J. Chem. Phys.* **115**, 3540 (2001).
- ¹⁰J. Heyd, G. E. Scuseria, and M. Ernzerhof, *J. Chem. Phys.* **118**, 8207 (2003).
- ¹¹T. Yanai *et al.*, *Chem. Phys. Lett.* **393**, 51 (2004).
- ¹²H. Sekino *et al.*, *J. Chem. Phys.* **126**, 014107 (2007).
- ¹³J.-D. Chai and M. Head-Gordon, *J. Chem. Phys.* **128**, 084106 (2008).
- ¹⁴M. Henderson, B. G. Janesko, and G. E. Scuseria, *J. Chem. Phys.* **128**, 194105 (2008).
- ¹⁵E. Livshits and R. Baer, *Phys. Chem. Chem. Phys.* **9**, 2932 (2007).
- ¹⁶T. Stein *et al.*, *J. Am. Chem. Soc.* **131**, 2818 (2009).
- ¹⁷T. Stein *et al.*, *J. Chem. Phys.* **131**, 244119 (2009).
- ¹⁸A. Neubig and M. Thelakkat (unpublished).
- ¹⁹P. J. Stevens *et al.*, *J. Phys. Chem.* **98**, 11623 (1994).
- ²⁰J. P. Perdew *et al.*, *Phys. Rev. Lett.* **77**, 3865 (1996).
- ²¹M. J. G. Peach *et al.*, *J. Chem. Phys.* **128**, 044118 (2008).
- ²²Z. Chen *et al.*, *J. Am. Chem. Soc.* **131**, 8 (2009).
- ²³X. Guo *et al.*, *J. Am. Chem. Soc.* **131**, 7206 (2009).
- ²⁴A. P. Zoombelt *et al.*, *J. Mater. Chem.* **19**, 5336 (2009).
- ²⁵H. Yan *et al.*, *Nature (London)* **457**, 679 (2009).
- ²⁶For the TDDFT calculations we used the qchem program package (Ref. 34) and the 6-311G(d,p) basis set.
- ²⁷J. Gierschner *et al.*, *Adv. Mater.* **19**, 173 (2007).
- ²⁸A. Klamt and G. Schüürmann, *J. Chem. Soc. Perkin Trans. 2* **1993**, 799.
- ²⁹J. Florián and A. Warshel, *J. Phys. Chem. B* **103**, 10282 (1999).
- ³⁰H. Meier *et al.*, *Acta Polym.* **48**, 379 (1997).
- ³¹R. Martin *et al.*, *Chem. -Eur. J.* **6**, 3622 (2000).
- ³²J. Rissler, *Chem. Phys. Lett.* **395**, 92 (2004).
- ³³S. Tretiak *et al.*, *Phys. Rev. Lett.* **89**, 97402 (2002).
- ³⁴Y. Shao *et al.*, *Phys. Chem. Chem. Phys.* **8**, 3172 (2006).

Publication 2

*Using optimally tuned range separated hybrid functionals
in ground-state calculations: Consequences and caveats*

A. Karolewski, L. Kronik, and S. Kümmel,
J. Chem. Phys. **138**, 204115 (2013).

© 2013 AIP Publishing LLC
DOI: 10.1063/1.4807325

2

Own Contribution

I did all calculations and wrote the first version of the manuscript.

Using optimally tuned range separated hybrid functionals in ground-state calculations: Consequences and caveats

Andreas Karolewski,¹ Leeor Kronik,² and Stephan Kümmel¹

¹Theoretical Physics IV, University of Bayreuth, 95440 Bayreuth, Germany

²Department of Materials and Interfaces, Weizmann Institute of Science, Rehovoth 76100, Israel

(Received 18 March 2013; accepted 7 May 2013; published online 31 May 2013)

Optimally tuned range separated hybrid functionals are a new class of implicitly defined functionals. Their important new aspect is that the range separation parameter in these functionals is determined individually for each system by iteratively tuning it until a fundamental, non-empirical condition is fulfilled. Such functionals have been demonstrated to be extremely successful in predicting electronic excitations. In this paper, we explore the use of the tuning approach for predicting ground state properties. This sheds light on one of its downsides – the violation of size consistency. By analyzing diatomic molecules, we reveal size consistency errors up to several electron volts and find that binding energies cannot be predicted reliably. Further consequences of the consistent ground-state use of the tuning approach are potential energy surfaces that are qualitatively in error and an incorrect prediction of spin states. We discuss these failures, their origins, and possibilities for overcoming them. © 2013 AIP Publishing LLC. [<http://dx.doi.org/10.1063/1.4807325>]

I. INTRODUCTION

Recent years have seen the advent of a new class of functionals in density functional theory (DFT) and time-dependent DFT (TDDFT). Functionals within this class are not and cannot be expressed explicitly, but are defined implicitly, often via a numerical procedure. Such functionals can be general and non-empirical, yet allow for considerably greater flexibility in the functional definition. Therefore, they are a promising route for improving the accuracy of practical DFT and TDDFT calculations without introducing empirical concepts. In the spirit of the famous classification of density functionals into three generations,¹ one may think of numerically defined functionals as the fourth generation. Examples for such functionals include the adiabatically exact approximation,² functionals based on inversion arguments,³ functionals based on the concepts of machine learning,⁴ and optimally tuned range separated hybrid (RSH) functionals.^{5,6} The latter are examined in this work.

The main idea in RSH functionals is the separation of the Coulomb repulsion term into a short- and a long-range part,^{7,8} e.g., in the form

$$\frac{1}{r} = \frac{1 - \text{erf}(\gamma r)}{r} + \frac{\text{erf}(\gamma r)}{r}, \quad (1)$$

where γ is a range separation parameter. For short distances, the first term on the right hand side of Eq. (1) is the dominant contribution. For large distances, the second term dominates. They equally contribute at around $0.5\gamma^{-1}$, the separation point between short and long-range. The two ranges of electron-electron distances are then treated with different functionals. The most common realization is to treat the short-range exchange with a semi-local functional and the long-range exchange exactly, with the correlation energy described by a semi-local functional without splitting into long-range and short-range parts. RSH functionals have become popu-

lar in recent years because the range separation allows for a self-interaction free description at large electron-electron distances while maintaining a balanced description of exchange and correlation in the short range, based on well known semi-local functional concepts. Different implementations of this idea have been suggested and discussed, e.g., in Refs. 9–14 and more general forms involving a fraction of short-range exact exchange have also been put forth, e.g., in Refs. 15 and 16.

The focus of this work is on investigating the specific way of choosing the range separation parameter γ , which has become known as “optimal tuning.” One way of determining γ is by empirical fitting against an appropriate training set.^{12,14–17} However, various studies, e.g., Refs. 18–22, have shown that the best value of γ can be strongly system-dependent and that capturing this dependence correctly is crucial for the quality of the results. “Optimal tuning” is a successful strategy for choosing γ in a system-specific but non-empirical way, in which γ is chosen so as to obey a known exact property.^{5,6} While other possibilities exist,²³ in the most popular and broadly applicable tuning approach γ is chosen such that the eigenvalue of the highest occupied molecular orbital (HOMO) is as close as possible to the negative ionization potential (IP) computed from total energy differences,¹² often for both the neutral and anionic system.²⁴ The optimally tuned RSH approach was already successfully employed for a great variety of systems. Two of its notable achievements were the correct prediction of charge transfer excitation energies, also in situations where other functionals designed for charge transfer fail,²¹ and fundamental gaps (see, e.g., Refs. 6, 18–21, 24–27 for an overview). For the fundamental gaps, it is particularly important to keep in mind that RSH functionals are implemented within the generalized Kohn-Sham scheme.²⁸ It is therefore possible to tune the generalized-Kohn-Sham HOMO-LUMO gap to be close to the physically meaningful fundamental gap.⁶

While virtually all applications of the optimal-tuning approach have so far confirmed a distinct system dependence of γ , such a dependence, when incorporated into a global parameter as in the tuning, clearly also possesses conceptual drawbacks, notably the violation of size consistency. It has long been known that this problem exists in principle.¹² With this work, taking seriously the concept of treating the tuned RSH functional as an implicitly defined one, we investigate how the formal drawbacks manifest themselves in errors obtained in practical scenarios. We demonstrate that there are situations in which not only the choice of the range separation parameter but also the choice of the semi-local approximation has a major influence on the results. After a brief description of the underlying methods in Sec. II and a detailed discussion of different tuning conditions in Sec. III, we quantify the size consistency error and examine its impact on binding energies in Sec. IV. In Sec. V, we show how related issues may result in problems with the prediction of electronic spin configuration and potential energy curves. Finally, we analyze and summarize the reasons for the observed failures and close with an outlook on approaches for overcoming these problems.

II. METHODOLOGY

As mentioned above, this work aims to quantify the size consistency error and to calculate the binding energies of molecules with optimally tuned RSH approaches in a comparative study of different tuning conditions and short-range exchange expressions. In order to keep the analysis – which is in fact quite involved – as transparent as possible, we focus on diatomic molecules. Of the various RSH functionals that are available we here examine two specific choices: the Baer-Neuhauser-Livshits (BNL) functional,^{11,12} which employs a short-range version of the local density approximation (LDA) exchange functional and Lee-Yang-Parr (LYP) semi-local correlation, and the ω PBE functional of Scusevia and co-workers¹³ which employs a short-range version of the Perdew-Burke-Ernzerhof (PBE) semi-local exchange functional²⁹ and semi-local PBE correlation.

For our calculations we used the program package QChem,³⁰ which has both the BNL and the ω PBE functionals implemented. All calculations were carried out using the aug-cc-pVQZ basis set, unless explicitly stated otherwise. Most of the results presented below change considerably if a cc-pVQZ basis set is used without diffuse functions, because calculations with anions are incorporated as part of the tuning procedure. Further details on basis set dependence are given in Sec. III.

III. TUNING CONDITIONS

The general idea behind the tuning approach is to demand that the HOMO is the negative of the IP – a condition that has to be fulfilled for the exact functional.^{31–34} One possibility for obtaining an approximation to the IP is the calculation of the difference between the total energies of the $N - 1$ and the N electron system. This leads to the tuning condition¹²

$$T_N(\gamma) = |\epsilon_{\text{HOMO}}^\gamma(N) + E^\gamma(N - 1) - E^\gamma(N)| = \min. \quad (2)$$

The minimum of T_N defines an optimal γ_N for which the HOMO energy is as close as possible to the approximate IP. γ_N has to be determined in an iterative procedure with successive ground state energy calculations for the N and the $N - 1$ electron system. For the ultimate functional, the condition of Eq. (2) would be perfectly fulfilled. For approximate functionals the approach is still approximate as per construction, even when $T_N(\gamma) = 0$ is reached, it is limited to the predictive power of the IP approximation—a price to pay for having a non-empirical tuning approach.

In order to obtain the fundamental gap from quasiparticle energy differences, it is tempting to use a similar condition for connecting the LUMO (lowest unoccupied molecular orbital) and the electron affinity (EA). However, there is no rigorous theoretical basis for such a connection. A convenient way around this problem is to apply the IP tuning to the $N + 1$ electron system. This leads to the second tuning condition²⁴

$$T_{N1}(\gamma) = |\epsilon_{\text{HOMO}}^\gamma(N + 1) + E^\gamma(N) - E^\gamma(N + 1)| = \min. \quad (3)$$

To obtain the optimal fundamental gap it would be necessary to enforce both conditions T_N and T_{N1} at the same time. However, this is not possible with just one parameter γ and therefore both conditions have to be combined in a least square approach to minimize the resulting error. This leads to the third condition⁶

$$T_{LS}(\gamma) = \sqrt{T_N^2(\gamma) + T_{N1}^2(\gamma)} = \min. \quad (4)$$

The optimal γ obtained from this tuning condition, γ_{LS} , lies between γ_N and γ_{N1} , i.e., the optimal γ 's that result from using T_N and T_{N1} as tuning conditions. It is thus a compromise between these both conditions. We note that a related, fourth tuning condition, used in some of our earlier publications^{19,21,24,25} combines the absolute values of T_N and T_{N1} ,

$$T_{J2}(\gamma) = |T_N(\gamma)| + |T_{N1}(\gamma)| = \min. \quad (5)$$

We do not consider this tuning condition in the following because it tends to produce γ_{J2} which is very close to either γ_N or γ_{N1} , depending on how the total and the HOMO energies vary with γ .

A first step in our work is to find the optimized γ -values and energies for representative atoms and diatomic molecules with these tuning conditions. A technical but important prerequisite to this task is to determine the basis set sensitivity of the method. Generally, the basis set quality required for a certain calculation strongly depends on the employed method and the property of interest. Because RSH functionals are in many ways similar to hybrid functionals, one could naively expect equivalent basis set requirements. For an RSH without tuning this is indeed the case, as demonstrated in Fig. 1 for the BNL functional, using the oxygen atom as an example. In these two graphs we compare different basis sets with the aug-cc-pVQZ basis set and plot the respective differences for the total energy and the HOMO-LUMO gap. As expected, data points obtained from B3LYP,³⁵ a popular conventional hybrid functional, are close to the “BNL without tuning” data points (where we used $\gamma = 0.6$). If we perform the T_{LS} tuning for each basis set separately, however, we observe severe

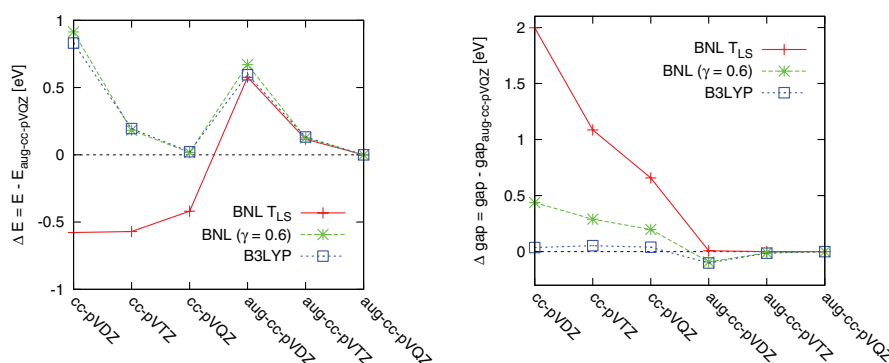


FIG. 1. Basis set dependence for the oxygen atom: Tuned BNL calculations with T_{LS} (solid line), BNL calculations with a constant $\gamma = 0.6$ (dashed line), and B3LYP calculations (dotted line). (Left) Difference of the ground-state energies obtained with the particular basis set and the aug-cc-pVQZ basis set. (Right) HOMO-LUMO gap difference obtained with the particular basis set and the aug-cc-pVQZ basis set.

deviations from the calculations with constant γ . There are two reasons for this increased basis set dependence. First, the tuning depends on the anion and the cation, which themselves have a basis set sensitivity (especially the anion). Second, changes due to the basis set enter a calculation twice. On the one hand due to the RSH calculation itself and on the other hand due to the tuning process. Hence it is necessary to choose the basis set carefully if doing a tuned RSH calculation and to use or compare to a basis set with diffuse functions if using the T_{N1} or the T_{LS} tuning, as both depend on the anion.

Having addressed the basis set issue, we turn to evaluating the tuning procedure itself. The upper part of Fig. 2 shows the optimized γ values for diatomic molecules composed of first and second row atoms. All three tuning conditions exhibit

a similar behavior. With only a few exceptions, the BNL γ 's are just slightly larger than the ω PBE ones. As mentioned in earlier work,^{18,20,21} the range separation parameter depends inversely on the system size. Our calculations confirm this finding, as seen by comparing γ to the inverse of the bond length in the lower part of Fig. 2. As a corollary, γ_N is larger than γ_{N1} , the latter being obtained for the (larger) anion, and consequently γ_{LS} is between γ_N and γ_{N1} . However, note that there is one clear exception: the BeS molecule. This exception is related to tuning problems with alkali and earth alkali atoms and is discussed in the following. We also note that this behavior is very sensitive to the basis set. If we use the cc-pVQZ instead of the aug-cc-pVQZ basis set, we obtain much smaller γ_N and γ_{LS} for BeS; however, γ_N of Be₂ is then considerably larger. That data points are missing for some systems indicates that the calculations in these cases lead to unstable anions. Therefore, the tuning conditions T_{N1} and T_{LS} are not well defined and are neglected in this graph and all other graphs of this work.

In the upper part of Fig. 3 we plot the γ values for atoms calculated again with both BNL and ω PBE. In the lower part of the same Figure we plot the inverse of the calculated atomic radii to demonstrate the system size dependence of γ as we would expect it. Clearly, the BNL γ_N and the BNL γ_{LS} values of all alkali and earth alkali atoms of this plot do not follow the general trend. Their γ values are out of scale, just as in the case of the BeS molecule. The reason is that for these systems $T_N(\gamma)$ of Eq. (2) never intersects the zero line, whereas a zero is found for all other systems that the authors know about. Moreover, $T_N(\gamma)$ exhibits just a shallow minimum at very large γ , or it has no minimum and converges to a small positive constant c , as in the case of Li. It is noteworthy that in these cases the minimum value (or the constant c) is very small (<0.5 eV) and therefore even in these cases the tuning approach predicts the fundamental gap reliably as demonstrated in Ref. 18. However, other properties, such as the total energy in the ground state, may differ from reference values by up to several 10 eV.

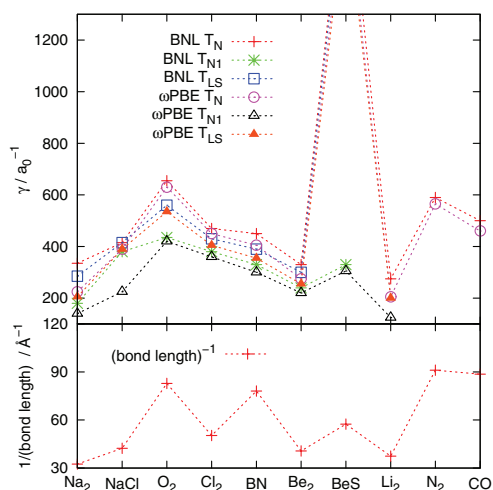


FIG. 2. (Upper part) Optimized γ values for diatomic molecules. The tuning conditions of Eqs. (2)–(4) were used. (Lower part) Inverse experimental³⁶ bond lengths.

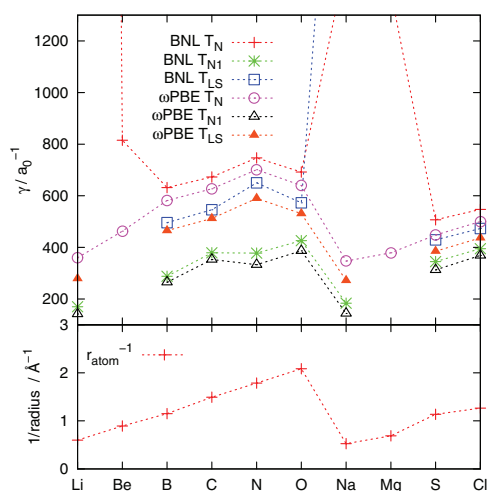


FIG. 3. (Upper part) Optimized γ values for selected atoms. The tuning conditions of Eqs. (2)–(4) were used. (Lower part) Inverse calculated³⁷ atomic radii.

IV. SIZE CONSISTENCY

A. Size consistency error

The size consistency criterion is a fundamental constraint that applies to any electronic structure approach, and thus also to approximations in DFT. It states that the sum of the energies E_A and E_B of two well-separated, independent subsystems A and B should be equal to the energy E that one obtains when A and B are considered as one large combined system. The RSH functional itself is expected to be properly size consistent if no tuning is performed, because all of its exchange and correlation ingredients are. Nevertheless, by construction a tuned RSH functional is not size consistent,¹² because due to its implicit definition it generally has different γ values for the whole system and the two separate subsystems. As a con-

sequence

$$\Delta_{\text{SC}} = E_{\gamma_A}(A) + E_{\gamma_B}(B) - E_{\gamma_{A+B}}(A+B) \neq 0, \quad (6)$$

with Δ_{SC} defining the size-consistency error. While this argument establishes that the tuning procedure in principle violates the size consistency condition, we do not know of any study so far that systematically quantified the error. Therefore, we examine it here in the transparent, hallmark test case of two atoms that are far from each other. In this situation we expect large γ differences due to the large γ variations seen in Fig. 3. Our theoretical setup is a system of two atoms with a distance of 20 Å, large enough such that all orbitals are localized on either one of the two atoms A or B with vanishing orbital overlap. Consider, for example, the simple T_N or T_{N1} tuning criteria. If we assume that the HOMO of the whole (neutral or anionic, respectively) system, A+B, is localized on atom A, we obtain $\gamma_{A+B} = \gamma_A$ as the range separation parameter for the whole system. The size consistency error can then be expressed as

$$\Delta_{\text{SC}} = E_{\gamma_A}(A) + E_{\gamma_B}(B) - E_{\gamma_A}(A+B) \quad (7)$$

and therefore reduces to $E_{\gamma_B}(B) - E_{\gamma_A}(B)$ owing to the size-consistency of the RSH functional itself. Whether the resulting size consistency error is negligible or worrisome depends on the difference $\gamma_A - \gamma_B$ and how strongly the total energy of B varies with γ .

In Fig. 4, we plot the size consistency errors of several diatomic molecules calculated with the BNL (left graph) and ω PBE functional (right graph). The error strongly depends on the system and the applied tuning condition. The largest errors are observed for (Na+Cl) and (Be+S). This is related to the fact that in these atom pairs the differences between the atomic γ values are the largest (compare Fig. 3). It is exacerbated by the fact that one atom dominates the ionization potential and therefore T_N , whereas the other atom dominates the electron affinity and therefore T_{N1} . The monoatomic systems (O+O) and (N+N) exhibit no size consistency error since the combined system has the same γ as its subsystems. Using an RSH approach without tuning is size consistent and is

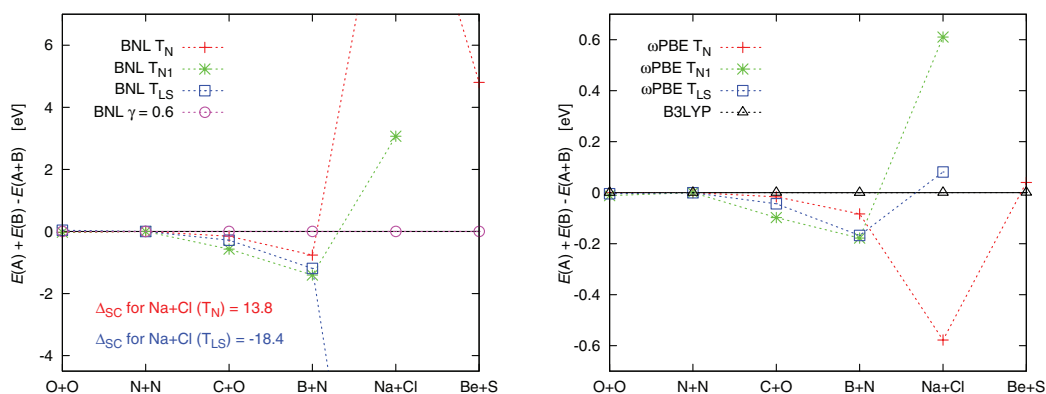


FIG. 4. The size consistency error according to Eq. (6) for atom pairs calculated with the BNL (left) and the ω PBE functional (right). The distance between the two subsystems is 20 Å. Note that B3LYP data points exhibit no size consistency error, which proves that the calculations were properly set up. The data points “BNL $\gamma = 0.6$ ” (no tuning, γ constant for all systems) are also all zero, confirming that the RSH approaches itself (without tuning) are size consistent (the same applies to ω PBE). Note the different scales on the energy axes in the left and right viewgraph.

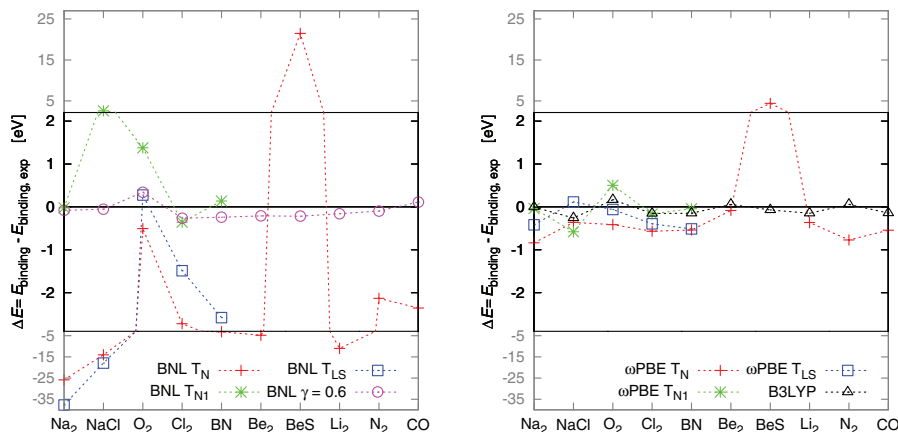


FIG. 5. Differences of calculated binding energies (according to Eq. (8)) and experimental binding energies. The calculations were performed with all three tuning conditions for the BNL functional (left) and the ω PBE functional (right). It also shows B3LYP data points (right) and data points for the case of BNL without tuning (“BNL $\gamma = 0.6$ ”, left). Note the change of scale in the energy axis. Missing T_{N1} and T_{LS} data points indicate that either the anion of the molecule or at least one of its atoms is unstable (cf. Sec. III).

demonstrated with the data points “BNL $\gamma = 0.6$ ” in the left part of Fig. 4 where we used a constant $\gamma = 0.6$ in all calculations. The comparison of the BNL and the ω PBE functional is the most noteworthy aspect of Fig. 4. The size consistency errors of both methods differ substantially, with the BNL error being one order of magnitude larger than the ω PBE one. (Na+Cl) is the most extreme case that we encountered, with an error of 18 eV for the T_{LS} tuning of BNL. We attribute this to the above-discussed abnormal tuning behavior of the sodium atom. Even when such extreme cases are disregarded, the size consistency violation for BNL is nevertheless generally severe, as a consequence of the strong γ dependence of the total energy (compare Fig. 7). This γ dependence is smaller for ω PBE (compare Fig. 7) resulting in a moderate error. However, even for ω PBE it may be considerably large, as in the case of (Na+Cl).

B. Binding energies of diatomic molecules

In this section, we address an important consequence of the violation of size consistency: the incorrect prediction of binding energies. As in Secs. III and IV A, we focus our analysis on diatomic molecules. In order to calculate their binding energies with the implicitly defined tuned RSH functionals, we have to conduct the tuning process for the atoms and the molecules separately. Therefore, we obtain a difference in the γ values of the molecule (γ_{AB}) and its constituent atoms (γ_A and γ_B). Due to this difference the resulting binding energy,

$$E_{\text{binding}} = E_{\gamma_A}(A) + E_{\gamma_B}(B) - E_{\gamma_{AB}}(AB), \quad (8)$$

incorporates an error that is closely connected to the size consistency error. We calculated these binding energies for diatomic molecules composed of first and second row elements with all three tuning approaches for the BNL and the ω PBE functional. In Fig. 5 we plot the differences of our calculated binding energies and the experimental binding energies.³⁸ The

graph shows severe deviations of the BNL calculations (left part of Fig. 5) from the experiment. A binding energy error of 1–3 eV is the normal case, but 10 eV and more are observed for the molecules containing alkali and earth alkali atoms. By using a constant range separation parameter, $\gamma = 0.6$ (chosen without specific optimization, but considered “reasonable” for thermochemistry¹²), the deviations from the experiment are less than 0.3 eV. This is the same order of error as observed for the B3LYP data points presented in the right part of Fig. 5. This part of Fig. 5 also shows the ω PBE calculations with a binding energy error smaller than 0.8 eV, consistent with the more moderate size consistency error of this functional. The only exception is BeS, with an error of 4.4 eV. This large error is related to the above-discussed abnormal tuning behavior of this system (cf. Sec. III).

On the whole, these results reflect the size consistency errors of Sec. IV A. The differences between the two applied RSH approaches are consistent with our finding that the total energies depend more strongly on γ for the BNL functional than for the ω PBE functional. This is reflected in Fig. 6, which shows the difference of γ_{AB} (molecule AB) to the mean atomic γ , i.e., the average of γ_A and γ_B . Although these differences are very similar for BNL and ω PBE (except for molecules containing alkali and earth alkali atoms), the binding energy errors are much larger for the BNL functional. Note that the general structure of the graphs in Fig. 6 (γ differences) and Fig. 5 (binding energy errors) is very similar. This falls in line with the other arguments in this section, i.e., the differences in the γ values obtained for molecules and atoms in the tuning approach are the main reason for the notable errors.

V. TUNING-RELATED SHORTCOMINGS

In this section, we address some situations where the tuning approach leads to problems in an indirect way that is not

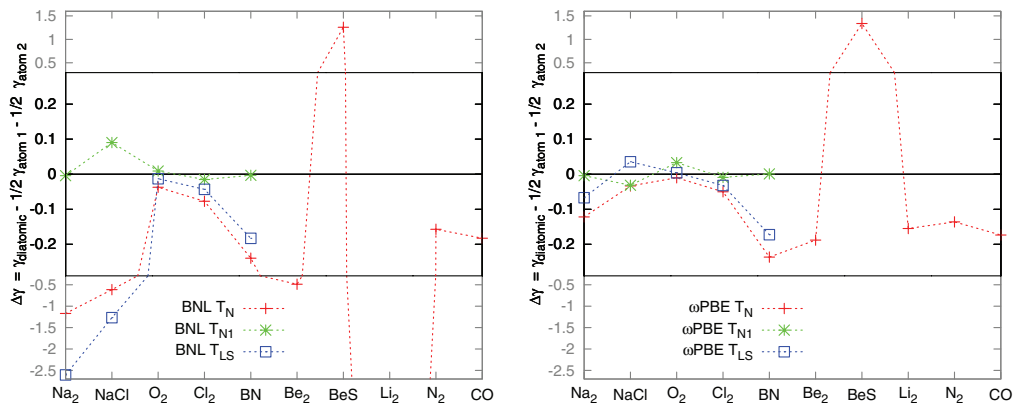


FIG. 6. Difference $\Delta\gamma$ between γ_{AB} (molecule) and $1/2(\gamma_A + \gamma_B)$ (average over atoms) for the BNL functional (left) and the ω PBE functional (right). Systems with a large $\Delta\gamma$ are expected to have a large binding energy error if calculated with tuned RSH functionals. Note the change of scale in the ordinate. Missing T_{N1} and T_{LS} data points indicate that either the anion of the molecule or at least one of its atoms is unstable (cf. Sec. III).

strictly related to the violation of size consistency. In these situations, tuning has to be conducted with great care, or not at all.

A. Spin configuration

Spin multiplicity introduces an additional problematic aspect of tuning. Generally, a modification of the spin configuration may modify the optimal value of γ and, in turn, introduce changes in the energy that go beyond the physical energy changes demanded by the changes in the spin configuration. To explore this effect, consider the prototypical example of the O_2 molecule, well-known to possess a triplet ground state. Fig. 7 shows the energy of the O_2 molecule, at the experimental bond length, as a function of γ . For both the BNL and the ω PBE functionals, the triplet energy is correctly identified as lower than the singlet energy, for any choice of γ .

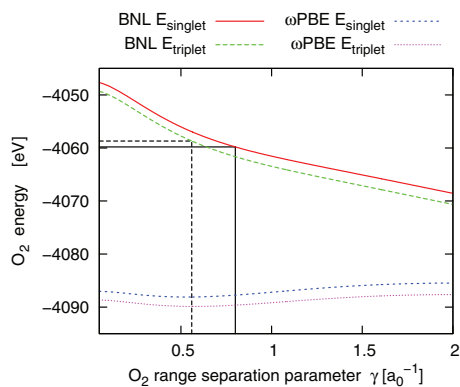


FIG. 7. Energy of the O_2 molecule at its experimental bond length³⁶ for different RSH approaches and spin configurations. The solid vertical and horizontal line illustrate the optimally tuned BNL γ_{LS} and its corresponding energy $E(\gamma_{LS})$ for the singlet state. The dashed vertical and horizontal line indicate γ_{LS} and $E(\gamma_{LS})$ of BNL for the triplet state.

For the BNL functional, however, the T_{LS} optimally tuned γ of the singlet state (solid vertical line) is larger than that of the triplet state (dashed vertical line). Due to the strong γ -dependence of the energy, the tuned singlet energy is lower than the tuned triplet energy, i.e., the triplet and singlet energy ordering at their respective optimal γ values (solid and dashed horizontal line, respectively) is erroneous. Note that due to the weaker γ -dependence of its energy, the ω PBE functional predicts the correct order of the singlet and the triplet energy (the singlet and triplet γ of ω PBE are close to the solid and dashed vertical line). However, the same quantitative limitation remains in force, even if it does not translate into a qualitative difference in this case. Thus, if one constructs the energy at optimal tuning as a function of bond length, as shown in Fig. 8, the equilibrium bond length is obtained correctly, at least qualitatively, but the predicted spin configuration itself is incorrect. For a system with a spin state that is unknown prior to calculation, a naive tuned-RSH approach may therefore be

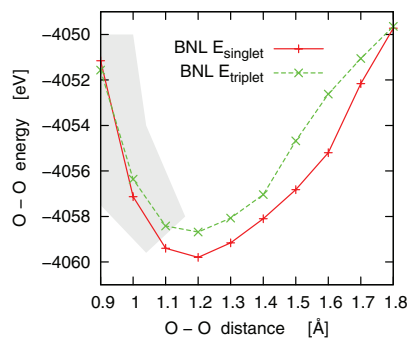


FIG. 8. Singlet (solid) and triplet (dashed) energy of the O_2 molecule as a function of the bond length calculated with the BNL functional with T_{LS} tuning. For the parts of the curves that are within the shaded area the tuning approach is not well defined. Although the neutral system is stable at these bond lengths the anion is unstable as the HOMO value of the anion calculated with the optimally tuned γ_{LS} is slightly positive.

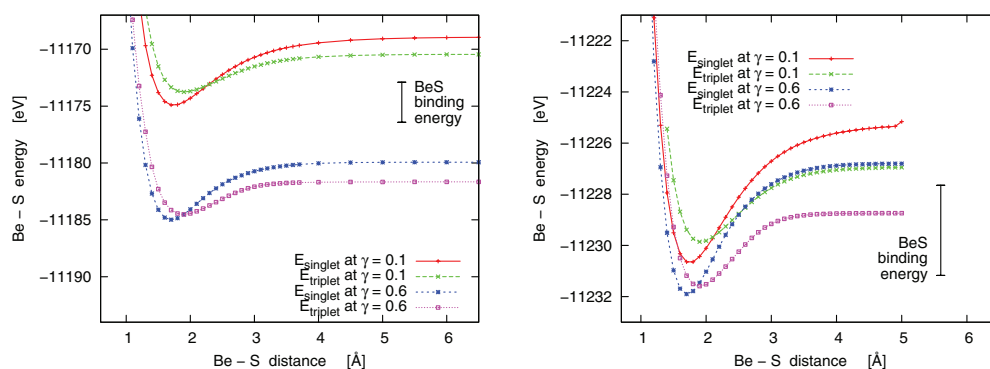


FIG. 9. BNL (left) and ω PBE (right) energy as a function of distance between Be and S for a singlet and a triplet spin configuration and for two different γ values.

misleading and the correct spin state has to be determined by considering a range of γ values (as in Fig. 7) and/or with a different functional beforehand.

B. Potential energy curve

In this subsection, we analyze how the tuning approach performs for the calculation of potential energy surfaces. We again focus on diatomic molecules as these allow for a transparent analysis. The discussion is motivated by and related to the effects reported in Sec. V A for O_2 close to its equilibrium bond length. However, here we discuss two additional conceptual problems.

In Subsection V A we pointed out possibly spurious spin-related issues of the neutral species. But even if no such issue arises, the energy of the neutral system may still exhibit a spurious dependence of the energy on the multiplicity of the anion and the cation of the system under consideration. By going from the equilibrium bond length to a very large one, the multiplicity of the system may change at a specific distance where a different spin configuration becomes more favorable, e.g., the systems could go from a singlet to a triplet state. The dilemma is that the anion and cation of the sys-

tem could also change their spin states and this could happen at a different distance or even several times, e.g., the multiplicity could change from 2 to 4 and then again from 4 to 6. For a specific example, consider the heterodimer comprised of beryllium (Be) and sulfur (S) with the following configuration:

	Neutral	Anion	Cation
Molecule (multiplicity)	1	2	2
Well separated (multiplicity)	3	2	4

For a common functional one would calculate a singlet and a triplet energy curve that would intersect at a certain bond length. The same applies to RSH functionals without tuning. Fig. 9 displays these singlet and triplet energy curves for Be and S for the BNL and ω PBE functionals (without tuning), for two different values of the range separation parameter. For both γ values, both functionals behave correctly and predict the correct binding energy of 3.5 eV,³⁸ as the difference of the triplet energy at large internuclear separation and the singlet energy at the equilibrium bond length. A different situation, however, occurs when either

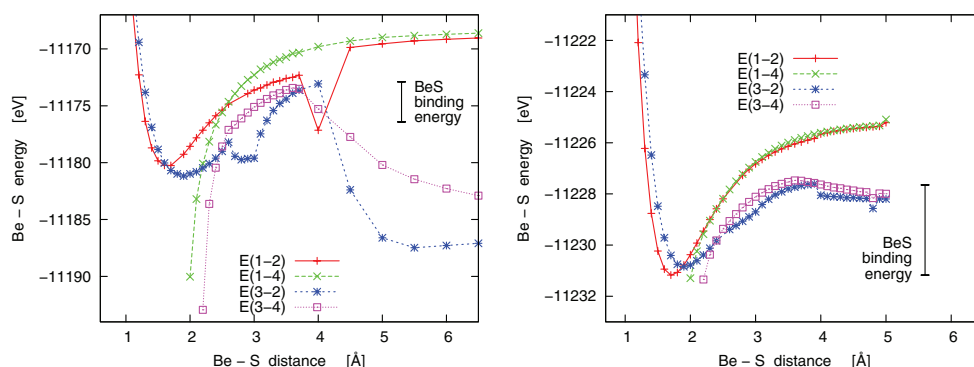


FIG. 10. Tuned BNL (left) and ω PBE (right) energies of Be-S as a function of distance between Be and S for four different spin configurations. The T_N tuning was applied at each distance separately. “E(x-y)” encodes the energy of the four different spin configurations according to $E(\langle \text{multiplicity of the neutral system} \rangle - \langle \text{multiplicity of the cation} \rangle)$. The multiplicity of the anion is always 2.

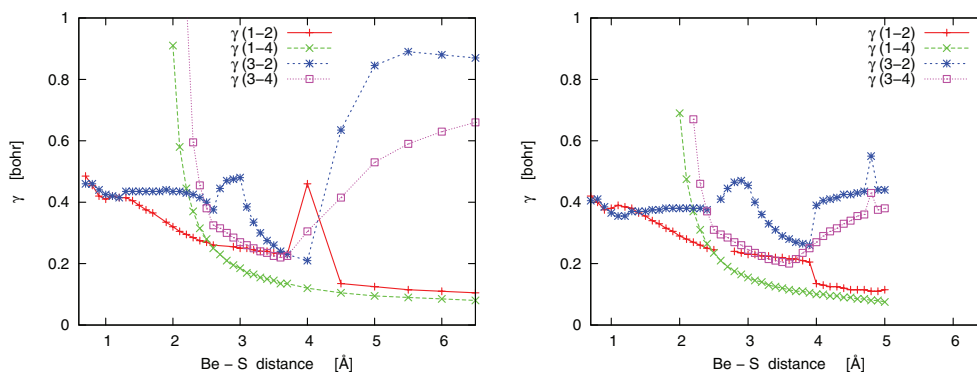


FIG. 11. γ values from T_N tuning for Be-S as a function of distance between Be and S for four different spin configurations, for the BNL (left) and ω PBE (right). The T_N tuning was applied at each distance separately. “ $\gamma(x-y)$ ” means $\gamma(\langle \text{multiplicity of the neutral system} \rangle - \langle \text{multiplicity of the cation} \rangle)$. The multiplicity of the anion is always 2.

functional is used in combination with the tuning approach. Because the tuning procedures depend on the anion and/or the cation, the spin states of the latter also affect the results. This means one would not simply get a singlet and triplet curve, but a singlet(neutral)-duplet(cation), a singlet(neutral)-quartet(cation), a triplet(neutral)-duplet(cation), and a triplet(neutral)-quartet(cation) curve (if we neglect the anion because its spin state does not change in the case of Be and S). The mere existence of these curves is physically incorrect. For Be and S they are depicted in Fig. 10 for the T_N tuning.

A second conceptual failure is connected to the basic concept of the tuning itself – the system dependence of the range separation parameter. It leads to a change of γ as a function of the distance between the two atoms. Fig. 11 demonstrates this dependence for Be and S for the different spin configurations. The consequence is that the potential energy curves exhibit unphysical trends, as seen in Fig. 10. The curve that one would obtain by choosing the lowest possible energy at each internuclear separation (not explicitly shown in Fig. 10 for reasons of clarity) zig-zags up and down and finally results in a negative binding energy for the optimally tuned BNL functional. The largest change occurs around 4 Å. This may be related to the transition from orbitals that are delocalized over the molecule to orbitals that are localized on the separate atoms. The unphysical curves can be understood by considering Fig. 9 again. Because γ mainly varies in the range between 0.1 and 0.6, the energy “jumps” between the curves of these two different γ values. In contrast to all other calculations in this paper, here we used the cc-pVQZ basis set because then the tuning is more well behaved than with the aug-cc-pVQZ basis set. However, the same effects can be observed for other basis sets as well. Furthermore, we found a similar behavior for all other tuning conditions and other diatomic systems such as BN, NaCl, CO, and O₂; sometimes the failures were not as pronounced as in this case and sometimes even more severe. For the ω PBE functional the curves are, again, generally better behaved because the γ dependence of the total energy is smaller. However, the conceptual problems remain for this functional too.

These results once more demonstrate that energies from calculations with different range separation parameters cannot be compared. Viewing γ as a system dependent quantity and performing the tuning for each configuration of a potential energy curve separately, generally leads to spurious results. As mentioned above, an alternative would be to apply the tuning procedure to molecules at their equilibrium bond length and to use the resulting γ also for all other bond lengths. However, this would be in contradiction to the general philosophy of regarding γ as an implicit density functional and in practice would lead to irreconcilable inconsistencies in the limit of large inter-nuclear separation. Clearly, this calls for a size consistent extension of the current tuning approach.

VI. SUMMARY

The main aim of this work was to analyze the tuning of RSH functionals with respect to the question of size consistency. For this purpose we examined diatomic systems at large distances, where we observed large size consistency errors – up to several electron volts. In the rest of the paper we discussed consequences of the size consistency violation. Likely the most prominent one is that the tuning approach may fail in predicting binding energies correctly and that a strict definition of potential energy surfaces is not possible. We also demonstrated that due to the tuning procedure, spin configurations might be predicted incorrectly and that tuning results depend also on the anion and/or cation of a system and their spin configurations. This, in fact, is an additional factor that can adversely influence potential energy surfaces.

The scenario considered throughout this work – a very small system with a very large difference in the optimal γ between its sub-systems – is in some sense a deliberately constructed “worst case scenario” for the optimal tuning method. It may well be that larger and/or more homogeneous systems, where the dependence on γ may be less pronounced, will exhibit more modest errors. This, in fact, has also been observed in some of the examples studied. We believe the information given here to be useful, as these extreme examples teach us most about potential pitfalls and allow us maximal

caution in the application of the method and the interpretation of its results. Specifically, a re-tuning during static or dynamic processes that changes the electronic configuration (including the case of reaction barriers) should be avoided if energetic changes are of interest. In cases where a tuned long-range correction is beneficial, it is advisable to conduct a tuning step just once. This procedure is not consistent with the interpretation of the tuning procedure as making the range-separation parameter an implicit density functional, but may lead to pragmatically more useful results. Interestingly, while all optimally tuned RSH functionals are subject to these limitations, they do not necessarily suffer from them to the same extent. In our case, ω PBE and BNL were found to perform very differently under identical tuning procedures. The size consistency errors for the ω PBE functional were nearly an order of magnitude smaller than the ones for the BNL functional, with a similar observation for binding energy errors. We attribute this behavior to the improved compatibility of the semi-local correlation and short-range exchange in the ω PBE functional.

What are the underlying reasons for the failures described above? A first observation is that with the tuning approach the functional is able to adjust its range separation parameter to a specific system. This adjustment has proven to be very important for the prediction of spectroscopic properties. The price to pay for this system dependence of γ are the limitations described in this work. They originate from the implicit construction of the functional itself. The tuning of γ , when being regarded as turning the range-separation parameter into an implicit density functional, must be seen as a definition of a highly non-local functional and global non-localities frequently lead to size-consistency violations.³⁹

A second observation is that one could simply think about γ as a parameter that is fixed anew for each system. From this perspective, different values for γ correspond to different functionals and it is therefore immediately obvious that energies obtained from the tuning approach cannot be compared. This perspective, however, is too simplistic. Due to the tuning, one is in fact using a system dependent range separation parameter that can in principle be seen as a functional of the density $\gamma[n]$. However, in taking the functional derivative to derive the exchange potential from the exchange energy, γ has been treated as a constant here as well as in all other applications of the optimally tuning idea that we know of. Yet, if one would take the concept of viewing γ as an implicit density functional seriously, then one should obtain an additional term in the exchange potential of the form

$$\frac{\partial E}{\partial \gamma} \frac{\delta \gamma[n]}{\delta \phi_i}, \quad (9)$$

that is not present if γ is held constant. The latter expression refers to a generalized Kohn-Sham approach,²⁸ where the exchange energy derivative has to be taken with respect to the generalized Kohn-Sham orbitals ϕ_i , i.e.,

$$\frac{\delta E[n, \gamma[n]]}{\delta \phi_i(\vec{r})}. \quad (10)$$

From this perspective, the optimally tuned calculations that have been done so far used an inconsistent combination of en-

ergy and potential, or, in other words, a potential that does not rigorously minimize the energy, because they neglected the term of Eq. (9). Energy-potential inconsistencies are known to generally lead to problems^{40,41} and the present case can be seen as a somewhat more subtle manifestation of this general principle.

VII. OUTLOOK

Which conclusions can we draw for the future use and development of tuned functionals in view of the presented findings on the size consistency error and related problems? One conclusion could be to avoid tuned functionals, at least in circumstances when ground-state energetics are relevant, and resort to other approaches. For example, it has been demonstrated that self-interaction free functionals based on exact Kohn-Sham exchange^{42,43} or a self-interaction correction (SIC) used in the Kohn-Sham framework⁴⁴⁻⁴⁶ tremendously improve on many of the deficiencies of semi-local functionals and lead to, e.g., occupied eigenvalues that are much more amenable to physical interpretation⁴⁷⁻⁵⁴ and an accurate description of charge transfer^{45,55} and charge transfer excitations.^{56,57} Some of these improvements may even be achieved with semi-local functionals.^{58,59}

Yet, in our opinion, avoiding tuned functionals altogether would be a serious misconception. The tuned RSH functionals and approaches such as the Kohn-Sham SIC each have their individual strengths and neither one makes the other superfluous. Rather, each offers specific advantages and one may choose one of the approaches depending on the requirements of the problem at hand. Advantages of, e.g., the Kohn-Sham SIC are the availability of a consistent energy-potential combination and the lack of the requirement to do many calculations to tune a parameter. On the other hand, the tuned RSH functionals offer opportunities that are beyond what can be reached with any Kohn-Sham approach. For example, recent work showed that tuning based on Eq. (4) results in a very good prediction of both fundamental gaps and IP's for both atoms^{18,60} and organic systems.^{18,20} Consequently, the derivative discontinuity – the discrepancy between the HOMO-LUMO gap and the fundamental gap – is nearly vanishing in the generalized Kohn-Sham system selected due to the tuning, also allowing for a successful mimicking of exciton binding when comparing the HOMO-LUMO gap to the optical gap obtained from time-dependent DFT.⁶ This can be a significant advantage in practical applications, in addition to the successful treatment of charge transfer energies.^{21,24,25,61-64}

Thus, it is worthwhile to discuss the possibilities for improving concepts of RSH functionals with a system dependent range separation. Some suggestions towards this goal were already made in the literature.⁶⁵ Here, we present some further thoughts, based on the perspective that the limitations of the current tuning process and the strong violation of size consistency could be rooted in the dependence of the tuning procedure only on the frontier orbitals. All the different tuning conditions, from Eq. (2) to Eq. (4), address frontier orbitals, which is of course related to the intention of producing reliable results for fundamental gaps and optical (in particular charge-transfer) excitations. Other properties, like the total

energy, that depend on the entire system may be described poorly, as discussed in the present work. The reason for this is that γ enters the functional via the well known long-range exchange energy expression

$$E_x^{\text{LR}} = -\frac{1}{2} \sum_{\sigma} \iint d\vec{r}_1^3 d\vec{r}_2^3 \frac{\text{erf}(\gamma |\vec{r}_1 - \vec{r}_2|)}{|\vec{r}_1 - \vec{r}_2|} \times \sum_{ij} \phi_{i\sigma}^*(\vec{r}_1) \phi_{j\sigma}^*(\vec{r}_2) \phi_{j\sigma}(\vec{r}_1) \phi_{i\sigma}(\vec{r}_2) \quad (11)$$

and in this way influences all orbital-orbital interactions (see, e.g., Eq. (4) of Ref. 9), despite having been adjusted only for the frontier orbitals. Because the orbitals of a specific system have various shapes and sizes, the description of their interaction may require distinct separations into long and short-range. This is especially true if we compare inner shell with outer shell or binding orbitals. One possibility could be to assign a range separation parameter γ_{ij} to each orbital pair $\{ij\}$ in order to describe their interaction accurately by a mix of semi-local short-range and exact long-range exchange. Consequently we would obtain

$$E_x^{\text{LR}} = -\frac{1}{2} \sum_{\sigma} \iint d\vec{r}_1^3 d\vec{r}_2^3 \sum_{ij} \frac{\text{erf}(\gamma_{ij}^{\sigma} |\vec{r}_1 - \vec{r}_2|)}{|\vec{r}_1 - \vec{r}_2|} \times \phi_{i\sigma}^*(\vec{r}_1) \phi_{j\sigma}^*(\vec{r}_2) \phi_{j\sigma}(\vec{r}_1) \phi_{i\sigma}(\vec{r}_2) \quad (12)$$

for the long-range exchange energy expression with orbital pair-dependent γ_{ij}^{σ} 's. Because the semi-local short-range expression, which is also γ -dependent, does not depend on orbital-orbital exchange directly, we could use the mean value $\gamma_{\text{SR}} = \sum_{ij\sigma} \frac{\gamma_{ij}^{\sigma}}{2N^2}$ instead. The question is how to determine the values for these γ_{ij}^{σ} 's. One approach may be to assign them according to the spatial extension of the orbitals that form the pair $\{ij\}$ and the distance between their centers of mass. The advantages of such an approach would be a generalization of the range separation in principle and a possible elimination of the time-consuming tuning step involving the anions and cations. Whether such a scheme can be realized in practice and how accurate it may be needs to be left to future work. In any case, considerations such as this one show that the idea of implicitly, numerically defined functionals does hold the potential for extensions that may increase the application range of concepts such as the optimal tuning.

ACKNOWLEDGMENTS

A.K. acknowledges stimulating discussions with E. Kraisler and S. Refaely-Abramson and the hospitality of the Weizmann Institute of Science. S.K. and L.K. acknowledge financial support from the German-Israeli Foundation. A.K. and S.K. further acknowledge support from DFG GRK 1640. L.K. further acknowledges support from the European Research Council and the Lise Meitner Minerva Center for Computational Chemistry.

¹T. Grabo, T. Kreibich, S. Kurth, and E. K. U. Gross, in *Strong Coulomb Correlation in Electronic Structure: Beyond the Local Density Approximation*, edited by V. Anisimov (Gordon & Breach, Tokyo, 2000).

²M. Thiele and S. Kümmel, *Phys. Rev. Lett.* **100**, 153004 (2008).

³I. Dreissigacker and M. Lein, *Chem. Phys.* **391**, 143 (2011).

⁴J. Snyder, M. Rupp, K. Hansen, K.-R. Müller, and K. Burke, *Phys. Rev. Lett.* **108**, 253002 (2012).

⁵R. Baer, E. Livshits, and U. Salzner, *Annu. Rev. Phys. Chem.* **61**, 85 (2010).

⁶L. Kronik, T. Stein, S. Refaely-Abramson, and R. Baer, *J. Chem. Theory Comput.* **8**, 1515 (2012).

⁷A. Savin and H.-J. Flad, *Int. J. Quantum Chem.* **56**, 327–332 (1995).

⁸T. Leininger, H. Stoll, H.-J. Werner, and A. Savin, *Chem. Phys. Lett.* **275**, 151 (1997).

⁹H. Iikura, T. Tsuneda, T. Yanai, and K. Hirao, *J. Chem. Phys.* **115**, 3540 (2001).

¹⁰M. J. G. Peach, P. Benfield, T. Helgaker, and D. J. Tozer, *J. Chem. Phys.* **128**, 044118 (2008).

¹¹R. Baer and D. Neuhauser, *Phys. Rev. Lett.* **94**, 043002 (2005).

¹²E. Livshits and R. Baer, *Phys. Chem. Chem. Phys.* **9**, 2932 (2007).

¹³T. M. Henderson, B. G. Janesko, and G. E. Scuseria, *J. Chem. Phys.* **128**, 194105 (2008).

¹⁴J.-D. Chai and M. Head-Gordon, *J. Chem. Phys.* **128**, 084106 (2008).

¹⁵T. Yanai, D. P. Tew, and N. C. Handy, *Chem. Phys. Lett.* **393**, 51 (2004).

¹⁶M. A. Rohrdanz, K. M. Martins, and J. M. Herbert, *J. Chem. Phys.* **130**, 054112 (2009).

¹⁷J.-W. Song, T. Hirose, T. Tsuneda, and K. Hirao, *J. Chem. Phys.* **126**, 154105 (2007).

¹⁸T. Stein, H. Eisenberg, L. Kronik, and R. Baer, *Phys. Rev. Lett.* **105**, 266802 (2010).

¹⁹S. Refaely-Abramson, R. Baer, and L. Kronik, *Phys. Rev. B* **84**, 075144 (2011).

²⁰T. Körzdörfer, J. S. Sears, C. Sutton, and J.-L. Brédas, *J. Chem. Phys.* **135**, 204107 (2011).

²¹A. Karolewski, T. Stein, R. Baer, and S. Kümmel, *J. Chem. Phys.* **134**, 151101 (2011).

²²M. A. Rohrdanz and J. M. Herbert, *J. Chem. Phys.* **129**, 034107 (2008).

²³E. Livshits and R. Baer, *J. Phys. Chem. A* **112**, 12789 (2008).

²⁴T. Stein, L. Kronik, and R. Baer, *J. Am. Chem. Soc.* **131**, 2818 (2009).

²⁵T. Stein, L. Kronik, and R. Baer, *J. Chem. Phys.* **131**, 244119 (2009).

²⁶N. Kuritz, T. Stein, R. Baer, and L. Kronik, *J. Chem. Theory Comput.* **7**, 2408 (2011).

²⁷Optimal tuning of the more general range-separated hybrid, involving a fraction of short-range exact exchange, has also been found recently to be useful for various applications in spectroscopy. See, e.g., M. Srebro and J. Autschbach, *J. Chem. Theory Comput.* **8**, 245 (2012); S. Refaely-Abramson, S. Sharifzadeh, N. Govind, J. Autschbach, J. B. Neaton, R. Baer, and L. Kronik, *Phys. Rev. Lett.* **109**, 226405 (2012); J. V. Koppen, M. Hapka, M. M. Szczepaniak, and G. Chalasiński, *J. Chem. Phys.* **137**, 114302 (2012); B. Moore, M. Srebro, and J. Autschbach, *J. Chem. Theory Comput.* **8**, 4336 (2012).

²⁸A. Seidl, A. Görling, P. Vogl, J. A. Majewski, and M. Levy, *Phys. Rev. B* **53**, 3764 (1996).

²⁹J. P. Perdew, K. Burke, and M. Ernzerhof, *Phys. Rev. Lett.* **77**, 3865 (1996).

³⁰Y. Shao, L. F. Molnar, Y. Jung, J. Kussmann, C. Ochsenfeld, S. T. Brown, A. T. B. Gilbert, L. V. Slipchenko, S. V. Levchenko, D. P. O'Neill, R. A. DiStasio, Jr., R. C. Lochan, T. Wang, G. J. O. Beran, N. A. Besley, J. M. Herbert, C. Y. Lin, T. V. Voorhis, S. H. Chien, A. Sodt, R. P. Steele, V. A. Rassolov, P. E. Maslen, P. P. Korambath, R. D. Adamson, B. Austin, J. Baker, E. F. C. Byrd, H. Dachsel, R. J. Doerksen, A. Dreuw, B. D. Dunietz, A. D. Dutoi, T. R. Furlani, S. R. Gwaltney, A. Heyden, S. Hirata, C.-P. Hsu, G. Kedziora, R. Z. Khallullin, P. Klunzinger, A. M. Lee, M. S. Lee, W. Liang, I. Lotan, N. Nair, B. Peters, E. I. Proynov, P. A. Pieniazek, Y. M. Rhee, J. Ritchie, E. Rosta, C. D. Sherrill, A. C. Simmonett, J. E. Subotnik, H. L. W. Iii, W. Zhang, A. T. Bell, A. K. Chakraborty, D. M. Chipman, F. J. Keil, A. Warshel, W. J. Hehre, H. F. S. Iii, J. Kong, A. I. Krylov, P. M. W. Gill, and M. Head-Gordon, *Phys. Chem. Chem. Phys.* **8**, 3172 (2006).

³¹J. P. Perdew, R. G. Parr, M. Levy, and J. L. Balduz, *Phys. Rev. Lett.* **49**, 1691 (1982).

³²M. Levy, J. P. Perdew, and V. Sahni, *Phys. Rev. A* **30**, 2745 (1984).

³³C.-O. Almbladh and U. von Barth, *Phys. Rev. B* **31**, 3231 (1985).

³⁴J. P. Perdew and M. Levy, *Phys. Rev. B* **56**, 16021 (1997).

³⁵P. J. Stephens, F. J. Devlin, C. F. Chabalowski, and M. J. Frisch, *J. Phys. Chem.* **98**, 11623 (1994).

³⁶“Experimental bond lengths, computational chemistry comparison and benchmark database, Section II.B.3,” 2012, see <http://cccbdb.nist.gov>.

³⁷E. Clementi, D. L. Raimondi, and W. P. Reinhardt, *J. Chem. Phys.* **47**, 1300 (1967).

³⁸“Experimental atomization energies, computational chemistry comparison and benchmark database, Section II.B.1,” 2012, see <http://cccbdb.nist.gov>.

- ³⁹S. Kümmel and L. Kronik, *Rev. Mod. Phys.* **80**, 3 (2008).
- ⁴⁰M. Mundt, S. Kümmel, R. van Leeuwen, and P.-G. Reinhard, *Phys. Rev. A* **75**, 050501(R) (2007).
- ⁴¹M. Mundt and S. Kümmel, *Phys. Rev. A* **74**, 022511 (2006).
- ⁴²R. T. Sharp and G. K. Horton, *Phys. Rev.* **90**, 317 (1953).
- ⁴³J. D. Talman and W. F. Shadwick, *Phys. Rev. A* **14**, 36 (1976).
- ⁴⁴T. Körzdörfer, M. Mundt, and S. Kümmel, *J. Chem. Phys.* **129**, 014110 (2008).
- ⁴⁵T. Körzdörfer, M. Mundt, and S. Kümmel, *Phys. Rev. Lett.* **100**, 133004 (2008).
- ⁴⁶D. Hofmann, S. Klüpfel, P. Klüpfel, and S. Kümmel, *Phys. Rev. A* **85**, 062514 (2012).
- ⁴⁷M. Städele, M. Moukara, J. A. Majewski, P. Vogl, and A. Görling, *Phys. Rev. B* **59**, 10031 (1999).
- ⁴⁸A. M. Teale and D. J. Tozer, *Chem. Phys. Lett.* **383**, 109 (2004).
- ⁴⁹M. Mundt, S. Kümmel, B. Huber, and M. Moseler, *Phys. Rev. B* **73**, 205407 (2006).
- ⁵⁰T. Körzdörfer, S. Kümmel, N. Marom, and L. Kronik, *Phys. Rev. B* **79**, 201205(R) (2009).
- ⁵¹T. Körzdörfer, S. Kümmel, N. Marom, and L. Kronik, *Phys. Rev. B* **82**, 129903(E) (2010).
- ⁵²E. Engel and R. Schmid, *Phys. Rev. Lett.* **103**, 036404 (2009).
- ⁵³T. Körzdörfer and S. Kümmel, *Phys. Rev. B* **82**, 155206 (2010).
- ⁵⁴M. Dauth, T. Körzdörfer, S. Kümmel, J. Ziroff, M. Wiessner, A. Schöll, F. Reiner, M. Arita, and K. Shimada, *Phys. Rev. Lett.* **107**, 193002 (2011).
- ⁵⁵D. Hofmann and S. Kümmel, *Phys. Rev. B* **86**, 201109(R) (2012).
- ⁵⁶D. Hofmann, T. Körzdörfer, and S. Kümmel, *Phys. Rev. Lett.* **108**, 146401 (2012).
- ⁵⁷D. Hofmann and S. Kümmel, *J. Chem. Phys.* **137**, 064117 (2012).
- ⁵⁸R. Armiento, S. Kümmel, and T. Körzdörfer, *Phys. Rev. B* **77**, 165106 (2008).
- ⁵⁹A. Karolewski, R. Armiento, and S. Kümmel, *J. Chem. Theory Comput.* **5**, 712 (2009).
- ⁶⁰Reference 18 mistakenly reports $T_{r2}(\gamma)$ as the tuning criterion but in fact the $T_{LS}(\gamma)$ criterion was employed throughout that work.
- ⁶¹J. Autschbach, *Chem. Phys. Chem.* **10**, 1757 (2009).
- ⁶²E. B. Isaacs, S. Sharifzadeh, B. Ma, and J. B. Neaton, *Phys. Chem. Lett.* **2**, 2531 (2011).
- ⁶³G. Sini, J. S. Sears, and J.-L. Bredas, *J. Chem. Theory Comput.* **7**, 602 (2011).
- ⁶⁴S. Zheng and E. Geva, B. D. Dunietz, *J. Chem. Theory Comput.* **9**, 1125 (2013).
- ⁶⁵A. V. Krukau, G. E. Scuseria, J. P. Perdew, and A. Savin, *J. Chem. Phys.* **129**, 124103 (2008).

Publication 3

Optical absorption in donor-acceptor polymers – alternating vs. random

A. Karolewski, A. Neubig, M. Thelakkat, and S. Kümmel,

Phys. Chem. Chem. Phys. **15**, 20016 (2013).

Reproduced by permission of the PCCP Owner Societies

DOI: 10.1039/c3cp52739e

3

Own Contribution

I did all calculations and wrote the first version of the manuscript except for the section "Synthesis and Characterization". This section was written by A. Neubig who also synthesized and characterized all compounds of this work.

Optical absorption in donor–acceptor polymers – alternating vs. random†

Cite this: *Phys. Chem. Chem. Phys.*, 2013, **15**, 20016

Andreas Karolewski,^{‡a} Anne Neubig,^{‡b} Mukundan Thelakkat*^b and Stephan Kümmel*^a

We investigate in a combined theoretical and experimental study the influence that the specific arrangement, e.g., alternating or random, of donor and acceptor units has on the optical absorption of extended molecules. Because of its important role in low gap polymers we discuss in particular the energetic position of the first electronic transition. We theoretically determine the excitations in extended oligomers with thiophene as the donor and 2,1,3-benzothiadiazole as the acceptor component by using time-dependent density functional theory based on non-empirically tuned range separated hybrid functionals. Corresponding systems are synthesized and theoretical and experimental data are critically compared to each other. We conclude that the influence of the specific arrangement of donor and acceptor monomers on the optical gap is limited and that effects beyond the single molecule level effectively limit the size of the experimentally observed optical gap.

Received 1st July 2013,
Accepted 8th October 2013

DOI: 10.1039/c3cp52739e

www.rsc.org/pccp

1 Introduction

The search for low gap polymers is an important step in improving the efficiency of organic solar cells based on conjugated polymers.^{1–5} For systematically designing low gap polymers it is beneficial to understand the complex electronic processes that typically occur in these systems. The absorption of light that results in an excitation (“exciton formation”) is one important step in the sequence of processes that determine solar cell efficiency.⁶ There are different strategies for obtaining low gap polymers.⁴ Among the most important ones are increasing the conjugation length, e.g., by increasing the planarity of the polymer, and the combination of electron rich (donor) and electron poor (acceptor) monomers along the conjugated polymer backbone.⁷ In the latter case the reduction of the bond length alternation and the formation of partial intramolecular charge transfer (CT) excitations between the donor (D) and acceptor (A) moieties are considered to be responsible for the low gap.^{4,8}

In this article we focus on donor acceptor (DA) polymers and analyze how far the specific arrangement of D and A units within a polymer influences the optical absorption. Specifically we address

the question of whether the optical gap and other absorption peaks differ considerably between a molecule with a random arrangement of D and A units and a molecule in which the same total number of D and A units is arranged in a strictly alternating way. The answer to this question is important for our fundamental understanding of DA systems and for developing future synthesis strategies. Usually low gap polymers based on D and A moieties are synthesized by arranging the D and A units in a strict alternating order. Whether this strict alternating order is necessary for lowering the gap is not studied. If this is not necessary and the D and A units can be arranged in any random order to obtain the same effect, then the synthetic strategy to obtain a variety of new low gap polymers can be more innovative involving different kinds of monomers in any random fashion. This also allows improving the solubility of such polymers. Therefore, the question of the importance of the ordering of the D and A units is discussed in this paper.

Our study is based on thiophene (T) as the D and 2,1,3-benzothiadiazole (B) as the A component. Both of these constituents are frequently used in the field of low gap oligomers and polymers for organic photovoltaic devices.^{9–15} We computationally analyze the low lying excitations of these systems in detail. In agreement with other studies of similar systems¹⁶ we find that they can be described as having, at best, “partial” CT character, and we compare the theoretical findings in detail to experiments.

The type of accurate, non-empirical calculations for systems of considerable size that we present here are made possible by

^a Theoretical Physics IV, University of Bayreuth, 95440 Bayreuth, Germany.

E-mail: stephan.kuemmel@uni-bayreuth.de

^b Macromolecular Chemistry I, University of Bayreuth, 95440 Bayreuth, Germany.

E-mail: mukundan.thelakkat@uni-bayreuth.de

† Electronic supplementary information (ESI) available. See DOI: 10.1039/c3cp52739e

‡ These authors contributed equally to this work.

recent progress in the development of (Time Dependent) Density Functional Theory ((TD) DFT).^{17–24} Specifically, we employ a range separated hybrid (RSH) functional in which the range separation parameter is chosen according to a non-empirical, self-consistent procedure designed to yield a reliable description of excitations in multichromophoric systems.^{21,25,26} Using the correct functional class to account for the complexity of the excitations in DA polymers is a decisive prerequisite for the type of computational study that we present here.

Our manuscript is organized as follows. In Section 2 we give a brief overview of the studied systems, followed by an outline of the theoretical approach and the experimental synthesis in Section 3. We present the results of our calculations in Section 4, comparing different D–A arrangements and oligomer sizes in a single molecule approach and predicting the effective saturated conjugation length. In the same section we compare the theoretical findings to the corresponding experimental data. Occurring differences are analyzed in Section 5. The maximum achievable conjugation length emerges as the main factor limiting the optical gap.

2 Systems

Fig. 1 and 2 schematically depict the oligomers that we examine in this article. a-BTT and a-BTT-H show strictly alternating arrangements of thiophene (T) as a donor and 2,1,3-benzothiadiazole (B) as an acceptor (upper left and left in Fig. 1 and 2, respectively). The difference between these two systems is the presence of hexyl side chains (H) on the thiophene units in a-BTT-H. The systems r-BTT and r-BTT-H (upper right and right in Fig. 1 and 2, respectively) are molecules in which T and B units are combined to yield random arrangements of T and BT (Fig. 3) components. For a-BTT and r-BTT we did calculations with the number n of repeat units ranging from $n = 1$ to $n = 12$. For illustration we show the optimized structures for the largest

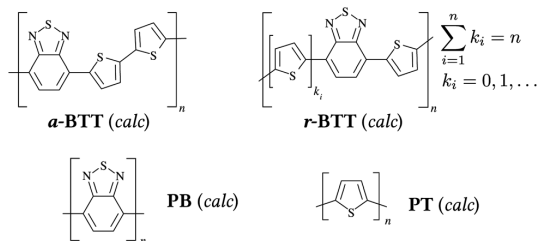


Fig. 1 Schematic of the oligomeric systems examined in the calculations.

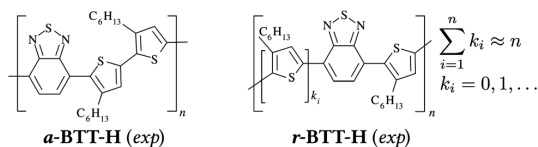


Fig. 2 Schematic of the oligomeric systems examined in experiments. The chain length n can only be determined on average (\bar{n}) from gel permeation chromatography.

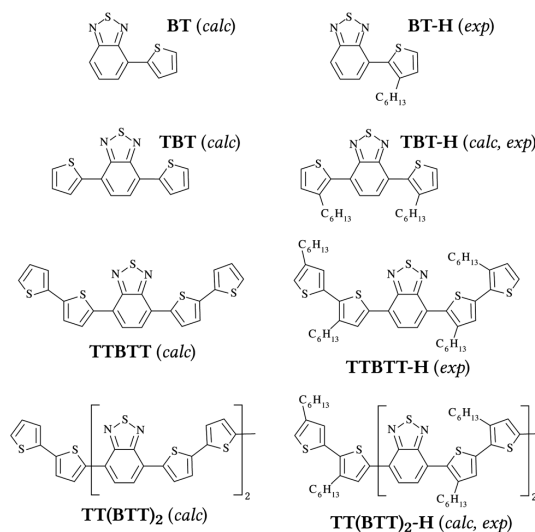


Fig. 3 Schematic of the well defined monodisperse low molecular weight systems examined in experiments (labeled with exp) and calculations (labeled with calc).

oligomeric calculated systems ($n = 12$) in Fig. 4. For reasons that become clear further below it is sufficient to study just one representative for r-BTT, *i.e.*, one specific random arrangement, for each chain length.

In our experiments we synthesized a-BTT-H with an average number \bar{n} of repeat units of $\bar{n} = 4$ and $\bar{n} = 15$ and a polydispersity $M_w/M_n = 1.7$ and 1.6 , as well as r-BTT-H with $\bar{n} = 5$ and $\bar{n} = 10$ and $M_w/M_n = 1.5$ and 1.6 (see caption of Fig. 2). The only difference to the systems that we use in the calculations are the hexyl side chains. The influence of such side chains is discussed in detail in Section 5.

It is important to note that in the calculations we always combined n B with $2n$ T. In this way we ensure that our results are only influenced by the DA arrangement (and not by different D and A ratios). In the synthesis, however, we were only able to obey this rule approximately in the case of r-BTT-H. For a deeper understanding of DA systems and the differences between calculations and experiment we furthermore investigated the donor-only oligomer PT, the acceptor-only oligomer PB as well as the donor-acceptor systems BT, TBT, TBT-H, TTBT, TTBT-H, TT(BTT)₂, and TT(BTT)₂-H as shown in Fig. 3 (monodisperse low molecular weight in experiment).

3 Methodology and synthesis

3.1 Methodology (theory)

The largest systems that we examined in our calculations are conjugated molecular chains with up to 36 aromatic rings. Our method of choice for systems of such size is DFT^{27,28} or TDDFT,^{29,30} respectively, because of its favorable ratio of reasonable quality of results to moderate computational cost. With appropriately chosen functionals, it also allows for little or no empiricism.

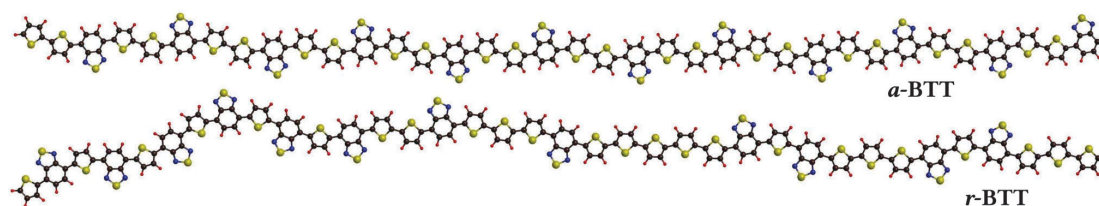


Fig. 4 Optimized geometries of a-BTT and r-BTT for $n = 12$, corresponding to a length of 15 nm. The optimization method is described in Section 3.

We optimized the geometries of the systems in Fig. 1 and 3 using the B3LYP functional³¹ with the def2-SV(P) basis set and the Grimme dispersion correction³² in Turbomole.^{33,34} This choice is pragmatically motivated by previous experience showing that this approach yields reliable geometries for this type of system.

For the calculation of the excitation energies, which is the critical step in our study, we used linear response TDDFT with the Baer–Neuhauser–Livshits (BNL) RSH functional. It combines LDA-type short range exchange and long range Fock exchange with the Lee–Yang–Parr correlation functional.^{35–37} Since we are calculating optical excitation energies we choose the least square gap tuning condition^{26,38}

$$T_{LS}(\gamma) = \sqrt{\sum_{i=N}^{N+1} [e_{\text{HOMO}}^i(i) + E^\gamma(i-1) - E^\gamma(i)]^2} = \min \quad (1)$$

to determine the range separation parameter γ , which corresponds to approximately twice the inverse of the separation length between short range and long range electronic exchange.^{39,40} $E^\gamma(i)$ is the γ -dependent total energy for a system with i electrons and $e_{\text{HOMO}}^i(i)$ the eigenvalue of the highest occupied generalized Kohn–Sham orbital. To account for the system specific magnitude of the highest occupied and lowest unoccupied orbitals we performed the tuning for each molecule separately. With the optimized γ we calculate the BNL excitation energies with the program package QChem⁴¹ and the 6-31G(d,p) basis set. We expect reliable results from this procedure because it has been shown, *e.g.* in ref. 16 and 25, that tuned RSH functionals can successfully be applied to DA systems that are similar to the ones studied here, and the resulting excitation energies are consistent with experimental absorption spectra.

In order to test the reliability of this approach we performed several control calculations. To check basis set limitations we optimized the geometries of BT, TBT, and TT(BTT)₂ also with the def2-TZVP basis set (in Turbomole) and performed the γ -tuning and the calculation of the BNL excitation energies with the 6-311G(d,p) basis set (in QChem). In comparison to the calculations with the basis sets mentioned in the previous paragraph, this lead to differences of less than 0.1 eV in the lowest excitation energy. As another test we checked how much using a different RSH functional alters the results. We used the ω PBE functional¹⁸ for the γ optimization as well as the TDDFT calculation on TT(BTT)₂. Compared to the BNL functional the lowest excitation energy changed by only about 0.02 eV. This is

in line with other studies showing that differences between various RSH approaches appear in the ground state energy³⁸ and not in optical and fundamental gaps.^{16,42} Finally, we tested how far environmental influences as described by the COSMO solvation model⁴³ within Turbomole affect the B3LYP geometries and TDDFT excitation energies and found an overall effect of only 0.04 eV.⁴⁴ These tests confirm the validity of our theoretical setup since all the discrepancies are within the limits of the predictive power of our method itself.

3.2 Synthesis and characterization

3.2.1 Monomer synthesis. The synthesis procedures of the monomers M1 and M2 are outlined in Fig. 5. The AB-type monomer M1 is not documented in the literature; the details of the synthesis are given in the ESI.† M1 was obtained by the Ir-catalyzed (Ir(COD)Cl₂) borylation of an asymmetrically substituted compound **1** in the presence of 4,4'-di-tert-butyl bipyridine (dtbpy). The other AB-type monomer M2 is known in the literature but we synthesized it starting from 2-bromo-3-hexylthiophene **2** with the Knochen–Hauser-base (2,2,6,6-tetramethylpiperidinylmagnesium chloride lithium chloride: TMPMgCl·LiCl). Details are given in the ESI.† M3 was synthesized by bromination of 3,4'-dihexyl-2,2'-bithiophene with *N*-bromosuccinimide according to published procedures.⁴⁵ M4 is commercially available.

3.2.2 Polymer synthesis. Following the synthetic route shown in Fig. 6, the AB-type monomers M1 and M2 were used to obtain the conjugated copolymers r-BTT-H ($\bar{n} = 4; 15$). Using monomers M3 and M4 the alternating copolymers a-BTT-H ($\bar{n} = 5; 10$) were obtained. All copolymers were synthesized *via* palladium catalyzed Suzuki coupling polycondensation. A variation of reaction conditions led to different molecular weights for r-BTT-H and a-BTT-H. For synthetic details and characterization see the ESI.†

All four conjugated copolymers are completely soluble in common organic solvents like toluene, tetrahydrofuran or

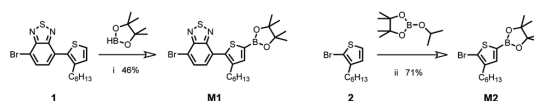


Fig. 5 Synthesis of monomers M1 and M2. Reaction conditions: (i) Ir(COD)Cl₂/dtbpy in tetrahydrofuran at reflux; (ii) TMPMgCl·LiCl in tetrahydrofuran at room temperature.

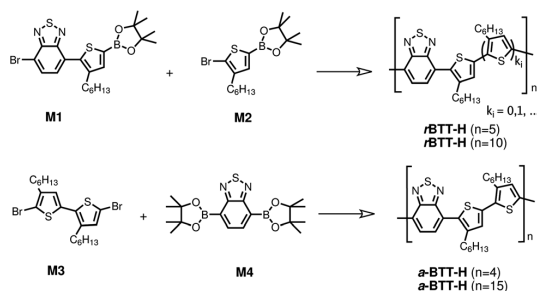


Fig. 6 Synthesis of copolymers r-BTT-H and a-BTT-H.

Table 1 Number average molecular weights (M_n) determined with GPC, polydispersity index (M_w/M_n) and absorption maximum (E_{\max}) of the synthesized compounds

	M_n [g mol ⁻¹] (GPC)	M_w/M_n (GPC)	E_{\max} [eV]
TBT-H			3.08
TTBT-H	913	1.01	2.46
TT(BTT) ₂ -H	1443	1.04	2.41
a-BTT-H (\bar{n} = 4)	1841	1.74	2.38
a-BTT-H (\bar{n} = 15)	7201	1.64	2.36
r-BTT-H (\bar{n} = 5)	2490	1.46	2.49
r-BTT-H (\bar{n} = 10)	4478	1.59	2.45

methylene chloride. The number average molecular weights of these copolymers were determined using oligomeric gel permeation chromatography (GPC). Polystyrene was used for calibration of molecular weights. The GPC traces of the copolymers are shown in Fig. S1 (ESI[†]), the respective data are summarized in Table 1.

3.2.3 Oligomer synthesis. The well-defined oligomers TTBT-H and TT(BTT)₂-H were obtained from polymer a-BTT-H ($n = 4$) by preparative GPC after extraction with particular solvents. The crude polymer was extracted sequentially with methanol, ethanol, acetone and methylene chloride. The acetone fraction was used for preparative GPC. Narrow fractions were collected and measured on an analytical GPC setup. Molecular weight analysis of TTBT-H and TT(BTT)₂-H was done by matrix assisted laser desorption ionization with time of flight detection (MALDI-ToF) mass spectrometry and GPC. The GPC traces and MALDI-ToF spectra of TTBT-H and TT(BTT)₂-H are shown in the ESI.[†]

4 Influence of the D and A arrangement on the gap

One of the key properties of a low gap system designed for the use in organic solar cells is the optical gap which is defined as the transition energy between the vibrational ground state (GS) of the electronic GS and the vibrational GS of the first excited electronic state. However, more accessible to theory is the vertical excitation energy that is close or identical to the absorption maximum E_{\max} (see Fig. 7). It is the energy

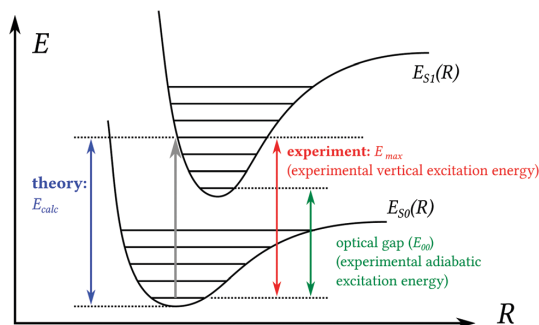


Fig. 7 Schematic of the different excitation energy expressions discussed in this work. R is a generalized coordinate. $E_{S0}(R)$ is the GS energy and $E_{S1}(R)$ the first excited state energy as a function of this coordinate.

difference of the GS and the first excited state with both states in the GS geometry. Hence, the vertical excitation energy is the optical gap (also called adiabatic excitation energy) plus a first or higher order vibrational energy. The energy that we obtain from a standard TDDFT calculation (E_{calc}) is the vertical excitation energy plus the vibrational zero point energy of the electronic GS. This zero point vibrational energy is below the accuracy of the calculation and the error of the experiment and can be neglected. Therefore E_{calc} and E_{max} are comparable. The situation and mentioned energies are illustrated in Fig. 7. In the following, if we write lowest or first excitation energy we mean E_{calc} in a calculation and E_{max} in an experiment.

Our focus in this section lies on the differences between the lowest excitation energies of the DA arrangements a-BTT and r-BTT. These differences directly reveal how large the influence of the DA arrangement on the optical gap is. We calculated these energies for the oligomers $n = 1$ up to $n = 12$ with the RSH approach explained in Section 3, studying one representation of r-BTT for each repeat unit n . The resulting energies E_{calc} are plotted in Fig. 8 as a function of the inverse number of double bonds N^{-1} along the molecular backbone. As discussed in earlier work²⁵ we use an exponential fit to extrapolate to the saturation limit. For the monomer ($n = 1$) both systems are identical. Hence, both curves start at the same point. During the progression to larger N the excitation energies of a-BTT and r-BTT almost overlap each other and saturate at 1.63 and 1.67 eV, respectively. Note that all data points are close to the exponential fitting curves. This confirms that for the purposes of our study it is not necessary to consider different statistical arrangements for r-BTT.

In addition to predicting the saturation energies we can draw two conclusions from this graph. The first one is the saturation length – the amount of repeat units at which the lowest excitation energy saturates. For both systems it lies between $n = 6$ and $n = 8$. The second conclusion concerns the influence of the relative ordering of D and A components on the first excitation energy. Comparing a-BTT with r-BTT we observe that the respective energy values are very close to each other. Thus, the relative order of D and A in the polymer chain has only a minor influence.

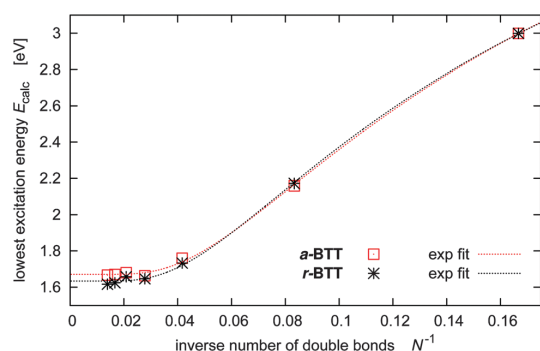


Fig. 8 Lowest calculated vertical absorption energies (TDDFT with tuned BNL and 6-31G(d,p) basis) as a function of the inverse number of double bonds N^{-1} .

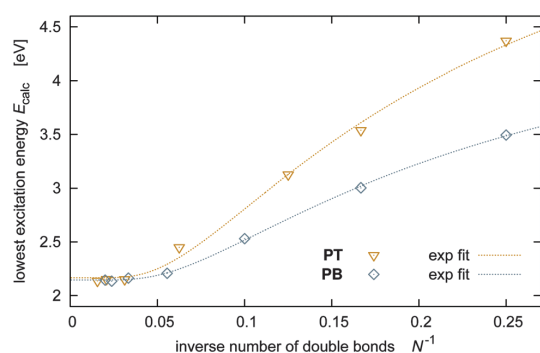


Fig. 9 Lowest calculated vertical absorption energies of T and B oligomers as a function of the inverse number of double bonds N^{-1} .

In order to further elucidate the question of how much the DA arrangement influences the first excitation energy we compare the above results to first excitation energies of oligomers that consist of only either D or A monomers. Fig. 9 shows these energies for T oligomers (PT, $n = 1$ to 32) and B oligomers (PB, $n = 1$ to 25) as a function of the inverse number of double bonds N^{-1} . Both systems coincidentally saturate at a vertical excitation energy of 2.15 eV, which is 0.5 eV above the respective energies of a-BTT and r-BTT. We thus observe the well known effect that combining D and A units reduces the first excitation energy, but in our calculations the magnitude of this reduction is at most 0.5 eV.

Similar conclusions hold when the analysis is extended to not only take the first excitation energies into account, but also the corresponding oscillator strengths and higher excitations. To this end we show the optical spectra of a-BTT and r-BTT for $n = 6$ in Fig. 10. It shows that both systems have very dominant first excitations with oscillator strengths of similar magnitude. Comparing the spectra obtained for different chain lengths (not shown here) confirms that the oscillator strength and dominance increase with n . Besides the main peak the spectra of a-BTT and r-BTT do not show large differences at higher energies. Thus, the calculations show that the conclusions

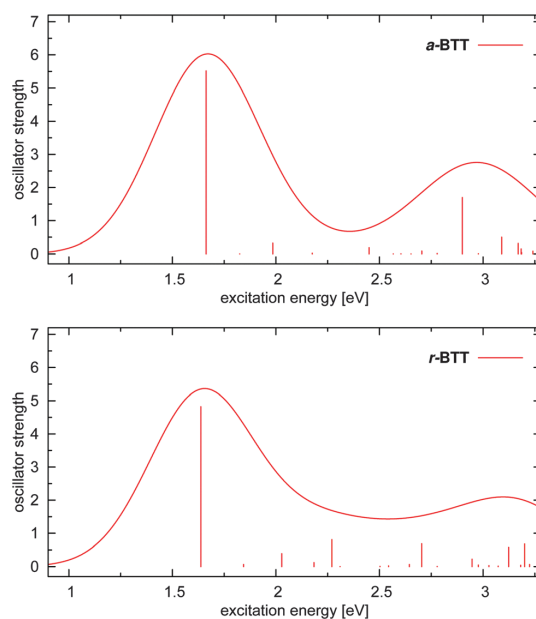


Fig. 10 Calculated electronic excitation spectra of a-BTT and r-BTT with $n = 6$ repeat units (6 B and 12 T units). The calculated positions and oscillator strengths are represented by the bars. Linewidths as present in typical experiments are mimicked by a Gaussian broadening with 0.3 eV HWHM (half width half maximum).

drawn previously for the first excitation energy are valid in a similar way for the overall optical spectrum: the rearrangement of D and A from a-BTT to r-BTT leads to only relatively small changes.

To gain further insight into the physics of these systems we analyze whether CT is important in the lowest excitations. CT excitations are defined as excitations where a transfer of electronic density from one part of a system to another part occurs during the excitation. Typically, CT excitations are prevalent in DA systems since they combine electron poor and electron rich components. In a figurative sense an electron leaves the donor, thus creating a hole, and is absorbed by the acceptor. It is not clear whether this picture holds in DA oligomers or polymers in which the D and A units are distributed along the molecular backbone such that D and A parts are not necessarily adjacent to each other.

In order to examine the CT character of a-BTT and r-BTT we calculated the most dominant natural transition orbital⁴⁶ (NTO) holes and electrons of the first excitation for both systems with a chain length $n = 10$. Fig. 11 (top) shows the most dominant NTO pair for r-BTT accounting for 54% of the excitation. The “hole orbital” and the corresponding “electron orbital” are localized on the same parts of the molecule and are nearly equal in extension. The only difference that we observe is that parts of the electron NTO are located on the sulfur and nitrogen atoms of the benzothiadiazole unit, whereas the hole NTO does not extend to these regions. This difference is so

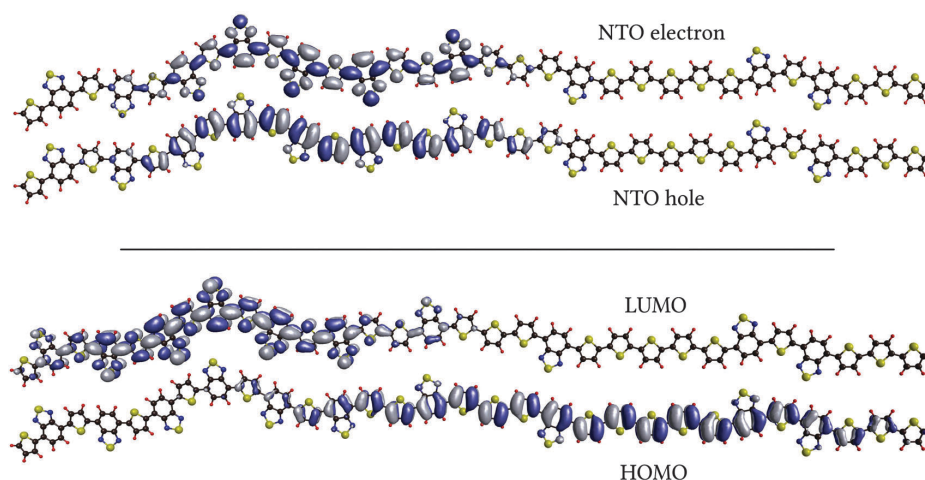


Fig. 11 Most dominant NTO hole/electron of the first excitation (top) and HOMO–LUMO plot (bottom) for *r*-BTT with $n = 10$. The NTO pair contribution to the excitation is 54% and from the HOMO–LUMO pair 8%. The next three less dominant NTO pairs (accounting for 93% of the excitation) also show no significant CT. The isosurface value is 0.01.

small that this excitation can be classified as having predominantly valence character and just a small CT component. An analysis of the less dominant NTO pairs (shown in Fig. S4 of the ESI†) shows that some of these have more CT character, but still overall the excitation appears as being of mixed valence-CT character at most, and not a hallmark CT one. Similar conclusions hold for *a*-BTT.

In this context it is worthwhile to draw attention to a limitation of the frequently used technique of using HOMO and LUMO orbital plots for analyzing the CT character of an excitation. The present systems are hallmark examples where such a simplified view would lead to even qualitatively wrong conclusions, because many different generalized Kohn–Sham orbital pairs contribute to the lowest excitations. In the case of *r*-BTT an analysis of the HOMO and LUMO orbitals (Fig. 11 (bottom)) would lead to the conclusion that long-range CT is very dominant here. However, the HOMO–LUMO pair accounts for only 8% of the excitation, *i.e.*, does not suffice to characterize its nature. The other orbital pairs with a significant contribution to the lowest excitation are shown in Fig. S5 of the ESI.† Their structure does not allow for clearly assigning a certain character to the excitation.

In the second part of this section, we compare the theoretical results with measurements of *a*-BTT-H ($\bar{n} = 4, 15$) and *r*-BTT-H ($\bar{n} = 5, 10$), corresponding to the calculated systems *a*-BTT and *r*-BTT. Fig. 12 shows the measured UV/vis spectrum of *a*-BTT-H and *r*-BTT-H in chloroform solution and Table 2 compares the maxima of the lowest absorption peaks to our calculated excitation energies. The measured and calculated values for the lowest excitation energy are a good approximation to the vertical excitation energy (*cf.* Section 4). The maxima of absorption for the longer oligomers of *a*-BTT-H and *r*-BTT-H are at 2.36 and 2.45 eV, respectively. The small difference with a magnitude of only 0.09 eV is in line with the

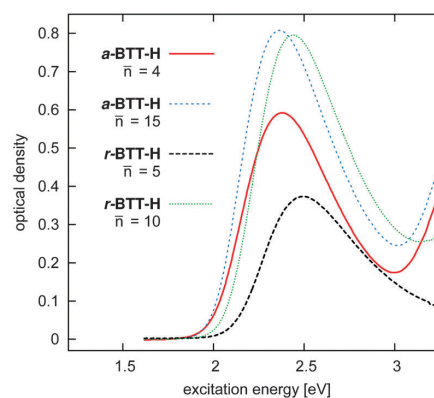


Fig. 12 UV/vis absorption spectra of *a*-BTT-H ($\bar{n} = 4, 15$) and *r*-BTT-H ($\bar{n} = 5, 10$) in chloroform solution (0.02 mg ml^{-1}) at room temperature.

theoretical finding that the nature of the arrangement of D and A has only a small influence on the optical gap. Regarding that the difference is not exactly the same – 0.05 eV *versus* 0.09 eV – one has to keep in mind possible small differences between the random arrangements in the calculation and the experiment: in the calculation *r*-BTT contains exactly twice as many thiophene rings as benzothiadiazole rings, whereas in experiments this ratio can only be achieved approximately.

The most noticeable difference between experiment and theory is found for the absolute values of the excitation energies. The experimental excitation energies are approximately 0.7 eV larger than the theoretical ones, *i.e.*, the difference is considerably larger than what one expects based on the accuracy of the experiments and calculations. We consider our experimental values as reliable since they are in accordance with measurements for similar systems.^{9–11,47,48} One may argue

Table 2 Lowest excitation energies: comparison of an alternating vs. random system in experiment and calculation, respectively. The calculations refer to $n = 12$ for both cases. The experiments refer to $\bar{n} = 15$ for a-BTT-H and $\bar{n} = 10$ for r-BTT-H. In both theory and experiment, the chosen numbers of repeat units lie in the saturated regime (compare Fig. 13 and Section 5)

First excitation energy [eV]			
	Alternating	Random	Δ (alt-random)
Calculation	1.67	1.62	0.05
First excitation energy [eV]			
	Alternating	Random	Δ (alt-random)
Experiment	2.36	2.45	-0.09

that it is a well known effect that TDDFT based on local, semilocal or hybrid functionals underestimates CT excitation energies^{25,49,50} and that this may explain the discrepancy. However, because of this reason we use the tuned RSH approach that remedies this problem and is known for very accurately predicting the lowest excitation energies of DA systems.^{§16,21,25,26} The discrepancy may thus be regarded as physically significant, and we elaborate on it in the following section.

5 Analysis of the differences between experiment and theory

In order to analyze the disagreement between the theoretical predictions and the experimental data we also synthesized DA systems with a smaller chain length and compared their lowest absorption energies to the corresponding calculated excitation energies. These additionally synthesized systems are BT, TBT-H, TT(BTT)₂-H, and TT(BTT)₂-H, as schematically represented in Fig. 3. The calculated systems are BT, TBT, TBT-H, TT(BTT)₂, and TT(BTT)₂-H, also shown in Fig. 3. We compare the measured and calculated lowest excitation energies in Fig. 13 along with results for the systems a-BTT and a-BTT-H as a function of the number of double bonds N . Additionally, we also show two data points for a-BTT with methyl side chains (indicated by “M” in the graph). In the left part of the graph (small systems) we have good agreement between theory and experiment. If the difference between theory and experiment were to be attributed solely to unreliability of the theoretical predictions, then the tuned RSH would have to be accurate for small systems but systematically fail for larger ones – a scenario that we do not consider likely, at least not in the size range studied here, given the previously published results obtained with the tuned RSH approach. We also note that the experimental values are in line with measurements of other, similar systems.^{8,52–55} Yet, as

§ B3LYP calculations would result in an even lower gap. For a-BTT one would obtain a saturated lowest excitation energy of 1.33 eV, 0.34 eV lower than our tuned BNL calculations.

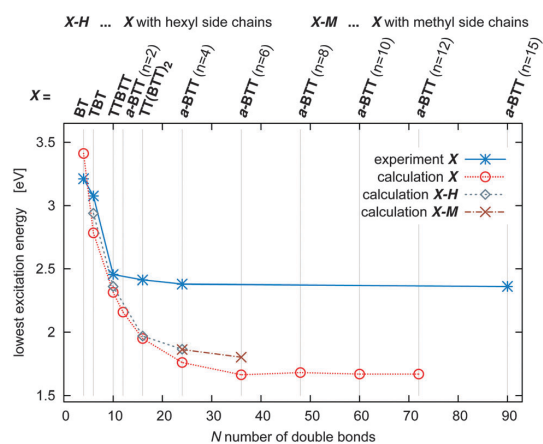


Fig. 13 Lowest excitation energies as a function of the number of double bonds N . The experimental data points reflect the maxima of the UV/vis spectra. The calculated data points are obtained from tuned BNL TDDFT linear response calculations. The dotted lines are drawn as guides to the eye. All systems in the experiment have hexyl side chains (C₆H₁₃) attached to the thiophene rings as shown in Fig. 2 and 3; for the calculations we show data points for systems with hexyl and methyl side chains⁵¹ and compare them to systems without side chains.

the systems get larger the difference between the experimental and the theoretical results increases.

In the experiment, the B units can have neighboring T units with hexyl chains pointing inwards, away, or in both directions. This can happen because during the synthesis the orientation of the bithiophene can change from one B to the next B unit (*cf.* Fig. 6). To examine the consequences that the different side-chain orientations can have we calculated the excitation energy for TBT with asymmetrically and symmetrically attached side chains. In the symmetric case the side chains point inwards and as a consequence lead to larger torsion angles between the thiophene and benzothiadiazole units. Furthermore, the chains are spatially closer and can therefore interact more. In line with this reasoning we observe in Fig. 14 that indeed in the symmetric case ((ii) in Fig. 14) the excitation energy changes by 0.15 eV whereas the changes are negligible for the asymmetric case ((i) in Fig. 14). Fig. 13 shows results that were obtained for different molecules with hexyl (H) and methyl (M) side chains attached as schematically shown in Fig. 2 (left side), *i.e.*, one of the neighboring T rings has a side chain pointing towards the B unit and the other pointing away. We chose this configuration in the calculations because it occurs on average in the experiment since the hexyl chains on the bithiophene units are asymmetrically attached (*cf.* Fig. 6). The lowest excitation shifts by at most 0.15 eV towards the experimental value. In summary these results indicate that the influence of the side chains may be able to explain part of the discrepancy between theory and experiment, but not all of it.

One possibility which we so far did not take into account and which may play a role in explaining the discrepancy are interactions between the systems and the solvent that may change the experimental excitation energies. Therefore, we explored the

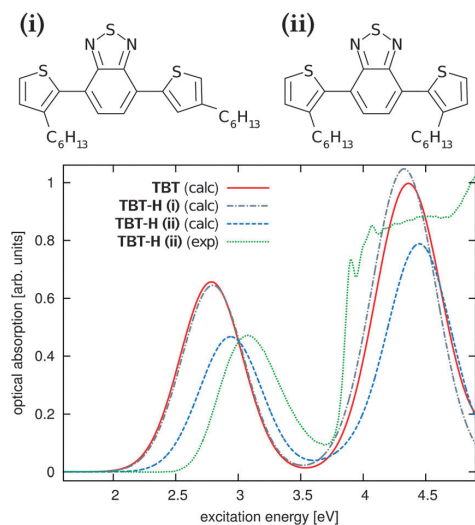


Fig. 14 Comparison of the calculated spectra (calc) for TBT and TBT-H and the UV/vis experimental spectrum (exp) for TBT-H in chloroform solution (0.02 mg ml⁻¹) at room temperature. For TBT-H we calculated a system with asymmetrically (i) and symmetrically (ii) attached hexyl side chains. Only case (ii) is examined in the experiment. As a guide to the eye the calculated peak positions are broadened with 0.3 eV HWHM and the measured optical density (experiment) is multiplied by a factor chosen to equalize the peak heights of the first peak of TBT-H (ii) in experiment and calculation.

influence of the solvent on some of the smaller systems. In the calculations, the solvent (as modeled by the solution model) has only little influence on the structure during geometry optimization. It also influences the excitation energies very little; the overall effect is less than 0.04 eV. Hence, solution models (*cf.* Section 3) cannot explain the large differences between experiment and theory. Also, the direct electronic effects of a solvent (*e.g.*, screening) should influence small and large systems in a similar way. On the experimental side we explored the effects of using different solvents. Besides chloroform we also measured the UV/vis spectrum of r-BTT-H with tetrahydrofuran and toluene. The observed shifts of the absorption maximum are less than 0.02 eV, *i.e.* very small. Thus, the discrepancies between experiments and calculations are not solvent dependent or at least similar for all tested solvents.

Another possibility is that the experimental geometries are more distorted than the stretched geometries that we used in the calculations (*cf.* Fig. 4). Although changing the orientation of the T vs. the B unit has only a small local influence on the structure (different cases have been discussed, *e.g.*, in ref. 56 and 57), it can change the global curvature of a chain, *e.g.*, from a stretched to a curved geometry. For r-BTT we constructed such a curved structure by choosing the sulfur atom of thiophene to always point in the opposite direction of the sulfur atom in benzothiadiazole. The optimized geometry of this system is displayed in Fig. 15. Compared to the stretched structure the excitation energy of this system changes by about 0.05 eV. This demonstrates that a globally curved structure can reach nearly as low a gap as a straight structure.

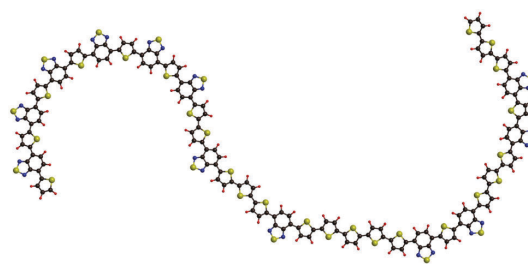


Fig. 15 Example of a curved structure for r-BTT with $n = 12$. Fig. 4 shows an example of a stretched version of r-BTT.

Another reason that could explain the discrepancy between theory and experiment is a difference in the effective conjugation length. Fig. 13 shows a significant difference in how the experimental and theoretical curves saturate with increasing system size. The experimental excitation energies already start to saturate at a number of double bonds of $N \approx 15$, whereas in theory the saturation is at $N \approx 35$. This corresponds to a BTT repeat unit of $n \approx 3$ for the experiment and $n \approx 6$ for theory. This result might not be unexpected, however, its extent is worrisome and may well explain that the minimal achievable lowest excitation energy in the experiment is 0.7 eV above the calculated saturated energy. There are different factors that may lead to an effective limitation of the conjugation length in the experiments. Likely candidates are interactions between different chains and between chains and the solvent, which may lead to kinks and torsions in the structure and may thus break the electronic conjugation along the molecular backbone. The effect could be intensified by the hexyl chains that are attached to the structures in the experiment.

Thus, the results for all our systems, which cover both the well defined small molecule range as well as the oligomeric/polymeric range, can be summarized as follows. For the case of small molecules, there is full agreement between theory and experiment. In the range of oligomers and polymers the theoretically found (first) excitation energies are by *ca.* 0.7 eV smaller than the ones found experimentally. However, the theoretical and the experimental results for the optical absorption agree with respect to the finding that different D and A arrangements lead to very similar excitation spectra. We extensively discussed the effects that can contribute to the 0.7 eV difference, and this brings us to our conclusion.

6 Conclusion

We studied theoretically and experimentally the influence that the relative ordering of D and A units has on the optical absorption of DA systems consisting of thiophene and benzothiadiazole. The lowest excitation energy changes only very little (< 0.1 eV) in our TDDFT calculations based on a tuned RSH functional when going from the alternating to the randomly arranged DA system. This result was confirmed by our experimental study. Analysis of the NTOs showed that long-range CT is

not dominant in the first optical excitation. Our calculations predicted the lowest possible excitation energy for a-BTT to be 1.67 eV with a saturation length of approximately 6 BTT repeat units. A comparison with measured excitation energies from a solution measurement reveals that the excitation already starts to saturate after 3 repeat units of BTT. Although the synthesized systems can have 15 repeat units or even more, they behave like oligomers with 3 BTT repeat units with respect to the optical properties. Thus, the maximum conjugation length in experiments is much lower than what appears to be theoretically achievable. Correspondingly, the minimum achievable optical gap is 2.36 eV, *i.e.*, *ca.* 0.7 eV larger than the theoretical prediction. Effects that may cause this discrepancy between the experiment and the theoretical prediction were discussed and, in agreement with work on other DA systems,^{56,57} we conclude that future work may need to go beyond the single molecule level. Such work could provide further guidance in the design of oligomers or polymers that have the effective conjugation length that is necessary for a lower optical gap.

Acknowledgements

The authors acknowledge financial support from the German Research Foundation (GRK 1640) and the Bavarian State Ministry of Science, Research, and the Arts for the Collaborative Research Network "Solar Technologies go Hybrid".

References

- 1 J. Roncali, *Chem. Rev.*, 1997, **97**, 173–206.
- 2 E. Bundgaard and F. C. Krebs, *Sol. Energy Mater. Sol. Cells*, 2007, **91**, 954–985.
- 3 R. Kroon, M. Lenes, J. C. Hummelen, P. W. M. Blom and B. de Boer, *Polym. Rev.*, 2008, **48**, 531–582.
- 4 Y.-J. Cheng, S.-H. Yang and C.-S. Hsu, *Chem. Rev.*, 2009, **109**, 5868–5923.
- 5 C. Risko, M. D. McGehee and J.-L. Brédas, *Chem. Sci.*, 2011, **2**, 1200–1218.
- 6 J.-L. Brédas, J. E. Norton, J. Cornil and V. Coropceanu, *Acc. Chem. Res.*, 2009, **42**, 1691–1699.
- 7 E. E. Havinga, W. t. Hoeve and H. Wynberg, *Polym. Bull.*, 1992, **29**, 119–126.
- 8 C. Kitamura, S. Tanaka and Y. Yamashita, *Chem. Mater.*, 1996, **8**, 570–578.
- 9 M. Helgesen, S. A. Gevorgyan, F. C. Krebs and R. A. J. Janssen, *Chem. Mater.*, 2009, **21**, 4669–4675.
- 10 J.-Y. Lee, M.-H. Choi, H.-J. Song and D.-K. Moon, *J. Polym. Sci., Part A: Polym. Chem.*, 2010, **48**, 4875–4883.
- 11 P. Sonar, E. L. Williams, S. P. Singh and A. Dodabalapur, *J. Mater. Chem.*, 2011, **21**, 10532–10541.
- 12 K.-H. Lee, H.-J. Lee, K. Kuramoto, Y. Tanaka, K. Morino, A. Sudo, T. Okauchi, A. Tsuge and T. Endo, *J. Polym. Sci., Part A: Polym. Chem.*, 2011, **49**, 3543–3549.
- 13 S. Albrecht, S. Janietz, W. Schindler, J. Frisch, J. Kurpiers, J. Knipert, S. Inal, P. Pingel, K. Fostiropoulos, N. Koch and D. Neher, *J. Am. Chem. Soc.*, 2012, **134**, 14932–14944.
- 14 W. Li, A. Furlan, K. H. Hendriks, M. M. Wienk and R. A. J. Janssen, *J. Am. Chem. Soc.*, 2013, **135**, 5529–5532.
- 15 B. A. D. Neto, A. A. M. Lapis, E. N. da Silva Júnior and J. Dupont, *Eur. J. Org. Chem.*, 2013, 228–255.
- 16 L. Pandey, C. Doiron, J. S. Sears and J.-L. Brédas, *Phys. Chem. Chem. Phys.*, 2012, **14**, 14243–14248.
- 17 H. Iikura, T. Tsuneda, T. Yanai and K. Hirao, *J. Chem. Phys.*, 2001, **115**, 3540–3544.
- 18 T. M. Henderson, B. G. Janesko and G. E. Scuseria, *J. Chem. Phys.*, 2008, **128**, 194105.
- 19 J.-D. Chai and M. Head-Gordon, *J. Chem. Phys.*, 2008, **128**, 084106.
- 20 M. A. Rohrdanz, K. M. Martins and J. M. Herbert, *J. Chem. Phys.*, 2009, **130**, 054112.
- 21 T. Stein, L. Kronik and R. Baer, *J. Am. Chem. Soc.*, 2009, **131**, 2818–2820.
- 22 D. Hofmann, T. Körzdörfer and S. Kümmel, *Phys. Rev. Lett.*, 2012, **108**, 146401.
- 23 D. Hofmann and S. Kümmel, *J. Chem. Phys.*, 2012, **137**, 064117.
- 24 I. Dabo, A. Ferretti, C.-H. Park, N. Poilvert, Y. Li, M. Cococcioni and N. Marzari, *Phys. Chem. Chem. Phys.*, 2013, **15**, 685.
- 25 A. Karolewski, T. Stein, R. Baer and S. Kümmel, *J. Chem. Phys.*, 2011, **134**, 151101.
- 26 L. Kronik, T. Stein, S. Refaely-Abramson and R. Baer, *J. Chem. Theory Comput.*, 2012, **8**, 1515–1531.
- 27 P. Hohenberg and W. Kohn, *Phys. Rev.*, 1964, **136**, B864–B871.
- 28 W. Kohn and L. J. Sham, *Phys. Rev.*, 1965, **140**, A1133–A1138.
- 29 E. Runge and E. K. U. Gross, *Phys. Rev. Lett.*, 1984, **52**, 997–1000.
- 30 M. E. Casida, in *Recent Advances in Computational Chemistry*, ed. D. P. Chong, World Scientific Publishing Co. Pte. Ltd., 1995, pp. 155–192.
- 31 P. J. Stephens, F. J. Devlin, C. F. Chabalowski and M. J. Frisch, *J. Phys. Chem.*, 1994, **98**, 11623–11627.
- 32 S. Grimme, *J. Comput. Chem.*, 2006, **27**, 1787–1799.
- 33 R. Ahlrichs, M. Bär, M. Häser, H. Horn and C. Kölmel, *Chem. Phys. Lett.*, 1989, **162**, 165–169.
- 34 *Turbomole V6.0*, 2009.
- 35 C. Lee, W. Yang and R. G. Parr, *Phys. Rev. B: Condens. Matter Mater. Phys.*, 1988, **37**, 785–789.
- 36 R. Baer and D. Neuhauser, *Phys. Rev. Lett.*, 2005, **94**, 043002.
- 37 E. Livshits and R. Baer, *Phys. Chem. Chem. Phys.*, 2007, **9**, 2932–2941.
- 38 A. Karolewski, L. Kronik and S. Kümmel, *J. Chem. Phys.*, 2013, **138**, 204115.
- 39 A. Savin and H.-J. Flad, *Int. J. Quantum Chem.*, 1995, **56**, 327–332.
- 40 T. Leininger, H. Stoll, H.-J. Werner and A. Savin, *Chem. Phys. Lett.*, 1997, **275**, 151–160.
- 41 Y. Shao, L. F. Molnar, Y. Jung, J. Kussmann, C. Ochsenfeld, S. T. Brown, A. T. B. Gilbert, L. V. Slipchenko, S. V. Levchenko, D. P. O'Neill, R. A. DiStasio Jr, R. C. Lochan, T. Wang, G. J. O. Beran, N. A. Besley, J. M. Herbert, C. Y. Lin,

- T. V. Voorhis, S. H. Chien, A. Sodt, R. P. Steele, V. A. Rassolov, P. E. Maslen, P. P. Korambath, R. D. Adamson, B. Austin, J. Baker, E. F. C. Byrd, H. Dachsel, R. J. Doerksen, A. Dreuw, B. D. Dunietz, A. D. Dutoi, T. R. Furlani, S. R. Gwaltney, A. Heyden, S. Hirata, C.-P. Hsu, G. Kedziora, R. Z. Khalliulin, P. Klunzinger, A. M. Lee, M. S. Lee, W. Liang, I. Lotan, N. Nair, B. Peters, E. I. Proynov, P. A. Pieniazek, Y. M. Rhee, J. Ritchie, E. Rosta, C. D. Sherrill, A. C. Simmonett, J. E. Subotnik, H. L. W. Iii, W. Zhang, A. T. Bell, A. K. Chakraborty, D. M. Chipman, F. J. Keil, A. Warshel, W. J. Hehre, H. F. S. Iii, J. Kong, A. I. Krylov, P. M. W. Gill and M. Head-Gordon, *Phys. Chem. Chem. Phys.*, 2006, **8**, 3172–3191.
- 42 T. Körzdörfer, J. S. Sears, C. Sutton and J.-L. Brédas, *J. Chem. Phys.*, 2011, **135**, 204107.
- 43 A. Klamt and G. Schüürmann, *J. Chem. Soc., Perkin Trans. 2*, 1993, 799–805.
- 44 The relevance of indirect influences of solvation, *e.g.*, on the RSH tuning approach, remains to be checked in future work.
- 45 H. Usta, C. Risko, Z. Wang, H. Huang, M. K. Delimeroglu, A. Zhukhovitskiy, A. Facchetti and T. J. Marks, *J. Am. Chem. Soc.*, 2009, **131**, 5586–5608.
- 46 R. L. Martin, *J. Chem. Phys.*, 2003, **118**, 4775–4777.
- 47 E. Bundgaard and F. C. Krebs, *Macromolecules*, 2006, **39**, 2823–2831.
- 48 A. A. El-Shehawey, N. I. Abdo, A. A. El-Barbary and J.-S. Lee, *Eur. J. Org. Chem.*, 2011, 4841–4852.
- 49 D. Tozer, *J. Chem. Phys.*, 2003, **119**, 12697.
- 50 S. Kümmel and L. Kronik, *Rev. Mod. Phys.*, 2008, **80**, 3.
- 51 As explained in Section 3.1 we tuned the range separation γ according to eqn (1) for all calculations of this manuscript. However, for a-BTT ($n = 4,6$) we did not re-tune γ when we attached the hexyl and methyl side chains. Since the HOMO orbital does not change considerably by attaching side chains the effects of re-tuning of γ are expected to be small.
- 52 H. a. M. van Mullekom, J. a. J. M. Vekemans and E. W. Meijer, *Chem.-Eur. J.*, 1998, **4**, 1235–1243.
- 53 M. Jayakannan, P. A. van Hal and R. A. J. Janssen, *J. Polym. Sci., Part A: Polym. Chem.*, 2002, **40**, 251–261.
- 54 P. Sonar, S. P. Singh, P. Leclère, M. Surin, R. Lazzaroni, T. T. Lin, A. Dodabalapur and A. Sellinger, *J. Mater. Chem.*, 2009, **19**, 3228–3237.
- 55 S. Ellinger, K. R. Graham, P. Shi, R. T. Farley, T. T. Steckler, R. N. Brookins, P. Taraneekar, J. Mei, L. A. Padilha, T. R. Ensley, H. Hu, S. Webster, D. J. Hagan, E. W. Van Stryland, K. S. Schanze and J. R. Reynolds, *Chem. Mater.*, 2011, **23**, 3805–3817.
- 56 M. C. Scharber, M. Koppe, J. Gao, F. Cordella, M. A. Loi, P. Denk, M. Morana, H.-J. Egelhaaf, K. Forberich, G. D. R. Gaudiana, D. Waller, Z. Zhu, X. Shi and C. J. Brabec, *Macromolecules*, 2010, **22**, 367.
- 57 L. Pandey, C. Risko, J. E. Norton and J.-L. Brédas, *Macromolecules*, 2012, **45**, 6405.

Publication 4

Electronic excitations and the Becke-Johnson potential:

*The need for and the problem of transforming
model potentials to functional derivatives*

A. Karolewski, R. Armiento, and S. Kümmel,
Phys. Rev. A **88**, 052519 (2013).

© 2013 American Physical Society
DOI: 10.1103/PhysRevA.88.052519

4

Own Contribution

I did all calculations and wrote the first version of the manuscript.

Electronic excitations and the Becke-Johnson potential: The need for and the problem of transforming model potentials to functional derivatives

Andreas Karolewski,¹ Rickard Armiento,² and Stephan Kümmel^{1,*}

¹Theoretical Physics IV, University of Bayreuth, 95440 Bayreuth, Germany

²Department of Physics, Chemistry and Biology (IFM), Linköping University, SE-58183 Linköping, Sweden

(Received 20 September 2013; published 25 November 2013)

Constructing approximations for the exchange-correlation (xc) potential in density functional theory instead of the energy appears attractive because it may provide for a way of easily incorporating desirable features such as a particle number discontinuity into xc functionals. However, xc potentials that are constructed directly are problematic: An xc potential that is not *a priori* derived as a functional derivative of some xc energy functional is most likely not a functional derivative of any density functional at all. This severely limits the usefulness of directly constructed xc potentials, e.g., for calculating electronic excitations. For the explicit example of the Becke-Johnson (BJ) potential we discuss defining corresponding energy expressions by density path integrals. We show that taking the functional derivative of these energies does not lead back to potentials that are close to the BJ one, and the new potentials do not share the attractive features of the original BJ expression. With further examples we demonstrate that this is a general finding and not specific to the BJ potential form.

DOI: 10.1103/PhysRevA.88.052519

PACS number(s): 31.15.E-, 71.15.Mb, 36.40.Vz

I. INTRODUCTION

Kohn-Sham density functional theory [1,2] (DFT) and time dependent DFT [3] (TDDFT) are well known for their practical usefulness in a wide range of applications. This is made possible by a variety of exchange-correlation (xc) functional approximations. Typically, the degree of sophistication that is needed for a functional approximation to fulfill its task grows with the degree of complexity of the physics that one aims to describe. A prominent and practically very relevant example of this type are long-range charge-transfer (CT) excitations. In order to be able to calculate them with at least reasonable accuracy, one so far needs to employ computationally demanding highly nonlocal xc functionals as discussed, e.g., in [4–10]. Many of the xc features that are important for describing long-range CT correctly can easily be directly identified in the xc potential. The field-counteracting behavior of the exact Kohn-Sham exchange potential [11,12] and the potential step structure [13] that is related [14] to the integer particle discontinuity [15] are such examples. It has therefore appeared as a promising strategy to switch perspective in xc functional development and develop approximations for the xc potential directly, instead of approximations for the xc energy.

Specifically, it appeared as a charming perspective to be able to design new xc potentials as expressions that are semilocal and computationally inexpensive to evaluate, yet able to perform difficult tasks such as the prediction of CT excitations. The Becke-Johnson (BJ) potential [16] is an example of a potential approximation that has shown promise in this regard [17,18]. It is defined by the simple expression

$$v^{\text{BJ}}(\mathbf{r}) = v_{\text{x}}^{\text{h}}(\mathbf{r}) + v^{\text{c}}(\mathbf{r}), \quad (1)$$

where $v_{\text{x}}^{\text{h}}(\mathbf{r})$ takes the role of the Coulomb potential of the exchange hole and

$$v^{\text{c}}(\mathbf{r}) = C \sqrt{\frac{2\tau(\mathbf{r})}{\rho(\mathbf{r})}} \quad (2)$$

is a correction that can be interpreted as playing the role of the response potential contribution. The noninteracting kinetic energy density $\tau(\mathbf{r}) = 2 \sum_{i=1}^N \frac{1}{2} |\nabla \phi_i(\mathbf{r})|^2$ is evaluated from the N occupied Kohn-Sham orbitals ϕ_i , and $C = \frac{1}{\pi} \sqrt{\frac{5}{12}}$. Here and in the following we assume a non-spin-polarized system for clarity and use hartree atomic units. It was shown that v^{BJ} is a good approximation to the exact exchange potential [16–19] including many of its important features such as the step structure, the derivative discontinuity, and a $\sim -\frac{1}{r}$ asymptotic behavior. In Ref. [17] it was demonstrated that the BJ potential shows features that are closely related to the discontinuous potential changes that occur in the exact exchange Kohn-Sham potential due to the derivative discontinuity. However, in the presence of an electric field the expression does not counteract the applied field and therefore, generalizations for this case were developed [17,20]. For one of these generalizations it was explicitly verified that it reliably predicts the static polarizabilities of acetylene oligomers [18], a capability closely connected to the accurate description of exact exchange features. The BJ potential was also applied [21] for the calculation of band gaps and improved results were found with a further modified expression [22]. Since the presence of the derivative discontinuity and other properties of the exchange potential are important for the description of ionization processes and CT [4,23] this simple potential expression is an ideal starting point for our purpose.

Most remarkably, though, is the fact that, except for the correct asymptotic behavior, the important properties that model exact exchange in the BJ potential arise from v^{c} —a solely semilocal expression. Via the orbital dependent (τ) term it incorporates the above mentioned features of exact exchange

*Corresponding author.

that are usually obtained from expressions that are nonlocal with respect to the orbitals. The low computational cost that is implied by semilocality makes the BJ potential very interesting from an application point of view.

However, potentials that are constructed as direct approximations and not obtained as functional derivatives of an energy functional have a significant downside. They are typically not the functional derivative of any density functional. This is in particular true for the BJ potential [18,24]. Such potentials do not comply with the requirements of Kohn-Sham theory [2] and from a formal perspective, their use is not justified. One could hope that this might be just a formal argument and that from a pragmatic point of view one may use such potentials and obtain good results. The Krüger-Li-Iafrate potential approximation [25] to the exact exchange optimized effective potential [26–28] is an example of a potential that is not a functional derivative, but nevertheless is very useful in practice.

However, a potential that is not a functional derivative is problematic also from a pragmatic point of view. First and most obviously, if there is no energy corresponding to the potential, then any form of a consistent energy minimizing calculation is impossible. Second, potentials that are not functional derivatives lack properties that proper xc potentials have, such as rotational and translational symmetry [29]. As a consequence they violate the zero-force theorem [30]. Especially in TDDFT this leads to serious problems as the TD Kohn-Sham equations can no longer be solved stably [31,32].

In this article we study ways that allow one to map xc potentials that are not functional derivatives to new potentials that are functional derivatives of some energy expression, with the aim of finding a map that preserves the relevant features of the original potential. This effort is motivated by the BJ potential that we see as an important step in the quest to find an easy-to-evaluate, computationally efficient semilocal functional that incorporates other nonlocal properties, such as a discontinuity at integer particle numbers, and thus, may be able to predict CT excitations. In the following we therefore focus on this example. However, most of the conclusions and results that we obtain from the analysis and modification of the BJ expression are also valid for other direct potential approximations that are not functional derivatives.

Our article is outlined as follows. In Sec. II we demonstrate that the BJ potential leads to problems when used in TDDFT, e.g., due to the violation of the zero-force theorem. Following this analysis we explain routes to modify v^{BJ} with the aim to obtain a potential that is a functional derivative. In Sec. III we discuss semilocal approximations for the hole potential of Eq. (1) in order to convert the whole potential into a semilocal expression. Thereafter, we define different energy expressions corresponding to v^{c} and take their functional derivative to derive new potentials. By comparing these newly defined expressions with v^{c} we discuss the prospects of this potential transformation approach (Sec. IV) and close with conclusions in Sec. V.

II. BJ POTENTIAL IN TDDFT

In this section we demonstrate which type of results are to be expected when the BJ potential is used in TDDFT. We have implemented v^{BJ} of Eq. (1) in our customized, time dependent

version [33] of the PARSEC [34] real-space code. The time dependent Kohn-Sham equations [3] are propagated in real time [35] on a real-space grid. For the xc potential we use the BJ expression in the adiabatic approximation, i.e.,

$$v^{\text{a-BJ}}(\mathbf{r}, t) = v^{\text{BJ}}(\{\{\varphi_i\}\}, \mathbf{r})_{\{\varphi_i\}=\{\varphi_i(\mathbf{r}, t)\}}. \quad (3)$$

Our main interest in the TDDFT implementation of the BJ potential is the calculation of excitation energies. One might hope that, just as $v^{\text{BJ}}(\mathbf{r})$ is close to the exact exchange potential in ground-state DFT, the adiabatic extension of the BJ potential $v^{\text{a-BJ}}(\mathbf{r}, t)$ (a-BJ) in TDDFT may exhibit important features of the time dependent exact exchange potential. As the ground-state BJ potential shows step structures that are related to the derivative discontinuity in DFT [15] and TDDFT [23,36], and as furthermore the a-BJ potential depends on the orbitals at time t , which themselves depend on the density at all prior times t' [37], the BJ potential in principle contains the elements that are considered necessary for capturing the spatial and temporal nonlocalities that are required for the description of CT excitations.

In order to obtain excitation energies from the propagation of the time dependent Kohn-Sham equations we apply a small boost $\exp(i\mathbf{r} \cdot \mathbf{k}_{\text{boost}})$ to the ground-state Kohn-Sham orbitals and calculate the time dependent dipole moment [35,38]

$$\mathbf{d}(t) = - \int d^3r \mathbf{r} \rho(\mathbf{r}, t). \quad (4)$$

From the Fourier transform $\tilde{\mathbf{d}}$ of the dipole moment one obtains the dipole power spectrum

$$D(\omega) = \sum_{i=1}^3 |\tilde{d}_i(\omega)|^2 \quad (5)$$

whose peak positions indicate the excitation energies [33,35]. As test cases we chose Na clusters. Their excitations are ordinary valence excitations that exhibit no CT. They are ideal for the purpose of testing v_{xc} approximations via propagation because they are known to be very sensitive to functional inconsistencies [31,39,40] while at the same time convergence with respect to numerical parameters such as time step and grid spacing is relatively easy to achieve.

As a first test we calculated the dipole power spectrum of the sodium dimer and compare it to the adiabatic local density approximation (a-LDA) and the adiabatic Krüger-Li-Iafrate approximation [25] of the exact exchange potential (a-xKLI) in Fig. 1. Na₂ is one of the systems which allowed for stable propagation in earlier tests [31] of the a-xKLI approximation, and we observe the same for the a-BJ approximation. Furthermore, the result shows that the a-BJ approximation for Na₂ leads to excitations that do not coincide with the ones from a-xKLI, but the transitions are at reasonable positions when compared to experimental results.

As a second test we investigated Na₅, a system that by now can be considered an established test case: It has been shown in previous studies that using potentials that are not functional derivatives in the propagation of the Na₅ orbitals leads to instabilities in the propagation [31,39,40]. We observe this effect so pronouncedly with the a-BJ approximation for Na₅ that we are not able to calculate an excitation energy spectrum at all. Even worse, when the system is propagated

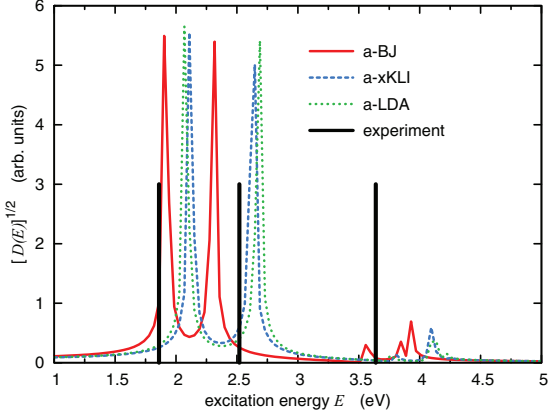


FIG. 1. (Color online) Dipole power spectrum of Na_2 for a-BJ, a-xKLI, and a-LDA after a boost energy of $E_{\text{boost}} = 10^{-5}$ eV, calculated with a time step of 0.003 fs and a total propagation time of 100 fs. Experimental excitation energies from Refs. [41,42] are indicated by vertical black lines (only the indicated energy is relevant, not the length of the line).

with the a-BJ potential without an external TD potential or a boost, i.e., propagated such that the orbitals should only acquire a trivial phase factor, a TD dipole moment of increasing magnitude develops.

We relate this finding to a violation of the zero-force theorem [30]

$$\int d^3r \rho(\mathbf{r}, t) \nabla v_{xc}(\mathbf{r}, t) = 0 \quad (6)$$

for the xc potential v_{xc} . The zero-force condition is not obeyed if a potential expression is used that is not a functional derivative of some energy functional. For Na_5 the violation of Eq. (6) is particularly severe. We demonstrate this by showing the left-hand side of Eq. (6) as a function of time in Fig. 2. The zero-force violation grows exponentially in time,

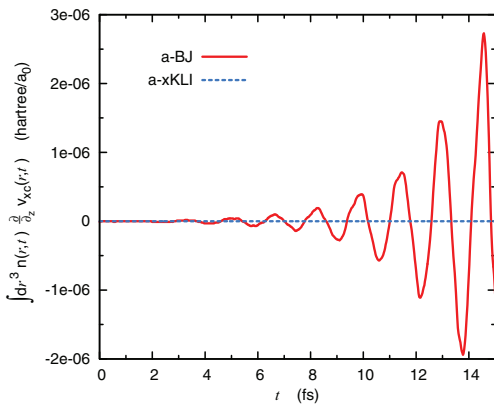


FIG. 2. (Color online) Left-hand side of Eq. (6) (zero-force theorem) for the z component as a function of time for the propagation of the ground state (no boost applied) of Na_5 . Solid line: a-BJ. Dashed line: a-xKLI.

leading to a fast self-excitation of the system. For reasons of comparison Fig. 2 also shows the left-hand side of Eq. (6) evaluated for the a-xKLI potential. Although a-xKLI also does not obey Eq. (6) and leads to a severe violation if a boost is applied [31], Fig. 2 shows that the zero-force violation of a-xKLI is negligible on the scale of the a-BJ violation when no boost is applied. Thus, Fig. 2 illustrates that the problems one has to expect due to the zero-force violation are more severe for a-BJ than for a-xKLI. The comparison also reveals that $v^c(\mathbf{r})$ is the problematic part of a-BJ and the main source of the self-excitation, because the hole potential $v_x^h(\mathbf{r})$ (which is also not a functional derivative) is also part of the a-xKLI potential. Problems with $v^c(\mathbf{r})$ are also expected since the evaluation of this term requires dividing by the density, and as the density becomes very small in the asymptotic regions of any finite system this may lead to numerical instabilities that may intensify the problems that arise from the violation of the zero-force theorem. Although there also is a division by the density in the a-xKLI potential, it is much less problematic there because the density is asymptotically dominated by the highest occupied orbital's density, and the latter appears in the numerator of the a-xKLI potential. Thus, numerical inaccuracies in the denominator can be canceled by the same inaccuracies in the numerator [32].

Finally, the comparison of the two tests, Na_2 and Na_5 , shows that the degree to which the violation of the zero-force condition manifests in practical calculations with the a-BJ potential does depend on the particular system that is studied. This is in line with similar observations for other xc potential approximations [31,39,40]. However, in any case our results show that the a-BJ potential as such can hardly be used for reliable TDDFT calculations. Moreover, as the a-BJ potential in its present form cannot be used reliably in TDDFT even for valence excitations (which are typically easier to get right than CT ones), hopes that it could be used for properly describing CT excitations are minimal. We thus did not explore this option any further.

III. SEMILOCAL REPLACEMENT OF THE SLATER POTENTIAL

Whereas the TDDFT tests reveal that $v^c(\mathbf{r})$ has problematic aspects, it is also necessary to change $v_x^h(\mathbf{r})$ if one wants to take full advantage of the possibilities that a BJ-like approach offers. In fact, it has already been pointed out in Ref. [16] that the first step for improving the BJ potential would be choosing a semilocal approximation for the hole potential v_x^h . There are two motivations for seeking such a replacement. One is the aim to turn the BJ potential into a functional derivative. This topic will be discussed in detail in Sec. IV. The other and even more obvious one is the great increase in computational efficiency that can be achieved by avoiding the many integrations that are needed in the evaluation of the Coulomb potential of the exact exchange hole, i.e., the Slater potential [43]

$$v_x^h(\mathbf{r}) = v_x^{\text{Slater}}(\mathbf{r}) = - \int d^3r' \frac{\hat{\rho}_x(\mathbf{r}, \mathbf{r}')}{|\mathbf{r} - \mathbf{r}'|}, \quad (7)$$

where the exchange hole is

$$\hat{\rho}_x(\mathbf{r}, \mathbf{r}') = \frac{2 \left| \sum_{i=1}^N \varphi_i^*(\mathbf{r}) \varphi_i(\mathbf{r}') \right|^2}{\rho(\mathbf{r})}. \quad (8)$$

So far, Eq. (7) was used in the BJ potential.

In the following we compare the exchange hole potential of different semilocal exchange functionals to the Slater potential and investigate whether any of these approximations can serve as a replacement. We obtain the hole potentials by appropriately factorizing the energy according to [44]

$$E_x = \int \frac{1}{2} \rho(\mathbf{r}) v_x^h(\mathbf{r}) d^3r \quad (9)$$

with E_x being the exchange energy. A summary of all hole potentials can be found in Appendix A.

In Fig. 3(a) we analyze different hole potentials for the Be atom as a function of the radial coordinate r . We compare the Slater potential with the exchange hole potentials of the Becke-Roussel (BR) [44], the Becke 88 (B88) [45], the Perdew-Burke-Ernzerhof (PBE) [46], the Perdew-Wang 86 (PW86) [47], the Becke 86 (B86) [48], and the local density approximation (LDA) exchange potential expressions. In Fig. 3(b) we show the inverse of these potential expressions for the same atom making the analysis of the asymptotic behavior more convenient. The BR hole potential is the one closest to the Slater potential, especially with respect to the $\sim -\frac{1}{r}$ asymptotic decay. The second best approximation is the B88 hole potential which also has the correct $\sim -\frac{1}{r}$ asymptotic behavior [45,49]. The LDA, B86, and PBE curves decay exponentially and as a consequence a modified v^{BJ} using one of these for the hole potential would lead to a qualitatively wrong asymptotic behavior. Figure 3 also shows that none of the plotted hole potentials approximates the Slater potential well in the center of the system. Here, the BR hole potential is even further off than the other approximations.

In Fig. 4 we performed the same analysis for a more extended system, the oligoacetylene C_6H_8 and plotted the corresponding exchange hole potentials along the direction of the molecular backbone (the plotting axis, the x axis, is centered between the C atoms). Qualitatively the observations here are the same as for the Be atom. In the center of the molecule all potentials have a similar structure. However, for all potentials except for the BR these structures are not as pronounced as for the Slater potential. B86, PW86, PBE, and B88 are very close to each other in the interior region of the molecule.

Among the available semilocal expressions the BR potential thus appears as the closest approximation to the Slater potential, followed by the B88 potential. Indeed, with some success previous studies [16,21,22] have already used the BR [44] instead of the Slater potential in the BJ approach. However, as explained in the next section, for our purposes of testing whether a potential can be constructed that is close to the BJ model yet at the same time a functional derivative, it is helpful to know the potential explicitly in terms of the density. This rules out the BR approximation and we therefore choose B88 for the following study, as it can be written explicitly in terms of the density while it still provides a reasonable approximation to the Slater potential.

IV. CONSTRUCTION OF A FUNCTIONAL DERIVATIVE

In this section we will explore ways of how a modified BJ expression that depends on the density semilocally can be turned into a potential that is a functional derivative of an

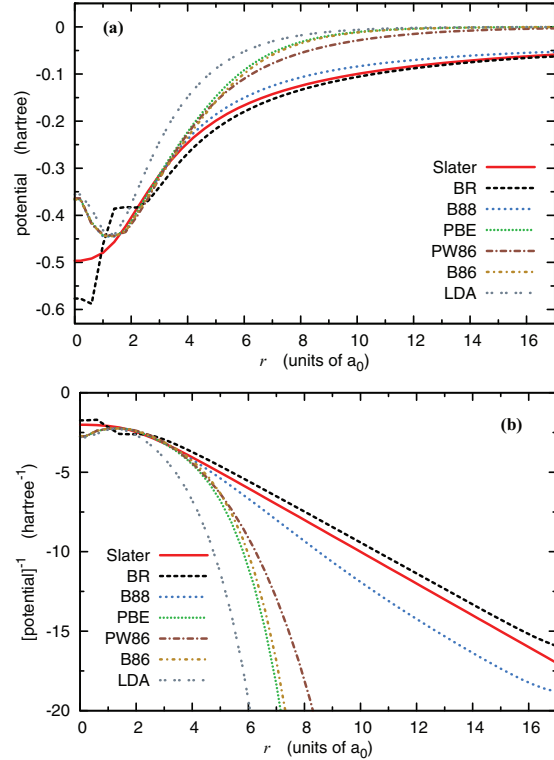


FIG. 3. (Color online) Comparison of different Coulomb hole potentials for the Be atom. See main text for details.

energy functional. To this end we use a line integral [50] in density space to define an energy functional for a potential v that is not a functional derivative

$$E^{\text{new}}[\rho] = \int_0^1 d\lambda \int d^3r v([\rho_\lambda], \mathbf{r}) \frac{d\rho_\lambda(\mathbf{r})}{d\lambda} \quad (10)$$

with the density path $\rho_\lambda(\mathbf{r})$ and $\rho_{\lambda=0}(\mathbf{r}) = 0$ and $\rho_{\lambda=1}(\mathbf{r}) = \rho(\mathbf{r})$. Defining a new energy functional for a potential that is not a functional derivative by using Eq. (10) was explored in Ref. [18] for a special line integral, the Levy-Perdew virial relation [30], and also for the exchange potential approximation of van Leeuwen and Baerends [51] for two different density paths in Ref. [52].

Once one has defined an energy via Eq. (10) one can calculate the potential that corresponds to this energy by taking the functional derivative with respect to the density,

$$\tilde{v} = \frac{\delta E^{\text{new}}[\rho]}{\delta \rho}. \quad (11)$$

In the following we investigate this procedure for the correction term $v^c(\mathbf{r}) = C \sqrt{\frac{2\tau(\mathbf{r})}{\rho(\mathbf{r})}}$ of Eq. (2). The decisive question is whether the newly defined potential \tilde{v}^c , which is a proper functional derivative of the energy functional E^{new} , is still close to the original potential v^c . Note that if one would insert a potential into Eq. (10) that already is a functional derivative of an energy functional, then the line integral would restore

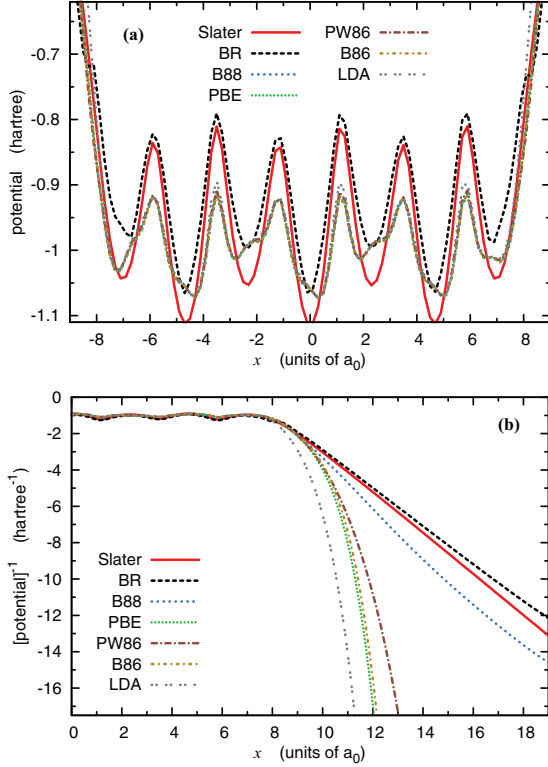


FIG. 4. (Color online) (a) Coulomb hole potential approximations and (b) the inverse Coulomb hole potential approximations of the C_6H_8 molecule.

exactly this energy functional and consequently Eq. (11) would give back the potential that was inserted.

For the general BJ expression there is a further technical hurdle. Due to the orbital dependence of v^c via τ we would have to evaluate the functional derivative of Eq. (11) in an optimized effective potential approach [26–28] and not as a direct analytical derivative. To avoid this difficulty we restrict our investigation to one-orbital systems with densities $\rho_1(\mathbf{r}) = |\varphi_1(\mathbf{r})|^2$. In this case the difference between the functional derivative with respect to the density and the one with respect to the orbital becomes trivial,

$$\frac{\delta E}{\delta \rho_1(\mathbf{r})} = \frac{1}{\varphi_1^*(\mathbf{r})} \frac{\delta E}{\delta \varphi_1(\mathbf{r})}, \quad (12)$$

making superfluous the optimized effective potential procedure: $\tilde{v}^c = u^c = u_1^c = \frac{1}{\varphi_1^*} \frac{\delta E^{\text{new}}}{\delta \varphi_1}$ can readily be calculated and compared to v^c .

First, we explore this procedure with the straight path (SP)

$$\rho_\lambda(\mathbf{r}) = \lambda \rho(\mathbf{r}). \quad (13)$$

When we use the orbital scaling $\varphi_{i,\lambda}(\mathbf{r}) = \sqrt{\lambda} \varphi_i(\mathbf{r})$ with v^c we obtain the energy integral [from Eq. (10)]

$$E^{\text{SP},c} = \int d^3r C \sqrt{2\tau(\mathbf{r})} \rho(\mathbf{r}). \quad (14)$$

From this we obtain the orbital specific potential

$$\begin{aligned} u_i^{\text{SP},c} &= \frac{1}{\varphi_i^*} \frac{\delta E^{\text{SP},c}}{\delta \varphi_i(\mathbf{r})} \\ &= C \left\{ \sqrt{\frac{\tau(\mathbf{r})}{2\rho(\mathbf{r})}} - \frac{1}{(2)^{3/2}} \nabla \left(\frac{\sqrt{\rho(\mathbf{r})} \nabla \varphi_i^*(\mathbf{r})}{\sqrt{\tau(\mathbf{r})}} \right) \frac{1}{\varphi_i^*(\mathbf{r})} \right\}. \end{aligned} \quad (15)$$

Second, we use the uniform scaling path (USP)

$$\rho_\lambda(\mathbf{r}) = \lambda^3 \rho(\lambda \mathbf{r}). \quad (16)$$

The orbital scaling for the uniform scaling path is $\varphi_{i,\lambda}(\mathbf{r}) = \lambda^{3/2} \varphi_i(\lambda \mathbf{r})$. Since v^c fulfills the scaling relation of the exchange potential

$$v^c([\rho_\lambda, \{\varphi_{i,\lambda}\}], \mathbf{r}) = \lambda v^c([\rho, \{\varphi_i\}], \lambda \mathbf{r}) \quad (17)$$

we obtain for the line integral [Eq. (10)]

$$E^{\text{USP},c} = \int d^3r v^c(\mathbf{r}) [3\rho(\mathbf{r}) + \mathbf{r} \cdot \nabla \rho(\mathbf{r})]. \quad (18)$$

This is the Levy-Perdew exchange virial relation [30]. The orbital functional derivative of this integral is

$$\begin{aligned} u_i^{\text{USP},c} &= \frac{1}{\varphi_i^*} \frac{\delta E^{\text{USP},c}}{\delta \varphi_i(\mathbf{r})} \\ &= -C \left\{ [3\rho + (\mathbf{r} \cdot \nabla)\rho] \sqrt{\frac{\tau}{2\rho^3}} + (\mathbf{r} \cdot \nabla) \sqrt{\frac{2\tau}{\rho}} \right. \\ &\quad \left. + \nabla \left[[3\rho + (\mathbf{r} \cdot \nabla)\rho] \sqrt{\frac{1}{2\tau\rho}} \right] \frac{\nabla \varphi_i^*}{\varphi_i} \right. \\ &\quad \left. + [3\rho + (\mathbf{r} \cdot \nabla)\rho] \sqrt{\frac{1}{2\tau\rho}} \frac{\nabla^2 \varphi_i^*}{\varphi_i^*} \right\}. \end{aligned} \quad (19)$$

In Fig. 5 we compare $u^{\text{SP},c}$ and $u^{\text{USP},c}$ to v^c for two different one-orbital densities. For part (a) we used an exponential function as the orbital and for part (b) a Gaussian function. Both graphs clearly demonstrate that $u^{\text{SP},c}$ and $u^{\text{USP},c}$ strongly differ from v^c . The qualitative difference is particularly striking in the case of the exponential function where v^c is constant (and supposed to be so for physical reasons [16]), whereas the newly derived potentials vary considerably. We also performed the test for other one-orbital densities, e.g., the $2p$ or $3s$ hydrogen orbitals, and obtained deviations of at least similar degree.

One could hope that the finding that the line-integral transformation changes the form of v^c substantially is unproblematic because ultimately one is interested in the transformation of the sum $v_x^h + v^c$. Hence, it is a possibility that the undesired features introduced by the line-integral transformation of v^c are compensated by opposite features introduced in the line-integral transformation of v_x^h . We investigate this possibility for the practically relevant case of the B88 hole potential. In Appendix B we show the transformation procedure for the B88 hole potential $[v_x^{h,\text{B88}}, \text{Eq. (A4)}]$ and calculate the functional derivative of the energy defined by Eq. (10) for the uniform scaling path. In this case it is possible to take the functional derivative with respect to the density directly. Figure 6 compares the newly defined potential $v_x^{\text{USP},h,\text{B88}}$ with the original B88 hole potential $v_x^{h,\text{B88}}$ for the exponential and

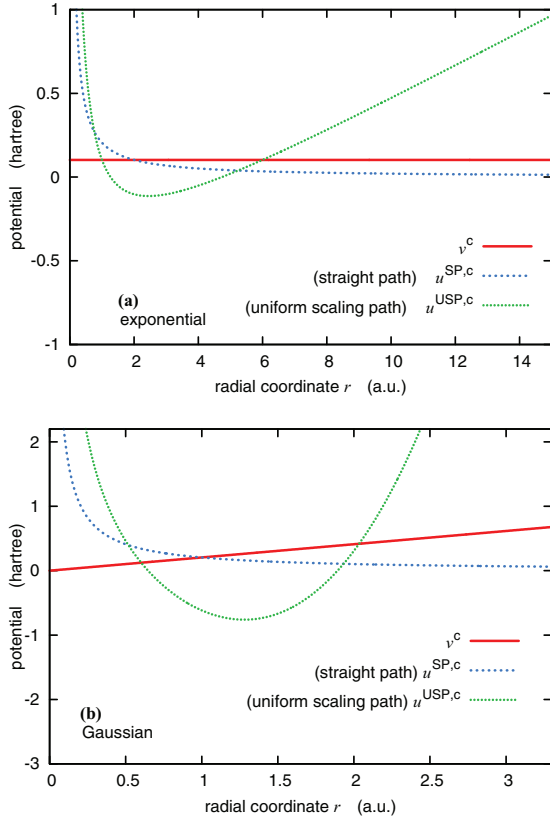


FIG. 5. (Color online) The potential expressions v^c [Eq. (2)], $u^{SP,c}$ [Eq. (15)], and $u^{USP,c}$ [Eq. (19)] for the exponential (a) and the Gaussian (b) spherical one-orbital densities.

Gaussian one-orbital densities. Similar to the transformation of v^c we observe strong deviations from the original hole potential expression. The most important features of the hole potential in the BJ expression—providing the overall potential structure and in particular the correct asymptotic behavior—are lost. We further see that indeed undesired features in the two transformed potentials can (at least in principle) cancel, because the deviations of $v_x^{USP,h,B88}$ from $v_x^{h,B88}$ are of opposite sign as the deviations of $u^{USP,c}$ from v^c . To check the extent of the cancellation Fig. 7 shows the sums $v_x^{USP,h,B88} + v^{USP,c}$ and $v_x^{h,B88} + v^c$. For intermediate values of r there is a certain cancellation, but for small and large r the discrepancies remain large.

We therefore conclude that the uniform density scaling and the straight path energy expressions define energy functionals whose functional derivatives are very different from the original v^{BJ} , despite two prior observations that one may have interpreted as suggesting otherwise: First, the form of v^{BJ} appears to be reasonable close to the exact exchange potential [16–18] and secondly, E^{USP} yields energy values close to exact exchange values [19]. Our results are consistent with Ref. [52] where the transformation of the Leeuwen-Baerends exchange potential [51] along the same density paths that we used here

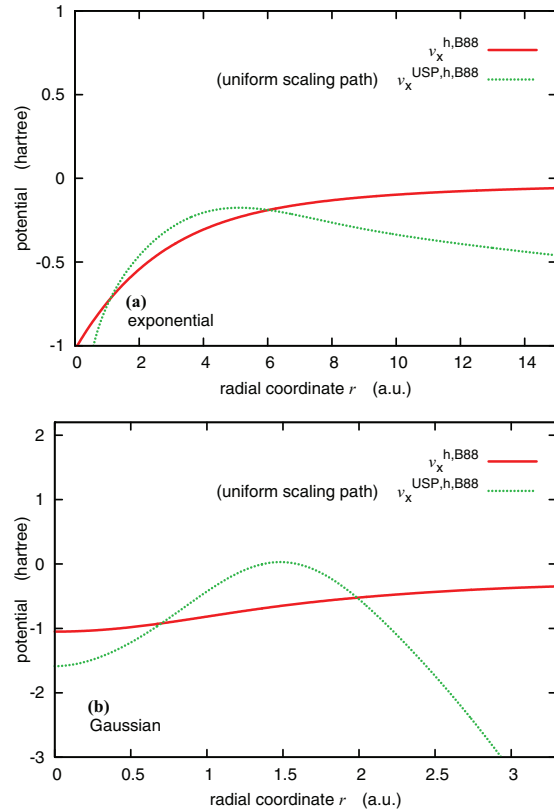


FIG. 6. (Color online) The potential expressions $v_x^{h,B88}$ [Eq. (A4)] and $v_x^{USP,h,B88}$ [Eq. (B2)] for the exponential (a) and the Gaussian (b) spherical one-orbital densities.

also lead to considerable deviations from the original potential for the Kr atom.

V. CONCLUSION

The BJ potential is not a functional derivative and therefore violates the zero-force theorem. In Sec. II we demonstrated that the theorem is not only violated in principle but also in practice and on a very relevant scale. Thus, the BJ potential as such is not applicable as a cost effective semilocal functional for the calculation of excitations.

After choosing the B88 hole potential as an appropriate semilocal replacement for the Slater potential we analyzed a procedure for transforming potentials which are not functional derivatives into ones that are. The procedure uses a line integral of a given potential expression along a certain density path to define a new energy functional. We investigated two density paths for transforming v^c . Comparing the newly defined potentials with the original expression for the case of one-orbital densities we found that the new potentials differ substantially from the original expression. The one-orbital test is a very relevant test because the density far away from a finite system's center is always dominated by one orbital that

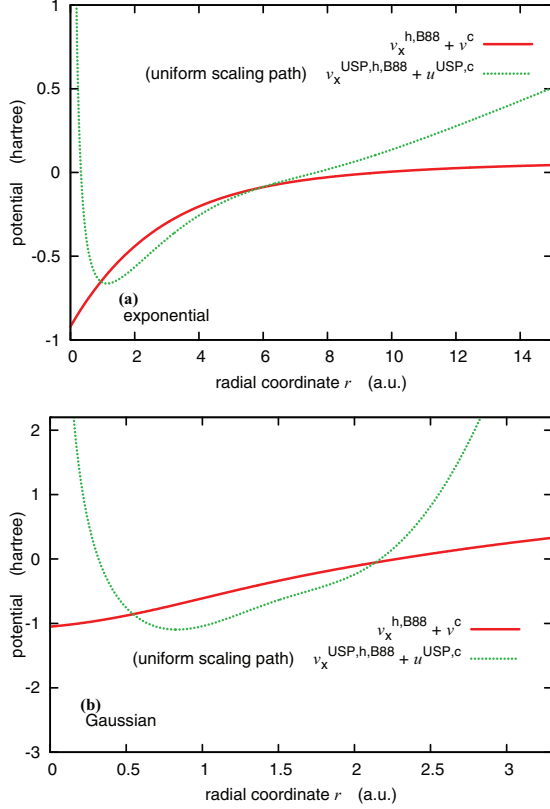


FIG. 7. (Color online) The potential expressions $v_x^{h,B88} + v^c$ [Eqs. (A4) and (2)] and $v_x^{USP,h,B88} + u^{USP,c}$ [Eqs. (B2) and (19)] for the exponential (a) and the Gaussian (b) spherical one-orbital densities.

decays exponentially. The finding that the transformations of BJ-type potentials do not preserve the good properties of the original potentials in such regions, and thus ruin one of the most attractive features of the BJ approach, is in itself already such a serious drawback that there is no point in going through the considerably more complicated many-orbital test.

One may speculate that the line integral transformation approach may be useful if the potential to which it is applied is already very close to a functional derivative in the mathematical sense. One possible route to achieve this could lie in the construction of a modified potential that already fulfills as closely as possible the constraints that a functional derivative would fulfill, e.g., the zero-force theorem [Eq. (6)] or the stronger constraint [50]

$$\frac{\delta v(\mathbf{r})}{\delta \rho(\mathbf{r}')} = \frac{\delta v(\mathbf{r}')}{\delta \rho(\mathbf{r})}. \quad (20)$$

However, one would need to find a modification of the BJ potential such that these expressions are fulfilled closely and at the same time the physics of the original BJ potential (e.g., the shell-structure steps) are not changed (e.g., similar to the idea

of Ref. [53]). As v^{BJ} is already close to the exact Kohn-Sham exchange potential in many ground-state situations, only those modifications would be helpful that “add an almost zero term” to the potential in these situations. Finding such modifications is not at all an easy task.

Therefore, one may resort to an alternative approach of exploiting the attractive features that are undoubtedly present in the BJ potential. By analyzing how the BJ potential achieves the derivative discontinuity and the shell-structure steps one may be able to build these features into a semilocal energy functional from which the potential is then obtained in the usual way of taking a functional derivative. Recent progress in developing a generalized gradient approximation functional that shows shell structure and exchange discontinuities [54] suggests that it is a worthwhile task to further explore this option. For addressing the CT problem, e.g., it appears as a promising direction of future work to extend the new generalized gradient approximation ideas of Ref. [54] along the lines of Ref. [17].

ACKNOWLEDGMENTS

S.K. and A.K. acknowledge financial support from German Science Foundation GRK 1640 and the German Israeli Foundation, and A.K. acknowledges discussions with J. P. Perdew during a visit to Tulane University. R.A. acknowledges support from the Swedish Research Council (VR), Grant No. 621-2011-4249 and the Linnaeus Environment at Linköping on Nanoscale Functional Materials (LiLi-NFM) funded by VR.

APPENDIX A: EXCHANGE HOLE POTENTIAL APPROXIMATIONS

In this Appendix we give an overview of the exchange hole potential approximations used in Sec. III. The potentials are shown in spin-polarized notation for consistency with earlier literature.

LDA exchange hole potential:

$$v_{x\sigma}^{h,LDA}(\mathbf{r}) = -3 \left(\frac{3}{4\pi} \right)^{1/3} \rho_{\sigma}^{1/3}. \quad (A1)$$

BR exchange hole potential [44]:

$$v_{x\sigma}^{h,BR}(\mathbf{r}) = -\frac{1 - e^{-x} - \frac{1}{2}xe^{-x}}{b}, \quad (A2)$$

where $b^3 = \frac{x^3 e^{-x}}{8\pi\rho_{\sigma}}$ and x is determined numerically from

$$\frac{xe^{-2x/3}}{x-2} = \frac{2}{3}\pi^{2/3} \frac{\rho_{\sigma}^{5/3}}{Q_{\sigma}}, \quad (A3)$$

where $Q_{\sigma} = \frac{1}{6}[\nabla^2\rho_{\sigma} - \gamma(4\tau_{\sigma} - \frac{1}{2}\frac{(\nabla\rho_{\sigma})^2}{\rho_{\sigma}})]$ with $\gamma = 0.8$ and $\tau_{\sigma} = \sum_{i=1}^N \frac{1}{2}|\nabla\varphi_{i\sigma}|^2$.

B88 exchange hole potential [45]:

$$v_{x\sigma}^{h,B88}(\mathbf{r}) = v_{x\sigma}^{h,LDA}(\mathbf{r}) - 2\beta\rho_{\sigma}^{1/3} \frac{x_{\sigma}^2}{1 + 6\beta x_{\sigma} \sinh^{-1}(x_{\sigma})} \quad (A4)$$

with $x_{\sigma} = \frac{|\nabla\rho_{\sigma}|}{\rho_{\sigma}^{3/4}}$ and $\beta = 0.0042$.

PBE exchange hole potential [46]:

$$v_x^{\text{h,PBE}}(\mathbf{r}, [\rho]) = 2A_x \rho^{1/3} \left[1 + \kappa - \frac{\kappa}{1 + \frac{\mu s^2}{\kappa}} \right],$$

$$v_{x\sigma}^{\text{h,PBE}}(\mathbf{r}, [\rho_\sigma]) = v_x^{\text{h,PBE}}(\mathbf{r}, [2\rho_\sigma]) \quad (\text{A5})$$

with $s = \frac{|\nabla\rho|}{2(3\pi^2)^{1/3}\rho^{4/3}}$, $A_x = -\frac{3}{4}(\frac{3}{\pi})^{1/3}$, $\kappa = 0.804$, and $\mu = 0.21951$.

PW86 exchange hole potential [47]:

$$v_x^{\text{h,PW86}}(\mathbf{r}, [\rho]) = 2A_x \rho^{1/3} \left[1 + 0.0864 \frac{s^2}{m} + bs^4 + cs^6 \right]^m,$$

$$v_{x\sigma}^{\text{h,PW86}}(\mathbf{r}, [\rho_\sigma]) = v_x^{\text{h,PW86}}(\mathbf{r}, [2\rho_\sigma]) \quad (\text{A6})$$

with $m = \frac{1}{15}$, $b = 14$, and $c = 0.2$. For definitions of s and A_x see above.

B86 exchange hole potential [48]:

$$v_{x\sigma}^{\text{h,B86}}(\mathbf{r}) = v_{x\sigma}^{\text{h,LDA}}(\mathbf{r}) - 2\beta\rho_\sigma^{1/3} \frac{x_\sigma^2}{1 + \gamma x_\sigma^2} \quad (\text{A7})$$

with $x_\sigma = \frac{|\nabla\rho_\sigma|}{\rho_\sigma^{4/3}}$ and $\beta = 0.0036$ and $\gamma = 0.004$.

APPENDIX B: TRANSFORMATION OF THE B88 EXCHANGE HOLE POTENTIAL

In this Appendix we transform the B88 exchange hole potential of Eq. (A4) with the transformation defined by Eqs. (10) and (11) for the uniform scaling path [Eq. (13)]. Since

the B88 hole potential fulfills the exchange scaling relation [Eq. (17)] we can write for the energy

$$E^{\text{USP,h,B88}} = \sum_\sigma \int d^3r v_{x\sigma}^{\text{h,B88}}(\mathbf{r}) [3\rho_\sigma(\mathbf{r}) + \mathbf{r} \cdot \nabla\rho_\sigma(\mathbf{r})]. \quad (\text{B1})$$

From this energy we obtain the functional derivative

$$v_{x\sigma}^{\text{USP,h,B88}} = \frac{\delta E^{\text{USP,h,B88}}}{\delta\rho_\sigma(\mathbf{r})}$$

$$= \left(\frac{1}{3}\rho_\sigma^{-2/3} M_\sigma + 3\rho_\sigma^{1/3} \right) (C - 2\beta Q_\sigma)$$

$$+ 2\beta \nabla \left[\frac{\nabla\rho_\sigma}{\rho_\sigma |\nabla\rho_\sigma|} M_\sigma \frac{dQ_\sigma}{dx_\sigma} \right]$$

$$+ \frac{8}{3}\beta \frac{|\nabla\rho_\sigma|}{\rho_\sigma^2} M_\sigma \frac{dQ_\sigma}{dx_\sigma} - \nabla[\rho_\sigma^{1/3} (C - 2\beta Q_\sigma) \mathbf{r}], \quad (\text{B2})$$

where

$$Q_\sigma = \frac{x_\sigma^2}{1 + 6\beta x_\sigma \sinh^{-1} x_\sigma}, \quad (\text{B3})$$

$$\frac{dQ_\sigma}{dx_\sigma} = \frac{2Q_\sigma}{x_\sigma} - \frac{6\beta Q_\sigma^2}{x_\sigma \sqrt{1 + x_\sigma^2}} - \frac{6\beta Q_\sigma^2 \sinh^{-1}(x_\sigma)}{x_\sigma^2}, \quad (\text{B4})$$

$$M_\sigma = 3\rho_\sigma + (\mathbf{r} \cdot \nabla)\rho_\sigma \quad \text{and} \quad C = -3 \left(\frac{3}{4\pi} \right)^{1/3}. \quad (\text{B5})$$

-
- [1] P. Hohenberg and W. Kohn, *Phys. Rev.* **136**, B864 (1964).
- [2] W. Kohn and L. J. Sham, *Phys. Rev.* **140**, A1133 (1965).
- [3] E. Runge and E. K. U. Gross, *Phys. Rev. Lett.* **52**, 997 (1984).
- [4] D. J. Tozer, *J. Chem. Phys.* **119**, 12697 (2003).
- [5] N. Maitra, *J. Chem. Phys.* **122**, 234104 (2005).
- [6] M. J. G. Peach, P. Benfield, T. Helgaker, and D. J. Tozer, *J. Chem. Phys.* **128**, 044118 (2008).
- [7] M. Hellgren and E. K. U. Gross, *Phys. Rev. A* **85**, 022514 (2012).
- [8] L. Kronik, T. Stein, S. Refaely-Abramson, and R. Baer, *J. Chem. Theory Comput.* **8**, 1515 (2012).
- [9] A. Karolewski, T. Stein, R. Baer, and S. Kümmel, *J. Chem. Phys.* **134**, 151101 (2011).
- [10] D. Hofmann, T. Körzdörfer, and S. Kümmel, *Phys. Rev. Lett.* **108**, 146401 (2012).
- [11] S. J. A. van Gisbergen, P. R. T. Schipper, O. V. Gritsenko, E. J. Baerends, J. G. Snijders, B. Champagne, and B. Kirtman, *Phys. Rev. Lett.* **83**, 694 (1999).
- [12] S. Kümmel, L. Kronik, and J. P. Perdew, *Phys. Rev. Lett.* **93**, 213002 (2004).
- [13] R. van Leeuwen, O. Gritsenko, and E. J. Baerends, *Z. Phys. D* **33**, 229 (1995).
- [14] D. Hofmann and S. Kümmel, *Phys. Rev. B* **86**, 201109(R) (2012).
- [15] J. P. Perdew, R. G. Parr, M. Levy, and J. L. Balduz, Jr., *Phys. Rev. Lett.* **49**, 1691 (1982).
- [16] A. D. Becke and E. R. Johnson, *J. Chem. Phys.* **124**, 221101 (2006).
- [17] R. Armiento, S. Kümmel, and T. Körzdörfer, *Phys. Rev. B* **77**, 165106 (2008).
- [18] A. Karolewski, R. Armiento, and S. Kümmel, *J. Chem. Theory Comput.* **5**, 712 (2009).
- [19] A. P. Gaiduk and V. N. Staroverov, *J. Chem. Phys.* **128**, 204101 (2008).
- [20] E. Räsänen, S. Pittalis, and C. R. Proetto, *J. Chem. Phys.* **132**, 044112 (2010).
- [21] F. Tran, P. Blaha, and K. Schwarz, *J. Phys.: Condens. Matter* **19**, 196208 (2007).
- [22] F. Tran and P. Blaha, *Phys. Rev. Lett.* **102**, 226401 (2009).
- [23] M. Mundt and S. Kümmel, *Phys. Rev. Lett.* **95**, 203004 (2005).
- [24] A. P. Gaiduk and V. N. Staroverov, *J. Chem. Phys.* **131**, 044107 (2009).
- [25] J. B. Krieger, Y. Li, and G. J. Iafrate, *Phys. Rev. A* **45**, 101 (1992).
- [26] R. T. Sharp and G. K. Horton, *Phys. Rev.* **90**, 317 (1953).
- [27] J. D. Talman and W. F. Shadwick, *Phys. Rev. A* **14**, 36 (1976).
- [28] S. Kümmel and L. Kronik, *Rev. Mod. Phys.* **80**, 3 (2008).
- [29] H. Ou-Yang and M. Levy, *Phys. Rev. Lett.* **65**, 1036 (1990).
- [30] M. Levy and J. P. Perdew, *Phys. Rev. A* **32**, 2010 (1985).
- [31] M. Mundt, S. Kümmel, R. van Leeuwen, and P.-G. Reinhard, *Phys. Rev. A* **75**, 050501 (2007).
- [32] M. Mundt and S. Kümmel, *Phys. Rev. A* **74**, 022511 (2006).
- [33] M. Mundt and S. Kümmel, *Phys. Rev. B* **76**, 035413 (2007).

- [34] L. Kronik, A. Makmal, M. L. Tiago, M. M. G. Alemany, M. Jain, X. Huang, Y. Saad, and J. R. Chelikowsky, *Phys. Status Solidi B* **243**, 1063 (2006).
- [35] K. Yabana and G. F. Bertsch, *Phys. Rev. B* **54**, 4484 (1996).
- [36] M. Lein and S. Kümmel, *Phys. Rev. Lett.* **94**, 143003 (2005).
- [37] N. T. Maitra, K. Burke, and C. Woodward, *Phys. Rev. Lett.* **89**, 023002 (2002).
- [38] F. Calvayrac, P.-G. Reinhard, and E. Suraud, *Ann. Phys.* **255**, 125 (1997).
- [39] P. M. Dinh, J. Messud, P.-G. Reinhard, and E. Suraud, *J. Phys.: Conf. Ser.* **248**, 012024 (2010).
- [40] D. Hofmann and S. Kümmel, *J. Chem. Phys.* **137**, 064117 (2012).
- [41] W. R. Fredrickson and W. W. Watson, *Phys. Rev.* **30**, 429 (1927).
- [42] S. P. Sinha, *Proc. Phys. Soc. A* **62**, 124 (1949).
- [43] J. C. Slater, *Phys. Rev.* **81**, 385 (1951).
- [44] A. D. Becke and M. R. Roussel, *Phys. Rev. A* **39**, 3761 (1989).
- [45] A. D. Becke, *Phys. Rev. A* **38**, 3098 (1988).
- [46] J. P. Perdew, K. Burke, and M. Ernzerhof, *Phys. Rev. Lett.* **77**, 3865 (1996).
- [47] J. P. Perdew and Y. Wang, *Phys. Rev. B* **33**, 8800 (1986).
- [48] A. D. Becke, *J. Chem. Phys.* **84**, 4524 (1986).
- [49] Contrary to the exchange hole potential the exchange potential of B88 decays asymptotically with $1/r^2$.
- [50] R. van Leeuwen and E. J. Baerends, *Phys. Rev. A* **51**, 170 (1995).
- [51] R. van Leeuwen and E. J. Baerends, *Phys. Rev. A* **49**, 2421 (1994).
- [52] A. P. Gaiduk and V. N. Staroverov, *J. Chem. Phys.* **136**, 064116 (2012).
- [53] Y. Kurzweil and M. Head-Gordon, *Phys. Rev. A* **80**, 012509 (2009).
- [54] R. Armiento and S. Kümmel, *Phys. Rev. Lett.* **111**, 036402 (2013).

Publication 5

*The influence of donor and acceptor ordering
on the fundamental and the optical gap*
A. Karolewski and S. Kümmel,
Manuscript.

5

Own Contribution

I did all calculations and wrote the first version of the manuscript.

The influence of donor and acceptor ordering on the fundamental and the optical gap

Andreas Karolewski¹ and Stephan Kümmel¹

Theoretical Physics IV, University of Bayreuth, 95440 Bayreuth, Germany

(Dated: 6 December 2013)

Understanding the electronic properties of donor-acceptor systems is an important prerequisite for systematically improving the performance of molecular electronic devices, in particular organic solar cells. In this theoretical study we investigate effects that are triggered by the rearrangement, e.g., from a strictly alternating to a diblock arrangement, of the donor and acceptor components in systems based on thiophene and 2,1,3-benzothiadiazole. We study the lowest optical excitation, i.e., optical gap, as well as the fundamental gap – the difference of ionization potential and electron affinity, and show that they are influenced differently by the rearrangement of donor and acceptor moieties. It is well known that the gaps can be related to bond length alternation and conjugation length. We take a closer look at these concepts and propose a definition of the bond length alternation that relates to the optical gap and allows for comparing systems composed of different subunits.

I. INTRODUCTION

Donor acceptor (DA) systems are frequently used in organic photovoltaic (OPV) devices due to their low first excited state energy.^{1–5} This excitation energy is decisive for the first step that occurs in the solar cell: the absorption of light. During this neutral excitation one part of the solar cell (typically the hole conducting part) passes from the electronic ground state to the first excited state. After this process multiple other processes occur until two separated charges emerge at the electrodes of the electron donating and accepting material.⁶ Besides the lowest excitation energy two other important properties exist that influence the usefulness of a material in organic solar cell applications, namely the ionization potential (IP) and the electron affinity (EA). Their difference defines the fundamental gap ($|IP - EA|$). The IP and EA define charged excitations with the former being the energy that is needed to remove an electron from the system and the latter the energy that is gained by adding an electron to the system. Both quantities also play an important role for OPV devices. The difference of the IP of the hole conducting material (\bar{D}) and of the EA of the electron conducting material (\bar{A}) define the upper energy limit that can be harvested at the electrodes of a simple OPV cell. An overview of the discussed quantities is shown in Fig. 1.

It is important to distinguish between the lowest excitation energy (or optical gap) and the fundamental gap because they originate from different physical processes. In this work we examine a set of DA oligomers especially suited for studying the differences between both quantities. All oligomers of the set contain the same amount of donor (D) and acceptor (A) monomers. They only differ by the arrangement of these monomer units, from a strictly alternating to a random to a diblock arrangement. We demonstrate that in this set the lowest excitation energy and the fundamental gap (or the IP and EA , respectively) follow different trends and are related to different material properties. For our study we em-

ploy thiophene (T) as the D and benzothiadiazole (B) as the A component. Both monomer units and their combination are frequently used in the field of organic solar cells.^{7–9}

Our study is based on calculations with Density Functional Theory (DFT)^{10,11} and Time Dependent DFT (TDDFT)^{12,13}. The functional class that we apply are range separated hybrid (RSH) functionals^{14–20} with a range separation parameter chosen according to a non-empirical tuning condition. The approach is designed to allow for a reliable prediction of the excitations discussed above, especially in systems with multichromophoric character.^{21–23} This method has already been used recently to evaluate the optical properties in a combined experimental and theoretical study.²⁴ Here, we go beyond this previous study and investigate not only the optical gap, but also examine the fundamental gap, the bond length alternation, the conjugation length, and the spatial extent and position of different orbital types and draw links to the optical and fundamental gap. This analysis is a key prerequisite for conceptual improvements of DA materials for the application in OPV devices. Furthermore, we identify the decisive factors that are responsible for the low gap of DA polymers.

Our manuscript begins with a description of the systems that we used in our calculations (Sec. II), followed by a brief overview of the employed theoretical approach (Sec. III). In Sec. IV we examine the IP , EA , and the fundamental gap of our set of DA systems. Thereafter, we focus on the analysis of the optical gap and classify the relation to other system properties in Sec. V. We also compare the optical gaps with the fundamental gaps in this section including a discussion of how the difference between them can be (approximately) understood in terms of different orbitals. We summarize and put our findings into a larger perspective in the concluding section.

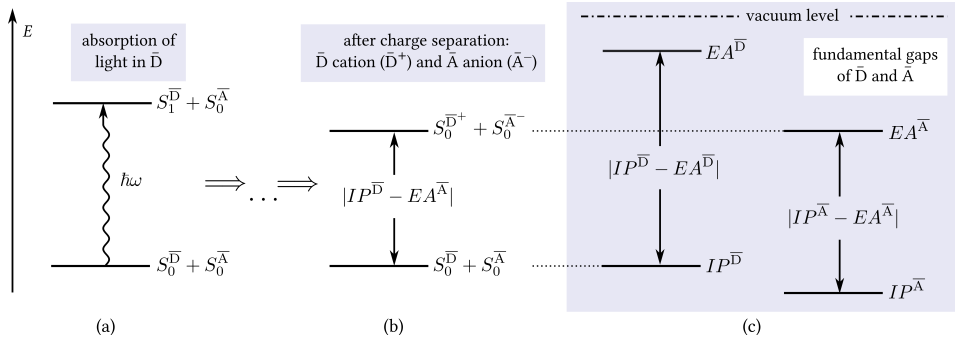


FIG. 1: Schematic of the energy levels involved in an ideal process of a simple organic solar cell. (a): The hole conducting material (\bar{D}) is excited (exciton formation) due to the absorption of light ($\hbar\omega$). For simplicity, we assume no light absorption in the electron conducting material (\bar{A}). (b): After multiple other processes (transport of the exciton to the $\bar{D} - \bar{A}$ interface, the charge separation, the transfer of the separated “hole” and “electron” to the respective electrodes) the upper energy limit that can be harvested at the electrodes is defined by $|IP^{\bar{D}} - EA^{\bar{A}}|$.⁶ S_0 denotes the electronic ground state and S_1 the first excited state. (c): Fundamental gaps of \bar{D} and \bar{A} defined by the difference of the IP and EA .

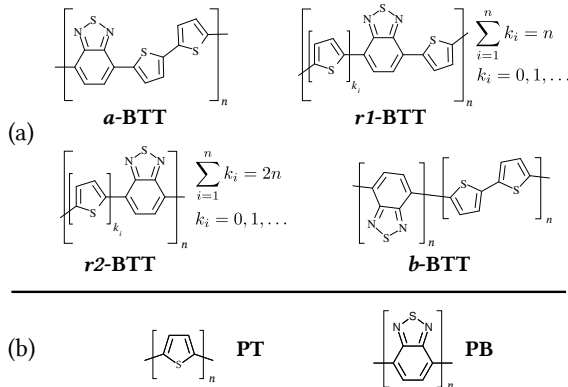


FIG. 2: (a) Schematic of the DA oligomers studied in this work ($n = 1$ to 12). They only differ in the arrangement of T and B subunits. (b) Schematic of the corresponding donor and acceptor only oligomers (PT: $n = 1$ to 32 , PB: $n = 1$ to 25).

II. SYSTEMS

Fig. 2 (a) schematically depicts the DA oligomers that we examine in this article. a -BTT is a strictly alternating arrangement of 2,2'-bithiophene (T_2) as donor and 2,1,3-benzothiadiazole (B) as acceptor. $r1$ -BTT and $r2$ -BTT are two examples for molecules in which thiophene (T) and B units are combined in random order. $r1$ -BTT is a random distribution of n T and n BT (Fig. 4) components whereas $r2$ -BTT is randomly composed of n B and $2n$ T components. Finally, b -BTT is a diblock oligomer of $2n$ T and n B monomer units. All systems contain

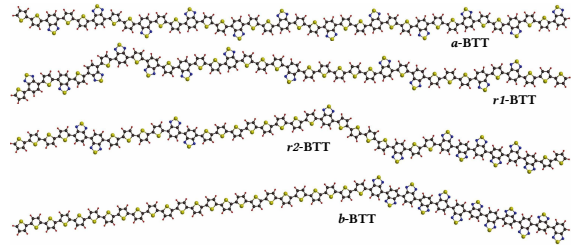


FIG. 3: Optimized geometries of a -BTT, $r1$ -BTT, $r2$ -BTT, and b -BTT for $n = 12$. The optimization method is described in Sec. III

exactly n B and $2n$ T units to ensure that only the DA arrangement is changed and not the ratio of D and A subunits. For all four system classes, i.e. a -BTT, $r1$ -BTT, $r2$ -BTT, and b -BTT, we did calculations with the number n of repeat units ranging from $n = 1$ to 12 . For illustration we show the optimized structures for the largest calculated systems ($n = 12$) in Fig. 3. Note that the longitudinal extent of these stretched systems is approximately 15 nm, i.e., a practically relevant length scale. Also note that the random arrangements $r1$ -BTT and $r2$ -BTT are not defined unambiguously because many different realizations exist for each setup. However, as discussed further below, our results show that it is sufficient to study only one specific random arrangement for each chain length. For a comparative study we furthermore examine the donor-only systems PT and the acceptor-only system PB (Fig. 2 (b)) as well as the low molecular weight systems T, T_2 , B, B_2 , and BT (Fig. 4).

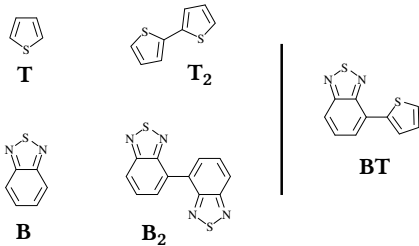


FIG. 4: Schematic of the low molecular weight systems studied in this work.

III. METHODOLOGY

In this work we calculate the IP s, EA s, and excitation energies of conjugated DA oligomers with up to 36 aromatic rings. We use DFT^{10,11} and TDDFT^{12,13}, respectively, because of its favorable ratio of reasonable quality of results to moderate computational cost. For all systems mentioned in Sec. II we optimized the geometries in TURBOMOLE^{25,26} using the B3LYP functional²⁷ in combination with the def2-SV(P) basis set and the Grimme dispersion correction.²⁸ The calculation of IP s, EA s, and excitation energies of DA systems requires a more sophisticated functional class. We use an RSH functional where the electronic exchange is split into long-range and short-range. As a specific choice we use the Baer-Neuhauser-Livshits (BNL) RSH functional which combines LDA-type short range exchange and long range Fock exchange with the Lee-Yang-Parr correlation functional.^{17,29,30} We expect that for spectroscopic properties³¹, other similar RSH functionals would perform equally for our purpose, independent of the finding that ground-state properties may depend much more strongly on the specific RSH functional³². The range-separation parameter γ is determined by a non-empirical tuning condition. We employ the least square gap tuning^{23,32}

$$T_{LS}(\gamma) = \sqrt{\sum_{i=N}^{N+1} [\epsilon_{\text{HOMO}}^\gamma(i) + E^\gamma(i-1) - E^\gamma(i)]^2} = \min \quad (1)$$

with $E^\gamma(i)$ being the γ -dependent total energy for a system with i electrons and $\epsilon_{\text{HOMO}}^\gamma(i)$ the highest occupied generalized Kohn-Sham orbital. This tuning condition is the optimal choice to calculate IP s, EA s, and excitation energies simultaneously in accordance with experimental results for organic molecules. The tuning process has to be performed for each molecule of this work separately to account for the system specific size of the highest occupied and lowest unoccupied orbitals. With the optimized γ 's we perform ground state calculations with the BNL functional to determine the IP and EA from the highest occupied molecular orbital (HOMO) energy value and the lowest unoccupied molecular orbital (LUMO) energy

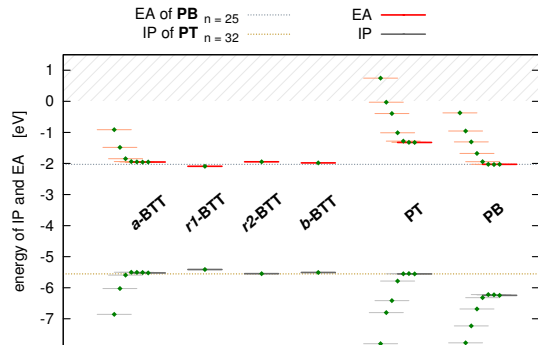


FIG. 5: Levels in dark color show IP and EA for a -BTT, $r1$ -BTT, $r2$ -BTT, and b -BTT ($n = 12$), for PT ($n = 32$), and to $n = 25$ for PB ($n = 25$). Levels in lighter color show IP and EA for a -BTT, PT, and PB for smaller n (a -BTT: $n = 1, 2, 4, 6, 8, 10, 12$; PT: $n = 2, 3, 4, 8, 16, 24, 32$; PB: $n = 1, 2, 3, 5, 9, 15, 21, 25$) and demonstrate the saturation with increasing chain length (different abscissa values chosen just for illustration).

value, respectively.^{23,33,34} Afterward, we calculated the excitation energies with linear response TDDFT by also using the BNL functional in combination with the optimized γ values.^{21,22} All these calculation were performed with the program package QChem³⁵ with the 6-31G(d,p) basis set. We refer to the methodology section of Ref. 24 for further information on the reliability of this approach regarding the employed functionals and basis sets.

IV. FUNDAMENTAL GAP AND IP/EA

In this section we examine the IP s, EA s, and fundamental gaps of DA systems. With the previously defined molecules a -BTT, $r1$ -BTT, $r2$ -BTT, and b -BTT we have a test set that is well suited for this study, because they all contain the same D and A components and only differ in the arrangement of D and A.

Fig. 5 shows their IP s and EA s in comparison to the oligomers PT and PB for different sizes. The IP s of all four DA arrangements are nearly identical to the IP of PT whereas the EA s are close to the EA of PB. This of course is only true for systems large enough to be saturated with respect to their IP and EA levels. It seems that the ionization of an electron is only determined by the T units and the absorption of an electron by the B units. Such a result is understandable for the case of b -BTT which is effectively a combination of PT and PB. However, in the case of a -BTT for example, T and B units are connected alternately, yet the IP nevertheless has the value of connected T units and the EA of

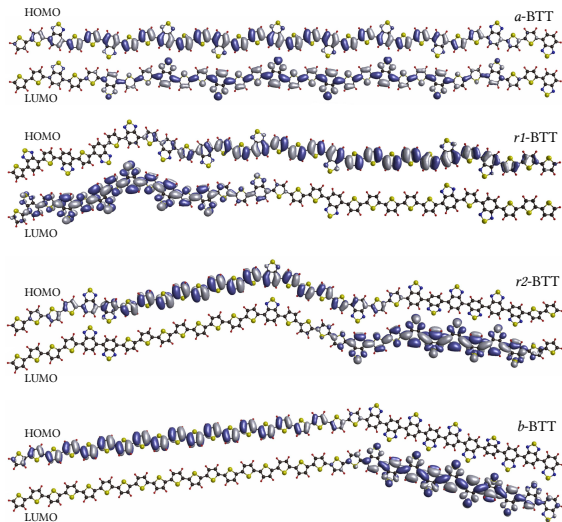


FIG. 6: HOMO and LUMO orbitals for *a*-BTT, *r1*-BTT, *r2*-BTT, and *b*-BTT (from top to bottom) for $n = 10$. The isosurface value is 0.01.

connected B units. This behavior can be understood by looking at the HOMO and LUMO orbital plots of *a*-BTT, *r1*-BTT, *r2*-BTT, and *b*-BTT in Fig. 6. In all four systems we encounter a similar situation. The HOMO orbital is mainly located on the T units and the LUMO orbital on the B units. This is consistent with the *IP* and *EA* results we obtained before. Note that with the help of these plots we are able to identify at which position in the molecule the ionization process (corresponds to the position of the HOMO orbital) and the electron absorption (corresponds to the position of the LUMO orbital) occurs. This might help in the design of efficient organic solar cells. If the ratio of D units is larger on one side of the molecule we are able to ensure that the ionization and related to that the transfer of an electron will appear at this position. The same argument holds for the absorption of an electron on this part of the molecule where the A ratio is dominant.

We close this section with a remark about fundamental gap differences of data obtained from calculations and experiment for organic molecules. Usually, in single molecule calculations the fundamental gap differs considerably from the difference of the *IP* and *EA* levels obtained from solution experiments (commonly determined by cyclic voltammetry (CV) measurements). Contrary, the lowest excitation energies calculated with a single molecule approach are usually close to optical gaps and the absorption maximum obtained from optical spectroscopy in a solution. We verify this statement by a comparison of calculated single molecule fundamental gaps and excitation energies as well as measured fundamental gaps from CV and first excitation energies of the

same systems in solution in Tab. I. The calculated fundamental gaps are approximately twice as large as the lowest excitation energy whereas in the experiment both quantities are close to each other. This difference is understandable as all our calculations are done for single molecules in vacuum and thus do not include intermolecular interactions. Optical excitation energies from solution experiments are typically similar to the ones of single molecules since they are neutral excitations causing only a little interaction with the surrounding molecules (due to some electron density redistribution caused by the excitation). But, fundamental gaps of systems surrounded by a solvent, *e.g.*, from CV measurements, might be very different because the *IP* and *EA* are determined by charged electronic excitations that have a significant impact on the surrounding. This impact can be simulated by using a solvation model in the calculation. In a simple approach we calculated the fundamental gap from total energy differences ($E(N-1) + E(N+1) - 2E(N)$). The total energies are calculated by using the QChem³⁵ solvation model chemsol³⁶ in combination with the BNL functional. We used the single molecule range separation parameter because we do not want to alter the interactions within the molecule. These solvation model fundamental gaps are also shown in Tab. I. They compare favorably with the fundamental gaps from CV measurements

V. FIRST EXCITATION ENERGIES

In this section we examine the first excitation energy of *a*-BTT, *r1*-BTT, *r2*-BTT, and *b*-BTT. It is one of the key properties of a low gap system designed for the use in organic solar cells and is as important as the optical gap. More accessible to theory is the vertical excitation energy which we refer to as lowest or first excitation energy and calculate in the following.³⁹ In Fig. 7 we show these excitation energies as a function of the inverse number of double bonds N^{-1} along the molecular backbone for all four DA arrangements. Since all systems are identical for $n = 1$ all four curves start with the same point. In Ref. 24 we already demonstrated that the excitation energies of *a*-BTT and *r1*-BTT are almost identical and saturate at 1.63 and 1.67 eV, respectively. The other two DA arrangements *r2*-BTT and *b*-BTT saturate at 1.81 and 2.04 eV, respectively. The latter has a discrepancy of 0.4 eV with respect to *a*-BTT. This represents the maximum possible effect one can obtain from changing the relative order of D and A. An analysis of the full optical spectra in appendix A confirms these findings. The changes in the overall spectrum are small from *a*-BTT to *r1*-BTT and larger to *r2*-BTT and *b*-BTT.

As explained in the introduction, an important aspect in organic solar cells is the interplay of the lowest excitation energy for the light absorption and the *IP* and *EA* for the transfer of an electron from the hole to the electron conducting material of the cell. In order to further

TABLE I: Comparison of the first excitation energies and fundamental gaps ($|IP - EA|$) from theory and experiment. The experimental values are from Refs. 37,38. The example systems are DA molecules composed of T and B units stringed together. Calculation and definition of TBT and TTBTT see Ref.²⁴.

Systems	Theory			Experiment	
	First excitation energy [eV]	single molecule Fundamental gap [eV]	solution model Fundamental gap [eV]	First excitation energy (maximum) [eV]	CV gap [eV]
BT	3.41	6.83	3.33	3.2	3.2
BTT (<i>a</i> -BTT, $n=1$)	3	5.94	2.86	2.9	2.7
TBT	2.78	5.87	2.84	2.8	2.4-2.7
TTBTT	2.32	4.9	2.43	2.5	2.3

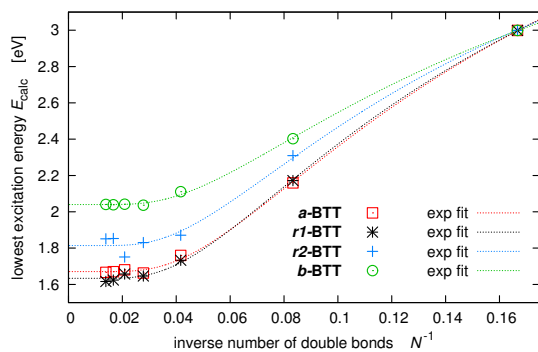


FIG. 7: Lowest calculated vertical absorption energies (TDDFT with tuned BNL and 6-31G(d,p) basis) as a function of the inverse number of double bonds N^{-1} . As discussed in earlier work²² we use an exponential fit to extrapolate to the saturation limit. Note that all data points are close to the exponential fitting curves (except for the “ $n = 8$ data point” of $r2$ -BTT). This confirms that for the purposes of our study it is not necessary to consider different statistical arrangements for $r1$ -BTT and $r2$ -BTT.

elucidate the understanding of these material properties we compare the first excitation energy and the fundamental gap ($|IP - EA|$) of a -BTT, $r1$ -BTT, $r2$ -BTT, and b -BTT in Fig. 8 alongside with the excitation energy and fundamental gap of PT and PB. All data points of this graph correspond to saturated values meaning that they do not change for larger chain lengths. The graph demonstrates that in all DA oligomers the fundamental gap is reduced by 0.6 to 0.8 eV compared to the D and A only system PT and PB. This reduction is nearly independent of the specific DA arrangement. In the case of the lowest excitation energy the reduction depends on the DA arrangement. It is the largest with 0.5 eV for a -BTT and $r1$ -BTT. However, the more similar ($r2$ -BTT) to a block copolymer the system becomes, the smaller is the reduction in the first excitation energy (0.3 eV). For the diblock system b -BTT we only observe a small effect with a re-

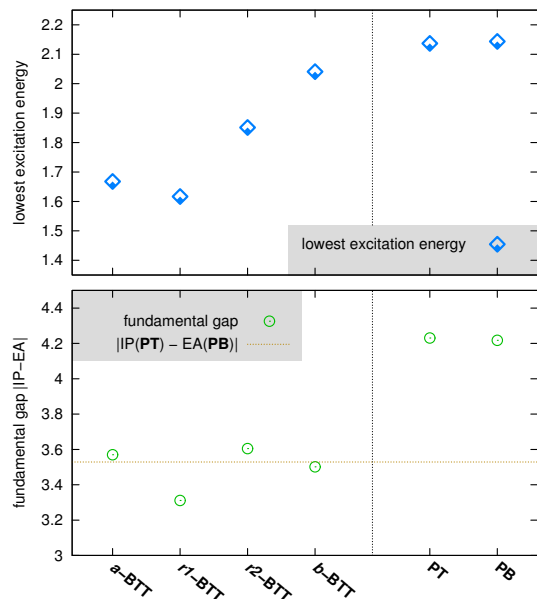


FIG. 8: Comparison of lowest excitation energy and fundamental gap. All values are saturated. $n = 12$ for a -BTT, $r1$ -BTT, $r2$ -BTT and b -BTT, $n = 32$ for PT and $n = 25$ for PB. For the saturation behavior of the excitation energy of PT and PB see Ref. 24.

duction of 0.1 eV. Hence, changing the DA arrangement enables us to modify the absorption properties without altering the fundamental gap (and connected to that the IP and EA .) Note that changes for the excitation energy are only considerable if the DA rearrangement is distinct enough (e.g., from a -BTT to $r2$ -BTT).

Below we want to critically examine which factors are important for obtaining a low excitation energy in DA systems. The previously defined and discussed molecules constitute a test set that is well suited for this type of study, because they all contain the same D and A components and nevertheless have different first excitation

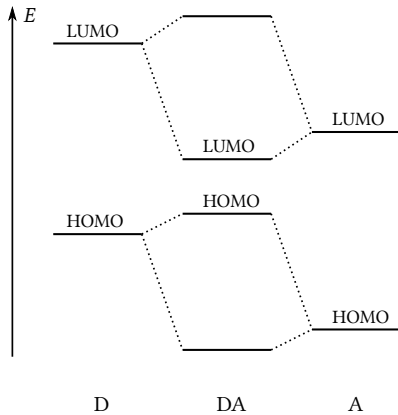


FIG. 9: Schematic illustration of the fictitious HOMO and LUMO levels (or *IPs* and *EAs*) of DA, D, and A.^{3,4}

energies. Factors that are generally regarded to reduce the gap in DA systems are an increase in the conjugation length and planarity, the occurrence of CT in the lowest excitation, and the reduction of the BLA.^{4,40} In the following we systematically examine these factors and verify which of them has a direct correlation with the lowest excitation energy or even cause a reduction of it.

A. Conjugation length

Fig. 7 and 5 demonstrate that the lowering of the excitation energy and the fundamental gap is strongly related to an increasing systems size. This is a well known characteristic of conjugated systems that can be understood by a particle in the box model: enlarging the box contracts the eigenvalue spectrum and therefore leads to lower excitation energies and fundamental gaps. In the systems under consideration the conjugation length can be seen as the property corresponding to the size of the box. In appendix B we introduce the definition of an effective conjugation length as the extent of the most dominant natural transition orbital (NTO) of the lowest excitation and use it to visualize the saturation of the lowest excitation energies.

In the following we want to emphasize the importance of the conjugation length by looking at a much simpler system, the BT molecule. A common way of explaining the favorable gap of a simple DA system is the comparison with the gap of a single D and A molecule, e.g., along the line of Fig. 9. However, this view disregards that the main effect for the low gap of DA compared to D and A alone is caused by the larger conjugation length of DA. In order to eliminate this effect it is necessary to compare systems with similar conjugation lengths. Fig. 10 compares the lowest excitation energy of BT with T and B alongside with T_2 and B_2 with a conjugation length

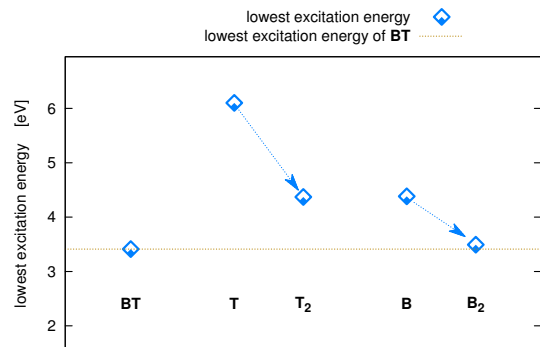


FIG. 10: Lowest calculated vertical absorption energies for BT, T, T_2 , B, and B_2 .

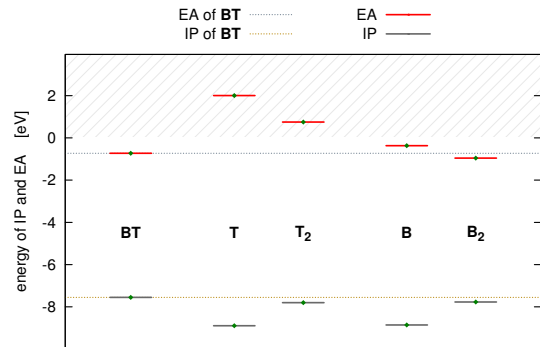


FIG. 11: *IP* and *EA* from tuned BNL/6-31G(d,p) calculations for BT, T, T_2 , B, and B_2 .

similar to the one of BT (for simplicity we assume that T and B equally contribute to the conjugation length). From T to BT the first excitation energy is reduced by approximately 2.5 eV and from T_2 to BT by only 1 eV. Only in the second comparison the reduction is an effect solely related to the combination of D and A. In the case of B_2 we see almost no reduction of the gap due to the combination with T although one would expect an effect if just comparing B with BT. This confirms the importance of the conjugation length.

We can draw a similar conclusion from an analysis of the *IPs* and *EAs* of these systems (Fig. 11). We observe that the energy levels of BT are very close to the ones of T_2 and B_2 , respectively. Fig. 11 could also explain why the lowest excitation energies of BT and B_2 are nearly equal in size since the *IP* of B is similar to the *IP* of T whereas the *EA* is larger.

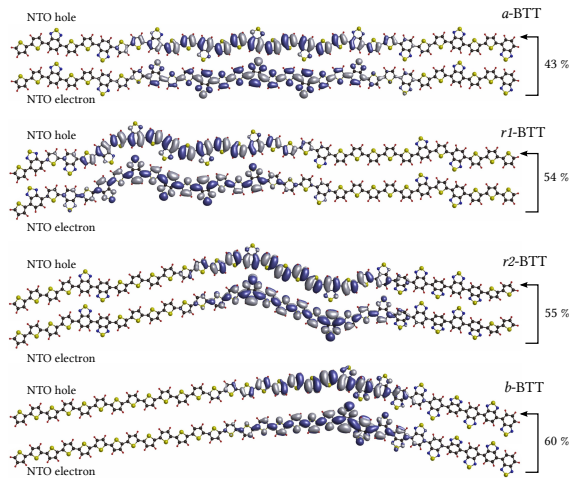


FIG. 12: Most dominant NTO pair of the lowest electronic excitation for each of the systems *a*-BTT, *r1*-BTT, *r2*-BTT, and *b*-BTT. The isosurface value is 0.01. The numbers on the right hand side denote the weight of the NTO pair contribution to the excitation.

B. NTO analysis

We further examine if the differences in the lowest excitation energy can be explained via an NTO analysis. We calculated the dominant NTO hole and electron of the first excitation for *a*-BTT, *r1*-BTT, *r2*-BTT, and *b*-BTT with a chain length $n = 10$. The “hole” and “electron orbital” are equal in size and localized in the same parts of the molecule. This also applies to the less dominant NTO pairs (not show here).

Only an insignificant CT characteristic appears around the sulfur and nitrogen atoms of the B units indicating that the excitations are essentially valence excitations. We already draw this conclusion for *a*-BTT and *r1*-BTT in Ref. 24. Surprisingly, even in the first excitation of *r2*-BTT and *b*-BTT no electron transfer from the D to the A part occurs although these parts are well separated in these molecules. Furthermore, since the nature of these excitations is similar in all four systems it does not explain why their energies are different.

It is important to note that this result is contrary to the perspective we would obtain from the HOMO and LUMO orbital pictures in Fig. 6. Although the ionization process takes place on the donor part of the molecule (HOMO) and the electron absorption on the acceptor part (LUMO) the excitation due to the absorption of light does not initiate such an electron transfer as the NTO picture demonstrates. This study reflects the different physics of these processes especially for *r2*-BTT and *b*-BTT.

Additionally to these results we can extract more in-

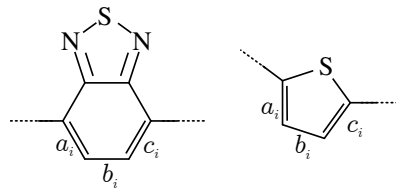


FIG. 13: Definition of the bond lengths a_i , b_i , and c_i used in Eq. 2 for a thiophene and a benzothiadiazole unit, respectively.

formation from the NTO plots of Fig. 12. Examining the extent of each NTO pair we observe that the length of the *a*-BTT and *r1*-BTT orbitals is noticeable larger than the one of the *r2*-BTT orbitals which is again larger than the one of the *b*-BTT orbitals. An interpretation of the NTO length as a measure of an effective conjugation length regarding the excitation would explain the discrepancy in the lowest excitation energies and underline the importance of the conjugation length for the lowest excitation energy. A low gap caused by a larger conjugation length can be the consequence of an increased planarity.^{4,40} This property is also influenced by the DA arrangement. Without a detailed analysis we note that *a*-BTT and *r1*-BTT are almost completely planar whereas the structures of *r2*-BTT and *b*-BTT show torsions between neighboring B units. This is also consistent with the first excitation energy values. The existence of torsions might also explain that the difference between the monomer and the polymer excitation energy is smaller for PB, *r2*-BTT, and *b*-BTT than for the planar structures of PT, *a*-BTT, and *r1*-BTT (Fig. 7, 8, and 10).

C. Bond length alternation

The connection between a low BLA – the average difference between the length of single and double bonds – and a low optical gap is a well established relationship.^{40–42} It is at least partly held responsible to cause the low gap in DA systems.⁴ In the following we study whether we can relate a lower gap (fundamental or optical) to a reduction of the BLA in our DA systems. For this purpose we first of all have to find an adequate definition of the BLA that enables us to compare systems composed of different subcomponents with each other, *e.g.*, *a*-BTT with PT. To us, two different definitions appear possible:

Definition 1: We define BLA_1 as the average difference of single and double bonds within either the thiophene or the benzol rings:

$$BLA_1 = \sum_i^{\text{T or B rings}} = \left(b_i - \frac{a_i + c_i}{2} \right), \quad (2)$$

where a_i , b_i , and c_i are defined in Fig. 13. This definition

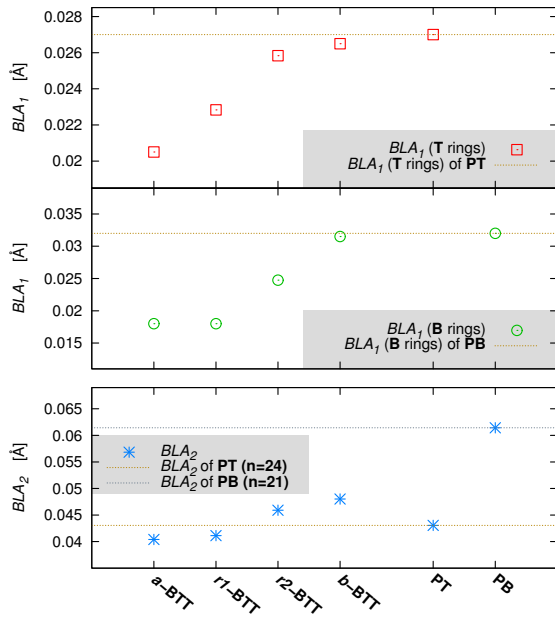


FIG. 14: BLA values from B3LYP/def2-SV(P) geometries for *a*-BTT, *r1*-BTT, *r2*-BTT, *b*-BTT, PT, and PB. The upper and center viewgraphs show values of BLA_1 , the lower viewgraph shows BLA_2 values. See text for definition of BLA_1 and BLA_2 .

allows for precisely defining the change in the BLA that occurs when we change the surrounding of T or B rings, respectively.

Definition 2: As BLA_2 we define the difference between single and double bonds, averaged over all bonds along the alternating molecular backbone. This corresponds more closely to the common definition of the BLA and may have the advantage of allowing for a closer connection to the lowest excitation energy, since BLA_2 is influenced by the molecule as a whole.

Fig. 14 shows BLA_1 and BLA_2 of *a*-BTT, *r1*-BTT, *r2*-BTT, and *b*-BTT, and also of PT and PB. If we compare the values of BLA_1 with the saturated first excitation energies of Fig. 8 we realize that both quantities follow the same trend. *a*-BTT and *r1*-BTT both have the lowest excitation energies and the lowest BLA_1 values, followed by *r2*-BTT and thereafter by *b*-BTT. The BLA_1 of PT and PB is slightly larger which is again in accordance with the first excitation energies. We obtain a different picture for BLA_2 . For this commonly used BLA definition results are not on a par with the lowest excitation energies. BLA_2 of PT lies between *r1*-BTT and *r2*-BTT opposed to their lowest excitation energies. For PB the BLA_2 is larger than *b*-BTT, however, the difference is disproportionate compared to the difference between *b*-BTT and *a*-BTT. If we restrict the analysis

to *a*-BTT, *r1*-BTT, *r2*-BTT, and *b*-BTT we realize that both BLA definitions draw a similar picture which is not surprising since these four systems contain exactly the same components (n B and $2n$ T units). Additionally we observe that contrary to the first excitation energy neither the BLA_1 results nor the BLA_2 results of Fig. 14 reflect the trends that are observed for the fundamental gap in Fig. 8. We draw similar conclusions from an analysis of BLA_1 and BLA_2 for the small systems BT, T, T₂, B, and B₂ in appendix C.

We conclude that BLA_1 is closely related to the optical excitation, and not BLA_2 . This is somewhat contrary to what one may have expected a priori, because the former takes only certain C-C bonds into account, whereas the latter, just like the first excitation, relates to all C-C bonds of the conjugated backbone. However, the BLA of oligomers composed of different monomers can not be compared directly and therefore the commonly used BLA definition (BLA_2) fails to predict trends of the excitation energy. We propose that with a simple BLA analysis based on BLA_1 one has a tool to predict trends for the optical gap without performing a relatively demanding tuned RSH TDDFT calculation. If this relationship is reconfirmed by calculations on other systems it facilitates the design of novel materials with a low absorption gap.

VI. CONCLUSION

In this work we examined the impact of rearranging D and A components on the optical gap as well as the *IP*, *EA* and fundamental gap in DA oligomers consisting of thiophene and benzothiadiazole by using DFT and TDDFT with a tuned RSH functional. For the optical gap (or first excitation energy) the rearrangement from *a*-BTT to *r1*-BTT causes only minor changes of the excitation energy (< 0.1 eV). However, the more drastic rearrangement from *a*-BTT to *r2*-BTT and *b*-BTT increases the excitation energy by 0.2 and 0.4 eV, respectively. This is a quite notable change in view of the finding that the decrease of the first excitation energy from polythiophene or benzothiadiazole to the donor-acceptor system *a*-BTT is itself only 0.5 eV. With respect to the second gap that is important for the use in organic solar cells, the fundamental gap, the results are different. *IP* and *EA* and consequently, the fundamental gap, are nearly identical for all four different DA arrangements. A detailed analysis of properties like the BLA, the planarity, and the extent of the dominant NTO's reveals that these properties are related to the optical gap, but not to the fundamental gap. Furthermore, we showed by NTO analysis that in all DA arrangements, even the diblock system, the first optical excitation has only a very limited, small CT character.

These results are helpful for understanding and systematically designing organic solar cell materials. A low optical and fundamental gap is achieved by both a strictly alternating and a random arrangement of D and A units.

Furthermore, we demonstrated that via a rearrangement of D and A to continuous blocks of D and A units it is possible to change the absorption properties and at the same time leave the IP and EA unchanged. The latter two properties are mostly determined by the respective energy levels of the D and A polymer, respectively. With selectively allocating different local fractions of D and A to different parts of the molecule it is possible to control the location where the electron leaves the molecule during the ionization or is absorbed during the inverse process. In solar cells that are specifically designed to take advantage of this effect the charge transfer and separation across the interface of the hole and electron conducting material could be enhanced.

We also specified the gain in lowering the optical gap that one can obtain by combining donor and acceptor molecules. The lowest excitation energy of a single thiophene and benzothiadiazole molecule is reduced from 6.1 eV and 4.4 eV, respectively, to 1.7 eV for the saturated alternating DA oligomer a -BTT. However, only 0.5 eV of this reduction originates from the combination of donor and acceptor components. The rest is caused by the increase of the conjugation length.

ACKNOWLEDGMENTS

The authors acknowledge financial support from the German Research Foundation (DFG, GRK 1640).

Appendix A: Optical spectra

In Fig. 15 we compare the optical spectra of a -BTT, $r1$ -BTT, $r2$ -BTT, and b -BTT for $n = 6$. It shows that the lowest excitation is the dominant excitation in all four systems with oscillator strengths of similar size. The differences for higher energies are small. a -BTT has a second considerable peak near 3 eV whereas $r2$ -BTT and b -BTT have a few other peaks closer to the lowest peak. A natural transition orbital⁴³ (NTO) analysis reveals that these other higher energy peaks are related to parts of the molecule that are either dominated by T or B units. These results confirm the conclusion drawn in Sec. V for the first excitation energies. The changes in the overall optical spectrum are relatively small for a rearrangement of D and A from a -BTT to $r1$ -BTT, whereas in $r2$ -BTT and b -BTT the changes are larger.

Appendix B: Saturation of a -BTT

An effective conjugation length for a certain excitation can be defined and visualized by looking at the extension of the dominant NTO pair. In Fig. 16 we plotted the most dominant NTO hole of the lowest excitation energy for a -BTT with repeat units of $n = 4, 6, 8$ and 10,

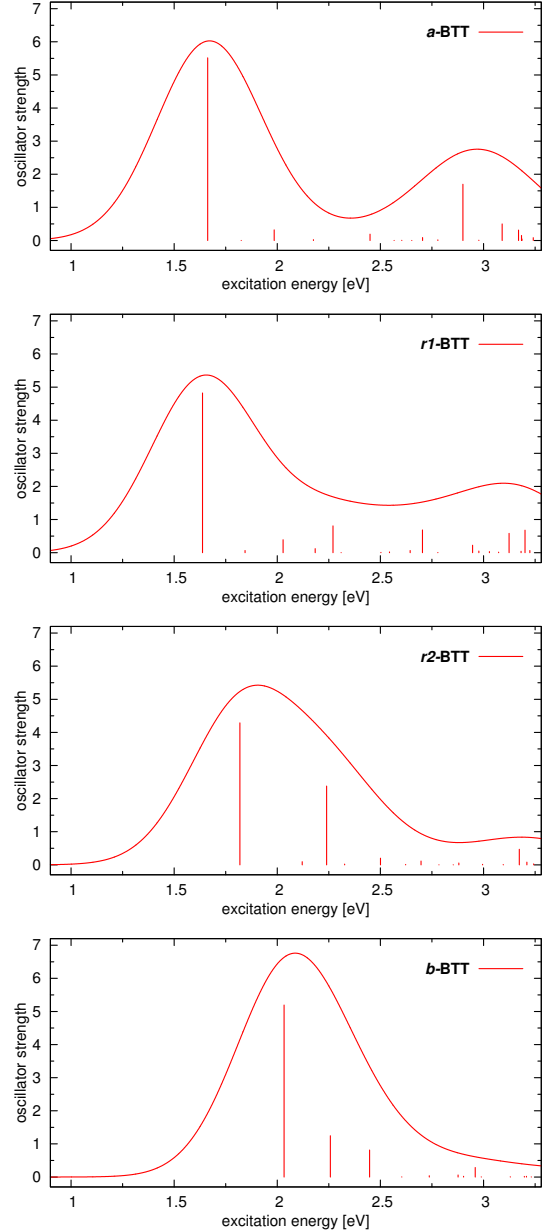


FIG. 15: Calculated electronic excitation spectra of four different DA arrangements, each with $n = 6$ repeat units (6 B and 12 T units). The calculated positions and oscillator strengths are represented by the bars. Linewidths as present in typical experiments are mimicked by a Gaussian broadening with 0.3 eV FWHM.

respectively. The size of these hole NTOs shows a saturation behavior similar to the lowest excitation energy (*cf.* Fig. 7), demonstrating its usefulness as a measure for an effective conjugation length.

Appendix C: Bond length alternation for monomeric systems

We draw a similar conclusion from Fig. 17 where we compare BLA_1 and BLA_2 for the small systems BT, T, T₂, B, and B₂. The BLA_1 values (upper and central part of the Figure) are qualitatively in line with results for the lowest excitation energies of Fig. 10. BLA_2 (lower part of the Figure), in contrast, disagrees with the trend of the excitation energies. Furthermore we note that in the case of a BLA analysis it is important to compare systems of similar size (likewise for excitation energies). The decrease of BLA_1 from T to T₂ or from B to B₂ illustrates that the main effect for the reduction of the BLA is related to the system size (or conjugation length) and not to the formation of a DA system.

- ¹E. E. Havinga, W. t. Hoeve, and H. Wynberg, *Polym. Bull.* **29**, 119 (1992).
- ²C. Kitamura, S. Tanaka, and Y. Yamashita, *Chem. Mater.* **8**, 570 (1996).
- ³E. Bundgaard and F. C. Krebs, *Sol. Energ. Mat. Sol. Cells* **91**, 954 (2007).
- ⁴Y.-J. Cheng, S.-H. Yang, and C.-S. Hsu, *Chem. Rev.* **109**, 5868 (2009).
- ⁵C. Risko, M. D. McGehee, and J.-L. Brédas, *Chem. Sci.* **2**, 1200 (2011).
- ⁶J.-L. Brédas, J. E. Norton, J. Cornil, and V. Coropceanu, *Acc. Chem. Res.* **42**, 1691 (2009).
- ⁷M. Helgesen, S. A. Gevorgyan, F. C. Krebs, and R. A. J. Janssen, *Chem. Mater.* **21**, 4669 (2009).
- ⁸J.-Y. Lee, M.-H. Choi, H.-J. Song, and D.-K. Moon, *J. Polym. Sci. A Polym. Chem.* **48**, 4875–4883 (2010).
- ⁹P. Sonar, E. L. Williams, S. P. Singh, and A. Dodabalapur, *J. Mater. Chem.* **21**, 10532 (2011).
- ¹⁰P. Hohenberg and W. Kohn, *Phys. Rev.* **136**, B864 (1964).
- ¹¹W. Kohn and L. J. Sham, *Phys. Rev.* **140**, A1133 (1965).
- ¹²E. Runge and E. K. U. Gross, *Phys. Rev. Lett.* **52**, 997 (1984).
- ¹³M. E. Casida, in *Recent Advances in Computational Chemistry*, edited by D. P. Chong (World Scientific Publishing Co. Pte. Ltd., 1995) pp. 155–192.
- ¹⁴T. Leininger, H. Stoll, H.-J. Werner, and A. Savin, *Chem. Phys. Lett.* **275**, 151 (1997).
- ¹⁵H. Iikura, T. Tsuneda, T. Yanai, and K. Hirao, *J. Chem. Phys.* **115**, 3540 (2001).
- ¹⁶T. Yanai, D. P. Tew, and N. C. Handy, *Chem. Phys. Lett.* **393**, 51 (2004).
- ¹⁷R. Baer and D. Neuhauser, *Phys. Rev. Lett.* **94**, 043002 (2005).
- ¹⁸J.-D. Chai and M. Head-Gordon, *J. Chem. Phys.* **128**, 084106 (2008).
- ¹⁹T. M. Henderson, B. G. Janesko, and G. E. Scuseria, *J. Chem. Phys.* **128**, 194105 (2008).
- ²⁰M. A. Rohrdanz, K. M. Martins, and J. M. Herbert, *J. Chem. Phys.* **130**, 054112 (2009).
- ²¹T. Stein, L. Kronik, and R. Baer, *J. Am. Chem. Soc.* **131**, 2818 (2009).
- ²²A. Karolewski, T. Stein, R. Baer, and S. Kümmel, *J. Chem. Phys.* **134**, 151101 (2011).
- ²³L. Kronik, T. Stein, S. Refaely-Abramson, and R. Baer, *J. Chem. Theory Comput.* **8**, 1515 (2012).
- ²⁴A. Karolewski, A. Neubig, M. Thelakkat, and S. Kümmel, *Phys. Chem. Chem. Phys.* **15**, 20016 (2013).
- ²⁵R. Ahlrichs, M. Bär, M. Häser, H. Horn, and C. Kölmel, *Chem. Phys. Lett.* **162**, 165 (1989).
- ²⁶“Turbomole V6.0,” (2009).
- ²⁷P. J. Stephens, F. J. Devlin, C. F. Chabalowski, and M. J. Frisch, *J. Phys. Chem.* **98**, 11623 (1994).
- ²⁸S. Grimme, *J. Comput. Chem.* **27**, 1787–1799 (2006).
- ²⁹C. Lee, W. Yang, and R. G. Parr, *Phys. Rev. B* **37**, 785 (1988).
- ³⁰E. Livshits and R. Baer, *Phys. Chem. Chem. Phys.* **9**, 2932 (2007).
- ³¹L. Pandey, C. Doiron, J. S. Sears, and J.-L. Brédas, *Phys. Chem. Chem. Phys.* **14**, 14243 (2012).
- ³²A. Karolewski, L. Kronik, and S. Kümmel, *The Journal of Chemical Physics* **138**, 204115 (2013).
- ³³T. Stein, H. Eisenberg, L. Kronik, and R. Baer, *Phys. Rev. Lett.* **105**, 266802 (2010).
- ³⁴S. Refaely-Abramson, R. Baer, and L. Kronik, *Phys. Rev. B* **84**, 075144 (2011).
- ³⁵Y. Shao, L. F. Molnar, Y. Jung, J. Kussmann, C. Ochsenfeld, S. T. Brown, A. T. B. Gilbert, L. V. Slipchenko, S. V. Levchenko, D. P. O’Neill, R. A. DiStasio Jr, R. C. Lochan, T. Wang, G. J. O. Beran, N. A. Besley, J. M. Herbert, C. Y. Lin, T. V. Voorhis, S. H. Chien, A. Sodt, R. P. Steele, V. A. Rassolov, P. E. Maslen, P. P. Korambath, R. D. Adamson, B. Austin, J. Baker, E. F. C. Byrd, H. Dachsel, R. J. Doerksen, A. Dreuw, B. D. Dunietz, A. D. Dutoi, T. R. Furlani, S. R. Gwaltney, A. Heyden, S. Hirata, C.-P. Hsu, G. Kedziora, R. Z. Khallullin, P. Klunzinger, A. M. Lee, M. S. Lee, W. Liang, I. Lotan, N. Nair, B. Peters, E. I. Proynov, P. A. Pieniazek, Y. M. Rhee, J. Ritchie, E. Rosta, C. D. Sherrill, A. C. Simmonett, J. E. Subotnik, H. L. W. Iii, W. Zhang, A. T. Bell, A. K. Chakraborty, D. M. Chipman, F. J. Keil, A. Warshel, W. J. Hehre, H. F. S. Iii, J. Kong, A. I. Krylov, P. M. W. Gill, and M. Head-Gordon, *Phys. Chem. Chem. Phys.* **8**, 3172 (2006).
- ³⁶J. Florián and A. Warshel, *J. Phys. Chem. B* **101**, 5583 (1997).
- ³⁷H. a. M. van Mullekom, J. a. J. M. Vekemans, and E. W. Meijer, *Chem. Eur. J.* **4**, 1235–1243 (1998).
- ³⁸M. Jayakannan, P. A. van Hal, and R. A. J. Janssen, *J. Polym. Sci. A Polym. Chem.* **40**, 251–261 (2002).
- ³⁹The energy that we obtain from a standard TDDFT calculation is the energy difference of the electronic ground state and the first excited state with both states in the ground state geometry. The difference to the experimental vertical excitation energy is the vibrational zero point energy of the electronic GS which is usually small and can be neglected. Cf. Fig 7 in Karolewski et al., *Phys. Chem. Chem. Phys.*, DOI: 10.1039/C3CP52739E (2013).
- ⁴⁰J. Roncali, *Chem. Rev.* **97**, 173 (1997).
- ⁴¹J.-L. Brédas, *J. Chem. Phys.* **82**, 3808 (1985).
- ⁴²C. Wu, S. Tretiak, and V. Y. Chernyak, *Chem. Phys. Lett.* **433**, 305 (2007).
- ⁴³R. L. Martin, *J. Chem. Phys.* **118**, 4775 (2003).

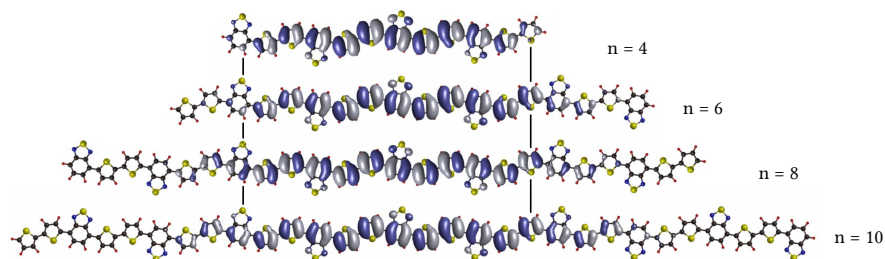


FIG. 16: Most dominant NTO hole of the lowest electronic excitation for *a*-BTT at different chain lengths ($n = 4, 6, 8, 10$). The isosurface value is 0.01.

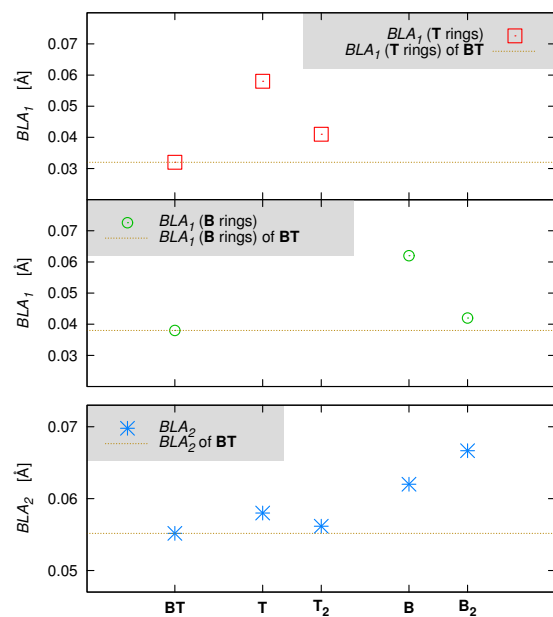


FIG. 17: BLA values from B3LYP/def2-SV(P) geometries for BT, T, T_2 , B, B_2 . See Fig. 14 for further explanation.

Erklärung

Hiermit erkläre ich, dass ich die vorliegende Arbeit selbstständig verfasst und keine anderen als die angegebenen Quellen und Hilfsmittel verwendet habe. Die Arbeit wurde weder in gleicher noch in ähnlicher Form bei anderen Prüfungsbehörden zur Erlangung eines akademischen Grades vorgelegt.

Weiterhin erkläre ich, dass ich keine Hilfe von gewerblichen Promotionsberatern bzw. -vermittlern oder ähnlichen Dienstleistern in Anspruch genommen habe und auch nicht beabsichtige diese zukünftig in Anspruch zu nehmen.

Weiterhin erkläre ich, dass ich bisher keinen anderweitigen Promotionsversuch unternommen habe.

Bayreuth, den 17. Oktober 2013

Andreas Karolewski